Designing Cellulose-Based Adsorbents For Water Remediation

by

Justin Trammell Harris

A dissertation submitted in partial fulfillment
of the requirements for the degree of
Doctor of Philosophy
(Chemistry)
in the University of Michigan
2021

Doctoral Committee:

Professor Anne J. McNeil, Chair
Professor Zhan Chen
Professor Joerg Lahann
Professor Adam J. Matzger

Justin T. Harris

justinha@umich.edu

ORCID iD: 0000-0002-6495-8248

Dedication

To my family, friends, and labmates.

Acknowledgements

I would first like to thank my advisor, Anne McNeil. Thank you for accepting me in your lab and helping me grow as a scientist. You guided me to become an effective presenter, concise scientific writer, and a critical thinker. I am continuously inspired by your passion for learning chemistry, and you have motivated me to become a life-long chemistry student. I am forever grateful for the time and effort you invested in me and the suggestions you provided over the years.

Thank you to my committee members, Professors Adam Matzger, Zhan Chen, and Joerg Lahann. Your comments and thoughts were always supportive and insightful, helping me advance my research project. A special thanks to Professor Matzger, as well, for providing assistance characterizing materials, letting me use your equipment, and answering all my science/job-related questions.

Next, I want to thank the collaborators I've worked with over the years. Thank you, Professor Thai, for providing project feedback. Thank you, Vikash Kumar, for making hydrogels in our joint publication. Lastly, thank you, Dr. Angela Devlin, for characterizing my cellulose fibers.

I would like to thank my undergraduate mentors and advisors for their guidance. Thank you, Professor Paul Mantica, for providing me with my first research experience and encouraging me to study chemistry. Thank you, Professor Matthew Becker, for inspiring me to pursue materials chemistry. Thank you, Professor James Dye, for being my undergraduate research advisor at MSU, teaching me how to perform research, and encouraging me to attend graduate school. Lastly, thank you, Professor Ned Jackson, for being my co-undergraduate research advisor, helping me solve research problems, and fostering my scientific curiosity.

I would like to thank past and present McNeil lab members for all their support: Dr. Gesine Veits, Dr. Mitchell Smith, Dr. Peter Goldberg, Dr. Ariana Hall, Dr. Chen Kong, Dr. Kendra Souther, Dr. Amanda Leone, Dr. Patrick Lutz, Dr. Danielle Fagnani, Dr. Tan Nguyen, Han Kim, Matthew Hannigan (best baymate!), Jessica Tami, Takunda Chazovachii, Emily Mueller, Gloria de la Garza, Bri Barbu, Vai Shastri, Izzy Zelaya, Morgan Young, Oscar Mota, and Joelle Anderson. You are all incredible people and thank you for helping me through the ups and downs of graduate school.

Lastly, I am blessed to have so many friends and family serve as my foundation throughout graduate school. Thank you to Dr. Ted McClain, Sam Michaud, Taylor Soucy, Jessi Wilson, Wes Pein, Matthew Lasky, and many more people for keeping me grounded with golf rounds, football Saturdays/Sundays, bar nights, etc. Thank you to Marcus Rivard and Morgan Kennedy for your generosity, friendship, advice, and most importantly, wine and dinner nights. Marcus, an additional thanks goes out to you for being an awesome roommate during my first years in graduate school, and I swear you'll get your 10% one day. Thank you to Stephen and Carolyn Rivard for providing me with examples of what hard work and determination look like in graduate school. Additionally, thank you, Stephen, for keeping me a Spartan in enemy territory. Thank you to my family: Steve, Sue, Leah, Micayla, Matt, Steve, Pat, Allison, and all of my extended family. I am extremely grateful for your love and support. Finally, thank you to my wife, Emily, for being my number one fan and source of strength throughout my graduate school career. I could not have done this without any of you.

Table of Contents

Dedication ii

Acknowledgements iii

List of Tables vii

List of Schemes xi

List of Figures xii

List of Equations xix

List of Appendices xxi

Abstract xxii

Chapter 1 Introduction 1

References 7

Chapter 2 Localized Hydrogels based on Cellulose Nanofibers and Wood Pulp for Rapid Removal of Methylene Blue* 10

Introduction 10

Experimental 13

Results and Discussion 18

Conclusions 24

References 25

Chapter 3 Rapid Removal of Poly- and Perfluoroalkyl Substances with Quaternized Wood Pulp 29

Introduction 29

Experimental 31

Results and Discussion 36

Conclusions 47
References 48
Chapter 4 Wood Pulp Adsorbents that Adsorb Methyl Orange Dye 54
Introduction 54
Experimental 56
Results and Discussion 67
Conclusions 73
References 74
Chapter 5 Conclusions and Future Directions 77
References 83
Appendices 86

List of Tables

Table 3.1. Initial and adsorbed moles of PFASs on QWP1.5. 41

Table 3.2. QWP1.5 adsorption % and capacity for PFASs after 30 s of contact time between QWP1.5 and PFASs. 43

Table 4.1. Reaction conditions for optimizing PWP synthesis. 73

Table A1.1. S-CNF/S-WP experimental conditions and results. 93

Table A1.2. S-CNF/S-WP conductometric titration results. 94

Table A1.3. Comparing S-CNF and S-WP sulfur contents (wt% S) as determined with conductometric titrations and elemental analysis (EA). 96

Table A1.4. Swelling of hydrogels prepared with various S-CNFs. 112

Table A1.5. Percentage of cellulose mass incorporated into gels using various S-CNFs. 113

Table A1.6. Swelling of hydrogels prepared with various S-WPs. 114

Table A1.7. Percentage of cellulose mass incorporated into gels using various S-WPs. 115

Table A1.8. Swelling of S-CNF-based hydrogels with various mass ratios. 117

Table A1.9. Percentage of cellulose mass incorporated into gels at various S-CNF:QHECE mass ratios. 118

Table A1.10. Swelling of S-WP-based hydrogels with various mass ratios. 119

Table A1.11. Percentage of cellulose mass incorporated into gels at various S-WP:QHECE mass ratios. 120

Table A1.12. Absorbance (661 nm) of MB solutions with various concentrations. 134

Table A1.13. MB adsorption % by S-CNF-based hydrogels as a function of initial MB concentration. 136

Table A1.14. MB adsorption % by S-WP-based hydrogels as a function of initial MB concentration. 138

Table A1.15. MB adsorption % by S-CNF-based hydrogels as a function of S-CNF concentration. 141

Table A1.16. Gelation conditions for monitoring MB adsorption over time. 144

Table A1.17. Decrease in MB concentration (conc.) over time in control and hydrogel-containing solutions. 146

Table A1.18. MB adsorption % by S-CNF-based flocs as a function of initial MB concentration. 148

Table A1.19. S-CNF-based hydrogel (white) and floc (gray) adsorption capacity as a function of initial MB concentration. 149

Table A1.20. MB adsorption % by S-CNF0.77-based flocs. 150

Table A1.21. MB adsorption % by S-CNF-based hydrogels in solutions with various pH values. 153

Table A1.22. MB adsorption % with S-CNF-based hydrogels in various NaCl solutions. 155

Table A1.23. Absorbance (661 nm) of MB in acidic ethanol solutions with various concentrations. 157

Table A1.24. S-CNF1.8-based hydrogels for MB desorption. 159

Table A1.25. MB desorption % over time from S-CNF1.8-based hydrogels. 160

Table A1.26. Comparing MB adsorption in S-CNF fibers and S-CNF-based gels. 163

Table A1.27. Mixing conditions for making the S-CNF1.9-based hydrogels that were added to 310 μM MB solutions. 165

Table A1.28. MB adsorption % over time when S-CNF1.9-based hydrogels are added to 310 μM MB solutions. 165

Table A2.1. QWP experimental conditions. 170

Table A2.2. QWP conductometric titration results. 170

Table A2.3. Comparing QWP nitrogen contents (wt% N) as determined with conductometric titrations and elemental analysis. 171

Table A2.4. PFOS adsorption (%) and capacity (mg/g) as a function of QWP charge density (mmol NR_3^+/g). 183

Table A2.5. PFOA adsorption (%) and capacity (mg/g) as a function of QWP charge density (mmol NR_3^+/g). 186

Table A2.6. PFOS adsorption (%) and capacity (mg/g) as a function of QWP1.5 concentration (mg/L). 188

Table A2.7. Measured and adjusted PFOS adsorption over time using QWP1.5. 190

Table A2.8. Measured and adjusted PFOA adsorption over time using QWP1.5. 190

Table A2.9. Pseudo-second-order adsorption parameters for PFOS and PFOA adsorption on QWP1.5. [QWP1.5] = 10 mg/L, $[PFOS]_0 = 3.5 \pm 0.1$ mg/L, $[PFOA]_0 = 3.9 \pm 0.1$ mg/L. 192

Table A2.10. Parameters for preparing adsorption isotherm samples. 196

Table A2.11. PFOS adsorption isotherm data. 197

Table A2.12. PFOA adsorption isotherm data. 198

Table A2.13. Langmuir isotherm parameters for PFOS and PFOA adsorption on QWP1.5. 201

Table A2.14. Freundlich isotherm parameters for PFOS and PFOA adsorption on QWP1.5. 202

Table A2.15. Leftover PFAS concentrations when adsorbing multiple PFASs with QWP1.5. Trials 1–5 and 11–15 were performed without HA, and trials 6–10 and 16–20 were performed with a HA concentration of 20.0 mg/L. 207

Table A2.16. QWP1.5 adsorption % and capacity for 7 PFASs after 30 s of contact time between QWP1.5 and PFASs. 208

Table A2.17. QWP1.5 adsorption % and capacity for 7 PFASs after 60 min of contact time between QWP1.5 and PFASs. 208

Table A2.18. PFOS and PFOA adsorption in solutions with various pHs. 216

Table A2.19. PFOS and PFOA adsorption in solutions with various [NaCl]. 220

Table A3.1. SWP experimental conditions. 224

Table A3.2. QWP experimental conditions. 224

Table A3.3. PWP synthesis conditions. 225

Table A3.4. SWP conductometric titration results. 225

Table A3.5. QWP conductometric titration results. 227

Table A3.6. PWP conductometric titration results. 228

Table A3.7. Comparing PWP nitrogen contents (wt% N) as determined with conductometric titrations and elemental analysis. 229

Table A3.8. Swell ratio of hydrogels prepared with various SWPs and QWPs. 231

Table A3.9. Baseline-corrected absorbance (464 nm) of MO solutions with various concentrations. 232

Table A3.10. MO adsorption as a function of SWP and QWP charge density. 234

Table A3.11. MO adsorption with only SWP and QWP fibers. 237

Table A3.12. MO adsorption (%) and capacity (mg/g) as a function of SWP and QWP concentration. 239

Table A3.13. MO adsorption as a function of SWP0.83:QWP0.77 mass ratio. 241

List of Schemes

Scheme 1.1. Combining oppositely charged anionic SCNFs and cationic QHECE results in a localized hydrogel formed via electrostatic crosslinking. 3

Scheme 1.2. MB adsorbed in a hydrogel made from SCNFs and QHECE. 4

Scheme 1.3. PFASs adsorbed with QWPs. 5

Scheme 1.4. MO adsorbed in hydrogel made with QWPs and SWPs. 6

Scheme 2.1. When combining oppositely charged polyions, a localized hydrogel forms via electrostatic crosslinks while rapidly adsorbing cationic pollutants. 12

Scheme 3.1. Synthesizing QWP fibers with various charge densities. 36

Scheme 4.1. A localized hydrogel forms via electrostatic interactions and adsorbs methyl orange when anionic SWPs and cationic QWPs are combined. 56

Scheme 4.2. Synthesis conditions for generating sulfated wood pulp (SWP) and quaternized wood pulp (QWP). 67

Scheme 5.1. Proposed syntheses to functionalize WP with hydrocarbon/fluorocarbon groups (top) and a variety of functional groups (bottom). 81

List of Figures

Figure 2.1. (A) Chemical structures for S-CNFs, S-WPs, and QHECE. (B) Procedure for making hydrogels. The gel shown is made from 0.050% (w/v) S-CNF1.9 and QHECE. 19

Figure 2.2. A localized hydrogel formed after adding aq. QHECE and S-CNF mixtures to a aq. solution containing MB ($[MB]_i$ = 94 μM; $[S\text{-}CNF1.8]_f$ = 0.08% w/v; $[QHECE]_f$ = 0.06% w/v). 21

Figure 2.3. (A) MB adsorption percent as a function of the initial dye concentration for S-CNF1.8 gels (●) and flocs (○). (B) MB adsorption capacity as a function of the initial dye concentration for S-CNF1.8 gels (●) and flocs (○). All gels and flocs were made using 0.080% w/v S-CNF1.8 and 0.060% w/v QHECE. 21

Figure 2.4. MB adsorption as a function of (A) pH and (B) NaCl concentration for S-CNF/QHECE hydrogels ([MB] = 94 μM, [S-CNF1.8] = 0.080% (w/v); [QHECE] = 0.060% (w/v)). 23

Figure 2.5. MB desorption % over time from gel sample 1 (●), gel sample 2 (○), and gel sample 3 (▼). 24

Figure 3.1. (A) Microscope image of a QWP1.5 fiber cross-section. (B) Raman spectra acquired at various positions on the fiber's cross-section. (The Raman spectra were normalized to the peak at 1096 cm^{-1}, which corresponds to the C–O and C–C stretches.) 37

Figure 3.2. (A) Effect of QWP charge density on PFOS (black) and PFOA (red) adsorption percent. ([QWP] = 50.0 mg/L, $[PFOS]_0$ = 4.2 mg/L, and $[PFOA]_0$ = 3.9 mg/L.) (B) PFOS (black) and PFOA (red) adsorption capacities (q_t) over time on QWP1.5. ([QWP1.5] = 10.0 mg/L, $[PFOS]_0$ = 3.5 mg/L, $[PFOA]_0$ = 3.9 mg/L.) Some error bars are not visible due to their small size. 38

Figure 3.3. Plot of PFOS adsorption (%) (black) and adsorption capacity (q, mg/g) (red) as a function of QWP1.5 concentration (mg/L). Some error bars are not visible due to their small size. 39

Figure 3.4. Plots of equilibrium adsorption capacities (q_e) versus equilibrium concentrations (C_e) for PFOS (A) and PFOA (B), fit with the Langmuir (solid black line) and Freundlich (dashed red line) models. ([QWP1.5] = 10.0 mg/L, $[PFOA]_0$ = ~920–8300 μg/L, $[PFOS]_0$ = ~750–8000 μg/L. Some error bars are not visible due to their small size.) 40

Figure 3.5. PFAS adsorption (%) on QWP1.5 with 30 s (white) and 60 min (gray) of contact time. ([QWP1.5] = 10.0 mg/L, $[PFAS]_0$ = ~2.5 µg/L.) Note: PFOS was removed below the limit of quantification (20 ng/L), so this limit was used in the adsorption % calculations) 42

Figure 3.6. PFOS (black) and PFOA (red) adsorption (%) as a function of pH (A) and NaCl concentration (B). ([QWP1.5] = 10.0 mg/L, $[PFAS]_{initial}$ < 2.8 µg/L.) Note: PFOS was removed below the limit of quantification (20 ng/L), so this limit was used for adsorption % calculations. Some error bars are not visible due to their small size. 44

Figure 4.1. (A) Adding SWP and QWP mixtures to a MO solution results in a hydrogel that adsorbs MO. ([MO] = 23 µM; [SWP0.83] = 0.60 mg/mL; [QWP1.6] = 0.80 mg/mL). (B) MO adsorption (%) as a function of SWP and QWP charge density. 69

Figure 4.2. (A) MO adsorption (%) as a function of QWP concentration (mg/mL). The mass ratio of SWP0.83:QWP0.77 was constant at 0.75. (B) MO adsorption (%) as function of SWP0.83:QWP0.77 mass ratio. The QWP concentration was fixed at 1.6 mg/mL. 70

Figure 5.1. Images of cellulose-based hydrogels used for adsorbing methylene blue (MB) and methyl orange (MO) dyes (left and middle), and an image of cationic wood pulp (WP) used for adsorbing PFASs (right). 77

Figure 5.2. Incorporating cellulose in a column for adsorption in flow. 82

Figure A1.1. Images of S-CNC-based hydrogels. 91

Figure A1.2. Calculating the charge density of a S-CNF1.1 sample. 95

Figure A1.3. Calculating the charge density of 2 QHECE samples. 98

Figure A1.4. SEM images of S-WP0.0. 100

Figure A1.5. SEM image of S-WP0.53. 100

Figure A1.6. SEM images of S-WP1.8. 101

Figure A1.7. SEM images of S-CNF0.0. 101

Figure A1.8. SEM images of S-CNF0.77. 102

Figure A1.9. SEM images of S-CNF1.1. 102

Figure A1.10. SEM images of S-CNF1.5. 103

Figure A1.11. SEM images of S-CNF1.9. 103

Figure A1.12. Determining the minimum amount of material needed to make S-CNF-based hydrogels. 106

Figure A1.13. Calculating f^- for S-CNF0.77-based hydrogels. 107

Figure A1.14. Determining the minimum amount of material needed to make S-WP-based hydrogels. 109

Figure A1.15. Calculating f^- for S-WP0.53-based hydrogels. 110

Figure A1.16. Hydrogel swell ratio as a function of S-CNF charge density. The line is present only to guide the eye. 112

Figure A1.17. Hydrogel swell ratio as a function of S-WP charge density. The line is present only to guide the eye. 115

Figure A1.18. Hydrogel swell ratio as a function of mass ratio between S-CNFs and QHECE. The line is present only to guide the eye. 117

Figure A1.19. Hydrogel swell ratio as a function of mass ratio between S-WPs and QHECE. The line is present only to guide the eye. 120

Figure A1.20. (A) Frequency and (B) oscillating stress sweep of S-CNF0.77 gels. 122

Figure A1.21. (A) Frequency and (B) oscillating stress sweep of S-CNF1.1 gels. 122

Figure A1.22. (A) Frequency and (B) oscillating stress sweep of S-CNF1.5 gels. 123

Figure A1.23. Frequency sweeps of S-CNF1.5 gels using gap heights of (A) 500 and (B) 1000 μm. 123

Figure A1.24. (A) Frequency and (B) oscillating stress sweep of S-CNF1.9 gels. 124

Figure A1.25. (A) Frequency and (B) oscillating stress sweep of S-WP0.53 gels. 124

Figure A1.26. (A) Frequency and (B) oscillating stress sweep of S-WP1.0 gels. 125

Figure A1.27. (A) Frequency and (B) oscillating stress sweep of S-WP1.3 gels. 125

Figure A1.28. (A) Frequency and (B) oscillating stress sweep of S-WP1.8 gels. 126

Figure A1.29. Frequency sweeps for SCNF1.8 gels made with a 0 μM initial MB concentration: (A) sample 1 and (B) sample 2. (C) Average frequency sweep from samples 1 and 2. 127

Figure A1.30. Frequency sweeps for SCNF1.8 gels made with a 313 μM initial MB concentration: (A) sample 1 and (B) sample 2. (C) Average frequency sweep from samples 1 and 2. 128

Figure A1.31. Frequency sweeps for SCNF1.8 flocs made with an 814 μM initial MB concentration: (A) sample 1, (B) sample 2, and (C) sample 3. (D) Average frequency sweep from samples 1, 2, and 3. 129

Figure A1.32. Frequency sweeps for SCNF1.8 flocs made with a 1628 μM initial MB concentration: (A) sample 1, (B) sample 2, and (C) sample 3. (D) Average frequency sweep from samples 1, 2, and 3. 130

Figure A1.33. Frequency sweeps for SCNF1.8 flocs made with a 3130 μM initial MB concentration: (A) sample 1, (B) sample 2, and (C) sample 3. (D) Average frequency sweep from samples 1, 2, and 3. 131

Figure A1.34. (A) Plot of absorbance (661 nm) versus concentration for MB in Millipore water. (B) Sample UV-vis spectrum of MB using the 31.3 μM solution. 135

Figure A1.35. UV-vis spectra of a 31.3 μM MB solution used in the MB calibration curve (■), and a MB solution after hydrogel dye adsorption using an initial MB concentration of 94 μM (○). 136

Figure A1.36. UV-vis spectra of a 31.3 μM MB solution used in the MB calibration curve (■), and a MB solution after hydrogel dye adsorption using an initial MB concentration of 31 μM (○). 138

Figure A1.37. Dye adsorption % as a function of the initial dye concentration for gels made with S-CNF1.8 (●) and S-WP1.8 (○), respectively. The lines are present only as guides for the eye. 139

Figure A1.38. UV-vis spectra of a 31.3 μM MB solution used in the MB calibration curve (■), and a MB solution after hydrogel dye adsorption using an initial MB concentration of 311 μM (○). 140

Figure A1.39. Dye adsorption % as a function of the final S-CNF1.8 concentration for samples where gels were (■) and were not (□) observed, respectively. The line is present only to guide the eye. 142

Figure A1.40. UV-vis spectra of a 31.3 μM MB solution used in the MB calibration curve (■), a MB solution after hydrogel dye adsorption for 3 min (○), and a MB solution after hydrogel dye adsorption for 3000 min (●). 145

Figure A1.41. MB concentration over time in a control solution (■) and solutions containing gel sample 1 (●), gel sample 2 (▽), and gel sample 3 (○). 146

Figure A1.42. UV-vis spectra of a 31.3 μM MB solution used in the MB calibration curve (■), and a MB solution after floc dye adsorption using an initial MB concentration of 814 μM (○). 148

Figure A1.43. (A) UV-vis spectra of a 31.3 μM MB solution used in the MB calibration curve (■), and a MB solution after hydrogel dye adsorption in a pH

11.51 solution (○). (B) UV-vis spectra of a 31.3 μM MB solution used in the MB calibration curve (■), and a MB solution after hydrogel dye adsorption in a pH 2.58 solution (○). 153

Figure A1.44. UV-vis spectra of a 31.3 μM MB solution used in the MB calibration curve (■), and a MB solution after hydrogel dye adsorption in a 98.5 mM NaCl solution (○). 155

Figure A1.45. (A) Plot of absorbance (661 nm) versus concentration for MB in acidic ethanol. (B) Sample UV-vis spectrum of MB in acidic ethanol using the 31.3 μM solution. 157

Figure A1.46. UV-vis spectra of a 31.3 μM MB in acidic ethanol (■), and a MB solution 1440 min after desorption from a hydrogel (○). 160

Figure A2.1. Calculating the charge density of a QWP1.5 sample. Points were included in the linear regression lines based on linearity and inclusion of extra points near the equivalence point did not significantly affect charge density calculations. 171

Figure A2.2. An image of a QWP1.5 fiber cross section overlayed with a Raman intensity ratio map using the intensity ratio between the peak at 724–810 cm^{-1} to the peak at 924–1183 cm^{-1}. The peak at 724–810 cm^{-1} corresponds to the symmetric $(CH_3)_3$-N^+ stretching from the quaternary amine group, and the peaks at 924–1183 cm^{-1} are C-C and C-O stretching in cellulose. The uniform color on the Raman intensity ratio map indicates that uniform amine functionalization occurred across the fiber cross section. The intensity ratio map was created using the Renishaw WiRE 5.3 software package. 172

Figure A2.3. Raman spectra of (A) QWP1.5 and (B) QWP0.0 fibers at various depths in the fibers. The arrow in (A) indicates the symmetric $(CH_3)_3$-N^+ stretching at 764 cm^{-1} from the quaternary amine group.[2] 173

Figure A2.4. (A) QWP1.5 fiber image along with (B) Raman spectra acquired at various positions on the fiber's surface. The colors of the dots in the fiber image correspond with the Raman spectra of similar color. The arrow in (B) indicates the symmetric $(CH_3)_3$-N^+ stretching at 764 cm^{-1} from the quaternary amine group.[2] 173

Figure A2.5. (A) Cross section microscope image of a QWP0.0 fiber. (B) Raman spectra acquired at various positions on the fiber's cross section. The Raman spectra were normalized to the peak at 1096 cm^{-1}. 174

Figure A2.6. (A) QWP0.0 fiber image along with (B) Raman spectra acquired at various positions on the fiber's surface. The colors of the dots in the fiber image correspond with the Raman spectra of similar color. 174

Figure A2.7. (A) TIC and (B) smoothed EIC for a 1.0 mg/L PFOS standard. 178

Figure A2.8. (A) TIC and (B) smoothed EIC for a 1.0 mg/L PFOA standard. 178

Figure A2.9. (A) TIC and (B) smoothed EIC for a PFOS sample 0.167 min after mixing with QWP1.5. 179

Figure A2.10. (A) TIC and (B) smoothed EIC for a PFOA sample 0.167 min after mixing with QWP1.5. 179

Figure A2.11. Examples of calibration curves generated for measuring (A) [PFOS] and (B) [PFOA]. 180

Figure A2.12. Plot of PFOS adsorption capacity (mg/g) over time (min) for QWP1.5 (blue), QWP0.99 (orange), QWP0.65 (magenta), QWP0.0 (red), and no QWPs (black). [QWP] = 50.0 mg/L. The data were fit using the pseudo second order model. 184

Figure A2.13. Plot of PFOA adsorption capacity (mg/g) over time (min) with QWP1.5 (blue), QWP0.99 (orange), QWP0.65 (magenta), QWP0.0 (red), and no QWPs (black). [QWP] = 50.0 mg/L. The data were fit using either the pseudo first or second order models to generate lines to guide the eye. 186

Figure A2.14. Plot of measured PFOS (black) and PFOA (red) adsorption capacities over time. PFOS (blue) and PFOA (magenta) control adsorption capacities over time are also given. Some error bars are not visible due to their small size. 191

Figure A2.15. Plot of t/q_t (min·g/mg) at various time (min) points for PFOS and PFOA adsorption over time. 192

Figure A2.16. Plot of adsorption capacity (mg/g) as a function of (A) PFOS and (B) PFOA equilibrium concentration (mg/L). 199

Figure A2.17. Plot of C_e/q_e (g/L) as a function of (A) PFOS and (B) PFOA equilibrium concentration (mg/L). 201

Figure A2.18. Plot of log q_e against log C_e for (A) PFOS and (B) PFOA adsorption. 202

Figure A2.19. UV-vis spectrum of a 20.0 mg/L humic acid solution. 210

Figure A3.1. Plot of conductivity (µS/cm) versus volume of 8.3 mM NaOH added (mL) during a titration to calculate the charge density of a SWP0.83 sample. 226

Figure A3.2. Plot of conductivity (µS/cm) versus volume of 10.0 mM $AgNO_3$ added (mL) during a titration to calculate the charge density of a QWP1.2 sample. Points were included in the linear regression lines based on linearity and inclusion of extra points near the equivalence point did not significantly affect charge density calculations. 227

Figure A3.3. Plot of conductivity (μS/cm) versus volume of 11.2 mM NaOH added (mL) during a titration to calculate the charge density of the PWP5 sample. Points were included in the linear regression lines based on linearity and inclusion of extra points near the equivalence point did not significantly affect charge density calculations. 228

Figure A3.4. (A) Plot of absorbance (464 nm) versus MO concentration in Millipore water. (B) Sample UV-vis spectrum of MO using the 30.6 μM solution. 233

Figure A3.5. UV-vis spectra of a 30.6 μM solution used in the MO calibration curve (black), and a MO solution after dye adsorption using a hydrogel made with SWP0.83 and QWP1.6 (red). 234

Figure A3.6. UV-vis spectra of a 30.6 μM solution used in the MO calibration curve (black), and MO solutions after adsorption using SWP1.1 (red) and QWP0.77 (blue) fibers. 236

Figure A3.7. UV-vis spectra of a 30.6 μM solution used in the MO calibration curve (black), and a MO solution after adsorption using a hydrogel made with 1.2 mg/mL SWP0.83 and 1.6 mg/mL QWP0.77 (red). 239

Figure A3.8. UV-vis spectra of a 30.6 μM solution used in the MO calibration curve (black), and a MO solution after adsorption in a hydrogel with a SWP0.83:QWP0.77 mass ratio of 0.25 (red). 240

List of Equations

Equation 2.1. Calculating MB desorption %. 18

Equation 4.1. Calculating MO adsorption %. 66

Equation A1.1. Calculating molar charge ratio in hydrogels. 105

Equation A1.2. Calculating swell ratio. 111

Equation A1.3. Calculating % cellulose in gels. 111

Equation A1.4. Calculating MB adsorption %. 133

Equation A1.5. Calculating MB adsorption capacity in gels. 141

Equation A1.6. Calculating the max ratio of MB/negative sites. 142

Equation A1.7. Calculating adsorption capacity for flocs. 149

Equation A1.8. Calculating MB desorption %. 159

Equation A2.1. Calculating PFAS adsorption %. 181

Equation A2.2. Calculating PFAS adsorption capacity. 181

Equation A2.3. Calculating pseudo-second order adsorption kinetics. 191

Equation A2.4. Calculating equilibrium adsorption capacity. 195

Equation A2.5. Langmuir model equation. 199

Equation A2.6. Freundlich model equation. 200

Equation A2.7. Calculating Langmuir parameters. 200

Equation A2.8. Calculating Freundlich parameters. 201

Equation A2.9. Calculating SUVA of HA. 210

Equation A2.10. pH equation. 214

Equation A2.11. Calculating pH for basic water solution. 214

Equation A2.12. Calculating salt concentration from conductivity. 219

Equation A3.1. Calculating WP-based hydrogel swell ratios. 230

Equation A3.2. Calculating MO adsorption capacity in WP-based hydrogels. 238

List of Appendices

Appendix 1 Supporting Information for Chapter 2 87

Appendix 2 Supporting Information for Chapter 3 167

Appendix 3 Supporting Information for Chapter 4 222

Abstract

Communities around the world are working to remove contaminants from freshwater sources. Adsorption is the primary technique utilized for remediation, but conventional adsorbents require long contact times to effectively remove pollutants. To overcome this limitation, we developed adsorbents using functionalized cellulose, a renewable, biodegradable, and inexpensive starting material, that rapidly remove pollutants from water via electrostatic interactions. More specifically, we demonstrated that functionalized cellulose fibers remove charged dyes and poly-/perfluoroalkyl substances (PFASs) from water in seconds.

In Chapter 1, we summarize adsorption techniques used for capturing water contaminants, with a focus on the limitations of currently used adsorbents. We highlight the advantages of cellulose-based materials and our motivation to utilize electrostatic interactions to adsorb two prevalent pollutants, dyes and PFASs.

Chapter 2 reports efforts designing localized cellulose-based hydrogels for rapidly removing methylene blue (MB), a cationic dye, from water. Specifically, we showed that anionic sulfated cellulose nanofibers (SCNFs) and quaternized hydroxyethyl cellulose ethoxylate (QHECE) form localized hydrogels and adsorb >90% of MB within 30 s of mixing. Adsorption was electrostatically driven and adsorption capacities for MB were greater than other cellulose-based hydrogels reported in the literature. This work showed that rapidly forming, localized hydrogels are promising adsorbents and may be useful as flocculating agents in water remediation.

Toxic PFASs are infiltrating freshwater supplies, but current adsorbents are incapable of rapidly removing these contaminants from water. Chapter 3 demonstrated that cationic wood pulp

(WP) fibers are an effective alternative adsorbent. Specifically, we showed that quaternized WPs (QWPs) adsorbed >90% of perfluorooctanesulfonic acid (PFOS) and >80% of perfluorooctanoic acid (PFOA) within 30 s of contact time at environmentally relevant concentrations. QWPs had adsorption capacities for PFOS and PFOA that rival conventional adsorbents. Furthermore, we found that adsorption was inhibited with humic acid present, but environmentally relevant solution pHs and salt concentrations had no effects on adsorption. These results indicated that WP is promising for removing PFASs from water.

Given the effectiveness of gels and WPs for adsorbing dyes and PFASs in previous chapters, Chapter 4 describes initial efforts adsorbing an anionic dye with WP-based hydrogels and fibers. We revealed that cationic QWPs and anionic SWPs formed localized hydrogels and adsorbed methyl orange (MO), an anionic dye, within seconds of mixing. MO adsorption was electrostatically driven, and SWP-QWP crosslinking reduced dye removal efficiency. Additionally, QWP fibers alone adsorbed more MO than hydrogels, suggesting that cationic fibers are promising for capturing anionic dyes. Further studies evaluating adsorbent properties such as adsorption capacity are needed before concluding whether gels or fibers are more effective for capturing dye. Finally, we detailed initial work synthesizing WP with primary amine groups for future use as an adsorbent. Future studies will show the utility of using these materials for removing dyes from water.

Chapter 5 summarizes each chapter and presents strategies for increasing the versatility of cellulose fiber adsorbents. Specifically, we intend to functionalize cellulose with groups complementary to other pollutants to expand the scope of contaminants that can be adsorbed. Additionally, adsorption will be performed in flow-based systems to evaluate functionalized cellulose fibers' potential in large scale water treatment operations. Overall, our work designing

cellulose-based adsorbents that rapidly capture pollutants is encouraging for advancing water treatment systems and will motivate researchers to develop improved adsorbents using renewable materials.

Chapter 1 Introduction

The United Nations included "ensure availability and sustainable management of water and sanitation for all" as one of their 17 Sustainable Development Goals to advance the health of people and the environment by 2030.[1] However, this goal is threatened by pollutants from industrial, agricultural, and municipal sources that have infiltrated water supplies around the world.[2,3] For example, an estimated 300–400 megatons of industrial waste and hundreds of millions of tons of sewage are released into water each year.[2,4,5] These quantities of waste are alarming considering that pollutants threaten human health and ecological biodiversity.[6,7] Thus, to minimize consequences stemming from pollution, it is imperative that we stop contaminating water and improve remediation systems to eliminate pollutants already in the environment.

Several technologies exist for removing contaminants from water including filtration,[8] chemical oxidation,[9] and liquid extraction.[10] The most common strategy, though, is adsorption because it is inexpensive and easily implemented.[11] Activated carbon (AC) is the leading adsorbent because it has high capacity and versatility for adsorbing different pollutants.[12] Despite these advantages, AC suffers from slow adsorption kinetics, needing long times (i.e., h to d) to achieve high levels of adsorption.[13,14,15] Additionally, AC is commonly made from coal,[16] and producing and regenerating AC requires harsh chemicals (e.g., phosphoric or sulfuric acid) and high temperatures (~800 ºC), making AC an unsustainable adsorbent.[12] Therefore, researchers are investigating alternative adsorbents.

To transition away from nonrenewable resources, scientists are developing adsorbents using renewable materials such as biomass and clay minerals.[3] Among the renewable options, cellulose

is promising because it is an inexpensive starting material and biodegradable.[17,18] Furthermore, cellulose is a versatile platform because it can be tailored with functional groups to target contaminants such as toxic organic chemicals, dyes, and heavy metals.[19] While these adsorbents are more sustainable compared to AC, most of them still require long time periods to effectively adsorb targeted contaminants. For example, a review by Mohammed et al. shows that multiple cellulose-based adsorbents require min to h of contact time to adsorb high levels of contaminants like dyes and heavy metals.[17] Similar times are reported for other toxic organic chemicals.[20,21] Additionally, these adsorbents are frequently less efficient in water containing realistic salt concentrations and solution pHs. A report by Liu et al. demonstrated that solutions with various NaCl concentrations and pHs caused dye adsorption to be inhibited on a cellulose adsorbent.[22] Ateia et al. showed that elevated pHs reduced adsorption of perfluorooctanoic acid (PFOA), a toxic fluorosurfactant, on cellulose microcrystals.[23] Overall, these shortcomings demonstrate the need for further research on cellulose-based adsorbents. We describe herein our efforts to overcome the deficiencies of current adsorbents by developing cellulose-based adsorbents that rapidly adsorb dyes and poly-/perfluoroalkyl substances (PFASs) under environmentally relevant conditions.

In Chapter 2, we report our work designing localized hydrogels (i.e., not sample-spanning) that rapidly adsorb organic dye during gelation.[24] Our approach to making localized hydrogels was inspired by flocculating agents which form suspensions with pollutants that are easily removed through filtration.[25] Additionally, because dyes are charged, we anticipated that dyes would effectively be captured by an adsorbent with charged functional groups. Thus, we explored making hydrogels, which have previously adsorbed dyes,[26] from polyionic complexes.[27] Moreover, we investigated creating hydrogels such that the gel was locally formed and easily removed from water, like a flocculant. Motivated by cellulose-based polyionic complex hydrogels described by

Boluk and coworkers,[28,29] we found that water-insoluble anionic sulfated cellulose nanofibers (SCNFs) form localized gels in ~20 s when mixed with water-soluble cationic quaternized hydroxyethyl cellulose ethoxylate (QHECE) (Scheme 1.1), likely driven by the entropy gain from counterion release into solution.[30] For localized gels to form, a minimum molar charge ratio, which is the ratio of negative charges to total charge, was required to effectively crosslink SCNFs with QHECE. Additionally, cellulose size impacted gel formation as sulfated cellulose nanocrystals, a material similar to SCNFs but with shorter lengths, were unable to form localized gels. We proposed that the longer SCNF fibers create more fiber/fiber entanglements, enabling the localized hydrogels to form rapidly.

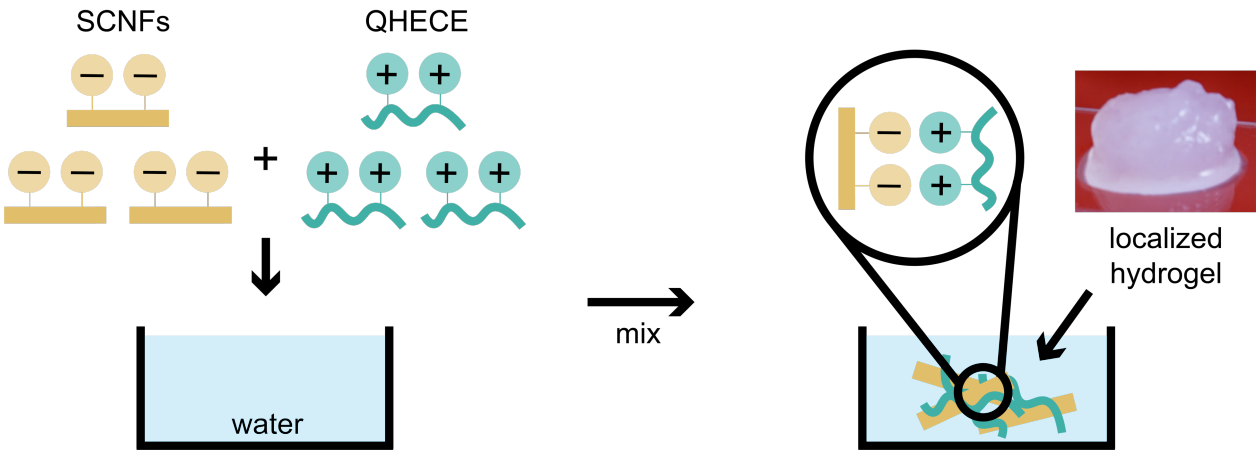

Scheme 1.1. Combining oppositely charged anionic SCNFs and cationic QHECE results in a localized hydrogel formed via electrostatic crosslinking.

After exploring gelation conditions, methylene blue (MB), a cationic dye, was removed from water with SCNF-based hydrogels. More specifically, we found that >90% of MB was adsorbed in under 60 s when gels were made in MB solutions (Scheme 1.2). We identified that gelation was dependent on dye concentration because gelation was inhibited at high MB concentrations (> 400 μM), due to reduced crosslinking between the anionic and cationic celluloses. Furthermore, when

gelation was inhibited, floc formation was observed, and the flocs adsorbed MB less efficiently than the gels. Overall, the maximum adsorption capacity for MB was greater than similar cellulose-based hydrogels.[31,32] To determine if MB/gel interactions were charge driven, MB was mixed with only anionic cellulose, and we observed that adsorption efficiency was similar to when MB was adsorbed by gels, indicating that MB adsorption primarily occurred through electrostatic interactions. MB was also adsorbed in solutions containing various pHs and NaCl concentrations, and we found that MB adsorption remained constant, which is an advantage compared to existing cellulose-based hydrogels used for dye removal.[31] To summarize, this work demonstrated that rapidly forming hydrogels are an effective material for removing dyes and may have future applications as flocculating agents in water purification.

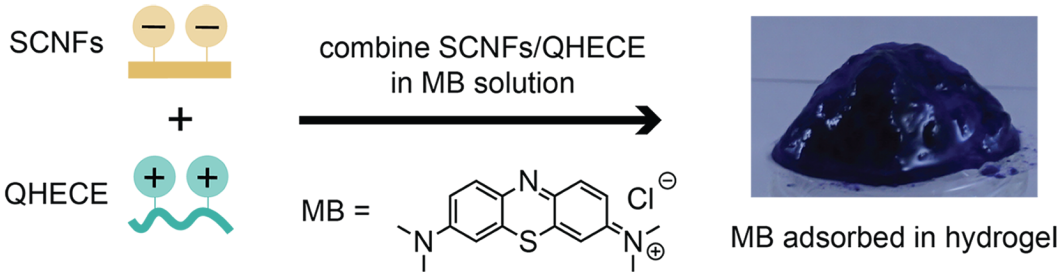

Scheme 1.2. MB adsorbed in a hydrogel made from SCNFs and QHECE.

Based on the work in Chapter 2 showing that electrostatic interactions are effective for removing a charged pollutant from water, Chapter 3 describes our efforts using cationic quaternized wood pulps (QWPs) to rapidly adsorb anionic PFASs (Scheme 1.3), which are toxic fluorosurfactants, from water via electrostatic interactions.[33] For this work, we were interested in developing a material for future use in flow systems, as opposed to a flocculating agent, to be competitive with currently used adsorbents. We investigated the effects of WP charge density (CD) and solution pH and salinity on PFAS adsorption. We observed that QWPs with higher charge

densities were more effective at removing perfluorooctanesulfonic acid (PFOS) and perfluorooctanoic acid (PFOA), and environmentally relevant solution pHs and NaCl concentrations had negligible effects on PFOS and PFOA adsorption. On the other hand, natural organic matter was found to significantly hinder PFAS removal. Despite this limitation, >80% of PFOS and PFOA could be removed from deionized water at environmentally relevant concentrations within 30 s of contact time, an advantage of QWPs compared to other adsorbents.[23,34,35,36,37] Using adsorption isotherms, we found that the QWPs had high adsorption capacities compared to adsorbents like AC and other sustainable adsorbents. Overall, Chapter 3 showed that QWPs are promising adsorbents for removing PFASs from water.

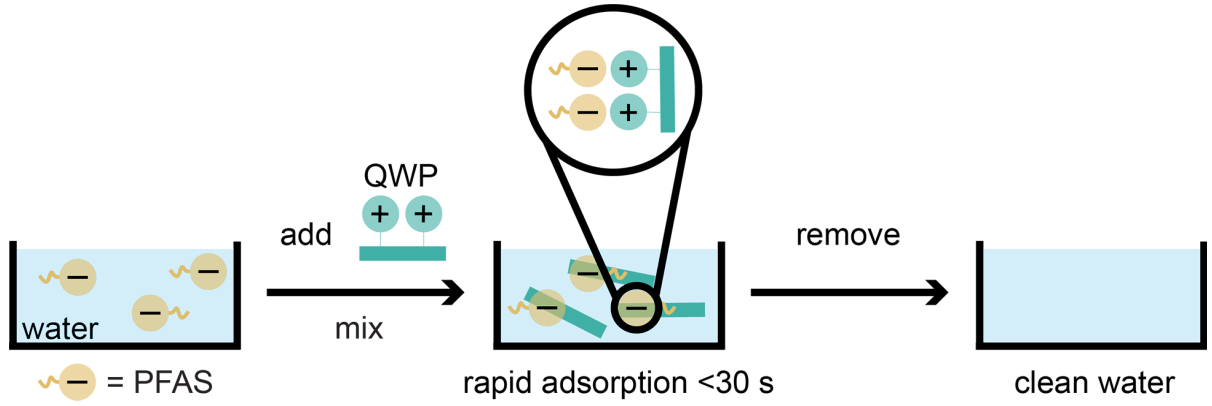

Scheme 1.3. PFASs adsorbed with QWPs.

Given the effectiveness of cellulose-based gels and QWPs for adsorbing cationic dyes and anionic PFASs, respectively, Chapter 4 outlines initial efforts using WP-based materials for adsorbing anionic dyes, which are another class of dye contaminant.[38] Specifically, we hypothesized that anionic dye adsorption would occur via electrostatic interactions in hydrogels with excess cationic charge. To investigate this hypothesis, we demonstrated that methyl orange (MO), an anionic dye, is adsorbed within seconds when anionic sulfated wood pulps (SWPs) are mixed with cationic QWPs to form a localized gel (Scheme 1.4). Adsorption was electrostatically

driven but inhibited by SWP-QWP electrostatic crosslinking. Additionally, we found that QWP fibers alone captured more MO than hydrogels, suggesting that cationic fibers may be promising adsorbents for anionic dyes. Future studies are necessary to optimize anionic dye adsorption and show these hydrogels/fibers are practical alternatives to conventional adsorbents. Finally, because Khalil et al. demonstrated that adsorbents with primary and secondary amines have higher adsorption capacities for some dyes than quaternary amines,[39] Chapter 4 reports preliminary work functionalizing WP with primary amines to generate a new cellulose fiber adsorbent. We anticipate that these efforts will motivate researchers to functionalize cellulose to increase the range of pollutants that can be adsorbed.

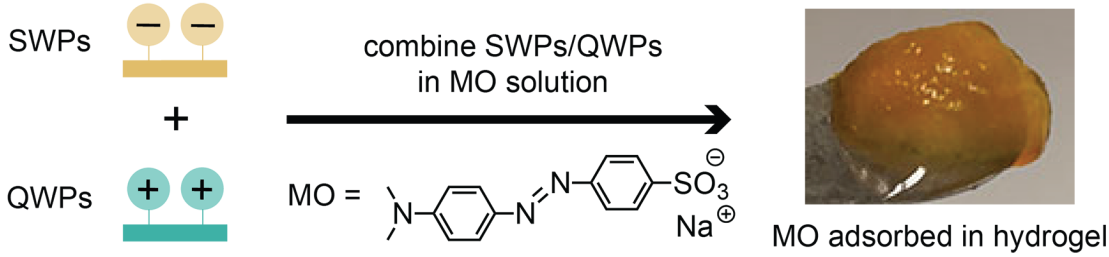

Scheme 1.4. MO adsorbed in hydrogel made with QWPs and SWPs.

In conclusion, this thesis demonstrates that cellulose-based adsorbents are efficient for removal of multiple pollutants from water. Specifically, cellulose fibers functionalized with anionic and cationic groups adsorb charged dyes and PFASs via electrostatic interactions. Compared to conventional adsorbents, the materials described herein rapidly adsorb pollutants and are unaffected by environmentally relevant solution pHs and salt concentrations. Moving forward, we intend to adsorb a larger scope of pollutants by functionalizing cellulose fibers with complementary groups specific to a pollutant. For example, to adsorb nonionic PFASs, cellulose will be functionalized with fluorocarbon moieties to enhance interactions with the PFAS fluorocarbon chain. Finally, we suggest future studies to use cellulose-based adsorbents for large

scale water treatment operations. Overall, biodegradable and renewable celluloses are encouraging for advancing water treatment systems.

References

(1) United Nations. The 17 Goals. https://sdgs.un.org/goals (accessed April 7, 2021).

(2) Boretti, A.; Rosa, L. Reassessing the projections of the world water development report. *npj Clean Water* **2019**, *2*.

(3) Green materials for wastewater treatment, 1st ed.; Naushad, M., Lichtfouse, E., Eds.; Environmental chemistry for a sustainable world, Vol. 38; Springer, **2020**.

(4) UNESCO. The global water quality challenge and SDGs. https://en.unesco.org/waterquality-iiwq/wq-challenge (accessed April 7, 2021).

(5) WWAP (United Nations World Water Assessment Program). *The united nations world water development report 2017*; Wastewater: the untapped resource.; UNESCO: Paris, **2017**.

(6) Yu, M.-H., Tsunoda, M., Tsunoda, H. Environmental toxicology: biological and health effects of pollutants, 3rd ed.; CRC Press, **2011**.

(7) UN Water. *Wastewater management–A UN-water analytical brief*; Policy and Analytical Briefs. **2015**.

(8) Van der Bruggen, B.; Vandecasteele, C. Removal of pollutants from surface water and groundwater by nanofiltration: overview of possible applications in the drinking water industry. *Environ. Pollut.* **2003**, *122*, 435–445.

(9) Bartolomeu, M.; Neves, M.G.P.M.S.; Faustino, M.A.F.; Almeida, A. Wastewater chemical contaminants: remediation by advanced oxidation processes. *Photochem. Photobiol. Sci.* **2018**, *17*, 1573–1598.

(10) Fredj, S.; Nobbs, J.; Tizaoui, C.; Monser, L. Removal of estrone (E1), 17ß-estradiol (E2), and 17α-ethinylestradiol (EE2) from wastewater by liquid–liquid extraction. *Chem Eng. J.* **2015**, *262*, 417–426.

(11) Cukierman, A.; Nunell, G.; Bonelli, P. Removal of emerging pollutants from water through adsorption onto carbon-based materials. In *Emerging and Nanomaterial Contaminants in Wastewater: Advanced Treatment Technologies*; Elsevier, **2019**; pp. 159–213.

(12) Pollard, S.J.T.; Fowler, G.D.; Sollars, C.J.; Perry, R. Low-cost adsorbents for waste and wastewater treatment: a review. *Sci. Total. Environ.* **1992**, *116*, 31–52.

(13) Srivastava, V.; Mall, I.; Mishra, I. Adsorption of toxic metal ions onto activated carbon: study of sorption behaviour through characterization and kinetics. *Chem. Eng. Process* **2008**, *47*, 1269–1280.

(14) Kaur, H.; Bansiwal, A.; Hippargi, G.; Pophali, G. Effect of hydrophobicity of pharmaceuticals and personal care products for adsorption on activated carbon: Adsorption isotherms, kinetics, and mechanism. *Environ. Sci. Pollut. Res.* **2018**, *25*, 20473–20485.

(15) Yu, Q.; Zhang, R.; Deng, S.; Huang, J.; Yu, G. Sorption of perfluorooctane sulfonate and perfluorooctanoate on activated carbons and resin: Kinetic and isotherm study. *Water Res.* **2009**, *43*, 1150–1158.

(16) Ahmadpour, A; Do, D. The preparation of active carbons from coal by chemical and physical activation. *Carbon* **1996**, *34*, 471–479.

(17) Mohammed, N.; Grishkewich, N.; Tam, K. Cellulose nanomaterials: promising sustainable nanomaterials for application in water/wastewater treatment processes. *Environ. Sci.: Nano* **2018**, *5*, 623–658.

(18) Varghese, A.; Paul, S.; Latha, M. Remediation of heavy metals and dyes from wastewater using cellulose-based adsorbents. *Environ. Chem. Lett.* **2019**, *17*, 867–877.

(19) Hokkanen, S.; Bhatnagar, A.; Sillanpaa, M. A review on modification methods to cellulose-based adsorbents to improve adsorption capacity. *Water Res.* **2016**, *91*, 156–173.

(20) Agarry, S.; Owabor, C.; Ajani, A.; Modified plantain peel as cellulose-based low-cost adsorbent for the removal of 2,6-dichlorophenol from aqueous solution: adsorption isotherms, kinetic modeling, and thermodynamic studies. *Chem. Eng. Comm.* **2013**, *200*, 1121–1147.

(21) Rathod, M.; Haldar, S.; Basha, S. Nanocrystalline cellulose for removal of tetracycline hydrochloridefrom water via biosorption: equilibrium, kinetic and thermodynamic studies. *Ecol. Eng.* **2015**, *84*, 240–249.

(22) Liu, L.; Gao, Z.; Su, X.; Chen, X.; Jiang, L.; Yao, J. Adsorption removal of dyes from single and binary solutions using a cellulose-based bioadsorbent. *ACS Sustainable Chem. Eng*. **2015**, *3*, 432−442.

(23) Ateia, M.; Attia, M.; Maroli, A.; Tharayil, N.; Alexis, F.; Whitehead, D.; Karanfil, T. Rapid removal of poly- and perfluorinated alkyl substances by poly(ethylenimine)-functionalized cellulose microcrystals at environmentally relevant conditions. *Environ. Sci. Technol. Lett*. **2018**, *5*, 764−769.

(24) Harris, J.; McNeil, A. Localized hydrogels based on cellulose nanofibers and wood pulp for rapid removal of methylene blue. *J. Polym. Sci.* **2020**, *58*, 3042–3049.

(25) Wilts, E.; Herzberger, J.; Long, T. Addressing water scarcity: cationic polyelectrolytes in water treatment and purification *Polym. Int.* **2018**, *67*, 799–814.

(26) Shalla, A.; Bhat, M.; Yaseen, Z. Hydrogels for removal of recalcitrant organic dyes: a conceptual overview. *J. Environ. Chem. Eng.* **2018**, *6*, 5938–5949.

(27) Meka, V.; Sing, M.; Pichika, M.; Nali, S.; Kolapalli, V.; Kesharwani, P. A comprehensive review on polyelectrolyte complexes. *Drug Discov. Today* **2017**, *22*, 1697–1706.

(28) Lu, A.; Wang, Y.; Boluk, Y. Investigation of the scaling law on gelation of oppositely charged nanocrystalline cellulose and polyelectrolyte. *Carbohydr. Polym.* **2014**, *105*, 214–221.

(29) Lu, A.; Song, Y.; Boluk, Y. Electrolyte effect on gelation behavior of oppositely charged nanocrystalline cellulose and polyelectrolyte. *Carbohyr. Polym.* **2014**, *114*, 57–64.

(30) Fu, J.; Schlenoff, J. Driving forces for oppositely charged polyion association in aqueous solutions: enthalpic, entropic, but not electrostatic. *J. Am. Chem. Soc.* **2016**, *138*, 980–990.

(31) Mohammed, N.; Grishkewich, N.; Berry, R.; Tam, K. Cellulose nanocrystal–alginate hydrogel beads as novel adsorbents for organic dyes in aqueous solutions. *Cellulose* **2015**, *22*, 3725–3738.

(32) Wang, D.; Yu, H.; Fan, X.; Gu, J.; Ye, S.; Yao, J.; Ni, Q. High aspect ratio carboxylated cellulose nanofibers cross-linked to robust aerogels for superabsorption−flocculants: paving way from nanoscale to macroscale. *ACS Appl. Mater. Interfaces* **2018**, *10*, 20755−20766.

(33) Harris, J.; Devlin, A.; McNeil, A. Rapid removal of poly- and perfluoroalkyl substances with quaternized wood pulp. *Submitted*.

(34) Ching, C.; Klemes, M.; Trang, B.; Dichtel, W.; Helbling, D. β-Cyclodextrin polymers with different cross-linkers and ion-exchange resins exhibit variable adsorption of anionic, zwitterionic, and nonionic PFASs. *Environ. Sci. Technol*. **2020**, *54*, 12693−12702.

(35) Du, Z.; Deng, S.; Bei, Y.; Huang, Q.; Wang, B.; Huang, J.; Yu, G. Adsorption behavior and mechanism of perfluorinated compounds on various adsorbents—A review. *J. Hazard. Mater.* **2014**, *274*, 443–454.

(36) Zhang, D.; Zhang, W.; Liang, Y. Adsorption of perfluoroalkyl and polyfluoroalkyl substances (PFASs) from aqueous solution - A review. *Sci. Total. Environ.* **2019**, *694*, 133606.

(37) Yang, A.; Ching, C.; Easler, M.; Helbling, D.; Dichtel, W. Cyclodextrin polymers with nitrogen-containing tripodal crosslinkers for efficient PFAS adsorption. *ACS Materials Lett.* **2020**, *2*, 1240–1245.

(38) Khan, S.; Malik, A. Environmental and health effects of textile industry wastewater. In *Environmental Deterioration and Human Health*; Malik, A., Akhtar, R., Grohmann, E., Eds.; Springer, **2014**.

(39) Khalil, M.; Aly, A. Use of cationic starch derivatives for the removal of anionic dyes from textile effluents. *J. Appl. Polym. Sci.* **2004**, *93*, 227–234.

Chapter 2 Localized Hydrogels based on Cellulose Nanofibers and Wood Pulp for Rapid Removal of Methylene Blue*

*Reproduced and modified with permission from Harris, J.; McNeil, A. Localized hydrogels based on cellulose nanofibers and wood pulp for rapid removal of methylene blue. *J. Polym. Sci*. **2020**, *58*, 3042–3049.

Introduction

Accessible, clean water is increasingly scarce due to pollutants discharged in the environment.[1] Many localities across the United States are grappling with extensive groundwater contamination by persistent pollutants.[2] Organic dyes are one major source of pollution: 10–15% of the approximately 10^5 tons of dye produced globally each year have been released into the environment.[3] Moreover, dyes have been linked to a variety of health problems in humans and aquatic life.[3,4] To minimize the negative consequences of dye release, improved water remediation systems are needed.

Several strategies for removing dyes from the environment have been investigated, including chemical oxidation, membrane filtration, ion exchange, and most commonly, adsorption.[5,6,7] The primary adsorbent material employed for water purification is activated carbon because of its high capacity, porosity, and versatility in adsorbing different pollutants.[8] Despite these useful properties, making and regenerating activated carbon is costly and unsustainable,[8] leading researchers to explore alternative adsorbents.[6,9,10,11,12]

Cellulose, which can be sustainably sourced and is biodegradable, has been evaluated as an alternative adsorbent for water purification.[13,14,15,16,17] For example, Tam and coworkers reported

that hydrogel beads made from sulfated cellulose nanocrystals (S–CNCs) and alginate could efficiently remove 97% of methylene blue (MB) from aqueous solutions.[18] In a different example, Yu and coworkers showed that carboxylated cellulose nanofiber (CNF) aerogels removed MB with up to 95% efficiency.[19] In both cases, however, the authors needed lengthy batch times (> 30 min) to reach these high adsorption efficiencies, highlighting the need for alternative cellulose-based materials with a more rapid adsorption.

To overcome this challenge, we hypothesized that rapid adsorption might occur if dye adsorption and gel formation are simultaneous. The rationale is that the cellulosic binding sites are more accessible before and during gelation, compared to after a gel has already formed. This approach was inspired by flocculating agents, which are commonly used in water treatment facilities.[20] Flocculants rapidly form a suspension when added to water, which allows for fast adsorption and easy removal through filtration. As a consequence, we hypothesized that an in situ-formed, localized (i.e., not sample-spanning), hydrogel could function like a flocculant, adsorbing pollutants while forming a suspended material for easy removal.

Both the hydrogel formation and adsorption processes need to be rapid for this approach to work. We anticipated that electrostatic crosslinking, which is both rapid and reversible, would be ideal for triggering localized gel formation (Scheme 2.1). We therefore targeted polyionic complexes,[21,22,23,24] which have previously been shown to form localized hydrogels in applications such as printable gels[25,26] and drug delivery systems.[27] In considering possible materials, we focused on cellulose-derived polymers due to their sustainable sourcing and biodegradability.

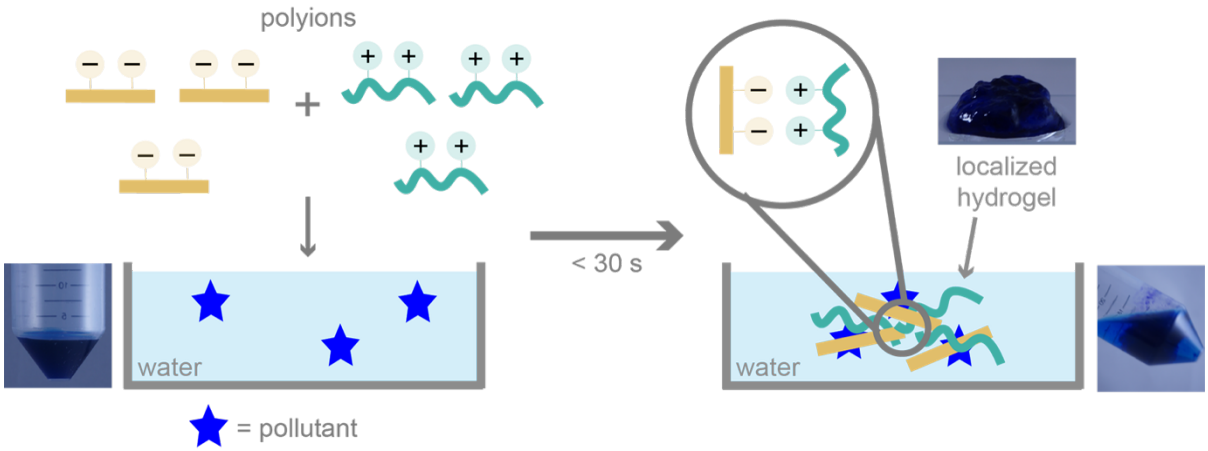

Scheme 2.1. When combining oppositely charged polyions, a localized hydrogel forms via electrostatic crosslinks while rapidly adsorbing cationic pollutants.

We initially focused on a system reported by Boluk and coworkers, wherein polyanionic S–CNCs and polycationic quaternized hydroxyethyl cellulose ethoxylate (QHECE) were mixed to form an all-cellulose based hydrogel.[28,29] Unfortunately, under their conditions, the gel formation was both slow (3 d) and not localized.[30] We hypothesized that longer cellulose fibers[31,32] – nanofibers (CNFs[33,34,35]) and wood pulp (WP)[36] – would create additional fiber/fiber entanglements, possibly enabling a faster-forming hydrogel.

Indeed, we report herein that sulfated CNFs (S-CNFs) and sulfated WPs (S-WPs) form localized hydrogels within 30 s when mixed with a water-soluble cationic cellulose derivative. In addition, we show that MB can be efficiently adsorbed while the localized gel forms, an advantage compared to traditional hydrogel adsorbents, which require lengthy batch times. Adsorption efficiencies above 90% are obtained across a wide range of dye concentrations, with a total adsorptive capacity of 340 mg dye/g cellulose. Both the solution pH and salt concentration had negligible effects on MB adsorption, indicating that the system is tolerant to a variety of water conditions. Overall, these locally formed cellulose-based hydrogels are effective adsorbents for cationic dyes and may be promising materials for other pollutants with alternative derivatization.

Experimental

Materials. Cellulose nanocrystals (spray-dried, Cellulose Lab Catalog Number CNC-SD) and cellulose nanofibrils (freeze-dried, Cellulose Lab Catalog Number CNF-FD) were purchased from Cellulose Lab. Bleached hardwood pulp was generously donated by Cellulose Lab. Chlorosulfonic acid and quaternized hydroxyethylcellulose ethoxylate (QHECE) were purchased from Aldrich and used without further purification. Deionized (DI) water purified by a Millipore Synergy water purification system was used as the water source, unless otherwise noted.

Sulfation of CNF and WP.

The synthesis was performed similar to Kumar and coworkers.[37]

(a) CNF and WP Dispersions. Unsulfated CNFs or WPs (400 mg) were placed in an oven-dried 100 mL flask with anhydrous DMF (50 mL), and the flask was capped with a septum. The mixture was soaked for 40 min without stirring under N_2. The mixture was then homogenized at a specified speed and time with an IKA T25 digital Ultra-Turrax (Table A1.1). The flask was re-capped and soaked for 10 min under N_2. The mixture was homogenized a second time at a specified speed and time (Table A1.1). Then a stir bar was added, the flask was sealed, and the mixture was stirred for 40 min under N_2.

(b) CSA Stock Solution (2.0 M in DMF). A Schlenk flask with stir bar and addition funnel were removed from the oven and assembled. The addition funnel was capped with a septum, and the system was cooled to room temperature under N_2. Anhydrous DMF (26 mL) was added to the Schlenk flask, and the solvent was cooled in an ice water bath for 10 min. Then, CSA (4 mL) was loaded into the addition funnel and added slowly over 5 min to the stirring DMF, with some HCl evolving. Once all the CSA was added, the addition funnel was removed and the Schlenk flask

was capped, removed from the ice-water bath, and warmed to room temperature to provide a 2.0 M solution of CSA in DMF.

(c) CNF and WP Sulfation. A specified amount of the 2.0 M CSA in DMF was added to the CNF or WP mixture dropwise over 0–2 min. The mixture was stirred for 20 min once all the CSA was added. Then, the reaction was quenched with methanol (~5 mL), and the mixture was stirred for 5 min.

The mixture was poured into a 250 mL centrifuge bottle, and the bottle was filled to ~90% capacity with DI water. The mixture was centrifuged at ~34,000 × g for ~25 min. The supernatant was discarded, and fresh DI water was added. Then a ~0.1 M NaOH solution was used to increase the pH to 7, as measured with pH paper. The mixture was centrifuged again at ~34,000 × g for ~25 min. The supernatant was discarded, and fresh DI water was added. The mixture was shaken by hand and then centrifuged a third time at ~34,000 × g for 25 min.

The fibers were then isolated using one of the two procedures described below. (i) If a white, gel-like mass remained in the centrifuge bottle, the supernatant was discarded, and the material was placed in smaller glass vials, frozen in liquid N_2, and dried under vacuum on a Schlenk line to remove excess water. (This procedure was used to access S-CNFs 0.77, 1.1, 1.5, 1.8, 1.9, and S-WP1.8.) (ii) If the fibers did not form a gel-like mass in the centrifuge bottle, ~90% of supernatant was discarded, and the remaining mixture was vacuum filtered using a Whatman polyamide membrane filter (0.2 μm, 47 mm). The fibers on the filter were then rinsed once with DI water (5 mL), and placed in smaller glass vials, frozen in liquid N_2, and dried under vacuum on a Schlenk line to remove excess water. (This procedure was used to access S-WPs 0.53, 1.0, and 1.3.)

Charge density measurements. Charge density measurements were carried out similar to the procedure given by Katz *et al*.[38,39] A known amount of S-CNFs or S-WPs (typically about 35 mg) was placed in a 20 mL vial with 0.1 M aq. HCl (15 mL) and a stir bar. The vial was capped and stirred for 90 min to protonate the S-CNFs or S-WPs. The mixture was then filtered over a polyamide membrane using vacuum filtration. The solids were rinsed with DI water until the conductivity of the filtrate was <10 μS/cm as measured by a Thermo Scientific Orion Star A215 pH/conductivity meter. The resulting solids were added to a tared 150 mL beaker followed by DI water (~20 mL) and a stir bar. The mixture was covered with weigh paper (of known mass), stirred for at least 5 min to uniformly disperse the solids, and then the stir bar was removed. The mixture was weighed to determine the total mass of the protonated S-CNF or S-WP mixture. Then, two aliquots of the mixture were removed, placed in separate tared 20 mL vials, accurately weighed (~2.5 g), and dried in a 110 °C oven. For all samples (except S-CNF0.0 and S-WP0.0), the mass of solids in each aliquot was used to determine the concentration of solids in the protonated S-CNF or S-WP mixture. For S-CNF0.0 and S-WP0.0, the mass of solids in each aliquot overestimated the amount of fibers that were present (likely because the fibers were non-uniformly clumped together in the mixture), so the aliquot masses were subtracted from the initial amount of S-CNF0.0 or S-WP0.0 used to give a total amount of titrated S-CNF0.0 and S-WP0.0 fibers.

A stir bar and recorded volume (~100 mL) of 1 mM NaCl were then added to the beaker containing the protonated S-CNF or S-WP mixture. The mixture was titrated, with stirring, by adding a volume with known concentration of NaOH solution (~0.01 M) to the protonated S-CNF or S-WP mixture and measuring the conductivity of the mixture 40 s after each addition of titrant. (The concentration of the NaOH solution was determined using the calibrated pH meter prior to the titration.) The volume-corrected conductivity was plotted as a function of the volume of NaOH

added, and the equivalence point was determined by the intersection of the linear least-squares regression lines from the positively and negatively sloped regions of the curve (Figure A1.2). Based on the mmols of NaOH added, the mmol of SO_3^- were calculated. The charge density was found by dividing the mmol SO_3^- by the mass of S-CNF or S-WP that was titrated. This procedure was repeated and the average is reported as the sample's charge density (Table A1.2). Throughout Chapter 2, S-CNF and S-WP samples will be identified by material type followed by the charge density (e.g., S-CNF1.1 is an S-CNF with a charge density of 1.1 mmol SO_3^-/g).

Dye adsorption measurements. S-CNF1.8 (25.0 mg) was soaked in DI water (12.5 mL) for 5 min. The mixture was then homogenized at 10k rpm for 1 min to make a 0.200% w/v S-CNF1.8 mixture. QHECE (30.0 mg) was dissolved in DI water (20.0 mL) to make a 0.150% w/v QHECE solution. MB (60.0 mg, 188 μmol) was dissolved in DI water (6.0 mL) in a 50 mL centrifuge tube to make a 31 mM MB solution.

A volume of 31 mM MB solution was added to a 50 mL centrifuge tube followed by DI water to give a total volume of 2.0 mL. Then, 4.0 mL of 0.200% w/v S-CNF1.8 mixture and 4.0 mL of 0.150% w/v QHECE solution were added simultaneously, over a recorded time (Table A1.13), directly to the bottom of the centrifuge tube with vortex mixing at a speed setting of 1.5. The centrifuge tube was then vortex mixed using a speed setting of 1.5 for an additional recorded "mixing" time. The centrifuge tube was then removed from the vortex mixer, and a gel was observed. An aliquot of water was removed from the centrifuge tube, placed in a cuvette, and the absorbance spectrum of the solution from 400–750 nm was obtained. The UV-vis measurement was performed within 1 min of the gel being formed. The absorbance spectrum for each gel sample was obtained and baseline corrected (Appendix 1 subsection "general procedure for calculating MB adsorption in gels and flocs"). The corrected absorbance at 661 nm was then recorded for each

gel sample, and the concentration of MB that was not adsorbed was determined using a calibration curve (Figure A1.34).

Dye desorption study. 0.200% w/v S-CNF1.8 mixtures, 0.150% w/v QHECE solutions, and a 31 mM MB solution were prepared according to the procedure in the "Dye adsorption measurements" section. An "acidic ethanol" solution (1:1 (v:v) EtOH:0.10 M aq. HCl solution, 50.0 mL) was prepared in a 50 mL polypropylene centrifuge tube ("tube 1"). The tube was wrapped in aluminum foil to minimize light and set aside for later use.

DI water (1.92 mL) was combined with an aliquot of 31 mM MB solution (80.0 μL) in a 50 mL polypropylene centrifuge tube ("tube 2"), and the solution was vortex mixed using a speed setting of 1.5 for 15 s. Then, S-CNF1.8-based gels were produced according to the procedure in the "Dye adsorption measurements" section. After a gel was formed, the gel was removed from tube 2 using a spatula and placed into tube 1. Tube 1 was capped and placed in a closed, dark drawer. Then, an aliquot of leftover solution from tube 2 was placed in a cuvette, and an absorbance spectrum from 400–750 nm was obtained and baseline corrected. The corrected absorbance at 661 nm was then recorded for each gel sample, and the mass of adsorbed MB (MAMB) that was adsorbed was determined using a calibration curve.

Then, at recorded time intervals, tube 1 was removed from the drawer and inverted to mix the contents of the tube. An aliquot of solution was then placed in a cuvette, and the absorbance spectrum of the solution was obtained and corrected. The aliquot was returned to tube 1, and the tube was placed back in a closed drawer. For the aliquots removed from tube 1, the mass of desorbed MB (MDMB) in solution at each time point was determined using a separate calibration curve that was generated for MB in acidic ethanol (Figure A1.45). The MB desorption % was then calculated at each time point using the following equation (Equation 2.1):

$$\text{MB desorption \%} = \frac{\text{MDMB}}{\text{MAMB}} \text{ x } 100$$

Equation 2.1. Calculating MB desorption %.

This procedure was performed for 3 hydrogel samples (Table A1.25 and Figure 2.5), and an average MB desorption % after 24 h is reported based on these samples.

Results and Discussion

Identifying conditions for quick-forming, localized hydrogels. As described above, we hypothesized that cellulose materials with longer lengths would generate more (physical) crosslinking sites, which would potentially lead to a faster, localized gelation. We also hypothesized that higher charge densities would lead to faster gelation due to rapid charge/charge interactions generating more (physical) crosslinks. To test both these hypotheses, we functionalized CNFs and WPs by reacting them with varying amounts of chlorosulfonic acid.[40,41] Previous studies on cellulose functionalization suggest that the sulfation likely occurs at the C6 and C2 positions on the glucose repeat unit.[42] Materials with charge densities ranging from 0.0 to 1.9 mmol SO_3^-/g were generated, as determined by conductometric titrations. Elemental analyses performed on a subset of samples showed that the conductometric titrations are accurate (i.e, less than 0.25% difference in S content, Table A1.3). The charge density on the other hydrogel component (commercial QHECE) was measured herein to be 1.23 mmol R_4N^+/g (Appendix 1 section "QHECE conductometric titration"). SEM images indicate that the size of S-CNFs and S-WPs did not change significantly after functionalization, but small changes in S-CNF structure (e.g., some fracturing) were observed for some charge densities (Appendix 1 section "SEM characterization of S-CNFs and S-WPs").

Localized gels[43] were formed within seconds when QHECE solutions were added to suspensions of aq. S-CNF or S-WP (Figure 2.1 and Appendix 1 section "Determining the minimum amount of material needed for S-CNF- and S-WP-based hydrogels"). Gel formation was impacted, as anticipated, by the CNF and WP charge density as well as by the molar charge ratio (f^-), which is the ratio of negative charges to total charge. For example, S-CNF-based gels only formed with a charge density ≥ 0.77 mmol SO_3^-/g and an f^- ≥ 0.39. Similarly, S-WP-based gels only formed with a charge density ≥ 0.53 mmol SO_3^-/g and an f^- ≥ 0.30. Both results indicate that there is a minimum amount of negative charge necessary to interact with QHECE and form an electrostatically crosslinked gel.

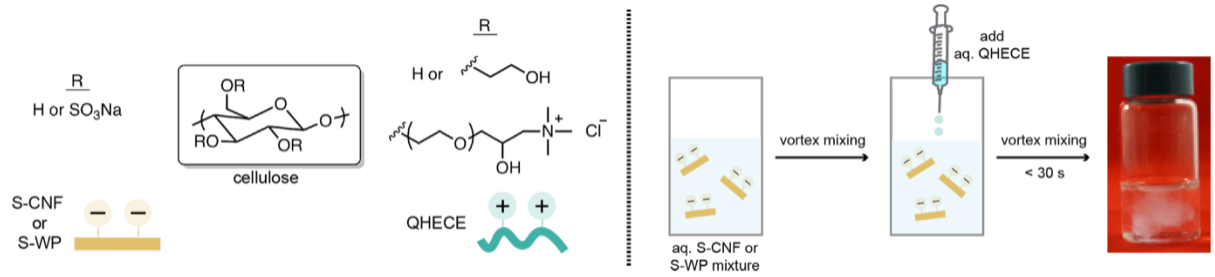

Figure 2.1. (A) Chemical structures for S-CNFs, S-WPs, and QHECE. (B) Procedure for making hydrogels. The gel shown is made from 0.050% (w/v) S-CNF1.9 and QHECE.

In both cases, gel formation was rapid (within 30 s) and localized, possibly driven by the entropy gain from the release of counterions into solution.[44] Surprisingly, the shorter S-CNFs formed gels at lower concentrations than the longer S-WPs, even when the charge densities were similar. (Localized gels could be formed with as little as 0.010% S-CNF and 0.0050% (w/v) QHECE.) This result is likely due to the thinner CNFs having more fiber/fiber interactions and entanglements compared to the same mass of the thicker WP. The S-CNF-based gels also exhibited higher swelling ratios relative to the analogous S-WP-based gels under otherwise identical conditions (Appendix 1 section "Evaluating hydrogel swelling"). This result may be attributable

to the larger interstitial volume present in gels made from the thinner S-CNF fibers, leading to more water retention via capillary forces.[45]

Examining the mass balance revealed that approximately 40–60% of the added cellulose was incorporated into the gels (Table A1.9 and Table A1.11). Most likely, the water-soluble QHECE is the dominant species in solution. The mechanical properties of the isolated S-CNF and S-WP hydrogels were probed using oscillatory shear rheology (Appendix 1 section "Rheological characterization of hydrogels"). The elastic modulus (G′) was nearly independent of frequency and greater than storage modulus (G″) in the frequency range of 0.1–50 rad/s. These results are characteristic of physical hydrogels.

Overall, the rapid, localized gel formation observed with both S-CNFs and S-WPs, suggests that the longer fiber lengths and higher charge densities played an important role, presumably by creating additional crosslinks. For the rest of the studies, we focused on the hydrogels made from S-CNFs with the highest charge density (1.8 mmol SO_3^-/g) because we anticipated that the highest adsorption would be achieved with gels containing the most negative sites.

Assessing dye adsorption. Because the insoluble cellulose component was anionic, we anticipated that these hydrogels would be best at adsorbing dyes with cationic charge. Gratifyingly, we observed over 90% MB adsorption within 1 min when the dye concentration was < 400 μM (Figure 2.2 and Figure 2.3A). This adsorption % held true as long as the ratio of dye/negative sites was kept below 0.35. MB adsorption only slightly increased over time (e.g., 96% at 3 min to 99% at 3000 min), likely due to a slower process of MB diffusion into the internal sites within the CNF fibers (Table A1.17).[46,47] The maximum capacity for MB adsorption was 94.5 ± 0.2 mg dye/g cellulose under these conditions.

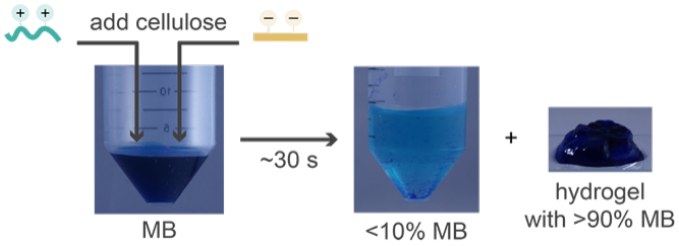

Figure 2.2. A localized hydrogel formed after adding aq. QHECE and S-CNF mixtures to a aq. solution containing MB ($[MB]_i$ = 94 μM; $[S\text{-}CNF1.8]_f$ = 0.08% w/v; $[QHECE]_f$ = 0.06% w/v).

At higher MB concentrations, we observed something similar to flocculation; rather than a single, localized hydrogel forming, we observed several smaller flocs.[48] Under these conditions, there is more MB than negative sites, leading to lower adsorption, and weaker gels. The maximum capacity for MB adsorption under these conditions was 340 ± 40 mg dye/g cellulose (Figure 2.3B). This value slightly outperforms related materials from the literature, with 256 mg dye/g of cellulose for CNC-based hydrogel beads reported by Tam and co-workers,[18] and 128 mg MB/g of cellulose for CNF-based aerogels reported by Yu and co-workers.[19] The advantage of our system (over these examples) is the rapid speed for both the adsorption (< 5 min) and gelation processes (< 30 s).

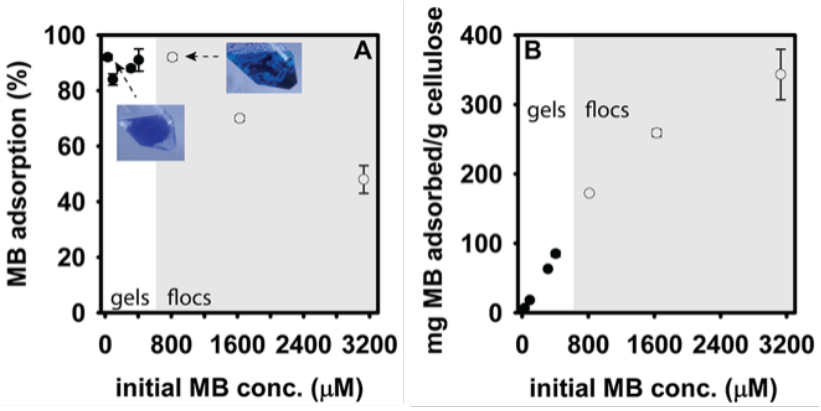

Figure 2.3. (A) MB adsorption percent as a function of the initial dye concentration for S-CNF1.8 gels (●) and flocs (○). (B) MB adsorption capacity as a function of the initial dye concentration for S-CNF1.8 gels (●) and flocs (○). All gels and flocs were made using 0.080% w/v S-CNF1.8 and 0.060% w/v QHECE.

We hypothesized that the MB/gel interactions were largely driven by charge complexation. To test this hypothesis, we first evaluated MB adsorption to S-CNF alone. Under conditions similar to above, the S-CNFs adsorbed approximately 85% of the MB, consistent with a charge-based complexation (Table A1.26). In a separate experiment, when an S-CNF with a lower charge density was used to form a gel, and all other variables were held constant, the maximum adsorption decreased (160 ± 30 mg dye/g cellulose, Table A1.20). This result also suggests that the primary driving force for adsorption is charge complexation. In addition, this result suggests that higher adsorption capacities might be accessible with higher S-CNF charge densities.

To demonstrate the advantages of having adsorption occur simultaneously with gelation, we added a pre-formed hydrogel into a solution of MB and monitored its adsorption over time. Gratifyingly, we observed slow adsorption with the pre-formed gel (e.g., 20% at 2 min) compared to in the in-situ system (>90% at 2 min). Only after 60 min did the pre-formed gel reach the same adsorption levels as our simultaneous system.

Effect of [salt] and pH on dye adsorption. Industrial effluent from dye manufacturing contains many other dissolved species, including acids and bases.[19] As such, we examined the influence of both salt concentration and solution pH on dye adsorption.

No significant decrease in dye adsorption was observed over a pH range of 2.5–11.5 (Figure 2.4A). These results were expected because there should be no change in charge for any of the species over this pH range. More specifically, QHECE is a quaternized amine with four alkyl groups, giving it a pH-insensitive permanent charge. The sulfate on the S-CNFs have an estimated pKa ~ 2,[49] indicating that they will be fully deprotonated under our conditions. Similarly, MB has an estimated pKa ~ 3[50] and is expected to be cationic over the pH range examined.

We also found that as salt concentration increases (from 0), the MB adsorption remains constant (Figure 2.4B), suggesting that Na^+ is not displacing the MB under these conditions.[51] However, gelation was inhibited above ~99 mM NaCl, indicating that the electrostatic-based crosslinking between S-CNF and QHECE was being disrupted.

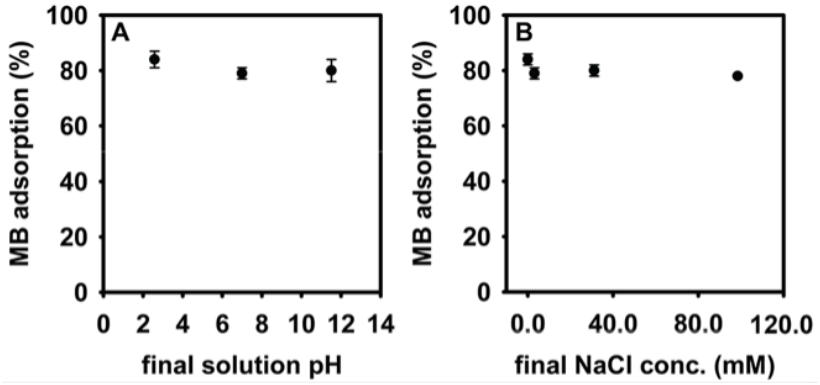

Figure 2.4. MB adsorption as a function of (A) pH and (B) NaCl concentration for S-CNF/QHECE hydrogels ([MB] = 94 μM, [S-CNF1.8] = 0.080% (w/v); [QHECE] = 0.060% (w/v)).

Dye Desorption. For water treatment applications, it would be advantageous to desorb the MB dye so that the cellulose-based gel can be re-used or biodegraded. As such, we soaked the used hydrogels in acidic EtOH (pH = 1.55) for 24 h (Figure 2.5 and Appendix 1 subsection "Monitoring MB desorption from S-CNF-based hydrogels over time").[18,52] Subsequent UV-vis spectroscopic analysis of the supernatant revealed approximately 55 ± 2% of the MB had desorbed, presumably via competitive binding of the H^+ to the sulfate groups. Clearly, further optimization will be necessary to fully recycle or recapture the spent materials.

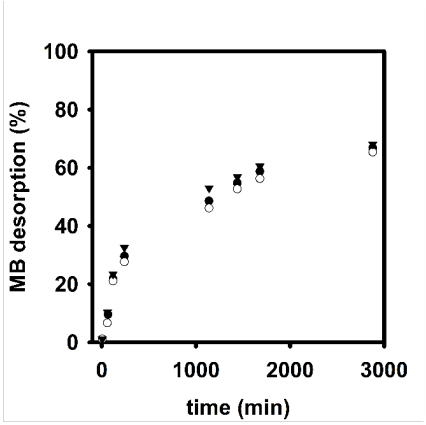

Figure 2.5. MB desorption % over time from gel sample 1 (●), gel sample 2 (○), and gel sample 3 (▼).

Conclusions

In summary, functionalized cellulose nanofibers and wood pulp were found to form localized hydrogels with an oppositely charged water soluble cellulose derivative, driven by electrostatic and physical crosslinking. These localized gels rapidly adsorb cationic dye during gelation, giving them an advantage over traditional hydrogel-based adsorbents. The maximum adsorption capacity was found to be 340 ± 40 mg methylene blue/g cellulose, which outperformed other cellulose-based physical gels.

Overall, we anticipate that these and related localized hydrogels may have future applications as flocculating agents in water purification. Moving forward, we intend to tailor the localized hydrogels to adsorb other contaminants that threaten freshwater supplies.[2,16,53] Towards this goal, we have successfully removed anionic dyes with cationic wood pulp-based gels. These and related studies will be reported in due course.

References

(1) Boretti, A.; Rosa, L. Reassessing the projections of the world water development report. *npj Clean Water* **2019**, *2*.

(2) U.S.E.P.A. National summary of state information. https://ofmpub.epa.gov/waters10/attains_nation_cy.control (accessed April 24, 2020).

(3) *Impact of Textile Dyes on Public Health and the Environment*; Wani, K., Jangid, N., Bhat, A., Eds.; IGI Global, **2020**.

(4) Khan, S.; Malik, A. In *Environmental Deterioration and Human Health*; Malik, A., Grohmann, E., Akhtar, R., Eds.; Springer **2014**; pp. 55–71.

(5) Salleh, M.; Mahmoud, D.; Karim, W.; Idris, A. Cationic and anionic dye adsorption by agricultural solid wastes: a comprehensive review. *Desalination* **2011**, *280*, 1–13.

(6) Singh, N.; Nagpal, G.; Agrawal, S.; Rachna. Water purification by using adsorbents: a review. *Environ. Technol. Innov.* **2018**, *11*, 187–240.

(7) Yagub, M.; Sen, T.; Afroze, S.; Ang, H. Dye and its removal from aqueous solution by adsorption: a review. *Adv. Colloid Interface Sci.* **2014**, *209*, 172–184.

(8) Pollard, S.; Fowler, G.; Sollars, C.; Perry, R. Low-cost adsorbents for waste and wastewater treatment: a review. *Sci. Total Environ.* **1992**, *116*, 31–52.

(9) Shalla, A.; Bhat, M.; Yaseen, Z. Hydrogels for removal of recalcitrant organic dyes: a conceptual overview. *Environ. Chem. Eng.* **2018**, *6*, 5938–5949.

(10) Van Tran, V.; Park, D.; Lee, Y. Hydrogel applications for adsorption of contaminants in water and wastewater treatment. *Environ. Sci. Pollut. Res.* **2018**, *25*, 24569–24599.

(11) Wang, H.; Ji, X.; Ahmed, M.; Huang, F.; Sessler, J. Hydrogels for anion removal from water. *J. Mater. Chem. A* **2019**, *7*, 1394–1403.

(12) de Luna, M.; Altobelli, R.; Gioiella, L.; Castaldo, R.; Scherillo, G.; Filippone, G. Role of polymer network and gelation kinetics on the mechanical properties and adsorption capacity of chitosan hydrogels for dye removal. *J. Polym. Sci., Part B: Polym. Phys* **2017**, *55*, 1843-1849.

(13) Chang, C.; Zhang, L. Cellulose-based hydrogels: present status and application prospects. *Carbohydr. Polym.* **2011**, *84*, 40–53.

(14) Hokkanen, S.; Bhatnagar, A.; Sillanpää, M. A review on modification methods to cellulose-based adsorbents to improve adsorption capacity. *Water Res.* **2016**, *91*, 156–173.

(15) Kang, H.; Liu, R.; Huang, Y. Cellulose-based gels. *Macromol. Chem. Phys.* **2016**, *217*, 1322–1334.

(16) Mohammed, N.; Grishkewich, N.; Tam, K. Cellulose nanomaterials: promising sustainable nanomaterials for application in water/wastewater treatment processes. *Environ. Sci. Nano* **2018**, *5*, 623–658.

(17) Varghese, A.; Paul, S.; Latha, M. Remediation of heavy metals and dyes from wastewater using cellulose-based adsorbents. *Environ. Chem. Lett.* **2019**, *17*, 867–877.

(18) Mohammed, N.; Grishkewich, N.; Berry, R.; Tam, K. Cellulose nanocrystal–alginate hydrogel beads as novel adsorbents for organic dyes in aqueous solutions. *Cellulose* **2015**, *22*, 3725–3738.

(19) Wang, D.; Yu, H.; Fan, X.; Gu, J.; Ye, S.; Yao, J.; Ni, Q. High aspect ratio carboxylated cellulose nanofibers cross-linked to robust aerogels for superabsorption-flocculants: paving way from nanoscale to macroscale. *ACS Appl. Mater. Interfaces* **2018**, *10*, 20755–20766.

(20) Wilts, E.; Herzberger, J.; Long, T. Addressing water scarcity: cationic polyelectrolytes in water treatment and purification. *Polym. Int.* **2018**, *67*, 799–814.

(21) Berger, J.; Reist, M.; Mayer, J.; Felt, O.; Gurny, R. Structure and interactions in covalently and ionically crosslinked chitosan hydrogels for biomedical applications. *Eur. J. Pharm. Biopharm.* **2004**, *57*, 35–52.

(22) Hujaya, S.; Lorite, G.; Vainio, S.; Liimatainen, H. Polyion complex hydrogels from chemically modified cellulose nanofibrils: Structure-function relationship and potential for controlled and pH-responsive release of doxorubicin. *Acta Biomater.* **2018**, *75*, 346–357.

(23) Meka, V.; Sing, M.; Pichika, M.; Nali, S.; Kolapalli, V.; Kesharwani, P. A comprehensive review on polyelectrolyte complexes. *Drug Discov. Today* **2017**, *22*, 1697–1706.

(24) Ingverud, T.; Larsson, E.; Hemmer, G.; Rojas, R.; Malkoch, M.; Carlmark, A. High water-content thermoresponsive hydrogels via electrostatic macrocrosslinking of cellulose nanofibrils. *J. Polym. Sci., Part A: Polym. Chem.* **2016**, *54*, 3415–3424.

(25) Cui, H.; Yu, Y.; Li, X.; Sun, Z.; Ruan, J.; Wu, Z.; Qian, J.; Yin, J. Direct 3D printing of a tough hydrogel incorporated with carbon nanotubes for bone regeneration. *J. Mater. Chem. B* **2019**, *7*, 7207–7217.

(26) Ng, W.; Yeong, W.; Naing, M. Polyelectrolyte gelatin-chitosan hydrogel optimized for 3D bioprinting in skin tissue engineering. *Int. J. Bioprinting* **2016**, *2*, 53–62.

(27) Tang, Y.; Heaysman, C.; Willis, S.; Lewis, A. Physical hydrogels with self-assembled nanostructures as drug delivery systems. *Expert Opin. Drug Deliv.* **2011**, *8*, 1141–1159.

(28) Lu, A.; Song, Y.; Boluk, Y. Electrolyte effect on gelation behavior of oppositely charged nanocrystalline cellulose and polyelectrolyte. *Carbohydr. Polym.* **2014**, *114*, 57–64.

(29) Lu, A.; Wang, Y.; Boluk, Y. Investigation of the scaling law on gelation of oppositely charged nanocrystalline cellulose and polyelectrolyte. *Carbohydr. Polym.* **2014**, *105*, 214–221.

(30) We were able to obtain faster forming hydrogels (350 s) with higher concentrations of both S-CNCs and QHECE (2.0% w/v each). With further optimization, hydrogels could be formed in 75 s with as little as 1.0% (w/v) S-CNCs and 0.5% (w/v) QHECE (Figure A1.1).

(31) De France, K.; Hoare, T.; Cranston, E. Review of hydrogels and aerogels containing nanocellulose. *Chem. Mater.* **2017**, *29*, 4609–4631.

(32) Reid, M.; Villalobos, M.; Cranston, E. Benchmarking cellulose nanocrystals: from the laboratory to industrial production. *Langmuir* **2017**, *33*, 1583–1598.

(33) Klemm, D.; Kramer, F.; Moritz, S.; Lindström, T.; Ankerfors, M.; Gray, D.; Dorris, A. Nanocelluloses: a new family of nature-based materials. *Angew. Chemie - Int. Ed.* **2011**, *50*, 5438–5466.

(34) Klemm, D.; Cranston, E.; Fischer, D.; Gama, M.; Kedzior, S.; Kralisch, D.; Kramer, F.; Kondo, T.; Lindström, T.; Nietzsche, S.; Petzold-Welcke, K.; Rauchfuß, F. Nanocellulose as a natural source for groundbreaking applications in materials science: today's state. *Mater. Today* **2018**, *21*, 720–748.

(35) Rodrigues, F.; Spagnol, C.; Pereira, A.; Martins, A.; Fajardo, A.; Rubira, A.; Muniz, E. Superabsorbent hydrogel composites with a focus on hydrogels containing nanofibers or nanowhiskers of cellulose and chitin. *J. Appl. Polym. Sci.* **2014**, *131*, 1–13.

(36) Sousa, S.; Costa, A.; Simões, R. Poly(lactic acid) composites reinforced with kraft pulp fibres: Production by a papermaking process and characterisation. *Compos. Part A Appl. Sci. Manuf.* **2019**, *121*, 273–282.

(37) Luo, J.; Semenikhin, N.; Chang, H.; Moon, R.; Kumar, S. Post-sulfonation of cellulose nanofibrils with a one-step reaction to improve dispersibility. *Carbohydr. Polym.* **2018**, *181*, 247–255.

(38) Katz, S.; Beatson, R.; Scallan, A. The determination of strong and weak acidic groups in sulfite pulps. *Sven. Papperstidning* **1984**, *87*, R48–R53.

(39) Pan, S.; Ragauskas, A. Enhancement of nanofibrillation of softwood cellulosic fibers by oxidation and sulfonation. *Carbohydr. Polym.* **2014**, *111*, 514–523.

(40) Wang, Y.; Wang, X.; Xie, Y.; Zhang, K. Functional nanomaterials through esterification of cellulose: a review of chemistry and application. *Cellulose* **2018**, *25*, 3703–3731.

(41) Zhu, L.; Qin, J.; Yin, X.; Ji, L.; Lin, Q.; Qin, Z. Direct sulfation of bacterial cellulose with a $ClSO_3H$/DMF complex and structure characterization of the sulfates. *Polym. Adv. Technol.* **2014**, *25*, 168–172.

(42) Eyley, S.; Thielemans, W. Surface modification of cellulose nanocrystals. *Nanoscale* **2014**, *6*, 7764–7779.

(43) Costalat, M.; Alcouffe, P.; David, L.; Delair, T. Macro-hydrogels versus nanoparticles by the controlled assembly of polysaccharides. *Carbohydr. Polym.* **2015**, *134*, 541–546.

(44) Fu, J.; Schlenoff, J. Driving forces for oppositely charged polyion association in aqueous solutions: enthalpic, entropic, but not electrostatic. *J. Am. Chem. Soc.* **2016**, *138*, 980–990.

(45) Zhou, Y.; Fu, S.; Zhang, L.; Zhan, H. Superabsorbent nanocomposite hydrogels made of carboxylated cellulose nanofibrils and CMC-g-p(AA-co-AM). *Carbohydr. Polym.* **2013**, *97*, 429–435.

(46) Jiang, F.; Dinh, D.; Hsieh, Y. Lo. Adsorption and desorption of cationic malachite green dye on cellulose nanofibril aerogels. *Carbohydr. Polym.* **2017**, *173*, 286–294.

(47) Deng, H.; Lu, J.; Li, G.; Zhang, G.; Wang, X. Adsorption of methylene blue on adsorbent materials produced from cotton stalk. *Chem. Eng. J.* **2011**, *172*, 326–334.

(48) Rheological studies performed on these flocs were consistent with a weak, physical gel, however, this result may be an artifact due to the compression of the flocs during sample preparation (Appendix 1 subsection "Procedure for characterizing MB-loaded gels and flocs").

(49) Wang, H.; Qian, C.; Roman, M. Effects of pH and salt concentration on the formation and properties of chitosan-cellulose nanocrystal polyelectrolyte-macroion complexes. *Biomacromolecules* **2011**, *12*, 3708–3714.

(50) Disanto, A.; Wagner, J. Pharmacokinetics of highly ionized drugs II: Methylene blue—absorption, metabolism, and excretion in man and dog after oral administration. *J. Pharm. Sci.* **1972**, *61*, 1086–1090.

(51) Maurya, N.; Mittal, A.; Cornel, P.; Rother, E. Biosorption of dyes using dead macro fungi: Effect of dye structure, ionic strength and pH. *Bioresour. Technol.* **2006**, *97*, 512–521.

(52) Hua, J.; Meng, R.; Wang, T.; Gao, H.; Luo, Z.; Jin, Y.; Liu, L.; Yao, J. Highly porous cellulose microbeads and their adsorption for methylene blue. *Fibers Polym.* **2019**, *20*, 794–803.

(53) Xiao, L.; Ching, C.; Ling, Y.; Nasiri, M.; Klemes, M.; Reineke, T.; Helbling, D.; Dichtel, W. Cross-linker chemistry determines the uptake potential of perfluorinated alkyl substances by β-cyclodextrin polymers. *Macromolecules* **2019**, *52*, 3747–3752.

Chapter 3 Rapid Removal of Poly- and Perfluoroalkyl Substances with Quaternized Wood Pulp

This work was done in collaboration with Dr. Angela Devlin, who carried out the Raman characterization of wood pulp fibers.

Introduction

Clean drinking water is increasingly challenging to acquire as many municipalities around the world struggle with pollutants.[1] For example, poly- and perfluoroalkyl substances (PFASs) are found in many fresh water supplies within the United States (US).[2,3,4,5] PFASs can be anionic, cationic, nonionic, or zwitterionic; however, anionic PFASs such as perfluorooctanesulfonic acid (PFOS) and perfluorooctanoic acid (PFOA) are most prevalent in the environment.[6,7] PFASs have been employed in aqueous film forming foam,[7] surfactants,[8] and other consumer goods,[9] but they are being phased out of production[10] because they been shown to negatively affect biota and human health.[11,12] To limit PFAS pollution, communities around the world are setting guidelines for maximum PFAS concentrations in potable water supplies.[13,14] For example, in 2016, the US Environmental Protection Agency set a health advisory limit of 70 ng/L for PFOS and PFOA,[15] and Michigan adopted even stricter maximum contaminant levels of 16 and 8 ng/L for PFOS and PFOA, respectively, in 2020.[16] Despite these regulations, however, PFASs are still found in potable water sources.[2,17]

Currently, several technologies exist for removing PFASs from water,[18] but adsorption is the most effective strategy. Activated carbon (AC) is the leading adsorbent for PFAS removal because it is inexpensive and exhibits moderate adsorption capacities.[19,20] However, AC typically suffers

from slow adsorption kinetics and long equilibration times (i.e., days).[21,22] Ion exchange (IX) resins are another common adsorbent because they are easy to implement, and they exhibit higher adsorption capacities than AC.[20] Despite these advantages, IX resins also suffer from slow adsorption kinetics and long equilibrium times (i.e., hours to days).[23] These limitations of AC and IX resins demonstrate the need for improved adsorbents with faster adsorption rates.

Researchers are developing adsorbents to overcome the limitations of AC and IX resins using sustainable materials, due to environmental concerns associated with nonrenewable resources. For example, the Dichtel and Helbling groups have together developed sustainably sourced cyclodextrin-based adsorbents for pollutant removal.[24,25] In particular, they have shown that cyclodextrins functionalized with amines and permanent cations quickly (contact time = 30 min) adsorb anionic PFASs like PFOS and PFOA at environmentally relevant concentrations.[26,27,28,29] Their materials also have shorter equilibration times than AC and distribution coefficients (K_D), which describe an adsorbate's affinity for an adsorbent, that rival AC and IX resins. Despite these critical advancements, the functionalized cyclodextrins are less efficient in water matrices that contain realistic salt concentrations and pHs, revealing the need for further improvements.[27,28,29]

Cellulose, a biodegradable and renewable biopolymer, is another potential material for generating effective adsorbents,[30] with some researchers already using it to adsorb PFASs.[31,32] For example, Ateia et al. showed that poly(ethylenimine)-functionalized cellulose microcrystals (PEI-CMCs) effectively adsorb >90% of several anionic PFASs.[31] In another example, Deng et al. demonstrated that cotton grafted with quaternary amines only adsorbs ~70% of PFOS and PFOA, but has high adsorption capacities of 1600 and 1300 mg/g, respectively.[32] In both cases, however, the adsorbents required more than 60 min to achieve these efficiencies, which is slow compared to Dichtel and Helbling's cyclodextrins. Additionally, while realistic salt concentrations were not

tested in either study, PFOA adsorption efficiency decreased under environmentally relevant pH conditions with Ateia's PEI-CMCs. These studies demonstrate the need for improved cellulose-based adsorbents with rapid PFAS adsorption under environmentally relevant pH and salt conditions.

In previous work, we observed that hydrogels made from anionic sulfated cellulose nanofibers rapidly (<30 s) and efficiently adsorbed (>90%) a cationic dye via electrostatic interactions.[33] Thus, we hypothesized that a cationic cellulose could be similarly used to rapidly adsorb anionic PFASs via electrostatic interactions. However, cellulose nanofibers are expensive due to their extensive processing, hence we evaluated an inexpensive alternative – wood pulp (WP). WP is a by-product of the papermaking industry and requires few energy-intensive production steps.[34] Herein, we report that WP functionalized with quaternary amines rapidly (<30 s) and efficiently adsorbs anionic PFASs. Adsorption efficiencies greater than 90% and 80% are achieved at environmentally relevant concentrations for PFOS and PFOA, respectively. Solution pH and salt concentration do not affect adsorption under realistic water conditions. Additionally, this quaternized wood pulp (QWP) has adsorption capacities of 763 and 605 mg/g for PFOS and PFOA, respectively, which are competitive with other existing adsorbents. Overall, this QWP adsorbent is effective for rapidly removing PFASs from water.

Experimental

Materials. Bleached hardwood pulp was generously donated by Cellulose Lab. Hydrochloric acid (ACS reagent, 37%), acetone, 2-propanol (IPA), glycidyl trimethyl ammonium chloride (GMAC, technical grade, contains 20–25% water), sodium nitrate, humic acid (HA), perfluorooctanoic acid (PFOA, CAS# 335-67-1), heptadecafluorooctane sulfonic acid potassium salt (PFOS, CAS# 2795-39-3), potassium nonafluoro-1-butanesulfonate (PFBS, CAS# 29420-49-

3), and heptafluorobutyric acid (PFBA, CAS# 375-22-4) were purchased from Aldrich. Undecafluoro-2-methyl-3-oxahexanoic acid (GenX, CAS# 13252-12-6) was purchased from Synquest Laboratories, and sodium 1H,1H,2H,2H-perfluorooctane sulfonate (6:2 FTS, CAS# 27619-94-9, 50 µg/mL in methanol) was purchased from Wellington Laboratories. Sodium chloride (NaCl), silver nitrate ($NaNO_3$), methanol (certified ACS), methanol (purge and trap suitable for volatile organic residue analysis), and disposable polypropylene 50 mL centrifuge tubes were purchased from Fisher. All reagents were used without further purification. Deionized water purified by a Millipore Synergy water purification system was used as a water source and is referred to as "Millipore water" where appropriate.

QWP synthesis. Note: Throughout the chapter, QWP samples are identified by their charge density (e.g., QWP1.5 is a sample with a charge density of 1.5 mmol $-NR_3^+$/g).

The synthesis of QWPs was carried out similar to literature procedures.[35,36,37] WP (1.0 g) was combined with Millipore water (50 mL) in a 100 mL round-bottom flask. The mixture was left alone for 15 min to wet the fibers, and then, the mixture was homogenized at 18k rpm for 2 min. The fibers were soaked for 5 min while the homogenizer was disassembled, cleaned with water and acetone to remove any clogged fibers, and reassembled. The mixture was homogenized again at 18k rpm for 2 min.

The mixture was divided into two 50 mL polypropylene centrifuge tubes and water was added to fill the tubes (~45 mL in each tube). The tubes were centrifuged at 2580 × g for 4 min, and the supernatant was discarded. The WP from each tube was combined into a round-bottom flask (note: a 100 mL round-bottom flask was used when making QWP1.5 and QWP0.65, but a 250 mL round-bottom flask was used when making QWP0.99, QWP0.97, and QWP0.0). 2-Propanol (50.0 mL) was added to the flask along with NaOH (333.4 mg, 8.335 mmol) and a stir bar. The flask was

then heated to 50 °C on a heating block and stirred for 45 min. After this activation time, a known volume of glycidyl trimethyl ammonium chloride (Table A2.1) was added with a micropipette over 0–4 min to the reaction, and the mixture was stirred for 2.25 h.

After the reaction time, the round-bottom flask was removed from the heating block and cooled in ice water for 5 min. The reaction was quenched with 5M HCl (~3 mL) and stirred for 5 min. The mixture was vacuum-filtered using VWR grade 413 filter paper and rinsed with Millipore water (1×~50 mL).

The fibers were then divided into two 50 mL polypropylene centrifuge tubes. Millipore water was added to fill the tubes (~45 mL in each tube), the tubes were centrifuged at 3260 × g for 7–10 min, and then the supernatant was discarded. This process was defined as 1 centrifuge cycle, and this centrifuge cycling was repeated 2 more times to remove excess acid and ions from the fibers. After the 3rd cycle (2nd cycle for QWP0.0), the pH of the supernatants was examined using pH paper and found to be ~7. In addition, the supernatant from one of the tubes was vacuum-filtered, and the conductivity of the supernatant was measured. If the conductivity was ≤ 25 μS/cm, the fiber purification was considered done. If the conductivity was > 25 μS/cm, the centrifuge cycling was repeated until the supernatant could be filtered and measured to have a conductivity ≤ 25 μS/cm. See Table A2.1 for the number of centrifuge cycles used to purify each QWP sample. After the fibers were purified, the fibers were removed from the centrifuge tubes with a spatula, placed in 20 mL vials, frozen in liquid N_2, and dried under vacuum to remove excess water.

Conductometric titrations. The titrations of QWPs were carried out similar to a literature procedure.[38] First, a 10.0 mM $AgNO_3$ solution was made by dissolving $AgNO_3$ (34.0 mg, 0.200 mmol) in Millipore water (20.0 mL). A 100 mM $NaNO_3$ solution was prepared by dissolving $NaNO_3$ (170.0 mg, 2.000 mmol) in Millipore water (20.0 mL).

Next, a known amount of QWPs (typically about 40 mg) were combined with Millipore water (50.0 mL) in a 150 mL beaker and soaked for 10 min. The fibers were homogenized at 18k rpm for 2 min to disperse the fibers, and then additional Millipore water (50.0 mL) and a stir bar were added to the beaker. The beaker was placed on a stir plate, a conductivity meter was inserted into the mixture, and the mixture was stirred. Then, 100 mM $NaNO_3$ solution (1.0 mL) was added to the beaker to increase the conductivity to a stable, non-fluctuating level, and the mixture was equilibrated for ~5 min. The mixture was then titrated using the 10.0 mM $AgNO_3$ solution by adding aliquots (~100–400 μL) of the $AgNO_3$ solution to the mixture over 10 s every 40 s. The conductivity was recorded as a function of the volume of 10.0 mM $AgNO_3$ added. Then, the volume-corrected conductivity was plotted as a function of the volume of 10.0 mM $AgNO_3$ added, and the equivalence point was determined by the intersection of the linear least-squares regression lines from the flat and positively sloped regions of the curve (Figure A2.1). Based on the mmol of $AgNO_3$ added, the mmol of $-NR_3^+$ were determined assuming a one-to-one ratio between Ag^+ and Cl^-. (Note that adding $NaNO_3$ did not affect the titration results because Na^+ and NO_3^- ions are not involved in the titration reaction between Ag^+ and Cl^-, which form AgCl precipitate.) The charge density was determined by dividing the mmol $AgNO_3$ by the mass of QWP that was titrated. This procedure was repeated two times for each QWP sample, and the average is reported as the sample's charge density (Table A2.2).

Raman spectroscopy of QWPs. Raman spectroscopy was performed, similar to literature,[35] to understand the spatial distribution of quaternary amine groups on the QWPs. Both QWP0.0 and QWP1.5 samples were analyzed via Raman mapping of the fiber surface, fiber depth, and fiber cross-sections.

Raman spectra were collected using a Renishaw inVia Qontor Raman spectrometer that is equipped with a Leica microscope, 532 nm laser, 1800 lines/mm grating, 50 μm slit size, and a 50x long working distance objective (NA = 0.5). Spectra were collected in static scan mode centered at 1050 cm^{-1} at a laser power of 5–10% with an exposure time of 3–5 s to avoid damage to the fibers. The spectrometer was calibrated with a silicon standard. All Raman spectra were normalized to the peak at 1096 cm^{-1}.

For lateral and depth Raman mapping, QWP samples were made in the following way: QWPs (12.5 mg) were soaked in Millipore water (10.0 mL) for 5 min in a 20 mL vial. The mixture was homogenized at 18k rpm for 1 min to generate a 1.25 mg/mL QWP mixture. A 0.125 mg/mL QWP mixture was then made by combining 2.0 mL of 1.25 mg/mL QWP mixture and 18.0 mL of Millipore water in a new 20 mL vial. Several drops of the 0.125 mg/mL QWP mixture were then spread on a glass slide. Raman maps of the fibers were collected in Streamline HR mode with 1 μm resolution at 5–10% power with a 3 s exposure time.

For the cross-section Raman maps, QWP fibers were placed into holes (1 mm diameter) that had been drilled into a glass slide such that the fibers were protruding from the hole by <0.5 mm. A razor blade was passed along the surface of the glass slide to cut the fibers. Raman mapping was done along the surface of the cut cross-sections with 200 nm lateral resolution.

General procedure for adsorbing PFASs. A known volume of PFAS solution was placed in a 50 mL polypropylene centrifuge tube, and in some experiments, a known volume of solution with measured pH, humic acid, or NaCl was added as well. Next, a volume of QWP mixture with known concentration and water were syringed over 10 s into the bottom of the centrifuge tube while vortex mixing at a speed of 1.5. The tube was vortex mixed for an additional 10 s using the same speed. The centrifuge tube was removed from the vortex mixer, and an aliquot was taken

with a 3 mL plastic syringe, filtered through a cellulose acetate syringe filter, and placed in either a 2 mL glass vial for in-house analysis or a 15 mL centrifuge tube so the sample could be sent to Eurofins Eaton Analytical for analysis (Appendix 2 section "PFAS adsorption experiments").

Results and Discussion

To test our hypothesis that cationic cellulose could rapidly adsorb PFASs via electrostatic interactions, several different QWPs were synthesized by varying the relative concentration of glycidyl trimethyl ammonium chloride (GMAC) to obtain charge densities ranging from 0.0–1.5 mmol -NR_3^+/g (Scheme 3.1).[35,36,37] Conductometric titrations were performed to determine charge densities, and elemental analysis was used to verify the titration results (Table A2.3).[38] Previous work functionalizing wood pulp with GMAC suggests that quaternary amines are functionalized at the C2 and C6 positions on the glucose repeat unit.[39]

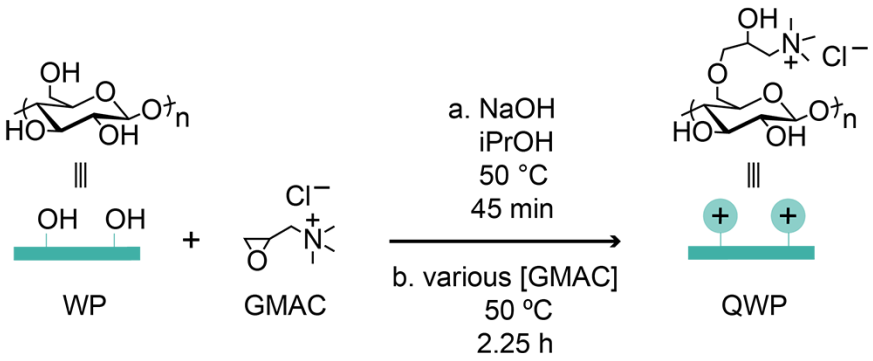

Scheme 3.1. Synthesizing QWP fibers with various charge densities.

WP fibers have both surface and interior (amorphous) sites that can be functionalized.[36,40,41] To determine where the functional groups were located, Raman spectroscopy was performed on the fiber surface, at different depths, and throughout a cross-section. More specifically, we used the quaternary amine's symmetric stretch at 764 cm^{-1} to map functional group location. Raman spectra acquired on a cross-section showed similarly intense symmetric stretches at all locations

(Figure 3.1 and Figure A2.2)[42] while lateral and depth maps also showed similar intensities (Figure A2.3 and Figure A2.4). As a control, the unfunctionalized QWP0.0 was also mapped, showing the expected absence of any peaks at 764 cm^{-1} (Figure A2.3, Figure A2.5, and Figure A2.6). Overall, these results indicate that amination occurs throughout QWP fibers and are not preferentially located on the surface.

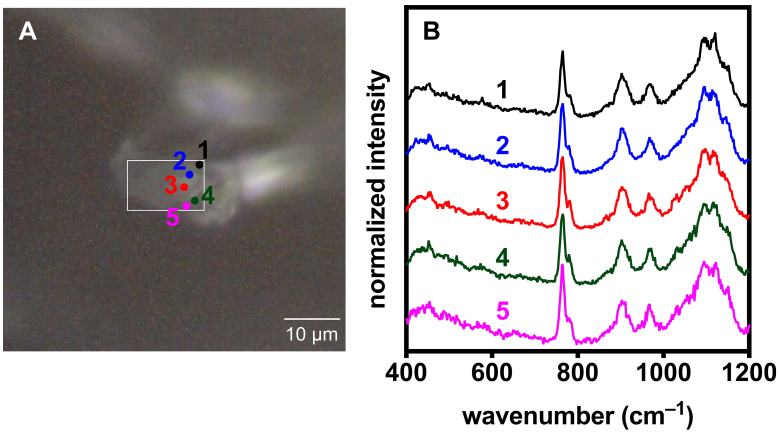

Figure 3.1. (A) Microscope image of a QWP1.5 fiber cross-section. (B) Raman spectra acquired at various positions on the fiber's cross-section. (The Raman spectra were normalized to the peak at 1096 cm^{-1}, which corresponds to the C–O and C–C stretches.)

After synthesizing QWPs with a range of charge densities (CDs), we next examined their PFAS adsorption efficiencies, anticipating that the wood pulp with highest charge density would exhibit the highest removal efficiency based on electrostatic interactions. To test this hypothesis, QWPs with CDs from 0.0–1.5 mmol -NR_3^+/g were mixed in PFOS or PFOA solutions, and adsorption was analyzed after 30 s of contact time (Figure 3.2A). As expected, nearly 100% of PFOS and 70% of PFOA were removed from solution with the highest CD QWP (QWP1.5) while QWPs with lower CDs (QWP0.99 and QWP0.65) adsorbed less than 16% of PFOS and 23% of PFOA. These results demonstrate that higher wood pulp CDs leads to more PFOS/PFOA adsorption under otherwise identical conditions. Moreover, because the unfunctionalized WP (i.e., with no cationic

charges) removed a negligible amount of anionic PFAS, we can conclude that the PFAS adsorption on QWPs likely occurs via electrostatic interactions. Moving forward, QWP1.5 was used for the remainder of the studies because it exhibited the highest adsorption percent compared to the other QWPs.

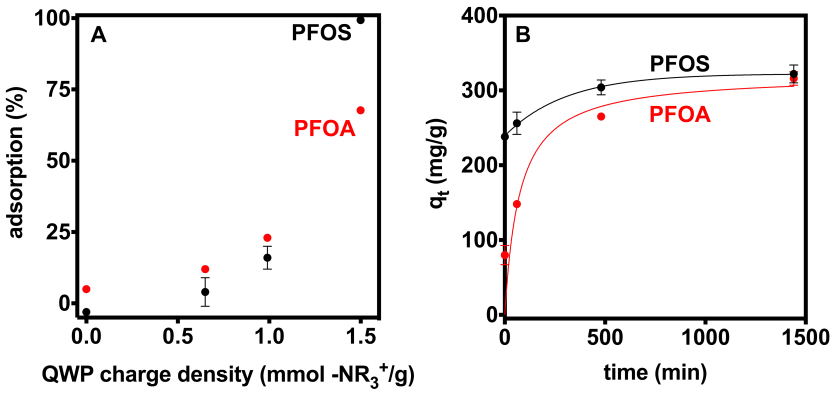

Figure 3.2. (A) Effect of QWP charge density on PFOS (black) and PFOA (red) adsorption percent. ([QWP] = 50.0 mg/L, $[PFOS]_0$ = 4.2 mg/L, and $[PFOA]_0$ = 3.9 mg/L.) (B) PFOS (black) and PFOA (red) adsorption capacities (q_t) over time on QWP1.5. ([QWP1.5] = 10.0 mg/L, $[PFOS]_0$ = 3.5 mg/L, $[PFOA]_0$ = 3.9 mg/L.) Some error bars are not visible due to their small size.

To optimize adsorption capacity, we added varying amounts of QWP1.5 to PFOS solutions and measured PFOS adsorption after 30 s of contact time (Figure 3.3). A small QWP1.5 dosage of 1.25 mg/L resulted in negligible PFOS adsorption but increasing the dosage to 12.5 mg/L resulted in a PFOS adsorption capacity of 263 ± 3 mg/g. Further increasing the dosage to 50.0 mg/L resulted in a decreased adsorption capacity of approximately 80 mg/g. This trend suggests that employing

too much QWP1.5 results in inefficient use of available cationic sites, and a moderate dosage maximizes PFAS adsorption. Thus, we utilized a dosage of 10.0 mg/L for the remaining studies.

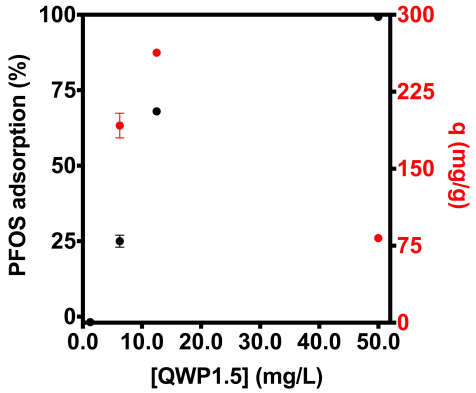

Figure 3.3. Plot of PFOS adsorption (%) (black) and adsorption capacity (q, mg/g) (red) as a function of QWP1.5 concentration (mg/L). Some error bars are not visible due to their small size.

To determine if adsorption equilibrium is achieved within 30 s of contact time, PFOS and PFOA adsorption capacities (q_t) on QWP1.5 were monitored over 24 h (Figure 3.2B). After 30 s of contact time, the PFOS adsorption capacity was 238 ± 5 mg/g, corresponding to 67 ± 1% of PFOS adsorbed, while PFOA adsorption capacity was 80 ± 10 mg/g, with 20 ± 3% of PFOA adsorbed. Moreover, the adsorption equilibrium required 8 and 24 h of contact time for PFOS and PFOA, respectively, suggesting that longer times are needed to reach higher adsorption capacities.

Adsorption isotherms were generated to determine QWP1.5's maximum adsorption capacity for PFOS and PFOA. Isotherm data was collected by soaking QWP1.5 in either PFOS or PFOA solutions for 24 h and measuring the equilibrium PFOS/PFOA concentrations (C_e) in solution (Figure 3.4, Table A2.11, and Table A2.12). The resulting data were fit with Langmuir and Freundlich isotherm models. The Langmuir model was found to best fit the data, according to a linear least-squares regression (Table A2.13 and Table A2.14). Because the Langmuir model best describes the equilibrium adsorption behavior, adsorption likely occurs at specific sites on the

cationic wood pulp with the PFASs adsorbing in one layer on the fiber surface.[43] Using the Langmuir model, we calculated that the maximum adsorption capacity (q_{max}) for PFOS and PFOA was 763 and 605 mg/g, respectively. The difference in q_{max} between PFOS and PFOA is attributed to a sulfate group's increased affinity for electrostatic interactions with charged amine groups relative to a carboxylate.[44,45] Additionally, because PFASs are typically found at concentrations from single-digit ng/L to hundreds of µg/L in the environment,[5,6,46] we calculated distribution coefficients (K_D, L/g), which characterize the affinity of adsorbates for an adsorbent and estimate the magnitude of adsorption that will occur at low PFAS concentrations, using the isotherm data.[47,48,49] K_D were determined using the linear portion of the adsorption isotherms (Figure A2.16), and resulted in a log K_D of 3.93 and 3.09 for PFOS and PFOA, respectively, which are comparable to other adsorbents.

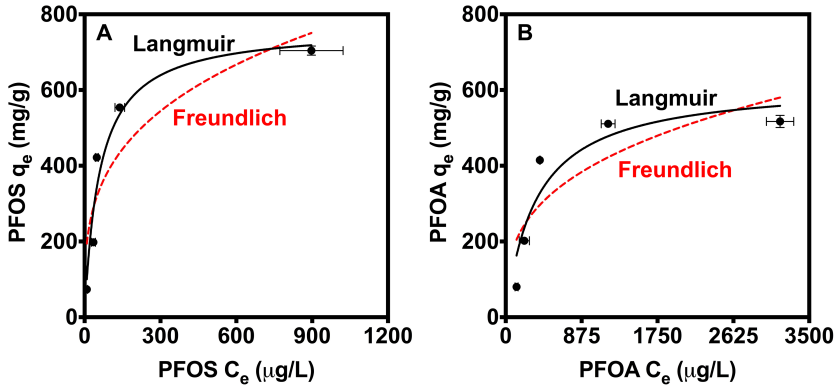

Figure 3.4. Plots of equilibrium adsorption capacities (q_e) versus equilibrium concentrations (C_e) for PFOS (A) and PFOA (B), fit with the Langmuir (solid black line) and Freundlich (dashed red line) models. ([QWP1.5] = 10.0 mg/L, $[PFOA]_0$ = ~920–8300 µg/L, $[PFOS]_0$ = ~750–8000 µg/L. Some error bars are not visible due to their small size.)

In nature, water contains other contaminants as well as a mixture of different PFASs at low concentrations (i.e., single-digit ng/L to hundreds of µg/L).[5,6,46] To determine whether QWP1.5 was effective for removing multiple types of PFASs, we monitored PFAS adsorption after the

cationic WP was mixed simultaneously with PFOS, PFOA, PFBS, PFBA, GenX, and 6:2 FTS. After just 30 s of contact time, we observed >80% adsorption of PFOS, PFOA, and 6:2 FTS (Figure 3.5). On the other hand, we found less efficient adsorption of PFBS, PFBA, and GenX, with adsorption between 13–29%. These differences in adsorption % correspond to approximately half as many moles of short chain PFASs (i.e., PFBS and PFBA) being adsorbed relative to long chain PFASs (i.e., PFOS, PFOA, and 6:2 FTS), despite adding approximately twice as many moles of short chain PFASs initially compared to long chain PFASs (Table 3.1).

Table 3.1. Initial and adsorbed moles of PFASs on QWP1.5.

	PFBA	**PFBS**	**GenX**	**6:2 FTS**	**PFOA**	**PFOS**
average initial mol added (pmol)	161 ± 8	91 ± 5	90 ± 20	47.6 ± 0.5	71 ± 1	48 ± 2
average adsorbed mol (pmol)	20 ± 10	27 ± 2	20 ± 10	44 ± 1	57 ± 2	48*

*Indicates that the measured PFAS concentration was below the limit of quantification (0.02 μg/L). Therefore, the limit of quantification was assumed to be the PFAS concentration. Accurate standard deviations could not be calculated for these entries because of this estimation.

After 60 min of contact time, only small increases in PFAS adsorption were observed, with PFBS having the largest change from 29 to 39%. Combined, these data reveal the impact of PFAS chain length on adsorption because the PFAS with longer chain lengths are adsorbed more efficiently than those with shorter chain lengths. To explain this phenomenon, we examined the PFASs' octanol/water partition coefficients (K_{ow}), which reflect a molecule's hydrophobicity. We found that longer PFASs had larger K_{ow} meaning they were more hydrophobic, likely due to their longer hydrophobic tails.[50,51] This finding suggests that hydrophobic interactions are likely complementing the electrostatic interactions during adsorption. More specifically, we propose that cellulose's hydrophobic backbone is enhancing QWP1.5's ability to efficiently adsorb the more hydrophobic (i.e., longer chain) PFASs. However, the effect of hydrophobicity should be explored in greater detail in future studies considering that QWP0.0, with no cationic groups, adsorbed

negligible amounts of PFASs. In addition, we observed that the PFAS functional group plays a role in adsorption wherein the PFASs with sulfate groups were more effectively adsorbed than the PFASs with carboxyl groups. We again attribute the increased adsorption to the sulfate group's known increased affinity for electrostatic interactions with charged amine groups.[44,45] The adsorption trends found in this study are consistent with other reports in literature.[31,52,53]

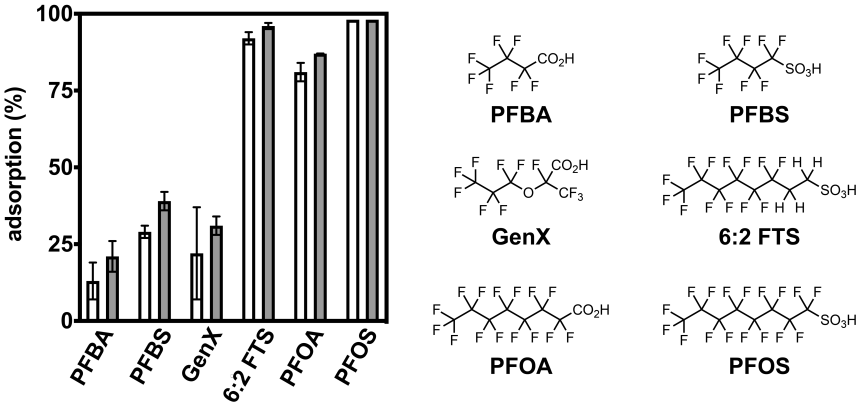

Figure 3.5. PFAS adsorption (%) on QWP1.5 with 30 s (white) and 60 min (gray) of contact time. ([QWP1.5] = 10.0 mg/L, $[PFAS]_0$ = ~2.5 μg/L.) Note: PFOS was removed below the limit of quantification (20 ng/L), so this limit was used in the adsorption % calculations)

Natural organic matter (NOM) refers to organic compounds naturally present in freshwater sources, and it has previously been shown to inhibit PFAS adsorption on conventional adsorbents.[54] To evaluate whether NOM inhibits adsorption with our cationic wood pulp fibers, we measured PFAS adsorption in the presence of humic acid (HA), a common type of NOM. We observed that HA significantly reduced PFAS adsorption, with ≤ 24% of each PFAS being adsorbed (Table 3.2).

Table 3.2. QWP1.5 adsorption % and capacity for PFASs after 30 s of contact time between QWP1.5 and PFASs.

PFAS	adsorption (%) without HA	adsorption capacity (mg/g) without HA	adsorption (%) with HA	adsorption capacity (mg/g) with HA
PFBA	13 ± 6	0.04 ± 0.02	3 ± 2	0.010 ± 0.007
PFBS	29 ± 2	0.08 ± 0.01	8 ± 3	0.021 ± 0.007
GenX	20 ± 20	0.06 ± 0.04	24 ± 3	0.07 ± 0.01
6:2 FTS	92 ± 2	0.187 ±0.004	8 ± 5	0.02 ± 0.01
PFOA	81 ± 3	0.237 ± 0.008	8 ± 4	0.02 ± 0.01
PFOS	98 ± 0*	0.238*	20 ± 5	0.05 ± 0.01

*Indicates that the measured PFAS concentration was below the limit of quantification (0.02 μg/L). Therefore, the limit of quantification was assumed to be the PFAS concentration. Accurate standard deviations could not be calculated for these entries because of this estimation.

Because HA is a complex mixture of charged and uncharged species, and the hydrophobicity/hydrophilicity can vary based on the source, we measured the specific UV absorbance at 254 nm ($SUVA_{254}$) to characterize our HA (Figure A2.19).[55] The $SUVA_{254}$ was 4.1, which suggests that the HA mainly consists of high molecular weight hydrophobic and aromatic materials.[56] Because the cellulose backbone is also hydrophobic, HA is likely adsorbing to the wood pulp via hydrophobic interactions, and blocking PFAS access to the cationic sites. Further research is needed to understand and then attenuate the detrimental impact of NOM on these cationic WP-based adsorbents.

Water pH often adversely impacts PFAS adsorption because some adsorbents lose their cationic charge at environmentally relevant pHs of 5–9.[22,57] The QWPs synthesized herein, on the other hand, should not be impacted by pH because the quaternary amine has a pH-insensitive permanent charge. Moreover, the PFOS/PFOA studied herein have pK_a values below 3,[58,59] meaning the sulfonyl and carboxyl groups will remain charged at pHs 5–9. As expected, after 30 s of contact time, we observed that pH had no effect on PFOS or PFOA adsorption (Figure 3.6A).

Moreover, the leftover PFOS concentration in solution was below the limit of quantification (< 20 ng/L), which is much lower than the EPA guidelines for PFOS in water.

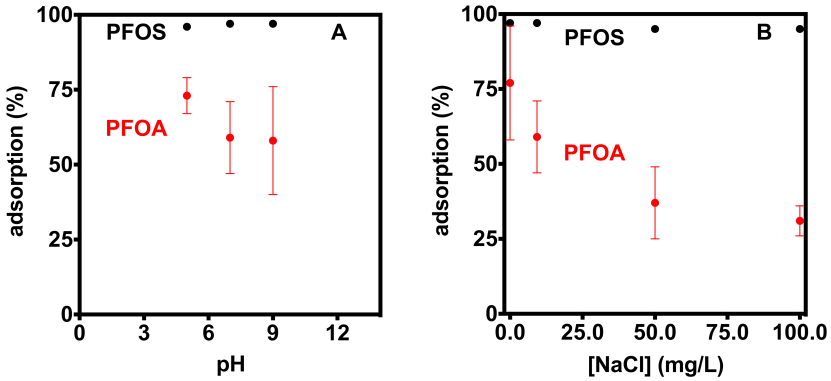

Figure 3.6. PFOS (black) and PFOA (red) adsorption (%) as a function of pH (A) and NaCl concentration (B). ([QWP1.5] = 10.0 mg/L, $[PFAS]_{initial}$ < 2.8 µg/L.) Note: PFOS was removed below the limit of quantification (20 ng/L), so this limit was used for adsorption % calculations. Some error bars are not visible due to their small size.

The influence of salt concentration on PFAS adsorption was also studied because water tends to have low concentrations of inorganic ions.[19,20] After 30 s of contact time, we observed that salt concentration had no impact on PFOS adsorption, similar to the pH experiment, with leftover PFOS concentrations below the limit of quantification (Figure 3.6B).[19,20] In contrast, PFOA adsorption decreased from >75% to nearly 30% as the NaCl concentration increased from 0 to 100 mg/L, likely due to electrostatic shielding between PFOA and the wood pulp's cationic sites. The difference in PFOS and PFOA adsorption is attributed, again, to the increased sulfate affinity for cationic amines, as Schlenoff and coworkers showed that sulfate/amine interactions are less affected by NaCl concentrations than carboxylate/amine interactions.[44] Despite the reduction in PFOA adsorption, it remains high (> 50%) for salt concentrations below 25 mg/L, which is the value usually observed in freshwater samples.[28,60]

To demonstrate QWP1.5's effectiveness for adsorbing PFASs, we compared PFAS adsorption capacities from this study with other adsorbents. We found that after 30 s of contact time in deionized water, PFOS and PFOA adsorption capacities were 238 ± 5 and 80 ± 10 mg/g on QWP1.5, which is better than the adsorption capacities for some ACs and IX resins that utilized similar adsorption conditions and longer contact times.[19,20] For example, Zhang et al. showed that AC adsorbs less than 20 mg/g of PFOS and PFOA after 40 h while Yu et al. revealed that an anionic exchange resin adsorbs ~125 and 300 mg/g of PFOS and PFOA, respectively, after 10 h.[22,61] Our result for PFOA after 30 s of contact time is also significantly larger than the PFOA capacity reported by Ateia et al. for poly(ethylenimine)-functionalized cellulose microcrystals after 24 h of contact time (2.32 mg/g).[31] Furthermore, the maximum adsorption capacities (q_{max}) for PFOS and PFOA in this study were calculated to be 763 and 605 mg/g, respectively, making QWP1.5 competitive with or better than the capacities of comparable adsorbents. For instance, ACs typically have q_{max} below 600 mg/g and IX resins have q_{max} ranging from ~200–2600 mg/g.[19,20] Dichtel and Helbling report q_{max} for PFOA of 457 and 33 mg/g for an amine- and unfunctionalized cyclodextrin-based adsorbent, respectively.[62,63] On the other hand, QWP1.5 has lower q_{max} than Deng et al.'s amine-grafted cotton, which has q_{max} values of 1600 mg/g for PFOS and 1300 mg/g for PFOA.[32]

The log K_D, which characterize the affinity of adsorbates for an adsorbent, were calculated as 3.93 for PFOS and 3.09 for PFOA adsorption on QWP1.5. These values were compared to AC and IX resins, which revealed that AC and IX resins have a log K_D less than 2.31.[21,28,64] As a consequence, the QWP1.5 synthesized herein has a better affinity for adsorbing PFOS and PFOA than conventional adsorbents. The amine-functionalized cyclodextrins reported by Dichtel and Helbling have log K_D values of 3.0 and 4.0 for PFOS and PFOA,[28] respectively, revealing that

cationic WP is also competitive with similar adsorbents that depend on ionic interactions to adsorb PFASs.

At environmentally relevant concentrations (~2.5 μg/L), QWP1.5 adsorbed >80% of PFOS, PFOA, and 6:2 FTS in deionized water within 30 s of contact time. Similar adsorption percents were achieved for Dichtel and Helbling's amine-functionalized cyclodextrins and Ateia's PEI-CMCs, but the amine-functionalized cyclodextrins and PEI-CMCs required more than 30 and 15 min, respectively, to achieve these efficiencies, highlighting QWP1.5's ability to rapidly adsorb long chain PFASs.[28,31] With respect to short chain PFASs, QWP1.5 adsorbed less than 29% of PFBS and PFBA, which is inferior to amine-functionalized cyclodextrins, which adsorbed greater than 75% of PFBS and PFBA after 30 min of contact time.[28] Additionally, when HA was present, PFAS adsorption on QWP1.5 was below 20%, which is worse than Dichtel and Helbling's cyclodextrins and Ateia's PEI-CMCs. However, PFAS adsorption by AC and IX resins is known to be similarly impacted by NOM.[52,29] Further research will be needed to attenuate the impact of HA on PFAS adsorption for these wood pulp-based adsorbents. On the other hand, PFAS adsorption on cationic WP was not affected by solution pH, even with short contact times, whereas adsorbents like AC and IX resins lose efficiency at pHs greater than 7 and 8, respectively,[22,57,65] and other adsorbents require long time periods (≥ 24 h) to reach similar adsorption efficiencies.[27,28,31,32] Elevated salt concentrations were found to decrease PFOA adsorption on QWP1.5 and have no effect on PFOS adsorption. These findings are in line with PFAS adsorption on AC, IX resins, and other adsorbents, showing that background ions inhibit PFAS adsorption.[28,60,66,67] Like the pH studies, however, the advantage of QWP1.5 in salt solutions is the rapid adsorption time whereas other adsorbents require long time periods (i.e., hours to days) to reach efficient adsorption. To summarize all these comparisons, the advantages of cationic WP are

the high adsorption capacities and distribution coefficients for PFOS and PFOA, and the rapid adsorption of long chain PFASs under most environmentally relevant conditions.

While beyond the scope of this article, the fate of spent QWP adsorbent eventually needs to be considered. Regeneration is often explored so that adsorbents can be reused; however, the processes involved in regeneration can potentially outweigh the benefits of using new adsorbent. For example, regenerating AC requires frequent costly and energy-intensive methods while regenerating IX resins entails harsh solvent combinations that are not financially feasible for large-scale operations.[19,23,52,68] One potential advantage of these cellulose-based adsorbents is the potential for environmental biodegradation after PFAS removal via emerging technologies such as irradiation[69] or microbial digestion.[70]

Conclusions

In summary, we demonstrated herein that cationic wood pulp is a promising adsorbent for removing PFASs from water. Accessing QWP involves a straightforward, one-step reaction, wherein the resulting charge density can be tailored by varying the reactant concentrations. At environmentally relevant concentrations (~2.5 μg/L), PFOS and PFOA were adsorbed in under 30 s, making QWPs advantageous compared to other adsorbents which require long adsorption times (>15 min). The maximum adsorption capacity for PFOS and PFOA on QWP1.5 outperforms similar adsorbents and activated carbon. Although adsorption was impacted by natural organic matter, it was unaffected by solution pH and low salt concentrations. Further research is necessary to advance these materials, especially with respect to the competitive adsorption with hydrophobic organic matter. Nevertheless, these materials are promising based on their performance and because wood pulp is bio-sourced, biodegradable, and inexpensive (~$0.90 per metric ton in

2021).[71] For these reasons, we remain optimistic that functionalized wood pulp will become a competitive, renewable alternative adsorbents to activated carbon for PFAS removal.

References

(1) Boretti, A.; Rosa, L. Reassessing the projections of the world water development report. *npj Clean Water* 2019, 2.

(2) Hu, X.; Andrews, D.; Lindstrom, A.; Bruton, T.; Schaider, L.; Grandjean, P.; Lohmann, R.; Carignan, C.; Blum, A.; Balan, S.; Higgins, C.; Sunderland, E. Detection of poly- and perfluoroalkyl substances (PFASs) in U.S. drinking water linked to industrial sites, military fire training areas, and wastewater treatment plants. *Environ. Sci. Technol. Lett.* **2016**, *3*, 344−350.

(3) Bai, X.; Son, Y. Perfluoroalkyl substances (PFAS) in surface water and sediments from two urban watersheds in Nevada, USA. *Sci. Total Environ.* **2021**, *751*, 141622.

(4) Barton, K.; Starling, A.; Higgins, C.; McDonough, C.; Calafat, A.; Adgate, J. Sociodemographic and behavioral determinants of serum concentrations of per- and polyfluoroalkyl substances in a community highly exposed to aqueous film-forming foam contaminants in drinking water. *Int. J. Hyg. Environ. Health* **2020**, *223*, 256–266.

(5) Boone, J.; Vigo, C.; Boone, T.; Byrne, C.; Ferrario, J.; Benson, R.; Donohue, J.; Simmons, J.; Kolpin, D.; Furlong, E.; Glassmeyer, S. Per- and polyfluoroalkyl substances in source and treated drinking waters of the United States. *Sci. Total Environ.* **2019**, *653*, 359–369.

(6) Nickerson, A.; Rodowa, A.; Adamson, D.; Field, J.; Kulkarni, P.; Kornuc, J.; Higgins, C. Spatial trends of anionic, zwitterionic, and cationic PFASs at an AFFF-impacted site. *Environ. Sci. Technol.* **2021**, *55*, 313–323.

(7) Barzen-Hanson, K.; Roberts, S.; Choyke, S.; Oetjen, K.; McAlees, A.; Riddell, N.; McCrindle, R.; Ferguson, P.; Higgins, C.; Field, J. Discovery of 40 classes of per- and polyfluoroalkyl substances in historical aqueous film-forming foams (AFFFs) and AFFF-impacted groundwater. *Environ. Sci. Technol.* **2017**, *51*, 2047−2057.

(8) Kissa, E. *Fluorinated surfactants and repellants*, 2nd Edition; Marcell Dekker, Inc. 2001.

(9) Kotthoff, M.; Muller, J.; Jurling, H.; Schlummer, M.; Fiedler, D. Perfluoroalkyl and polyfluoroalkyl substances in consumer products. *Environ. Sci Pollut. Res*. **2015**, *22*, 14546–14559.

(10) U.S. EPA. PFOA Stewardship Program Baseline Year Summary Report. https://www.epa.gov/assessing-and-managing-chemicals-under-tsca/pfoa-stewardship-program-baseline-year-summary-report (accessed March 11, 2021).

(11) Stahl, T.; Mattern, D.; Brunn, H. Toxicology of perfluorinated compounds. *Environ. Sci. Eur*. **2011**, *23*, 38.

(12) Chohan, A.; Petaway, H.; Rivera-Diaz, V.; Day, A.; Colaianni, O.; Keramati, M. Per and polyfluoroalkyl substances scientific literature review: water exposure, impact on human health, and implications for regulatory reform. *Rev. Environ. Health* **2020**. DOI: 10.1515/reveh-2020-0049.

(13) Cordner, A.; De La Rosa, V.; Schaider, L.; Rudel, R.; Richter, L.; Brown, P. Guideline levels for PFOA and PFOS in drinking water: the role of scientific uncertainty, risk assessment decisions, and social factors. *J. Expo. Sci. Environ Epidemiol.* **2019**, *29*, 157–171.

(14) Interstate Technology and Regulatory Council (ITRC). ITRC PFAS regulations, guidance and advisories fact sheets. https://pfas-1.itrcweb.org/fact-sheets/ (accessed March 11, 2021).

(15) Fact sheet: PFOA and PFOS drinking water health advisories; EPA 800-F-16-003; U.S. EPA: Washington, DC, 2016.

(16) Michigan Department of Environment, Great Lakes, and Energy. New state drinking water standards pave way for expansion of Michigan's PFAS clean-up efforts. https://www.michigan.gov/egle/0,9429,7-135--535602--,00.html (accessed March 11, 2021).

(17) EWG. Mapping the PFAS contamination crisis: new data show 2,337 sites in 49 States. https://www.ewg.org/interactive-maps/pfas_contamination/ (accessed March 11, 2021).

(18) Kucharzyk, K.; Darlington, R.; Benotti, M.; Deeb, R.; Hawley, E. Novel treatment technologies for PFAS compounds: A critical review. *J. Environ. Manage* **2017**, *204*, 757–764.

(19) Du, Z.; Deng, S.; Bei, Y.; Huang, Q.; Wang, B.; Huang, J.; Yu, G. Adsorption behavior and mechanism of perfluorinated compounds on various adsorbents—A review. *J. Hazard. Mater.* **2014**, *274*, 443–454.

(20) Zhang, D.; Zhang, W.; Liang, Y. Adsorption of perfluoroalkyl and polyfluoroalkyl substances (PFASs) from aqueous solution - A review. *Sci. Total. Environ.* **2019**, *694*, 133606.

(21) Xiao, X.; Ulrich, B.; Chen, B.; Higgins, C. Sorption of poly- and perfluoroalkyl substances (PFASs) relevant to aqueous film-forming foam (AFFF)-impacted groundwater by biochars and activated carbon. *Environ. Sci. Technol*. **2017**, *51*, 6342−6351.

(22) Yu, Q.; Zhang, R.; Deng, S.; Huang, J.; Yu, G. Sorption of perfluorooctane sulfonate and perfluorooctanoate on activated carbons and resin: kinetic and isotherm study. *Water Res*. **2009**, *43*, 1150–1158.

(23) Zaggia, A.; Conte, L.; Falletti, L.; Fant, M.; Chiorboli, A. Use of strong anion exchange resins for the removal of perfluoroalkylated substances from contaminated drinking water in batch and continuous pilot plants. *Water Res.* **2016**, *91*, 137–146.

(24) Alsbaiee, A.; Smith, B.; Xiao, L.; Ling, Y.; Helbling, D.; Dichtel, W. Rapid removal of organic micropollutants from water by a porous β-cyclodextrin polymer. *Nature* **2016**, *529*, 190–194.

(25) Ling, Y.; Klemes, M.; Xiao, L.; Alsbaiee, A.; Dichtel, W.; Helbling, D. Benchmarking micropollutant removal by activated carbon and porous β-cyclodextrin polymers under environmentally relevant scenarios. *Environ. Sci. Technol*. **2017**, *51*, 7590−7598.

(26) Klemes, M.; Ling, Y.; Ching, C.; Wu, C.; Xiao, L.; Helbling, D.; Dichtel, W. Reduction of a tetrafluoroterephthalonitrile-β-cyclodextrin polymer to remove anionic micropollutants and perfluorinated alkyl substances from water. *Angew. Chem. Int. Ed*. **2019**, *58*, 12049 –12053.

(27) Wu, C.; Klemes, M.; Trang, B.; Dichtel, W.; Helbling, D. Exploring the factors that influence the adsorption of anionic PFAS on conventional and emerging adsorbents in aquatic matrices. *Water Res.* **2020**, *182*, 115950.

(28) Ching, C.; Klemes, M.; Trang, B.; Dichtel, W.; Helbling, D. β-cyclodextrin polymers with different cross-linkers and ion-exchange resins exhibit variable adsorption of anionic, zwitterionic, and nonionic PFASs. *Environ. Sci. Technol*. **2020**, *54*, 12693−12702.

(29) Wang, R.; Ching, C.; Dichtel, W.; Helbling, D. Evaluating the removal of per- and polyfluoroalkyl substances from contaminated groundwater with different adsorbents using a suspect screening approach. *Environ. Sci. Technol. Lett.* **2020**, *7*, 954−960.

(30) Hokkanen, S.; Bhatnagar, A.; Sillanpaa, M. A review on modification methods to cellulose-based adsorbents to improve adsorption capacity. *Water Res.* **2016**, *91*, 156–173.

(31) Ateia, M.; Attia, M.; Maroli, A.; Tharayil, N.; Alexis, F.; Whitehead, D.; Karanfil, T. Rapid removal of poly- and perfluorinated alkyl substances by poly(ethylenimine)-functionalized cellulose microcrystals at environmentally relevant conditions. *Environ. Sci. Technol. Lett*. **2018**, *5*, 764−769.

(32) Deng, S.; Zheng, Y.; Xu, F.; Wang, B.; Huang, J.; Yu, G. Highly efficient sorption of perfluorooctane sulfonate and perfluorooctanoate on a quaternized cotton prepared by atom transfer radical polymerization. *Chem. Eng. J.* **2012**, *193–194*, 154–160.

(33) Harris, J.; McNeil, A. Localized hydrogels based on cellulose nanofibers and wood pulp for rapid removal of methylene blue. *J. Polym. Sci.* **2020**, *58*, 3042–3049.

(34) *Biermann's Handbook of Pulp and Paper*, 3rd ed.; Bajpai, P., Ed.; Elsevier 2018. DOI: 10.1016/B978-0-12-814240-0.12001-4

(35) Olszewska, A.; Eronen, P.; Johansson, L.; Malho, J.; Ankerfors, M.; Lindstrom, T.; Ruokolainen, J.; Laine, J.; Osterberg, M.; The behaviour of cationic nanofibrillar cellulose in aqueous media. *Cellulose*, **2011**, *18*, 1213–1226.

(36) Odabas, N.; Amer, H.; Bacher, M.; Henniges, U.; Potthast, A.; Rosenau, T. Properties of cellulosic material after cationization in different solvents. *ACS Sustainable Chem. Eng*. **2016**, *4*, 2295−2301.

(37) Wang, Z.; Carlsson, D.; Tammela, P.; Hua, K.; Zhang, P.; Nyholm, L.; Stromme, M. Surface modified nanocellulose fibers yield conducting polymer-based flexible supercapacitors with enhanced capacitances. *ACS Nano* **2015**, *9*, 7563–7571.

(38) Hasani, M.; Cranston, E.; Westman, G.; Gray, D. Cationic surface functionalization of cellulose nanocrystals. *Soft Matter* **2008**, *4*, 2238–2244.

(39) de la Motte, H.; Westman, G.; Regioselective cationization of cellulosic materials using an efficient solvent-minimizing spray-technique. *Cellulose* **2012**, *19*, 1677–1688.

(40) Agarwal, U.; Ralph, S.; Reiner, R.; Baez, C. Probing crystallinity of never-dried wood cellulose with Raman spectroscopy. *Cellulose* **2016**, *23*, 125–144.

(41) Wikberg, H.; Maunu, S. Characterisation of thermally modified hard- and softwoods by 13C CPMAS NMR. *Carbohydr. Polym*. **2004**, *58*, 461–466.

(42) Pigorsch, E. Spectroscopic characterisation of cationic quaternary ammonium starches. *Starch* **2009**, *61*, 129–138.

(43) Limousin, G.; Gaudet, J.; Charlet, L.; Szenknect, S.; Barthes, V.; Krimissa, M. Sorption isotherms: A review on physical bases, modeling and measurement. *Appl. Geochemistry* **2007**, *22*, 249–275.

(44) Dubas, S.; Schlenoff, J. Swelling and smoothing of polyelectrolyte multilayers by salt. *Langmuir* **2001**, *17*, 7725–7727.

(45) Fu, J.; Fares, H.; Schlenoff, J. Ion-pairing strength in polyelectrolyte complexes. *Macromolecules* **2017**, *50*, 1066–1074.

(46) Crone, B.; Speth, T.; Wahman, D.; Smith, S.; Abulikemu, G.; Kleiner, E.; Pressman, J. Occurrence of per- and polyfluoroalkyl substances (PFAS) in source water and their treatment in drinking water. *Crit. Rev. Environ. Sci. Technol*. **2019**, *49*, 2359–2396.

(47) Kamlet, M.; Doherty, R.; Abraham, M.; Taft, R. Linear solvation energy relationships. 33. An analysis of the factors that influence adsorption of organic compounds on activated carbon. *Carbon* **1985**, *23*, 549–554.

(48) Luehrs, D.; Hickey, J.; Nilsen, P.; Godbole, K.; Rogers, T. Linear solvation energy relationship of the limiting partition coefficient of organic solutes between water and activated carbon. *Environ. Sci. Technol*. **1996**, *30*, 143–152.

(49) Ling, Y.; Klemes, M.; Steinschneider, S.; Dichtel, W.; Helbling, D. QSARs to predict adsorption affinity of organic micropollutants for activated carbon and β-cyclodextrin polymer adsorbents. *Water Res*. **2019**, *154*, 217–226.

(50) Deng, S.; Zhang, Q.; Nie, Y.; Wei, H.; Wang, B.; Huang, J.; Yu, G.; Xing, B. Sorption mechanisms of perfluorinated compounds on carbon nanotubes. *Environ. Pollut*. **2012**, *168*, 138–144.

(51) Arp, H.; Niederer, C.; Goss, K. Predicting the partitioning behavior of various highly fluorinated compounds. *Environ. Sci. Technol*. **2006**, *40*, 7298-7304.

(52) Gagliano, E.; Sgroi, M.; Falciglia, P.; Vagliasindi, F.; Roccaro, P. Removal of poly- and perfluoroalkyl substances (PFAS) from water by adsorption: Role of PFAS chain length, effect of organic matter and challenges in adsorbent regeneration. *Water Res*. **2020**, *171*, 115381.

(53) Eschauzier, C.; Beerendonk, E.; Scholte-Veenendaal, P.; De Voogt, P. Impact of treatment processes on the removal of perfluoroalkyl acids from the drinking water production chain. *Environ. Sci. Technol*. **2012**, *46*, 1708−1715.

(54) Yu, J.; Lv, L.; Lan, P.; Zhang, S.; Pan, B.; Zhang, W. Effect of effluent organic matter on the adsorption of perfluorinated compounds onto activated carbon. *J. Hazard. Mater*. **2012**, *225*, 99–106.

(55) Sillanpaa, M; Matilainen, A.; Lahtinen, T. Characterization of NOM. In Natural Organic Matter in Water, 1st edition; IWA Publishing, **2015**; pp 17–53.

(56) Edzwald, J.; Tobiason, J. Enhanced coagulation: US requirements and a broader view. *Wat. Sci. Tech*. **1999**, *40*, 63–70.

(57) Dixit, F.; Barbeau, B.; Mostafavi, S.; Mohseni, M. PFOA and PFOS removal by ion exchange for water reuse and drinking applications: role of organic matter characteristics. *Environ. Sci.: Water Res. Technol*. **2019**, *5*, 1782–1795.

(58) Goss, K. The pKa values of PFOA and other highly fluorinated carboxylic acids. *Environ. Sci. Technol*. **2008**, *42*, 456–458.

(59) Brooke, D.; Footitt, A.; Nwaogu, T. Environmental Risk Evaluation Report: Perfluorooctanesulphonate (PFOS); Environment Agency, 2004.

(60) Ling, Y.; Alzate-Sanchez, D.; Klemes, M.; Dichtel, W.; Helbling, D. Evaluating the effects of water matrix constituents on micropollutant removal by activated carbon and β-cyclodextrin polymer adsorbents. *Water Res*. **2020**, *173*, 115551.

(61) Zhang, D.; Luo, Q.; Gao, B.; Chiang, S.; Woodward, D.; Huang, Q. Sorption of perfluorooctanoic acid, perfluorooctanesulfonate and perfluoroheptanoic acid on granular activated carbon. *Chemosphere* **2016**, *144*, 2336–2342.

(62) Yang, A.; Ching, C.; Easler, M.; Helbling, D.; Dichtel, W. Cyclodextrin polymers with nitrogen-containing tripodal crosslinkers for efficient PFAS adsorption. *ACS Materials Lett*. **2020**, *2*, 1240–1245.

(63) Xiao, L.; Ling, Y.; Alsbaiee, A.; Li, C.; Helbling, D.; Dichtel, W. β-cyclodextrin polymer network sequesters perfluorooctanoic acid at environmentally relevant concentrations. *J. Am. Chem. Soc*. **2017**, *139*, 7689–7692.

(64) Liu, C.; Werner, D.; Bellona, C. Removal of per- and polyfluoroalkyl substances (PFASs) from contaminated groundwater using granular activated carbon: a pilot-scale study with breakthrough modeling. *Environ. Sci.: Water Res. Technol*. **2019**, *5*, 1844–1853.

(65) Deng, S.; Yu, Q.; Huang, J.; Yu, G. Removal of perfluorooctane sulfonate from wastewater by anion exchange resins: Effects of resin properties and solution chemistry. *Water Res*. **2010**, *44*, 5188–5195.

(66) Maimaiti, A.; Deng, S.; Meng, P.; Wang, W.; Wang, B.; Huang, J.; Wang, Y.; Yu, G. Competitive adsorption of perfluoroalkyl substances on anion exchange resins in simulated AFFF-impacted groundwater. *Chem. Eng. J*. **2018**, *348*, 494–502.

(67) Saeidi, N.; Kopinke, F.; Georgi, A. Understanding the effect of carbon surface chemistry on adsorption of perfluorinated alkyl substances. *Chem Eng. J*. **2020**, *381*, 122689.

(68) Miguel, G. S.; Lambert, S. D.; Graham, N. J. D. The regeneration of field-spent granular activated carbons. *Water Res*. **2001**, *35*, 2740–2748.

(69) Trojanowicz, M.; Bartosiewicz, I.; Bojanowska-Czajka, A.; Szreder, T.; Bobrowski, K.; Nalecz-Jawecki, G.; Meczynska-Wielgosz, S.; Nichipor, H. Application of ionizing radiation in decomposition of perfluorooctane sulfonate (PFOS) in aqueous solutions. *Chem. Eng. J*. **2020**, *379*, 122303.

(70) Huang, S.; Jaffe, P. R. Defluorination of perfluorooctanoic acid (PFOA) and perfluorooctane sulfonate (PFOS) by Acidimicrobium sp. Strain A6. *Environ. Sci. Technol*. **2019**, *53*, 11410–11419.

(71) index mundi. Wood Pulp Monthly Price. https://www.indexmundi.com/commodities/?commodity=wood-pulp&months=120&currency=eur (accessed April 16, 2021).

Chapter 4 Wood Pulp Adsorbents that Adsorb Methyl Orange Dye

Introduction

Clean water is essential for human survival, but pollution makes acquiring water challenging for many communities.[1] One source of pollution is organic dyes as the textile industry generates approximately 20% of industrial water pollution,[2,3] stemming from textile dyeing and treatment.[4,5] Considering that dyes are linked to a variety of health issues in humans and damaging to the environment,[6,7] the textile industry needs to develop strategies to limit exposure to dyes. These strategies include minimizing dye release and removal of dyes from contaminated water.

Among several technologies that exist for removing dyes from water, adsorption is most commonly used.[8,9,10,11] The leading adsorbent is activated carbon (AC) due to its high adsorption capacity and broad affinity for different pollutants.[12] However, producing and regenerating AC is expensive and energy intensive,[12,13] making AC unsustainable and demonstrating the need for alternative adsorbents.

Cellulose, a renewable and biodegradable biopolymer, is a promising adsorbent for purifying water,[14,15] with researchers already employing it to adsorb dyes.[16,17] A major limitation of these cellulose-based materials, however, is the long contact times (i.e., min to h) required for effective adsorption.[18,19,20] To overcome this limitation, we designed rapidly forming, localized (i.e., not sample-spanning) hydrogels in Chapter 2, made by mixing anionic sulfated cellulose nanofibers (SCNFs) and cationic quaternized hydroxyethyl cellulose ethoxylate, which were effective for removing methylene blue (MB), a cationic dye, from water in only 30 s.[21] Because the dyeing

industry also discharges anionic dyes into the environment,[6] we were motivated to modify the hydrogel materials to rapidly adsorb other dyes.

In Chapter 3, we showed that cationic quaternized wood pulp (QWP) was an effective adsorbent for removing anionic perfluoroalkyl substances from water in under 30 s via electrostatic interactions.[22] Thus, we hypothesized that QWP-based adsorbents would rapidly adsorb anionic dyes, like the commonly used methyl orange (MO) dye, via electrostatic interactions. For this work, we were interested in using both localized hydrogels, similar to flocculating agents,[23] and QWP fibers alone, for future use in flow systems, to adsorb the anionic dye. WP was used to make the charged cellulose polyions in this chapter because WP is inexpensive relative to CNFs, which are derived from WP and require more energy-intensive production methods.[24,25] We report herein our initial efforts optimizing localized hydrogels, made from mixing anionic sulfated WP (SWP) and cationic QWP, for removing MO from water (Scheme 4.1). We also present preliminary findings using QWP fibers alone to adsorb MO. Lastly, we describe initial experiments synthesizing WP with primary amine groups for future use as an adsorbent, motivated by literature work showing that starches with primary and secondary amines have higher adsorption capacities for some dyes than quaternary amines.[26]

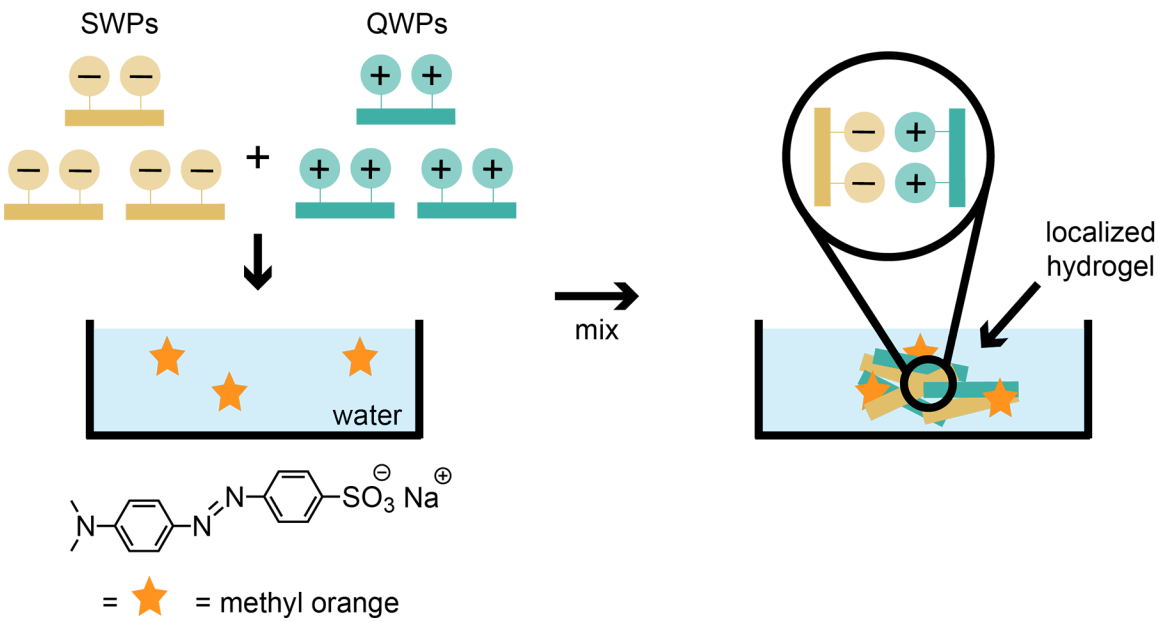

Scheme 4.1. A localized hydrogel forms via electrostatic interactions and adsorbs methyl orange when anionic SWPs and cationic QWPs are combined.

Experimental

Materials. Bleached hardwood pulp was generously donated by Cellulose Lab. Chlorosulfonic acid (CSA), anhydrous *N,N*-dimethylformamide (DMF), hydrochloric acid, sodium hydroxide (NaOH), 2-propanol (IPA), ethylene diamine (EDA), glycidyl trimethyl ammonium chloride (GMAC), methyl orange (MO), sodium nitrate, Whatman polyamide membrane filters (0.2 µm, 47 mm), and Whatman 1 filter paper (55 mm) were purchased from Aldrich and used without further purification. Absolute ethanol (EtOH), anhydrous dimethyl acetamide (DMA), triethylamine (TEA), toluenesulfonyl chloride (TsCl, Alfa Aesar), sodium chloride (NaCl), silver nitrate ($NaNO_3$), methanol, 20 mL vials, UV grade PMMA cuvettes (Globe Scientific), and disposable polypropylene 50 mL centrifuge tubes were purchased from Fisher and used without further purification. Deionized (DI) water (referred to as "Millipore water") was purified by a Millipore Synergy water purification system and used as the water source, unless otherwise noted. VWR grade 413 qualitative filter paper (5.5 cm) was purchased from VWR.

SWP synthesis. DI water from our house DI water system was used as the water source during synthesis and purification of SWP0.0, SWP0.53, and SWP1.7. Water purified by a Millipore Synergy water purification system was used as the water source during synthesis and purification of SWP0.83 and SWP1.1 and is referred to as "Millipore water."

The synthesis of SWPs was carried out similar to previous methods.[21] A 50 mL Schlenk flask with stir bar and 20 mL addition funnel were removed from the oven and assembled while hot. The addition funnel was capped with a septum, and the system was cooled to rt under N_2. Anhydrous DMF (26 mL) was added to the Schlenk flask, and the solvent was cooled in an ice-water bath for 10 min. Then, CSA (4 mL) was loaded into the addition funnel and added slowly over 5 min to the stirring DMF, with some HCl evolving. Once all the CSA was added, the addition funnel was removed and the Schlenk flask was capped, removed from the ice-water bath, and warmed to rt to provide a 2.0 M solution of CSA in DMF.

WPs (Table A3.1) were placed in an oven-dried round-bottom flask (note: a 100 mL flask was used when making SWP0.0, SWP0.53, and SWP1.7, but a 250 mL flask was used when making SWP0.83 and SWP1.1) with anhydrous DMF (Table A3.1), and the flask was capped with a septum. The mixture was soaked for 30–40 min under N_2 without stirring to wet the fibers. The septum was removed, and the mixture was then homogenized at a specified speed and time with an IKA T25 digital Ultra-Turrax (Table A3.1). The septum was added, and the WP was soaked for 10 min under N_2. The septum was removed, and the mixture was homogenized a second time at a specified speed and time (Table A3.1). Then, a stir bar was added, the septum was added, and the mixture was stirred for 30–40 min under N_2. A specified amount of the 2.0 M CSA in DMF was added to the WP mixture dropwise over 2 min. The mixture was stirred for 20 min once all the

CSA was added. Then, the reaction was quenched with methanol (~5–20 mL), and the mixture was stirred for 5 min.

SWP0.0, SWP0.53, and SWP1.7 purification. The mixture was poured into a 250 mL centrifuge bottle, and the bottle was filled to ~90% capacity with DI water. The mixture was centrifuged at ~34,000 × g for ~25 min using a Sorvall RC5C Plus centrifuge. The supernatant was discarded via pouring, and fresh DI water was added to fill the bottle to ~90% capacity. Then a ~0.1 M NaOH solution was used to increase the pH to 7, as measured with pH paper. The mixture was centrifuged again at ~34,000 × g for ~25 min. The supernatant was discarded via pouring, and fresh DI water was added to fill the bottle to ~90% capacity. The mixture was shaken by hand and then centrifuged a third time at ~34,000 × g for 25 min.

SWP0.83 and SWP1.1 purification. The mixture was filtered over Whatman 1 filter paper, and the fibers were rinsed with Millipore water (1 × 30 mL). The fibers were then divided into two 50 mL polypropylene centrifuge tubes. Millipore water was added to fill the tubes (~45 mL in each tube), the tubes were centrifuged at 3260 × g for 5 min using a Thermo Scientific Sorvall ST8 centrifuge, and then the supernatant was discarded via pouring. This process is defined as 1 centrifuge cycle, and the process was repeated once more. After the 2nd cycle, the pH of the supernatant was examined using pH paper and found to be ~3. The supernatant was discarded, and fresh Millipore water was added to each tube (~45 mL in each tube). Then, a ~0.1 M NaOH solution was used to increase the pH to 7, as measured with pH paper. The tubes were centrifuged at 3260 × g for 5 min, the supernatant was discarded via pouring, and fresh Millipore was added to each tube (~45 mL in each tube). The pH of the supernatant was found to be ~4 using pH paper, and the ~0.1 M NaOH solution was used to increase the pH to 7, as measured with pH paper. Then, two additional centrifuge cycles were performed.

Isolation of fibers. The fibers were then isolated using one of the following two procedures. (i) If a white, gel-like mass remained in the centrifuge bottle/tube, the supernatant was discarded via pouring, and the material was transferred to 20 mL glass vials, frozen in liquid N_2, and dried under vacuum on a Schlenk line to remove excess water. (This procedure was used for SWP0.83, SWP1.1, and SWP1.7.) (ii) If the fibers did not form a gel-like mass in the centrifuge bottle/tube, ~90% of supernatant was discarded via pouring, and the remaining mixture was vacuum filtered using a Whatman polyamide membrane filter (0.2 μm, 47 mm). The fibers on the filter were then rinsed once with DI water (5 mL), and placed in 20 mL glass vials, frozen in liquid N_2, and dried under vacuum on a Schlenk line to remove excess water. (This procedure was used for SWPs 0.0 and 0.53.)

QWP synthesis. Millipore water was used in the synthesis and purification of QWPs.

The synthesis of QWPs was carried out similar to previous methods.[22] WP (Table A3.2) was combined with Millipore water (Table A3.2) in either a 20 mL vial (for QWP1.6) or 100 mL round-bottom flask (for QWP0.77, QWP1.2, and QWP1.3). The fibers were soaked for 10–15 min without stirring to wet the fibers, and then, the mixture was homogenized at 18k rpm for 2 min. For all samples besides QWP1.6, the fibers went through a second homogenization cycle because they were not uniformly distributed in the mixture like the QWP1.6 fibers. To perform this 2nd cycle, the fibers were first soaked without stirring for 5 min while the homogenizer was disassembled, cleaned with water and acetone to remove any clogged fibers, and reassembled. Then, the mixture was homogenized again at 18k rpm for 2 min.

The mixture was divided into two 50 mL polypropylene centrifuge tubes (note: for QWP1.6, only one tube was used) and water was added to fill the tubes (~45 mL in each tube). The tubes were centrifuged at 2580 × g for 4 min, and the supernatant was discarded via pouring. The WP

from each tube was combined into a round-bottom flask (note: a 50 mL round-bottom flask was used when making QWP1.6, but 100 mL round-bottom flasks were used when making QWP0.77, QWP1.2, and QWP1.3). 2-Propanol (IPA, Table A3.2) was added to the flask along with NaOH (Table A3.2) and a stir bar. The flask was then heated to 50 °C on a heating block and stirred for 45 min. After this time, a known volume of glycidyl trimethyl ammonium chloride (GMAC, Table A3.2) was added with a micropipette over 4 min to the reaction, and the mixture was stirred for 2.25 h. Then, the round-bottom flask was removed from the heating block and cooled with stirring in ice-water for 5 min. The reaction was quenched with aq. HCl (5 M, ~3 mL) and stirred for 5 min. The mixture was vacuum filtered using VWR grade 413 filter paper and rinsed with Millipore water (1×50 mL).

QWP purification. The fibers were then divided into two 50 mL polypropylene centrifuge tubes (note: only 1 tube for QWP1.6). Millipore water was added to fill the tubes (~45 mL in each tube), and then, the tubes were centrifuged at 3260 × g for ~10 min. The supernatant was discarded via pouring. This process was defined as 1 centrifuge cycle, and this centrifuging process was repeated 2–3 more times to remove excess acid and ions from the fibers. After the 3rd cycle, the pH of the supernatant was examined using pH paper and found to be ~7. In addition, after the 3rd cycle (QWP0.77 and QWP1.2) or 4th cycle (QWP1.3 and QWP1.6), the supernatant from one of the tubes was vacuum filtered, and the conductivity of the solution was measured. If the conductivity was less than or equal to 25 μS/cm, the fiber purification was considered done. If the conductivity was above 25 μS/cm, the centrifuge cycling was repeated until the supernatant could be filtered and measured to have a conductivity less than or equal to 25 μS/cm. See Table A3.2 for the number of centrifuge cycles used to purify each QWP sample. After the fibers were purified, the fibers

were removed from the centrifuge tubes with a spatula, placed in 20 mL vials, frozen in liquid N_2, and dried under vacuum on a Schlenk line to remove excess water.

PWP Synthesis. Millipore water was used in the synthesis of PWPs.

The synthesis of PWPs was carried out similar to literature.[27] WP (300.0 mg) was combined with anhydrous DMA (40.0 mL) in a 100 mL round-bottom flask (labelled as "rxn 1"), and the flask was capped with a septum. The mixture was placed under N_2 for 10 min without stirring to wet the fibers. Then, the septum was removed, and the mixture was homogenized at 20k rpm for 3–5 min. A stir bar was added to the flask, the flask was recapped with a septum, and the flask was placed under N_2 atmosphere. For all samples except PWP6, TEA (Table A3.3) was added dropwise over 1 min to the mixture with stirring at rt. The mixture was then cooled with an ice-water bath for 5 min. For PWP6, the flask was placed in an IPA bath cooled to 0 °C with a Thermo Scientific Neslab CC100 Immersion cooler (because the reaction would be cooled overnight). After 5 min, TEA (Table A3.3) was added dropwise over 1 min with stirring to the mixture.

Meanwhile, TsCl (Table A3.3) was dissolved in anhydrous DMA (5.0 mL) in a 20 mL vial. The TsCl/DMA solution was then added dropwise with pipette over 1 min to the cooled flask containing WP and TEA. For all samples except PWP6, the reaction flask was then removed from the ice-water bath and stirred at rt for ~16–18 h under N_2. For PWP6, the reaction flask was left in the 0 °C bath and stirred for ~16 h under N_2.

To quench the reaction, the mixture was poured into ice water (~50 mL). Then, the mixture was vacuum filtered with Whatman 1 filter paper (55 mm), followed by washing the fibers with Millipore water (3×50 mL), acetone (1×50 mL), ethanol (2×50 mL), and diethyl ether (2×50 mL).

Next, the fibers were placed in a new 100 mL round-bottom flask (labelled as "rxn 2") with a stir bar and anhydrous DMA (40.0 mL). The mixture was stirred for 2 min to disperse the fibers.

The flask was heated to 85 °C with stirring. EDA (Table A3.3) was then added dropwise to the mixture over 1 min. A reflux condenser was attached to the flask, capped with septum, and the mixture was placed under N_2. For all samples except PWP7, the mixture was refluxed at 85 ºC for 5–6 h. For PWP7, the mixture was refluxed at 85 ºC for 23 h. After the reflux time, the mixture was cooled to rt and vacuum filtered on Whatman 1 filter paper. The fibers were washed with EtOH (3×50 mL) and diethyl ether (50 mL).

SWP conductometric titrations. Conductometric titrations were carried out according to the charge density measurements in Appendix 1. A known amount of SWPs (typically about 35 mg) was placed in a 20 mL vial with 0.1 M aq. HCl (15 mL) and a stir bar. The vial was capped and stirred for 90 min to protonate the SWPs. The mixture was then filtered over a polyamide membrane using vacuum filtration. The solids were rinsed with Millipore water (~20 mL), and the conductivity of the filtrate was measured by a Thermo Scientific Orion Star A215 pH/conductivity meter. If the conductivity was >10 μS/cm, the filtrate was discarded via pouring, and the solids were rinsed with additional 20 mL portions of Millipore water until the conductivity of the filtrate was <10 μS/cm. The resulting solids were added to a tared 150 mL beaker, followed by DI water (~20 mL) and a stir bar. The mixture was covered with weigh paper (of known mass), stirred for at least 5 min to uniformly disperse the solids, and then the stir bar was removed. The mixture was weighed to determine the total mass of the protonated SWP mixture. Then, two aliquots of the mixture were removed, placed in separate tared 20 mL vials, accurately weighed (~2.5 g), and dried in a 110 °C oven. For all samples (except SWP0.0), the mass of solids in each aliquot was used to determine the concentration of solids in the protonated SWP mixture. For SWP0.0, the mass of solids in each aliquot overestimated the amount of fibers that were present (likely because

the fibers were non-uniformly clumped together in the mixture), so the aliquot masses were subtracted from the initial amount of SWP0.0 used to give a total amount of titrated SWP0.0 fibers.

A stir bar and recorded volume (~100 mL) of 1 mM NaCl were then added to the beaker containing the protonated SWP mixture. The mixture was titrated, with stirring, by adding a volume with known concentration of NaOH solution (~0.01 M) to the protonated SWP mixture and measuring the conductivity of the mixture 40 s after each addition of titrant. (The concentration of the NaOH solution was determined using the calibrated pH meter prior to the titration.) The volume-corrected conductivity[28] was plotted as a function of the volume of NaOH added, and the equivalence point was determined by the intersection of the linear least-squares regression lines from the positively and negatively sloped regions of the curve (Figure A3.1). Based on the mmol of NaOH added, the mmol of SO_3^- were calculated. The charge density was found by dividing the mmol SO_3^- by the mass of SWP that was titrated. This procedure was repeated, and the average is reported as the sample's charge density (Table A3.4). Throughout Chapter 4 and Appendix 3, SWP samples will be identified by material type followed by the charge density (e.g., SWP0.53 is a SWP with a charge density of 0.53 mmol SO_3^-/g).

QWP conductometric titrations. Conductometric titrations were carried out according to the charge density measurements in Appendix 2. First, a 10.0 mM $AgNO_3$ solution was made by dissolving $AgNO_3$ (34.0 mg, 0.200 mmol) in Millipore water (20.0 mL). A 100 mM $NaNO_3$ solution was prepared by dissolving $NaNO_3$ (170.0 mg, 2.000 mmol) in Millipore water (20.0 mL).

Next, a known amount of QWPs (typically about 50 mg) were combined with Millipore water (50.0 mL) in a 150 mL beaker and soaked for 10 min. The fibers were homogenized at 18k rpm for 2 min to disperse the fibers, and then additional Millipore water (50.0 mL) and a stir bar were added to the beaker. Note: water was added in 2 × 50 mL portions to the beaker because 1 × 100

mL sprays water when homogenized. The beaker was placed on a stir plate, a conductivity meter was inserted into the mixture, and the mixture was stirred. Then, 100 mM $NaNO_3$ solution (1.0 mL) was added to the beaker to increase the conductivity of the mixture to a stable, non-fluctuating level, and the mixture was equilibrated for ~5 min. The mixture was then titrated using the 10.0 mM $AgNO_3$ solution by adding aliquots (~100–400 μL) to the mixture over 10 s every 40 s. The conductivity was recorded as a function of the volume of 10.0 mM $AgNO_3$ added. Then, the volume-corrected conductivity was plotted as a function of the volume of 10.0 mM $AgNO_3$ added, and the equivalence point was determined by the intersection of the linear least-squares regression lines from the flat and positively sloped regions of the curve (Figure A3.2). Based on the mmol of $AgNO_3$ added, the mmol of R_3N^+ present were calculated assuming a one-to-one ratio between Ag^+ and Cl^- (note: adding $NaNO_3$ did not affect the titration results because Na^+ and NO_3^- ions are not involved in the titration reaction between Ag^+ and Cl^-, which form the precipitate AgCl). The charge density was found by dividing the mmol $AgNO_3$ by the mass of QWP that was titrated. This procedure was repeated two times for each QWP sample, and the average is reported as the sample's charge density (Table A3.5). Throughout Chapter 4 and Appendix 3, QWP samples are identified by their charge density (e.g., QWP1.6 is a sample with a charge density of 1.6 mmol - NR_3^+/g).

PWP conductometric titrations. PWP titrations were carried out similar to literature.[29] A known amount of PWP (typically about 100 mg) was added to a 150 mL beaker with Millipore water (100 mL) and a stir bar. The mixture was stirred, and a previously calibrated pH meter was inserted into the mixture. Using ~0.1 M HCl, the pH of the mixture was adjusted to ~3, and the mixture was stirred for 25 min. The pH meter was removed (because drift was observed during titrations when the pH meter was left in the beaker), and the conductivity meter was inserted. The

mixture was titrated, with stirring, by adding a volume with known concentration of NaOH solution (~0.01 M) to the PWP mixture over 5 s and measuring the conductivity of the mixture 35 s after each addition of titrant. (The concentration of the NaOH solution was determined using the calibrated pH meter prior to the titration.) The volume-corrected conductivity[28] was plotted as a function of the volume of NaOH added, and 2 equivalence points were found: the first represents titration of excess acid and the second represents titration of primary amines (Figure A3.3). The first equivalence point was determined by the intersection of the linear least-squares regression lines from the negatively and flat sloped regions of the curve, and the second equivalence point was ascertained from the intersection of the linear least-squares regression lines from the positively and flat sloped regions of the curve. The first equivalence point was subtracted from the second equivalence point to obtain the volume of ~0.01 M NaOH required to titrate the primary amines. Based on the mmols of NaOH added, the mmol of $-NH_3^+$ were calculated. The charge density was found by dividing the mmol $-NH_3^+$ by the mass of PWP that was titrated. This procedure was repeated for PWP2 only, and the average is reported as the sample's charge density (Table A3.6).

General preparation of MO solutions and SWP and QWP mixtures. MO solutions (3.1 mM) were made by dissolving either 12.5 mg MO (38.2 μmol) in 12.5 mL of Millipore water or 8.0 mg MO (24.4 μmol) in 8.0 mL of Millipore water in a 50 mL polypropylene centrifuge tube. Bath sonication (~2 min) was used to dissolve the MO.

SWP and QWP mixtures were made by first soaking a known mass of SWP or QWP in a known volume of Millipore water in a 20 mL vial for 5 min. Then, the mixture was homogenized at 18k rpm for 1 min to generate SWP or QWP mixtures with known concentrations.

General procedure for adsorbing MO with SWP/QWP gels. A 75.0 μL portion of 3.1 mM MO solution was added to a 50 mL polypropylene centrifuge tube with 1.925 mL of Millipore

water. Then, 4.0 mL of a SWP mixture and 4.0 mL of a QWP mixture, both with known concentrations, were added simultaneously via syringe to the centrifuge tube over a recorded time while vortex mixing at a speed setting of 1.5. The centrifuge tube was vortex mixed for an "additional" mixing time using a speed setting of 1.5. The centrifuge tube was then removed from the vortex mixer, and a gel was formed if the following criteria were met: (1) There was one cohesive hydrogel with minimal amounts of small polyionic complexes that were not connected to the gel. (2) The centrifuge tube could be rotated 90° from a vertical to horizontal position without the localized gel breaking into smaller complexes. An aliquot of leftover solution was removed from the centrifuge tube, placed in a disposable PMMA cuvette, and the absorbance spectrum of the solution from 400–750 nm was obtained. The UV-vis measurement was performed within 2 min of the gel being formed.

A baseline correction was performed on all MO absorbance spectra to account for non-zero baselines. More specifically, the absorbance values for wavelengths 740–750 nm were averaged (because 740–750 nm was a region where the spectrum's absorbance was closest to 0), and this average absorbance was then subtracted from the entire spectrum. The corrected absorbance at 464 nm was then recorded for each MO solution. The concentration (C, μM) of MO that was not adsorbed by a gel was determined using the MO calibration curve (Figure A3.4).

The MO adsorption % was then determined using the following equation:

$$\text{MO adsorption \%} = \frac{C_0 - C}{C_0} \text{ x } 100$$

Equation 4.1. Calculating MO adsorption %.

where C_0 was the initial MO concentration (23 μM) in the centrifuge tube. The initial MO concentration was determined by calculating the mols of MO initially added to the centrifuge tube and using a total volume of 10 mL.

All MO adsorption experiments were performed in triplicate, unless noted, and average MO adsorption % values from the 3 trials are reported for each set of experimental conditions.

Results and Discussion

To test the hypothesis that WP-based hydrogels would rapidly adsorb MO, we first synthesized SWPs and QWPs by separately reacting WP with varying amounts of chlorosulfonic acid (CSA) and glycidyl trimethyl ammonium chloride (GMAC), respectively, according to previously developed methods (Scheme 4.2).[21,22] SWPs with charge densities (CDs) of 0.0–1.7 mmol SO_3^-/g and QWPs with CDs of 0.77–1.6 mmol NR_3^+/g were generated, as determined by conductometric titrations (samples are denoted by material type followed by charge density: e.g., SWP0.53 is a SWP sample with CD of 0.53 mmol SO_3^-/g). Previous reports on cellulose and WP functionalization suggest that sulfate and quaternary amine groups are located primarily on the C2 and C6 positions of the glucose repeat unit.[30,31,32]

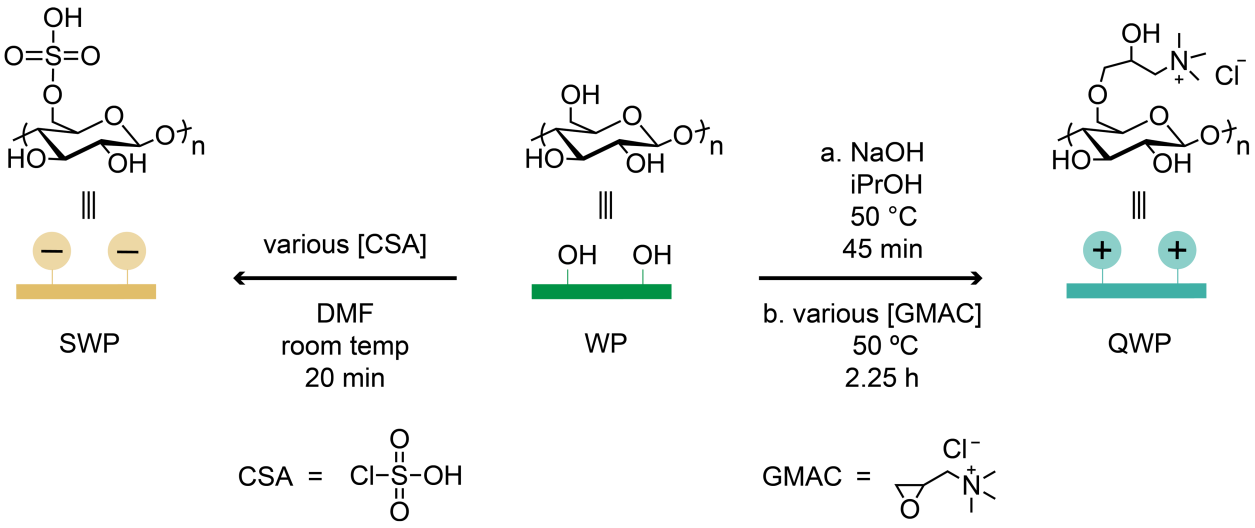

Scheme 4.2. Synthesis conditions for generating sulfated wood pulp (SWP) and quaternized wood pulp (QWP).

When anionic WP mixtures were mixed simultaneously with cationic QWP mixtures and MO solutions, localized hydrogels that adsorbed MO were formed within 30 s (Figure 4.1A). We hypothesized that hydrogels utilizing high charge density QWPs would remove the most MO from water because more cationic sites would be available for electrostatic interactions with MO. To test this hypothesis, MO adsorption was monitored on hydrogels made with SWP0.83 and either QWP0.77 or QWP1.6 (Figure 4.1B). Unexpectedly, we observed that 64 ± 3% and 61 ± 2% of MO was adsorbed in hydrogels made with QWP0.77 or QWP1.6, respectively, indicating that QWP charge density plays a negligible role in determining adsorption efficiency. Therefore, we hypothesized that hydrogels utilizing high charge density SWPs would remove less MO because SWPs are competing with MO for cationic sites on QWPs and more SWP-QWP electrostatic crosslinking causes fewer MO-QWP electrostatic interactions. By monitoring MO adsorption on hydrogels made with SWP1.7 and either QWP0.77 or QWP1.6, we found that 54 ± 3% of MO was adsorbed regardless of which QWP was used. Contrary to our hypothesis, this result demonstrates that SWP charge density plays a negligible role in removing MO because adsorption % remained approximately constant despite doubling the SWP CD.

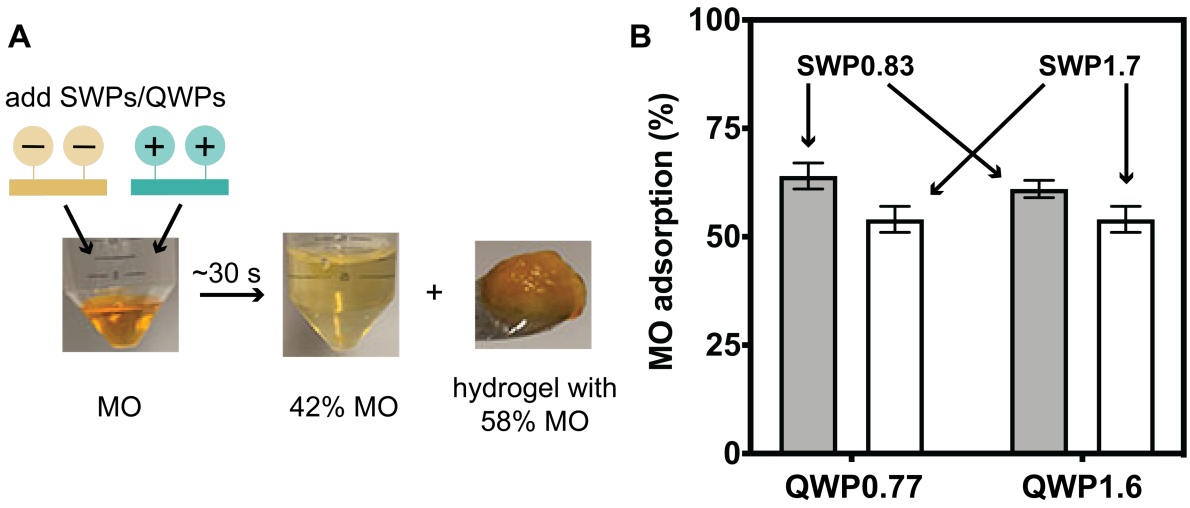

Figure 4.1. (A) Adding SWP and QWP mixtures to a MO solution results in a hydrogel that adsorbs MO. ([MO] = 23 µM; [SWP0.83] = 0.60 mg/mL; [QWP1.6] = 0.80 mg/mL). (B) MO adsorption (%) as a function of SWP and QWP charge density.

To increase the MO % adsorbed by hydrogels in short time frames, the QWP concentration was increased in hydrogels while keeping the mass ratio between SWP0.83:QWP0.77 constant at 0.75 (Figure 4.2A). We observed that small QWP0.77 concentrations of 0.2 mg/mL exhibited 29% MO adsorption and increasing the QWP concentration to 1.6 mg/mL resulted in 75% MO adsorption. Adsorption plateaued near 80% above QWP concentrations of 1.6 mg/mL. These results indicate that more dye can be adsorbed in hydrogels with higher QWP concentrations, but a maximum amount of dye can be adsorbed for a given mass ratio, likely because many SWPs are competing with MO for accessible binding sites on a single QWP. Thus, we hypothesized that decreasing the SWP:QWP mass ratio in hydrogels would result in higher MO adsorption %. To test this hypothesis, MO adsorption was monitored on hydrogels made with varying SWP0.83 amounts and a QWP0.77 concentration of 1.6 mg/mL (Figure 4.2B). We observed that 70% of MO was adsorbed when a SWP0.83:QWP0.77 mass ratio of 1 was used to make a hydrogel. Decreasing the mass ratio to 0.25 and 0.063 resulted in 85 and 81% of MO adsorbed, respectively.

As expected, these initial results demonstrated that higher MO adsorption occurred in hydrogels when fewer SWPs were present for crosslinking with QWPs and a greater number of cationic sites were available for interaction with dye. However, further experiments are necessary to determine if the differences in adsorption %, stemming from different mass ratios, are significant. Additionally, we propose that longer contact times, allowing dye diffusion into the hydrogel, may result in higher removal efficiencies.

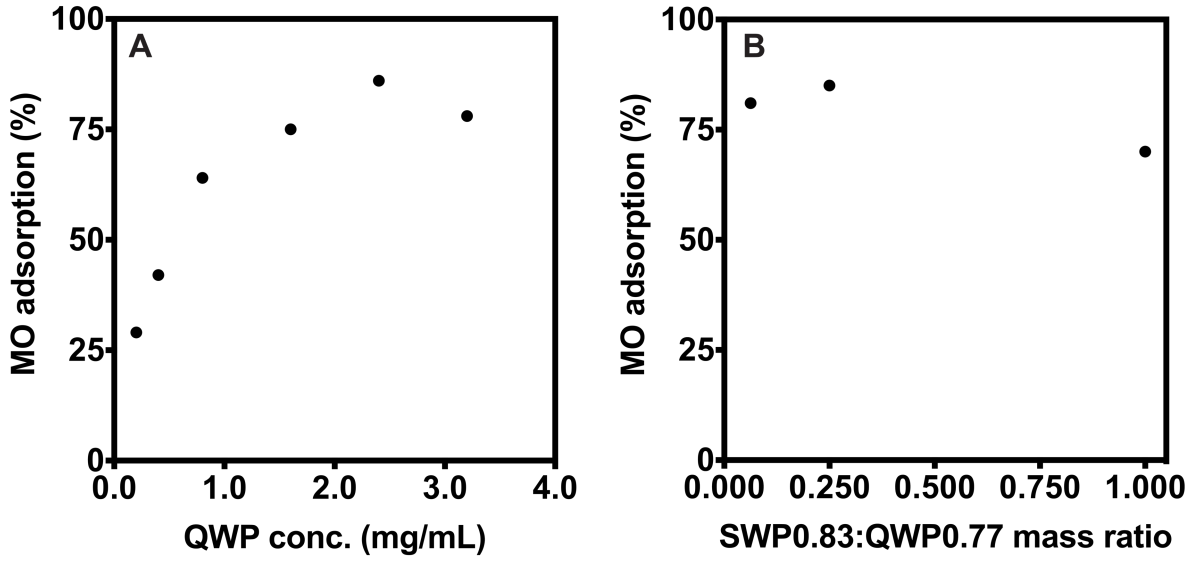

Figure 4.2. (A) MO adsorption (%) as a function of QWP concentration (mg/mL). The mass ratio of SWP0.83:QWP0.77 was constant at 0.75. (B) MO adsorption (%) as function of SWP0.83:QWP0.77 mass ratio. The QWP concentration was fixed at 1.6 mg/mL.

To further evaluate the influence of electrostatic crosslinking on MO adsorption with hydrogels and begin examining dye removal with QWP fibers alone, we investigated MO adsorption on unfunctionalized WP, SWP, and QWP fibers individually (Table A3.11). We observed that cationic QWP1.6 and QWP0.77 adsorbed 73 ± 1% and 82 ± 1% of MO, respectively. We speculate that QWP1.6 adsorbed less MO than QWP0.77 because the dye molecular size is greater than the distance between neighboring cationic groups, leading to steric blocking of cationic sites.[26] Further

studies are needed to support this explanation. On the other hand, unfunctionalized WP and anionic SWP1.1 adsorbed negligible amounts of MO. Together, these results indicated that MO adsorption is electrostatically driven because cationic WP adsorbed more dye than unfunctionalized and anionic WP. Finally, because individual cationic WPs adsorbed more MO than gels formed with SWPs (~64%, Figure 4.1B), SWP-QWP electrostatic crosslinking is likely reducing MO adsorption in hydrogels. This observation also suggests that cationic WP fibers alone may be more effective than hydrogels for adsorbing anionic dyes. Future studies examining properties such as adsorption capacity, which describes the amount of dye adsorbed per mass of cellulose, are necessary to understand the advantages of hydrogels and cationic WP fibers.

In a previous report, Khalil et al. showed that starches with charged primary and secondary amines have higher adsorption capacities for some dyes than quaternary amines due to reduced steric hindrance between the charged amines and dyes.[26] Thus, we were interested in installing various amounts of primary amine groups on WP to enhance dye adsorption in rapidly forming hydrogels. Here, we describe initial attempts at synthesizing primary amine WPs (PWPs) with a range of charge densities (mmol NH_3^+/g). In the first reaction performed, we generated a baseline for synthesizing PWPs by first reacting unfunctionalized WP with triethylamine (TEA) and p-toluenesulfonyl chloride (TsCl) in anhydrous dimethylacetamide (DMA) to generate tosylated WPs (TWPs). In the second step, TWPs were reacted with ethylene diamine (EDA), resulting in a PWP with a charge density of 0.15 mmol NH_3^+/g (PWP1, Table 4.1).[33] We then hypothesized that PWPs with higher charge densities could be synthesized using larger reagent concentrations, assuming bimolecular reactions were occurring. We observed that performing the reaction with larger concentrations of TEA and TsCl, separately, resulted in WP with more amines installed, as demonstrated by the higher CDs for these samples (PWP2 and PWP4). On the other hand,

increasing the concentration of EDA did not increase the amine content on WP (PWP3), suggesting that the reaction with TEA and TsCl is the limiting step. Performing a reaction with increased concentrations of both TEA and TsCl provided a PWP with the highest charge density of 0.20 mmol NH_3^+/g (PWP4). These results indicated that TEA and TsCl influence PWP synthesis more than EDA, likely because EDA only reacts with TWP at tosylated sites. Future studies using higher concentrations of TEA and TsCl should be performed to determine if PWPs with higher charge densities can be synthesized. To further optimize PWP synthesis, we examined the role of temperature during the tosylation reaction and time for the EDA reaction. Because McCormick and coworkers demonstrated that low temperatures (0–10 ºC) suppress chlorodeoxycellulose formation during cellulose tosylation,[34] we hypothesized that using a lower reaction temperature would lead to more efficient tosylation and higher charge density PWPs. We found that performing the tosylation reaction at 0 ºC resulted in no increase in amines installed on WP relative to the baseline reaction (PWP6). Additionally, increasing the EDA reaction time from ~5–6 to 23 h provided no additional amines on the WP (PWP7). These results suggest other factors such as lower tosylation reaction temperatures (<0 ºC) and longer tosylation reaction times (>17 h) need to be explored to increase the range of primary amines functionalized on WP. Finally, because PWPs with a limited range of charge densities were accessed (0.14–0.20 mmol NH_3^+/g), the roles of various reaction conditions are inconclusive.

Table 4.1. Reaction conditions for optimizing PWP synthesis.

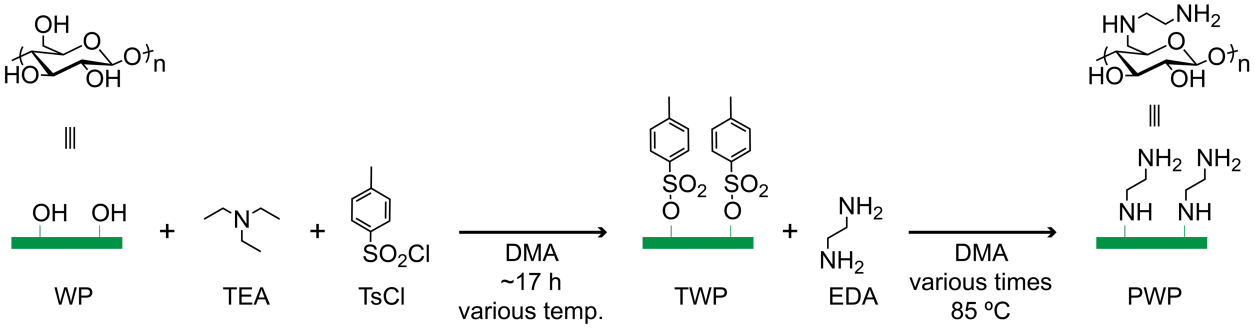

sample	[TEA] (mM)	[TsCl] (mM)	TsCl rxn temp (ºC)	[EDA] (mM)	EDA rxn time (h)	charge density (mmol NH_3^+/g)
PWP1	137	68.6	25	221	~5–6	0.15
PWP2	137	137	25	221	~5–6	0.18 ± 0.01
PWP3	137	68.6	25	436	~5–6	0.15
PWP4	269	67.3	25	221	~5–6	0.17
PWP5	269	135	25	221	~5–6	0.20
PWP6	269	135	0	221	~5–6	0.14
PWP7	269	135	25	221	23	0.17

Conclusions

In conclusion, we demonstrated that QWP-based hydrogels and fibers rapidly adsorb methyl orange, an anionic dye, within seconds. We discovered that MO adsorption is driven by electrostatic interactions with QWPs, and crosslinking between the anionic and cationic WP leads to reduced MO adsorption in hydrogels. QWP fibers alone adsorbed more MO than gels, indicating that cationic cellulose fibers are promising adsorbents for anionic dye. Future work will optimize MO adsorption on QWP-based hydrogels and fibers to demonstrate that cationic WP is a viable alternative to current adsorbents. Furthermore, we anticipate that the hydrogels described here may be useful flocculating agents for water purification.[23] Additionally, we described initial attempts installing primary amine groups on WPs but the roles of various reaction conditions were inconclusive because PWPs were produced with a small range of charge densities. Future work

will identify optimized reaction conditions for generating PWPs and determine if PWPs effectively adsorb dyes.

References

(1) Boretti, A.; Rosa, L. Reassessing the projections of the world water development report. *npj Clean Water* **2019**, *2*.

(2) The World Bank. The Bangladesh responsible sourcing initiative: a new model for green growth? https://openknowledge.worldbank.org/handle/10986/20764 (accessed May 3, **2021**).

(3) Kant, R. Textile dyeing industry an environmental hazard. *Natural Science* **2012**, *4*, 22–26.

(4) Chequer, F.M.D.; de Oliveira, G.A.R.; Ferraz, E.R.A.; Cardoso, J.C.; Zanoni, M.V.B.; de Oliveira, D.P. Textile dyes: dyeing process and environmental Impact. In *Eco-friendly textile Dyeing and Finishing*; Gunay, M., Ed.; IntechOpen, **2013**.

(5) Yaseen, D.A.; Scholz, M. Textile dye wastewater characteristics and constituents of synthetic effluents: a critical review. *Int. J. Environ. Sci. Technol.* **2019**, *16*, 1193–1226.

(6) Khan, S.; Malik, A. Environmental and health effects of textile industry wastewater. In *Environmental deterioration and human health*; Malik, A., Akhtar, R., Grohmann, E., Eds.; Springer, **2014**.

(7) *Impact of textile dyes on public health and the environment*; Wani, K., Jangid, N., Bhat, A., Eds; IGI Global, **2019**.

(8) Ahmad, A.; Mohd-Setapar, S.; Chuong, C.; Khatoon, A.; Wani, W.; Kumar, R.; Rafatullah, M. Recent advances in new generation dye removal technologies: novel search for approaches to reprocess wastewater. *RSC Adv.* **2015**, *5*, 30801–30818.

(9) Hassan, M.; Carr, C. A critical review on recent advancements of the removal of reactive dyes from dyehouse effluent by ion-exchange adsorbents. *Chemosphere* **2018**, *209*, 201–219.

(10) Vikrant, K.; Giri, B.; Raza, N.; Roy, K.; Kim, K.; Rai, B.; Singh, R. Recent advancements in bioremediation of dye: current status and challenges. *Bioresour. Technol.* **2018**, *253*, 355–367.

(11) Yagub, M.; Sen, T.; Afroze, S.; Ang, H.M. Dye and its removal from aqueous solution by adsorption: a review. *Adv. Colloid Interface Sci.* **2014**, *209*, 172–184.

(12) Pollard, S.; Fowler, G.; Sollars, C.; Perry, R. Low-cost adsorbents for waste and wastewater treatment: a review. *Sci. Total. Environ.* **1992**, *116*, 31–52.

(13) Miguel, G.S.; Lambert, S.D.; Graham, N.J.D. The regeneration of field-spent granular activated carbons. *Water Res.* **2001**, *35*, 2740–2748.

(14) Hokkanen, S.; Bhatnagar, A.; Sillanpaa, M. A review on modification methods to cellulose-based adsorbents to improve adsorption capacity. *Water Res.* **2016**, *91*, 156–173.

(15) Mohammed, N.; Grishkewich, N.; Tam, K.C. Cellulose nanomaterials: promising sustainable nanomaterials for application in water/wastewater treatment processes. *Environ. Sci.: Nano* **2018**, *5*, 623–658.

(16) Salleh, M.; Mahmoud, D.; Karim, W.; Idris, A. Cationic and anionic dye adsorption by agricultural solid wastes: a comprehensive review. *Desalination* **2011**, *280*, 1–13.

(17) Varghese, A.; Paul, S.; Latha, M. Remediation of heavy metals and dyes from wastewater using cellulose-based adsorbents. *Environ. Chem. Lett.* **2019**, *17*, 867–877.

(18) Mohammed, N.; Grishkewich, N.; Berry, R.; Tam, K.C. Cellulose nanocrystal–alginate hydrogel beads as novel adsorbents for organic dyes in aqueous solutions. *Cellulose* **2015**, *22*, 3725–3738.

(19) Jin, L.; Li, W.; Xu, Q.; Sun, Q. Amino-functionalized nanocrystalline cellulose as an adsorbent for anionic dyes. *Cellulose* **2015**, *22*, 2443–2456.

(20) Chen, Y.; Liu, H.; Geng, B.; Ru, J.; Cheng, C.; Zhao, Y.; Wang, L. A reusable surface quaternized nanocellulose-based hybrid cryogel loaded with N-doped TiO2 for self-integrated adsorption/photo-degradation of methyl orange dye. *RSC Adv.* **2017**, *7*, 17279–17288.

(21) Harris, J.; McNeil, A. Localized hydrogels based on cellulose nanofibers and wood pulp for rapid removal of methylene blue. *J. Polym. Sci.* **2020**, *58*, 3042–3049.

(22) Harris, J.; Devlin, A.; McNeil, A. Rapid removal of poly- and perfluoroalkyl substances with quaternized wood pulp. *Submitted*.

(23) Wilts, E.; Herzberger, J.; Long, T. Addressing water scarcity: cationic polyelectrolytes in water treatment and purification. *Polym. Int.* **2018**, *67*, 799–814.

(24) Tejado, A.; Alam, M.; Antal, M.; Yang, H.; van de Ven, T. Energy requirements for the disintegration of cellulose fibers into cellulose nanofibers. *Cellulose* **2012**, *19*, 831–842.

(25) Osong, S.; Norgren, S.; Engstrand, P. Processing of wood-based microfibrillated cellulose and nanofibrillated cellulose, and applications relating to papermaking: a review. *Cellulose* **2016**, *23*, 93–123.

(26) Khalil, M.; Aly, A. Use of cationic starch derivatives for the removal of anionic dyes from textile effluents. *J. Appl. Polym. Sci.* **2004**, *93*, 227–234.

(27) Pereira, A.; Soares, L.; Teodoro, F.; Elias, M.; Ferreira, G.; Savedra, R.; Siqueira, M.; Martineau-Corcos, C.; da Silva, L.; Prim, D.; Gurgel, L. Aminated cellulose as a versatile adsorbent for batch removal of As(V) and Cu(II) from mono- and multicomponent aqueous solutions. *J. Colloid Interface Sci.* **2020**, *576*, 158–175.

(28) Garcia, J.; Schultz, L. Determination of sulfate by conductometric titration: and undergraduate laboratory experiment. *J. Chem. Educ.* **2016**, *93*, 910–914.

(29) Akhlaghi, S.; Zaman, M.; Mohammed, N.; Brinatti, C.; Batmaz, R.; Berry, R.; Loh, W.; Tam, K. Synthesis of amine functionalized cellulose nanocrystals: optimization and characterization. *Carbohydr. Res.* **2015**, *409*, 48–55.

(30) Eyley, S.; Thielemans, W. Surface modification of cellulose nanocrystals. *Nanoscale* **2014**, *6*, 7764–7779.

(31) Stratz, J.; Liedmann, A.; Heinze, T.; Fischer, S.; Groth, T. Effect of sulfation route and subsequent oxidation on derivatization degree and biocompatibility of cellulose sulfates. *Macromol. Biosci.* **2020**, *20*, 1900403.

(32) de la Motte, H.; Westman, G.; Regioselective cationization of cellulosic materials using an efficient solvent-minimizing spray-technique. *Cellulose* **2012**, *19*, 1677–1688.

(33) Pereira, A.; Soares, L.; Teodoro, F.; Elias, M.; Ferreira, G.; Savedra, R.; Siqueira, M.; Martineau-Corcos, C.; da Silva, L.; Prim, D.; Gurgel, L. Aminated cellulose as a versatile adsorbent for batch removal of As(V) and Cu(II) from mono- and multicomponent aqueous solutions. *J. Colloid Interface Sci.* **2020**, *576*, 158–175.

(34) McCormick, C.; Dawsey, T.; Newman, J. Competitive formation of cellulose p-toluenesulfonate and chlorodeoxycellulose during homogeneous reaction of p-toluenesulfonyl chloride with cellulose in N,N-dimethylacetamide-lithium chloride. *Carbohydr. Res.* **1990**, *208*, 183–191.

Chapter 5 Conclusions and Future Directions

Despite the United Nation's plan to "ensure availability and sustainable management of water and sanitation for all,"[1] communities struggle with water pollution, especially in Michigan.[2] For example, a recent water crisis in Flint, Michigan exposed thousands of people to harmful levels of poisonous lead.[3] Additionally, toxic poly-/perfluoroalkyl substances (PFASs) have been discovered in water across Michigan,[4,5] despite the state adopting strict maximum contaminant levels for two prevalent PFASs, perfluorooctanesulfonic acid (PFOS) and perfluorooctanoic acid (PFOA).[6]

Thus, it is imperative we develop adsorbents to prevent waste from contaminating the environment and adversely impacting human and ecological health.[7] This thesis describes our efforts to develop renewable and biodegradable cellulose-based adsorbents to advance water remediation technology. More specifically, we showed that functionalized cellulose materials were effective for rapidly removing two prevalent pollutants, dyes and PFASs, from water (Figure 5.1).

Figure 5.1. Images of cellulose-based hydrogels used for adsorbing methylene blue (MB) and methyl orange (MO) dyes (left and middle), and an image of cationic wood pulp (WP) used for adsorbing PFASs (right).

Cellulose-based hydrogels are promising adsorbents,[8] but they often require long times (i.e., min to h) to effectively adsorb dyes.[9,10,11,12] To overcome this limitation, we hypothesized in Chapter 2 that localized hydrogels, made from polyionic complexes, might rapidly adsorb charged dyes if gelation and dye adsorption happen concomitantly.[13] Thus, we first demonstrated that localized gels formed when anionic sulfated cellulose nanofibers (SCNFs) and cationic quaternized hydroxyethyl cellulose ethoxylate (QHECE) were mixed for less than 30 s. The localized gels were then generated in solutions containing methylene blue (MB), an anionic dye, and >90% adsorption was observed within seconds, an advantage compared to common adsorbents like activated carbon which require h to d to achieve high removal efficiencies.[14,15,16,17] The maximum adsorption capacity for MB was greater than other cellulose-based hydrogels and similar to activated carbon.[9,10,16] We showed that electrostatics drive dye adsorption and that using solutions with salt concentrations and pHs similar to environmental conditions did not inhibit adsorption. As a result, these hydrogels may be useful as flocculating agents[18] for adsorbing other charged contaminants. One current shortcoming, however, is that the charged pollutant disrupts gelation by competing with QHECE for accessible sites on SCNFs. To overcome this limitation, we propose making hydrogels with SCNFs that have increased amounts of anionic groups and with QHECE that has fewer cationic groups to increase the number of negatively charged locations available for binding the pollutant. More specifically, SCNFs with a higher charge density and QHECE with a lower charge density could be synthesized and utilized for making hydrogels. Additionally, using smaller QHECE:SCNF mass ratios may lead to hydrogels that have fewer adsorption sites consumed by crosslinking and more anionic sites available for pollutant binding.

Toxic PFASs are prevalent in freshwater sources,[19,20] especially in Michigan,[4] but adsorbents require long times (i.e., min to h) to effectively extract PFASs from water.[21,22,23,24] Thus, in Chapter

3, we hypothesized, based on results from Chapter 2, that cationic cellulose fibers may be effective for rapidly removing PFASs from water via electrostatics.[25] For this work, however, we were interested in using only cellulose fibers, as opposed to hydrogels, to be competitive with currently utilized flow-based adsorbents. To evaluate the hypothesis that cationic cellulose could rapidly adsorb PFASs, quaternized wood pulps (QWPs) were synthesized and utilized for adsorbing PFOS and PFOA. We found that at environmentally relevant concentrations, more than 90% of PFOS and 80% of PFOA were adsorbed within seconds, and adsorption capacities comparable to conventional adsorbents were achieved.[26,27] We also found that adsorption was inhibited with humic acid present, but environmentally relevant solution pHs and salt concentrations had no effects on adsorption. Overall, cationic cellulose was promising for rapidly removing PFASs from water, and we plan on tailoring WP to improve adsorption when humic acid is present and to adsorb cationic, nonionic, and zwitterionic PFASs. This future work is described in more detail below.

In Chapter 4, we combined the idea of localized gels from Chapter 2 and the use of cationic WP in Chapter 3 to begin developing QWP-based adsorbents that rapidly adsorb anionic dyes via electrostatic interactions. Specifically, we were interested in using both localized hydrogels, like flocculating agents, and QWP fibers alone, for future use in flow systems, to adsorb anionic dye. We demonstrated that methyl orange (MO), an anionic dye, is adsorbed within seconds when cationic QWPs (Chart 5.1) are mixed with anionic sulfated WPs (SWPs) to form localized gels. Adsorption was driven by electrostatic interactions, and SWP-QWP electrostatic crosslinking reduced adsorption. We also observed in preliminary studies that QWP fibers adsorbed more MO than hydrogels, suggesting that cationic fibers alone are promising for capturing anionic dyes. Future work optimizing SWP:QWP mass ratios in hydrogels and QWP fiber charge densities is

needed before determining whether gels or fibers are more effective for adsorbing MO. Additionally, studies evaluating adsorbent properties such as adsorption capacity will demonstrate the advantages of hydrogels and cationic WP fibers. Finally, because Khalil et al. demonstrated that adsorbents with charged primary and secondary amines have higher adsorption capacities for dyes than quaternary amines,[28] we preliminarily explored synthesizing primary amine WPs (PWPs) (Chart 5.1). Future work is required to synthesize PWPs with larger charge densities and to examine dye adsorption on these fibers.

Chart 5.1. Charged PWPs and QWPs studied in Chapter 4.

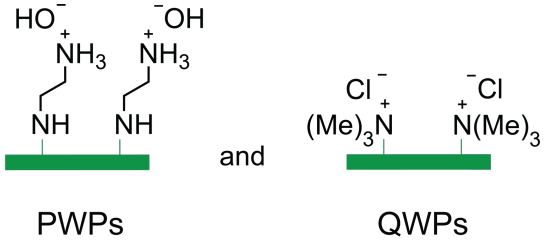

Moving forward, we are interested in functionalizing cellulose fibers with different groups to adsorb emerging contaminants.[7,29,30] Because these contaminants have diverse functionalities, we anticipate that functionalizing cellulose with complementary groups specific to a pollutant will be an effective strategy. For example, because we plan on tailoring WP to improve anionic PFAS adsorption % in the presence of HA, WPs with bulky cationic groups will be synthesized to electrostatically interact with PFASs and prevent HA adsorption. More specifically, we envision installing different amine groups (i.e., secondary, tertiary, and quaternary) and organic cations (e.g., phosphonium) with bulky substituents (e.g., phenyl groups) on the WP. We anticipate that the bulky cations will sterically block HA from interacting with the hydrophobic cellulose backbone while adsorbing PFASs through electrostatic interactions. To adsorb nonionic and

zwitterionic PFASs, which are being discovered in water,[31,32] cellulose will be functionalized with hydrocarbon and fluorocarbon groups to increase hydrophobic interactions with the PFAS fluorocarbon chain (Scheme 5.1). Finally, we expect effective adsorption of multiple PFAS species can be achieved by incorporating cationic, anionic, and hydrocarbon/fluorocarbon moieties on one WP batch (Scheme 5.1). Towards these goals, literature reports describing cellulose functionalized with phosphonium[33] and hydrocarbon/fluorocarbon[34,35] groups have been identified, and we will adapt these reports and others to functionalize WPs and adsorb PFASs.

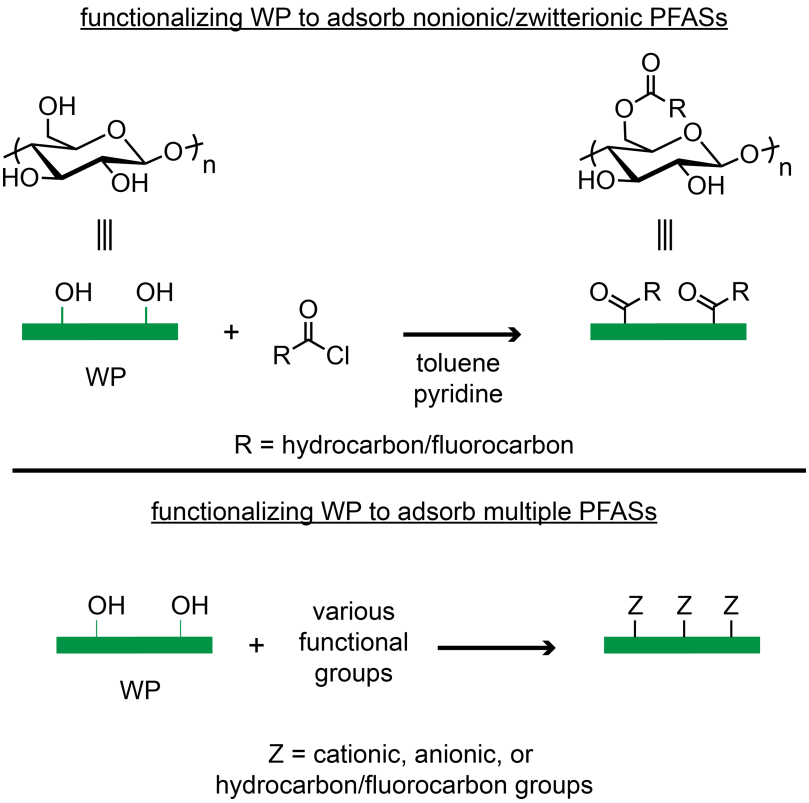

Scheme 5.1. Proposed syntheses to functionalize WP with hydrocarbon/fluorocarbon groups (top) and a variety of functional groups (bottom).

To expand the utility of functionalized cellulose fibers beyond use as flocculating agents, we intend to evaluate them in packed-bed filtration systems. While batch methods, which were used in this thesis, are useful for evaluating the feasibility of adsorbate-adsorbent systems, they are

typically only used for cleaning smaller quantities of water.[36] Packed-bed systems, on the other hand, are widely used because they purify larger water volumes in flow.[36] To evaluate functionalized cellulose in packed-bed systems, we intend to follow rapid small scale column test (RSSCT) protocols,[37,38] which predict a material's performance in large scale settings using small columns and quantities of materials (Figure 5.2). By optimizing variables such as cellulose size, flow rate, and column diameter, we anticipate achieving effective adsorption of targeted pollutants. In the long term, this work will demonstrate whether functionalized cellulose is a practical alternative to activated carbon for adsorbing pollutants in large scale operations.

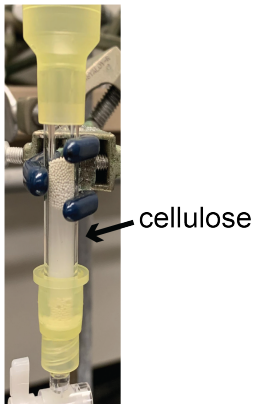

Figure 5.2. Incorporating cellulose in a column for adsorption in flow.

In conclusion, this work aimed to advance water remediation technologies. More specifically, we reported that cellulose-based materials adsorb pollutants within seconds via electrostatic interactions, making them advantageous compared to conventional adsorbents which require long contact times. Additionally, because cellulose-based adsorbents are renewable, biodegradable, and derived from inexpensive starting materials, they are a promising platform for improving adsorption. We optimistically anticipate that this work will motivate researchers to develop additional adsorbents based on renewable materials.

References

(1) United Nations. The 17 goals. https://sdgs.un.org/goals (accessed April 7, 2021).

(2) Boretti, A.; Rosa, L. Reassessing the projections of the world water development report. *npj Clean Water* **2019**, *2*.

(3) USA CDC. Flint water crisis. https://www.cdc.gov/nceh/casper/pdf-html/flint_water_crisis_pdf.html (accessed May 4, **2021**).

(4) Michigan Department of Environment, Great Lakes, and Energy. PFAS sites. https://www.michigan.gov/pfasresponse/0,9038,7-365-86511_95645---,00.html (accessed May 4, **2021**).

(5) Moody, C.; Hebert, G.; Strauss, S.; Field, J. Occurrence and persistence of perfluorooctanesulfonate and other perfluorinated surfactants in groundwater at a fire-training area at Wurtsmith Air Force Base, Michigan, USA. *J. Environ. Monit.* **2003**, *5*, 341–345.

(6) Michigan Department of Environment, Great Lakes, and Energy. New state drinking water standards pave way for expansion of Michigan's PFAS clean-up efforts. https://www.michigan.gov/egle/0,9429,7-135--535602--,00.html (accessed March 11, **2021**).

(7) *Environmental deterioration and human health*; Malik, A., Akhtar, R., Grohmann, E., Eds.; Springer, 2014.

(8) Hokkanen, S.; Bhatnagar, A.; Sillanpaa, M. A review on modification methods to cellulose-based adsorbents to improve adsorption capacity. *Water Res.* **2016**, *91*, 156–173.

(9) Mohammed, N.; Grishkewich, N.; Berry, R.; Tam, K.C. Cellulose nanocrystal–alginate hydrogel beads as novel adsorbents for organic dyes in aqueous solutions. *Cellulose* **2015**, *22*, 3725–3738.

(10) Wang, D.; Yu, H.; Fan, X.; Gu, J.; Ye, S.; Yao, J.; Ni, Q. High aspect ratio carboxylated cellulose nanofibers cross-linked to robust aerogels for superabsorption−flocculants: paving way from nanoscale to macroscale. *ACS Appl. Mater. Interfaces* **2018**, *10*, 20755−20766.

(11) Jin, L.; Li, W.; Xu, Q.; Sun, Q. Amino-functionalized nanocrystalline cellulose as an adsorbent for anionic dyes. *Cellulose* **2015**, *22*, 2443–2456.

(12) Chen, Y.; Liu, H.; Geng, B.; Ru, J.; Cheng, C.; Zhao, Y.; Wang, L. A reusable surface quaternized nanocellulose-based hybrid cryogel loaded with N-doped TiO2 for self-integrated adsorption/photo-degradation of methyl orange dye. *RSC Adv.* **2017**, *7*, 17279–17288.

(13) Harris, J.; McNeil, A. Localized hydrogels based on cellulose nanofibers and wood pulp for rapid removal of methylene blue. *J. Polym. Sci.* **2020**, *58*, 3042–3049.

(14) Pathania, D.; Sharma, S.; Singh, P. Removal of methylene blue by adsorption onto activated carbon developed from Ficus carica bast. *Arab. J. Chem.* **2017**, *10*, S1445–1451.

(15) Sharma, Y.; Uma. Optimization of parameters for adsorption of methylene blue on a low cost activated carbon. *J. Chem. Eng. Data* **2010**, *55*, 435–439.

(16) El Qada, E.; Allen, S.; Walker, G. Adsorption of methylene blue onto activated carbon produced from steam activated bituminous coal: A study of equilibrium adsorption isotherm. *Chem. Eng. J.* **2006**, *124*, 103–110.

(17) Bardhan, M.; Novera, T.; Tabassum, M.; Islam, M.; Jawad, A.; Islam, M. Adsorption of methylene blue onto betel nut husk-based activated carbon prepared by sodium hydroxide activation process. *Water Sci. Technol.* **2020**, *82*, 1932–1949.

(18) Wilts, E.; Herzberger, J.; Long, T. Addressing water scarcity: cationic polyelectrolytes in water treatment and purification. *Polym. Int.* **2018**, *67*, 799–814.

(19) Hu, X.; Andrews, D.; Lindstrom, A.; Bruton, T.; Schaider, L.; Grandjean, P.; Lohmann, R.; Carignan, C.; Blum, A.; Balan, S.; Higgins, C.; Sunderland, E. Detection of poly- and perfluoroalkyl substances (PFASs) in U.S. drinking water linked to industrial sites, military fire training areas, and wastewater treatment plants. *Environ. Sci. Technol. Lett.* **2016**, *3*, 344−350.

(20) Boone, J.; Vigo, C.; Boone, T.; Byrne, C.; Ferrario, J.; Benson, R.; Donohue, J.; Simmons, J.; Kolpin, D.; Furlong, E.; Glassmeyer, S. Per- and polyfluoroalkyl substances in source and treated drinking waters of the United States. *Sci. Total Environ*. **2019**, *653*, 359–369.

(21) Zhang, D.; Zhang, W.; Liang, Y. Adsorption of per-fluoroalkyl and polyfluoroalkyl substances (PFASs) from aqueous solution - A review. *Sci. Total. Environ*. **2019**, *694*, 133606.

(22) Ateia, M.; Attia, M.; Maroli, A.; Tharayil, N.; Alex-is, F.; Whitehead, D.; Karanfil, T. Rapid removal of poly- and perfluorinated alkyl substances by poly(ethylenimine)-functionalized cellulose microcrystals at environmentally relevant conditions. *Environ. Sci. Technol. Lett*. **2018**, *5*, 764−769.

(23) Deng, S.; Zheng, Y.; Xu, F.; Wang, B.; Huang, J.; Yu, G. Highly efficient sorption of perfluorooctane sulfonate and perfluorooctanoate on a quaternized cotton prepared by atom transfer radical polymerization. *Chem. Eng. J*. **2012**, *193–194*, 154–160.

(24) Ching, C.; Klemes, M.; Trang, B.; Dichtel, W.; Helbling, D. β-cyclodextrin polymers with different cross-linkers and ion-exchange resins exhibit variable adsorption of anionic, zwitterionic, and nonionic PFASs. *Environ. Sci. Technol*. **2020**, *54*, 12693−12702.

(25) Harris, J.; Devlin, A.; McNeil, A. Rapid removal of poly- and perfluoroalkyl substances with quaternized wood pulp. *Submitted*.

(26) Kamlet, M.; Doherty, R.; Abraham, M.; Taft, R. Linear solvation energy relationships. 33. An analysis of the factors that influence adsorption of organic compounds on activated carbon. *Carbon* **1985**, *23*, 549–554.

(27) Luehrs, D.; Hickey, J.; Nilsen, P.; Godbole, K.; Rogers, T. Linear solvation energy relationship of the limiting partition coefficient of organic solutes between water and activated carbon. *Environ. Sci. Technol*. **1996**, *30*, 143–152.

(28) Khalil, M.; Aly, A. Use of cationic starch derivatives for the removal of anionic dyes from textile effluents. *J. Appl. Polym. Sci.* **2004**, *93*, 227–234.

(29) Richardson, S.; Kimura, S. Water analysis: emerging contaminants and current issues. *Anal. Chem.* **2020**, *92*, 473–505.

(30) Patel, M.; Kumar, R.; Kishor, K.; Mlsna, T.; Pittman, C.; Mohan, D. Pharmaceuticals of emerging concern in aquatic systems: chemistry, occurrence, effects, and removal methods. *Chem. Rev*. **2019**, *119*, 3510−3673.

(31) Nickerson, A.; Rodowa, A.; Adamson, D.; Field, J.; Kulkarni, P.; Kornuc, J.; Higgins, C. Spatial trends of anionic, zwitterionic, and cationic PFASs at an AFFF-Impacted Site. *Environ. Sci. Technol.* **2021**, *55*, 313–323.

(32) Barzen-Hanson, K.; Roberts, S.; Choyke, S.; Oetjen, K.; McAlees, A.; Riddell, N.; McCrindle, R.; Ferguson, P.; Higgins, C.; Field, J. Discovery of 40 classes of per- and polyfluoroalkyl substances in historical aqueous film-forming foams (AFFFs) and AFFF-impacted groundwater. *Environ. Sci. Technol.* **2017**, *51*, 2047−2057.

(33) Xiong, W.; Hu, D. Fabrication of phosphonium bamboo cellulose by triphenylphosphine: preparation, characterization, and adsorption of Acid Black 24. *Environ. Sci. Pollut. Res.* **2019**, *26*, 1880–1891.

(34) Bashar, M.; Zhu, H.; Yamamoto, S.; Mitsuishi, M. Superhydrophobic surfaces with fluorinated cellulose nanofiber assemblies for oil–water separation. *RSC Adv.* **2017**, *7*, 37168–37174.

(35) Khanjani, P.; King, A.; Partl, G.; Johansson, L.; Kostiainen, M.; Ras, R. Superhydrophobic paper from nanostructured fluorinated cellulose esters. *ACS Appl. Mater. Interfaces* **2018**, *10*, 11280−11288.

(36) Patel, H. Fixed-bed column adsorption study: a comprehensive review. *Appl. Water Sci.* **2019**, *9*, 45.

(37) Crittenden, J.; Berrigan, J.; Hand, D. Design of rapid small-scale adsorption tests for a constant diffusivity. *Jour. WPCF* **1986**, *58*, 312–319.

(38) Poddar, M.; Nair, A.N.; Mahindrakar, A. A Review on the use of rapid small scale column test (RSSCT) on predicting adsorption of various contaminants. *IOSR-JESTFT* **2013**, *3*, 77–85.

Appendices

Appendix 1 Supporting Information for Chapter 2

I. Materials 89

II. General Experimental 89

III. S-CNC-based Hydrogel Formation with QHECE Using a Hand-Shaker 91

IV. Synthesis and Characterization of Sulfated CNFs (S-CNFs) and Wood Pulps (S-WPs) 92

A. Synthesis of S-CNFs and S-WPs 92

B. Preparation of unsulfated CNFs and WPs 92

C. Conductometric Titrations for S-CNFs and S-WPs 94

D. Elemental analysis (EA) 96

V. QHECE Conductometric Titration 97

VI. SEM Characterization of S-CNFs and S-WPs 99

A. General procedure for preparing SEM samples 99

VII. Determining the Minimum Amount of Material Needed for S-CNF- and S-WP-based Hydrogels 104

A. S-CNF-based hydrogels 104

B. S-WP-based hydrogels 107

VIII. Evaluating Hydrogel Swelling 110

A. General procedure for making gels during swelling studies 110

B. Procedure for measuring S-CNF-based hydrogel swelling as a function of charge density 111

C. Procedure for measuring S-WP-based hydrogel swelling as a function of charge density 113

D. Procedure for measuring S-CNF-based hydrogel swelling as a function of mass ratio 116

E. Procedure for measuring S-WP-based hydrogel swelling as a function of mass ratio 118

IX. Rheological Characterization of Hydrogels 121

A. Procedure for characterizing S-CNF- and S-WP-based gels 121

B. Procedure for characterizing MB-loaded gels and flocs 126

X. Dye Adsorption Experiments 132

A. General preparation of S-CNF mixtures 132

B. General preparation of QHECE solutions 132

C. General preparation of MB solutions 132

D. General procedure for calculating MB adsorption in gels and flocs 132

E. Generating a calibration curve for MB dissolved in Millipore water 134

F. Procedure for quantifying MB adsorption in S-CNF-based hydrogels for dye concentration versus MB adsorption % plot 135

G. Procedure for quantifying MB adsorption in S-WP-based hydrogels for dye concentration vs MB adsorption % plot 137

H. Procedure for measuring MB adsorption % as a function of S-CNF concentration 139

I. Determining the maximum ratios of dye/negative sites where gelation occurs 142

J. Monitoring MB adsorption in S-CNF-based hydrogels over time 143

K. Procedure for quantifying MB adsorption in S-CNF-based flocs for dye concentration versus MB adsorption % plot 147

L. Calculating MB adsorption capacity for S-CNF-based hydrogels and flocs 149

M. Procedure for quantifying MB adsorption in S-CNF0.77-based flocs 150

N. Influence of solution pH on dye adsorption 151

O. Influence of salt concentration on dye adsorption 154

P. Generating a calibration curve for MB dissolved in acidic ethanol 156

Q. Monitoring MB desorption from S-CNF-based hydrogels over time 157

R. Determining the pH of acidic ethanol solutions 161

S. Comparing MB adsorption on S-CNF fibers and in S-CNF-based gels 161
T. MB adsorption in premade S-CNF gels 163
XI. References 166

I. Materials

Cellulose nanocrystals (spray-dried, Cellulose Lab Catalog Number CNC-SD) and cellulose nanofibrils (freeze-dried, Cellulose Lab Catalog Number CNF-FD) were purchased from Cellulose Lab. Bleached hardwood pulp was generously donated by Cellulose Lab. Chlorosulfonic acid, anhydrous N,N-dimethylformamide (DMF), hydrochloric acid, sodium hydroxide, Whatman polyamide membrane filters (0.2 μm, 47 mm), and quaternized hydroxyethylcellulose ethoxylate (QHECE) were purchased from Aldrich and used without further purification. Absolute ethanol (EtOH), sodium chloride, silver nitrate, methylene blue (MB) (Alfa Aesar), UV grade PMMA cuvettes (Globe Scientific), and disposable polypropylene 50 mL centrifuge tubes were purchased from Fisher and used without further purification. Deionized (DI) water purified by a Millipore Synergy water purification system was used as the water source, unless otherwise noted, and is referred to as "Millipore water."

II. General Experimental

A Thermo Scientific Orion Star A215 pH/conductivity meter was used for the conductometric titrations. Before use each day, the pH and conductivity meters were calibrated. The pH meter was calibrated using Orion 4.01 (catalog number 910104), 7.00 (catalog number 910107), and 10.01 (catalog number 910110) pH buffers. The conductivity meter was calibrated using Orion 1413 μS/cm (catalog number 011007) conductivity standards.

An IKA T25 digital Ultra-Turrax homogenizer equipped with a S25N-10G-ST dispersing tool was utilized for homogenizing cellulose nanofiber (CNF) and wood pulp (WP) mixtures.

All UV-vis spectra were collected using a Thermo Scientific Evolution 220 UV-visible Spectrophotometer.

Scanning electron microscopy (SEM) images were obtained on a JEOL JSM-7800F scanning electron microscope, housed in the University of Michigan's Robert B. Mitchell Electron Microbeam Analysis Lab, using a 10-kV accelerating voltage. Samples were gold-coated prior to imaging using a Denton Vacuum Desk II Sputter Coater. Carbon conductive tabs (PECLO Tabs, 6 mm OD, product number 16084-6) and JEOL Aluminum Specimen Mounts (product number 16231) from Ted Pella, Inc. were utilized for making SEM samples.

During S-CNF and S-WP synthesis, a Sorvall RC5C Plus centrifuge equipped with a Thermo Scientific SLA-1500 rotor was used along with 250 mL Thermo Scientific Nalgene PPCO centrifuge bottles (catalog number 3141-0250).

In dye adsorption studies, when gels were <u>not</u> made, a Thermo Scientific Sorvall ST8 centrifuge was used along with disposable polypropylene 50 mL centrifuge tubes.

A Fisher Scientific standard microplate vortex mixer (catalog number 02-216-100) was used for making S-CNF- and S-WP-based hydrogels.

Elemental analysis was performed by Midwest Microlab.

S-CNF and S-WP samples are identified by material type followed by the charge density (e.g., S-CNF1.1 is a S-CNF sample with a charge density of 1.1 mmol SO_3^- g^{-1}).

III. S-CNC-based Hydrogel Formation with QHECE Using a Hand-Shaker

According to the information provided by Cellulose Lab, the S-CNCs had a sulfur content of 0.29 mmol g^{-1}. First, S-CNC suspensions with concentrations of 1.00 and 2.00% w/v were prepared by combining S-CNCs (100.0 mg) with Millipore water (10.0 mL or 5.0 mL) and vortex mixing at a speed setting of 10.0 until the S-CNCs were uniformly dispersed in solution (~10 min). S-CNC mixtures with lower concentrations were prepared through serial dilutions using the 1.00% w/v S-CNC mixture and Millipore water. Then, a mass of QHECE was placed in a 4 mL vial, and 1 mL of a S-CNC mixture was added to the vial. The vial was then placed on a Scinics Corporation Cocktail Shaker for a recorded time using the fastest speed setting. After the shaking time, the shaker was turned off and the vial was rested on the shaker for a designated time. The vial was then removed from the shaker and inverted. A gel was formed if the material in the bottom of the vial did not move before 5 s (see Figure A1.1).

% w/v QHECE	2.0	1.0	0.50	0.50	0.25
% w/v S-CNC	2.0	1.0	1.0	0.50	1.0
mixing/rest time (s)	290/60	160/30	65/10	65/10	65/10

Figure A1.1. Images of S-CNC-based hydrogels.

IV. Synthesis and Characterization of Sulfated CNFs (S-CNFs) and Wood Pulps (S-WPs)

Note: DI water from our house DI water system was used as the water source in "Synthesis of S-CNFs and S-WPs" and "Preparation of unsulfated CNFs and WPs".

A. Synthesis of S-CNFs and S-WPs

See Chapter 2 experimental section for the procedure.

B. Preparation of unsulfated CNFs and WPs

Samples of unsulfated CNFs (S-CNF0.0) and WPs (S-WP0.0) were subjected to the same reaction conditions as S-CNFs and S-WPs to ensure that CSA is the only reactant imparting functionality to the fibers.

A sample of unsulfated CNFs was made in the following way: unsulfated CNFs (300 mg) were placed in an oven-dried 100 mL flask with anhydrous DMF (50 mL), and the flask was capped with a septum. The mixture was soaked for 40 min under N_2. The mixture was then homogenized with an IKA T25 digital Ultra-Turrax for 4 min at 11k rpm. The flask was re-capped and soaked for 10 min under N_2. The mixture was homogenized again for 4 min at 11k rpm, and then the flask was re-capped while adding a stir bar. The mixture was stirred for 40 min under N_2. Then, the mixture was poured into a 250 mL centrifuge bottle, and the bottle was filled to ~90% capacity with DI water. The mixture was then centrifuged at ~34,000 × g for 25 min, the supernatant was discarded, and fresh DI water was added. The mixture was shaken by hand to disperse the fibers in the mixture, and a ~0.1 M NaOH solution was then used to increase the pH of the mixture to 7, as measured with pH paper. The mixture was centrifuged again at ~34,000 × g for 25 min. The supernatant was discarded, and fresh DI water was added. The mixture was shaken by hand to disperse the fibers in the mixture, and then centrifuged a third time at ~34,000 × g for 25 min. The

supernatant was discarded, and the material was placed in smaller glass tubes, frozen in liquid nitrogen, and dried under vacuum on a Schlenk line to remove excess water. This procedure generated S-CNF0.0.

The above procedure was repeated using WPs (300 mg) to access S-WP0.0. However, to isolate the S-WP after the third centrifuge cycle, most of the supernatant was carefully discarded, and the mixture was vacuum filtered using a polyamide membrane filter. The remaining fibers were then rinsed once with Millipore water (5 mL), and placed in smaller glass tubes, frozen in liquid nitrogen, and dried under vacuum on a Schlenk line to remove excess water.

Table A1.1. S-CNF/S-WP experimental conditions and results.

sample	first homogenization	second homogenization	volume of 2.0 M CSA added (mL)	CSA concentration in reaction mixture (mM)
S-CNF0.0	4 min @11k rpm	4 min @ 11k rpm	0.0	0.0
S-CNF0.77	4 min @12k rpm	4 min @12k rpm	1.0	39
S-CNF1.1	4 min @12k rpm	4 min @12k rpm	1.7	66
S-CNF1.5	4 min @12k rpm	4 min @12k rpm	2.1	81
S-CNF1.8A[a]	4 min @12k rpm	4 min @12k rpm	2.6	99
S-CNF1.8B[a]	1 min @15k rpm 3 min @11k rpm	1 min @15k rpm 3 min @11k rpm	3.3	120
S-CNF1.8C[a]	1 min @15k rpm 3 min @11k rpm	1 min @15k rpm 3 min @11k rpm	3.3	120
S-CNF1.9	4 min @11k rpm	4 min @11k rpm	3.0	110
S-WP0.0	4 min @11k rpm	4 min @ 11k rpm	0.0	0.0
S-WP0.53	1 min @15k rpm 3 min @11k rpm	1 min @15k rpm 3 min @11k rpm	1.1	43
S-WP1.0	1 min @15k rpm 3 min @11k rpm	1 min @15k rpm 3 min @11k rpm	1.8	69
S-WP1.3	1 min @15k rpm 3 min @11k rpm	1 min @15k rpm 3 min @11k rpm	2.5	95
S-WP1.8A[b]	1 min @15k rpm 3 min @11k rpm	1 min @15k rpm 3 min @11k rpm	3.2	120
S-WP1.8B[b]	1 min @15k rpm 3 min @11k rpm	1 min @15k rpm 3 min @11k rpm	3.4	127

[a]Three S-CNF1.8 samples were made for this work, and since they have the same charge density, they are referred to as the same sample.
[b]Two S-WP1.8 samples were made for this work, and since they have the same charge density, they are referred to as the same sample.

C. Conductometric Titrations for S-CNFs and S-WPs

See Chapter 2 experimental section for the procedure.

Table A1.2. S-CNF/S-WP conductometric titration results.

sample	first charge density (mmol/g)[a]	second charge density (mmol/g)[a]	average charge density (mmol/g)
S-CNF0.0	0.0427	0.0393	0.041 ± 0.002
S-CNF0.77	0.775	0.758	0.77 ± 0.01
S-CNF1.1	1.11	1.15	1.1 ± 0.0
S-CNF1.5	1.55	1.46	1.5 ± 0.1
S-CNF1.8A	1.79	1.78	1.8 ± 0.0
S-CNF1.8B	1.70	1.84	1.8 ± 0.1
S-CNF1.8C	1.85	1.71	1.8 ± 0.1
S-CNF1.9	1.94	1.87	1.9 ± 0.0
S-WP0.0	0.0439	0.0471	0.046 ± 0.002
S-WP0.53	0.529	0.530	0.53 ± 0.00
S-WP1.0	1.02	0.944	1.0 ± 0.1
S-WP1.3	1.33	1.28	1.3 ± 0.0
S-WP1.8A	1.72	1.86	1.8 ± 0.1
S-WP1.8B	1.75	1.76	1.8 ± 0.0

[a]The data in this column contain one extra significant figure to show how the average charge density was calculated for each sample.

1) determining mass of SCNF mixture in titration beaker:
mass beaker + water + weigh paper + protonated SCNFs = 83.6000 g
– (mass beaker + weigh paper) = 62.4260 g
mass protonated SCNF mixture = 21.1740 g

2) determining concentration of SCNFs in titration beaker:
mass aliquot 1 = 2.6627 g → dry mass of aliquot 1 = 4.4 mg → SCNF conc. = 1.652 mg/g
mass aliquot 2 = 2.6047 g → dry mass of aliquot 2 = 4.2 mg → SCNF conc. = 1.612 mg/g
→ average SCNF conc. = 1.632 mg/g

3) determining mass of SCNFs titrated:
mass protonated SCNF mixture after aliquot removal = 15. 9066 g
mass protonated SCNF = 26.0 mg

4) conductometric titration plot:

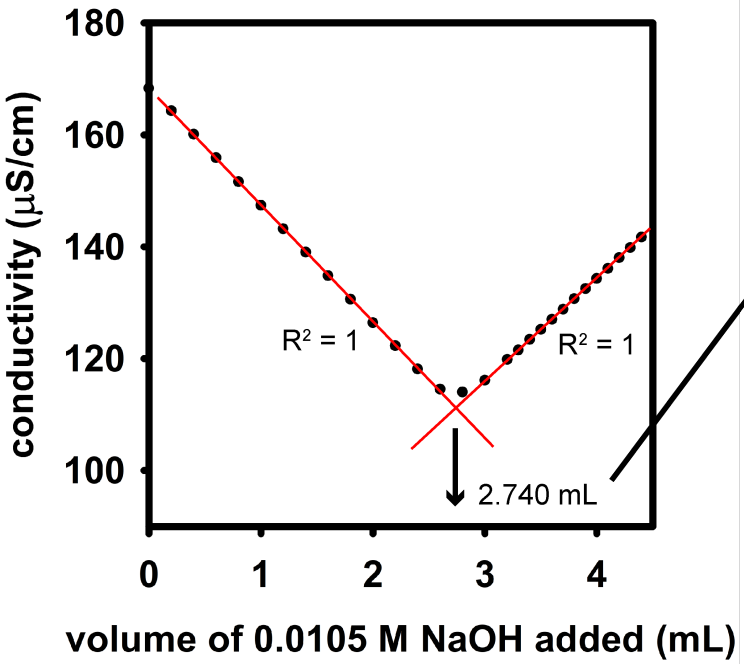

5) determining charge density:

$$\frac{2.740\ \text{mL} \times 0.0105\ \text{M NaOH}}{0.026\ \text{g SCNF}}$$

= 1.1 mmol SO_3^- g^{-1}

Figure A1.2. Calculating the charge density of a S-CNF1.1 sample.

D. Elemental analysis (EA)

A was performed on 6 S-CNF and 2 S-WP samples to determine the sulfur content (wt% S) in each sample. The results from EA were then compared to sulfur contents found using conductometric titrations, assuming a 1:1 ratio of sulfur:sulfate groups. The S-CNFs and S-WPs used for EA were prepared and characterized similar to the above procedures, but are not reported in Table A1.1 and Table A1.2 because they were not used for making gels.

Table A1.3. Comparing S-CNF and S-WP sulfur contents (wt% S) as determined with conductometric titrations and elemental analysis (EA).

sample[a]	wt% S by titration	wt% S by EA
S-CNF0.21	0.67	0.62
S-CNF0.61	1.95	2.09
S-CNF1.1a	3.52	3.20
S-CNF1.1b	3.52	3.48
S-CNF1.6	5.12	5.09
S-CNF2.0	6.40	6.15
S-WP0.8	2.56	2.55
S-WP1.3	4.16	4.14

[a]Note: These samples are not the same as in Table A1.1 and Table A1.2.

V. QHECE Conductometric Titration

The titration of QHECE was carried out similar to literature.[1] First, a 12.0 mM $AgNO_3$ solution was made by dissolving $AgNO_3$ (40.8 mg, 0.240 mmol) in deionized water (20.0 mL). Then, a known amount of QHECE was dissolved in deionized water (10.0 mL) and added to a 150 mL beaker with stir bar. An additional amount of deionized water (100.0 mL) was added to the beaker along with a previously calibrated Thermo Scientific Orion Star A215 pH/conductivity meter. The mixture was titrated by adding a specific volume (~100–200 μL) of 12.0 mM $AgNO_3$ solution to the QHECE solution over 5 s and measuring the conductivity of the mixture 40 s after each addition of titrant. The volume-corrected conductivity was plotted as a function of the volume of 12.0 mM $AgNO_3$ added, and the equivalence point was determined by the intersection of the linear least-squares regression lines from the positively and negatively sloped regions of the curve. Based on the mmols of $AgNO_3$ added, the mmol of R_4N^+ present were calculated assuming a one-to-one ratio between Ag^+ and Cl^-. The charge density was found by dividing the mmol $AgNO_3$ by the mass of QHECE that was titrated. This procedure was repeated to give a total of 2 charge density measurements, and the conductometric titration curves for both experiments can be seen in Figure A1.3 along with the calculations for both charge density measurements. The average of these 2 measurements is reported as QHECE's charge density. The experimental charge density of 1.23 ± 0.04 mmol g^{-1} is in good agreement with the mass % N (1.5–2.2%) that is given by Sigma.

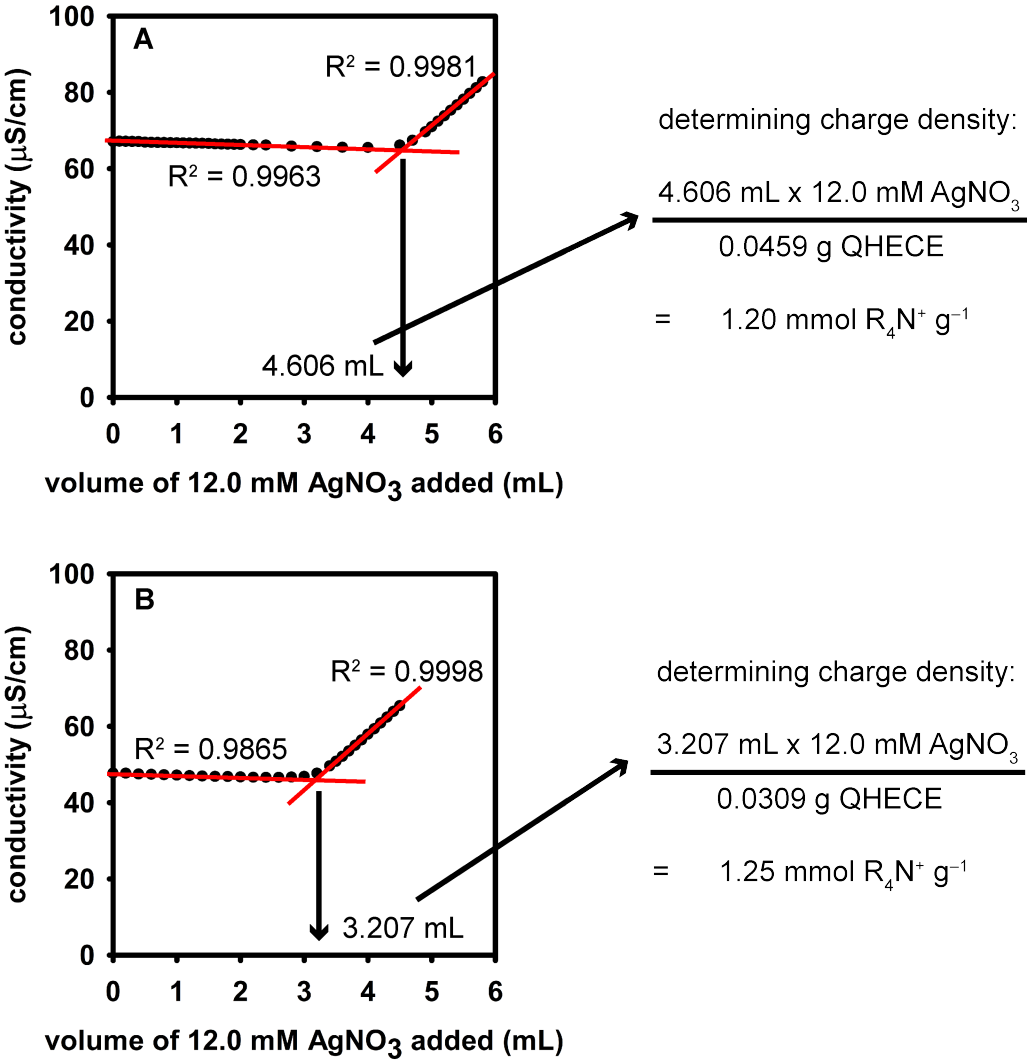

Figure A1.3. Calculating the charge density of 2 QHECE samples.

VI. SEM Characterization of S-CNFs and S-WPs

A. General procedure for preparing SEM samples

A sample of S-CNF or S-WP fibers (25.0 mg) was soaked in Millipore water (12.5 mL) for 5 min. The mixture was then homogenized at 10k rpm for 1 min to make a 0.200% w/v S-CNF or S-WP mixture.

To dilute S-CNF samples, the 0.200% w/v S-CNF mixture (0.5 mL) was combined with Millipore water (19.5 mL) in a new 20 mL vial to make a 0.005% w/v S-CNF mixture. This procedure was utilized to access 0.005% w/v mixtures of S-CNF0.0, S-CNF0.77, S-CNF1.1, S-CNF1.5, and S-CNF1.9

To dilute S-WP samples, the 0.200% w/v S-WP mixture (1 mL) was combined with Millipore water (3 mL) in a new 20 mL vial to make a 0.05% w/v S-WP mixture. The 0.05% w/v S-WP mixture (0.1 mL) was combined with Millipore water (0.9 mL) in a new 4 mL vial to make a 0.005% w/v S-WP mixture. This procedure was used to access 0.005% w/v mixture of S-WP0.0, S-WP0.53, and S-WP1.8.

A carbon conductive tab (Ted Pella, Inc., PELCO Tabs, 6 mm OD, product number 16084-6) was placed on top of a JEOL aluminum specimen SEM mount (Ted Pella, Inc., product number 16231). A S-CNF or S-WP mixture (~5 drops, 0.005% w/v) was then drop-cast onto the carbon-coated SEM mount, and the water was allowed to evaporate at room temperature overnight. The fibers were then sputter-coated with Au for 60 s to reduce charge build-up during imaging. All samples were imaged on a JEOL JSM-7800F scanning electron microscope using a 10-kV accelerating voltage. The images were recorded digitally.

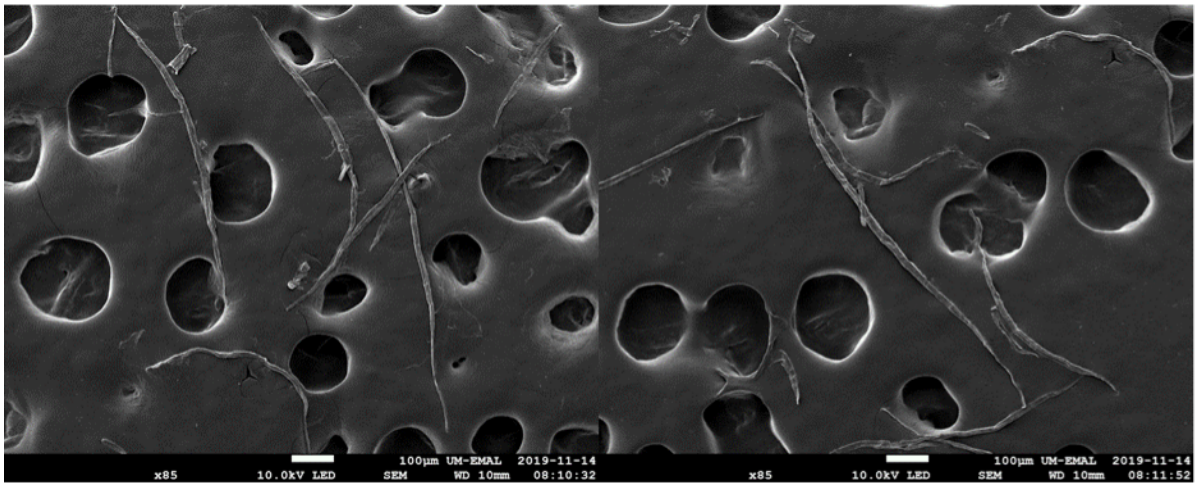

Figure A1.4. SEM images of S-WP0.0.

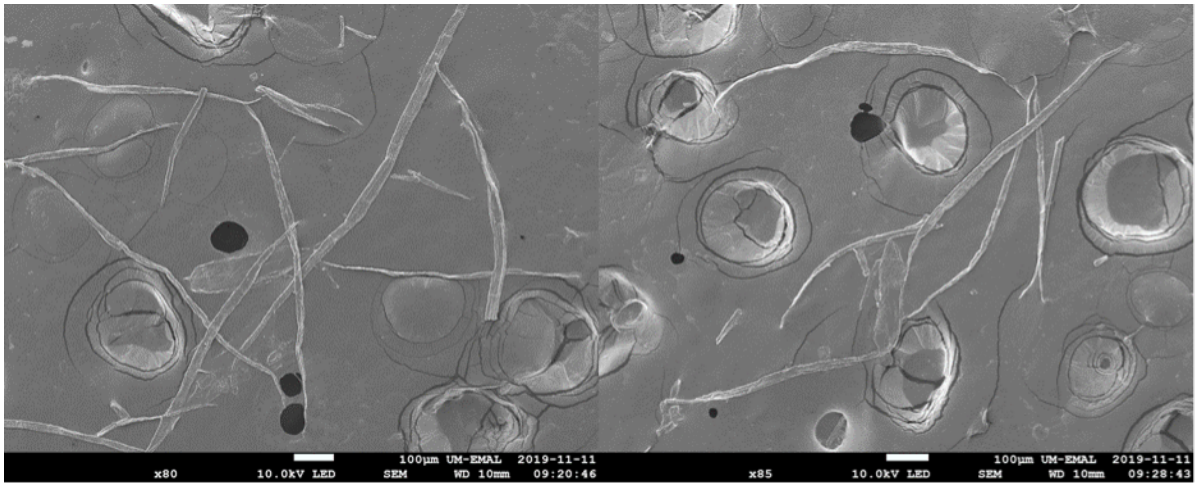

Figure A1.5. SEM image of S-WP0.53.

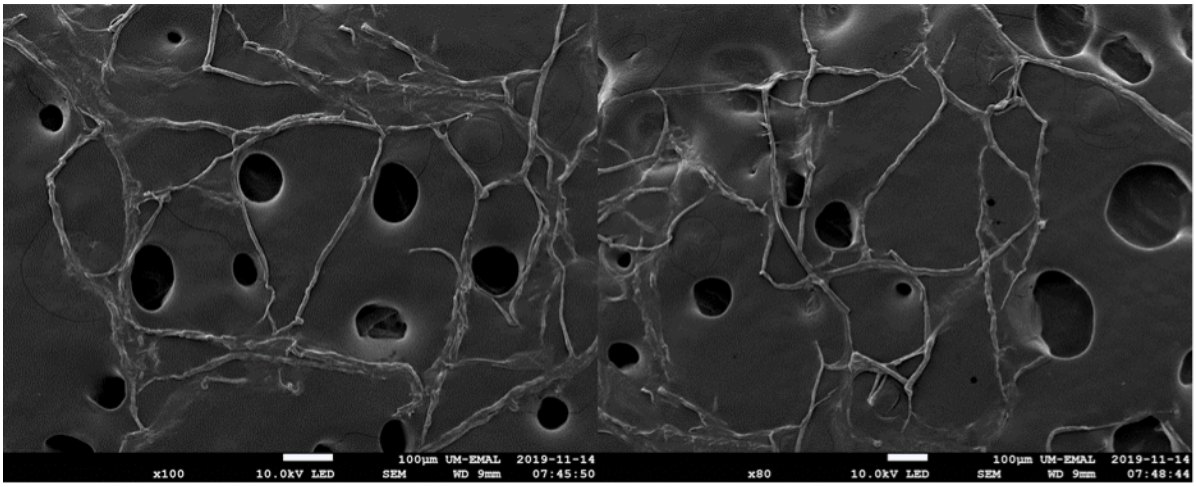

Figure A1.6. SEM images of S-WP1.8.

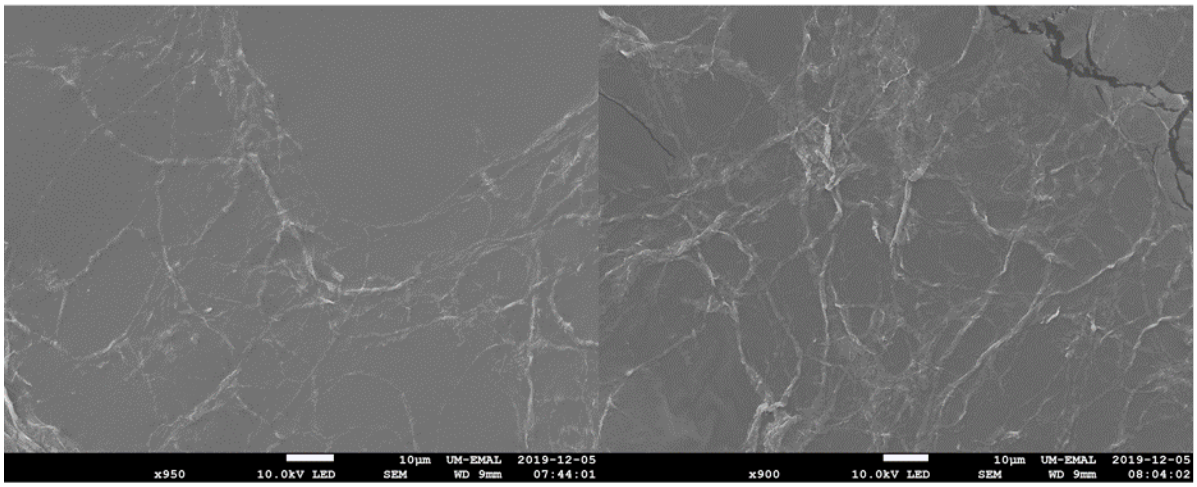

Figure A1.7. SEM images of S-CNF0.0.

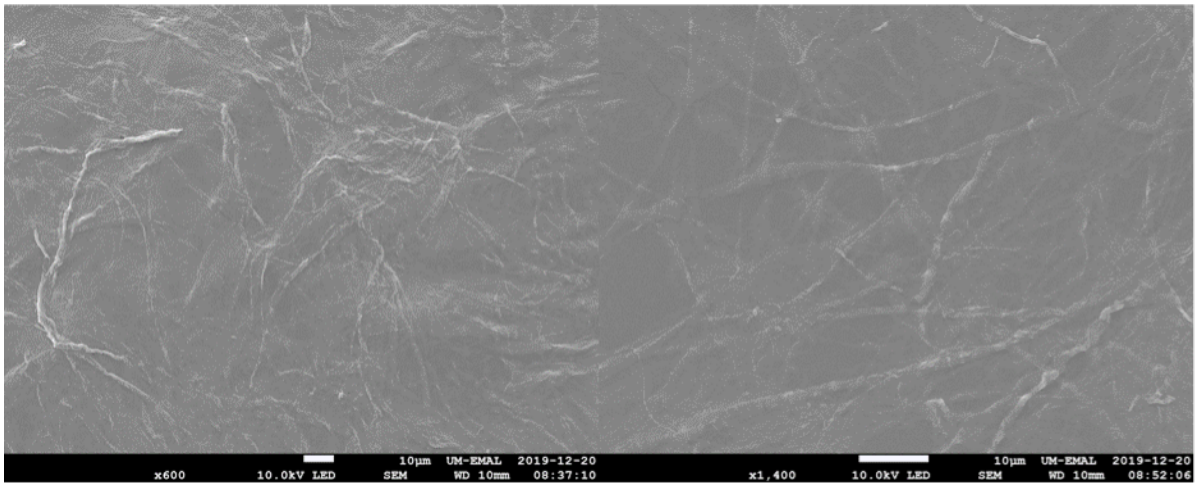

Figure A1.8. SEM images of S-CNF0.77.

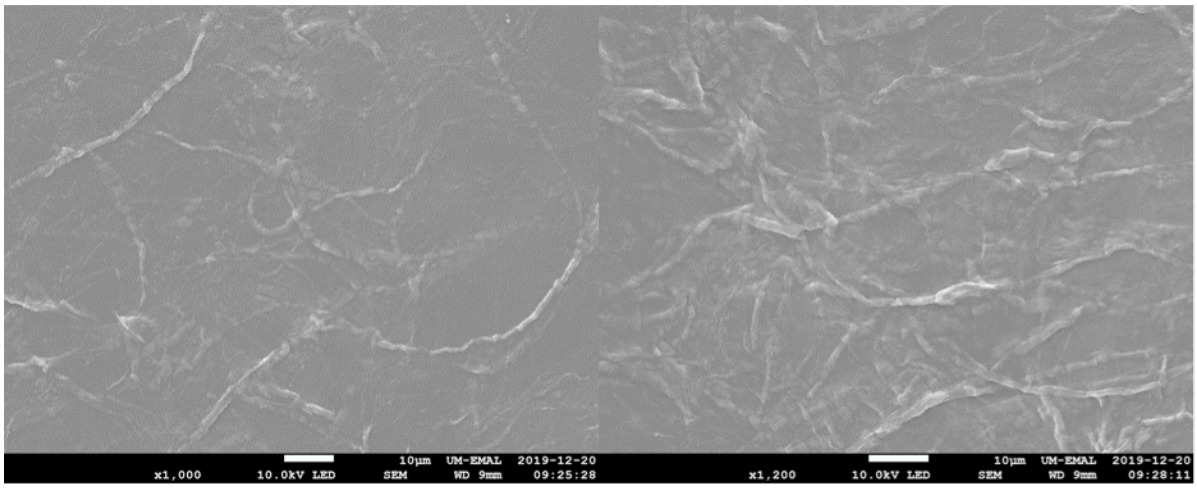

Figure A1.9. SEM images of S-CNF1.1.

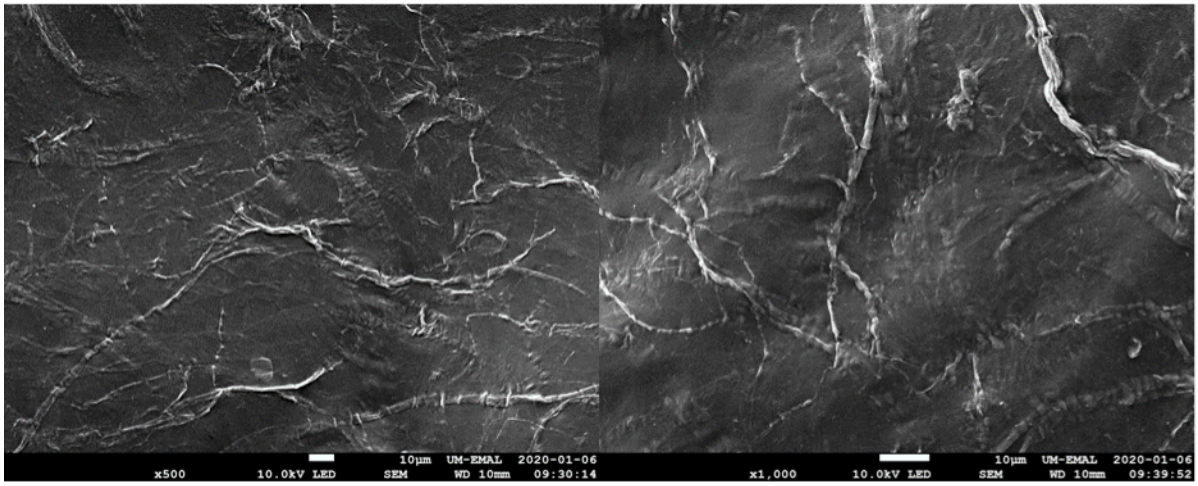

Figure A1.10. SEM images of S-CNF1.5.

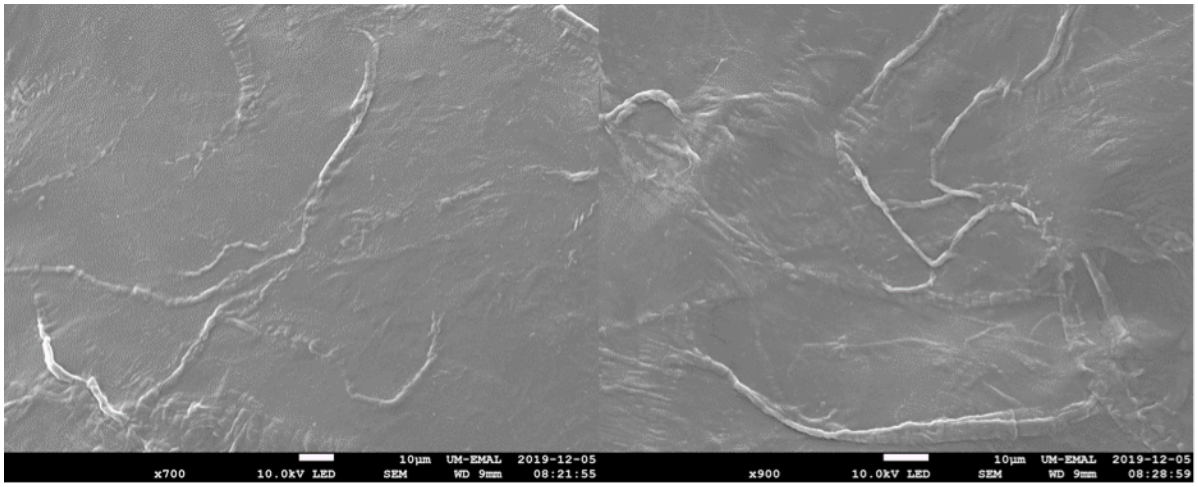

Figure A1.11. SEM images of S-CNF1.9.

VII. Determining the Minimum Amount of Material Needed for S-CNF- and S-WP-based Hydrogels

A. S-CNF-based hydrogels

S-CNF fibers (25.0 mg) were soaked in Millipore water (12.5 mL) for 5 min in a 20 mL vial. The sample was then homogenized at 10k rpm for 1 min. This method made a 0.200% w/v S-CNF mixture, and the process was repeated to make 0.200% w/v mixtures of S-CNF0.0, S-CNF0.77, S-CNF1.1, S-CNF1.5, and S-CNF1.9. To obtain lower concentration mixtures, serial dilutions were performed with each sample and Millipore water.

Three QHECE solutions with concentrations of 0.200, 0.100, and 0.0500% w/v were prepared by dissolving 40.0, 20.0, or 10.0 mg QHECE, respectively, in Millipore water (20.0 mL) in a 20 mL vial. Lower concentration QHECE solutions were prepared via serial dilutions using the 0.0500% w/v QHECE solution and Millipore water.

To make gels, a volume (4.0 mL) with a known concentration of S-CNF mixture was placed in a new 20 mL vial. The vial was then handheld on the vortex at a mixing speed of 1.0. A volume (4.0 mL) with a known concentration of QHECE solution was added to the S-CNF vial, while vortex mixing at a speed of 1.0, over the course of a recorded time. The vial was vortexed for an additional mixing time using a vortex mixing speed of 1.0. See Figure A1.12 for images of hydrogels, QHECE addition/mixing times, and final S-CNF/QHECE concentrations. From here, a localized gel was determined to be made if: (1) There was one cohesive hydrogel with minimal amounts of small polyionic complexes that were not connected to the gel. (2) The vial could be rotated 90° from a vertical to horizontal position without the localized gel breaking into smaller complexes.

Additionally, rheology performed on hydrogels suggested that gels made with this procedure are elastic, crosslinked networks. Rheological measurements can be found in the "rheological characterization of hydrogels" section. Hydrogels for rheology were made such that the final S-CNF and QHECE concentrations were both 0.100% w/v.

To understand the charge balance, between S-CNFs and QHECE, required to make hydrogels, a molar charge ratio[2] (f^-) was calculated according to:

$$f^- = \frac{[-]}{[+]+[-]}$$

Equation A1.1. Calculating molar charge ratio in hydrogels.

which is the ratio between the concentration of negative charges added to the system, [–], and the total concentration of charged groups added to the system, [+] + [–]. f^- was calculated for each S-CNF sample according to the example in Figure A1.13. f^- values of 0.00, 0.39, 0.47, 0.55, and 0.61 were calculated for gels made using S-CNF0.0, S-CNF0.77, S-CNF1.1, S-CNF1.5, and S-CNF1.9, respectively.

Figure A1.12. Determining the minimum amount of material needed to make S-CNF-based hydrogels.

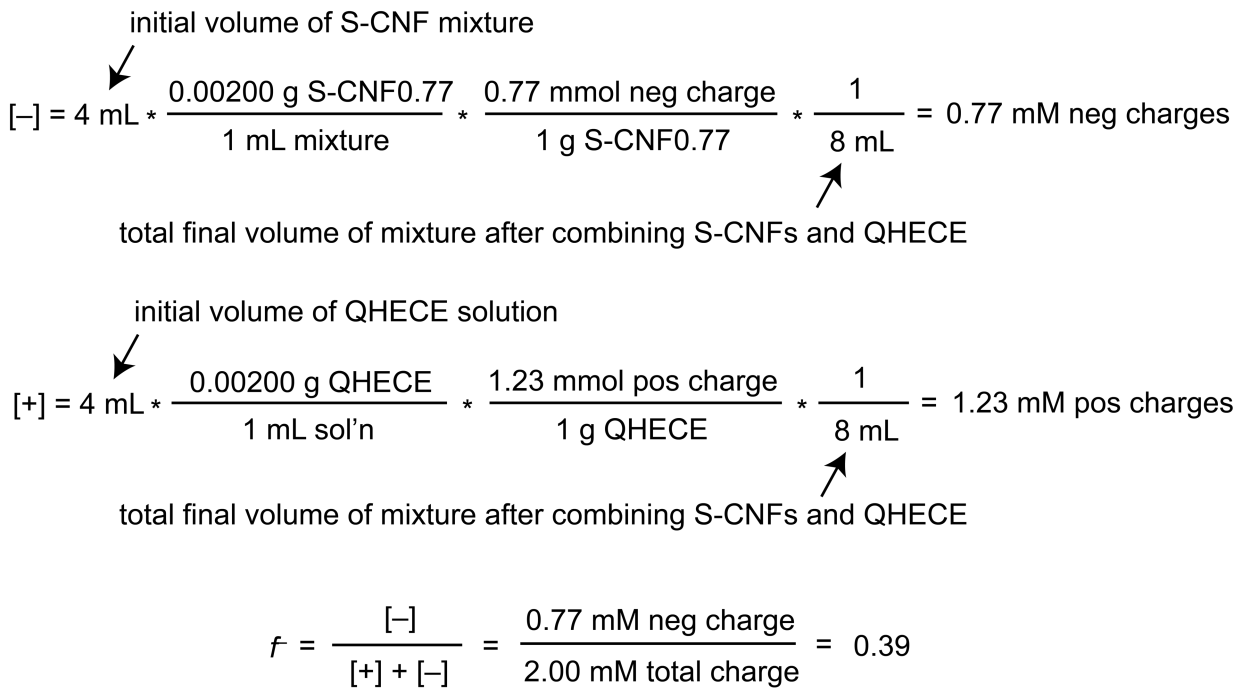

Figure A1.13. Calculating f^- for S-CNF0.77-based hydrogels.

B. S-WP-based hydrogels

S-WP fibers (25.0 mg) were soaked in Millipore water (12.5 mL) for 5 min in a 20 mL vial. The sample was then homogenized at 10k rpm for 1 min. This method made a 0.200% w/v S-WP mixture, and the process was repeated to make 0.200% w/v mixtures of S-WP0.0, S-WP0.53, S-WP1.0, S-WP1.3, and S-WP1.8. To obtain lower concentration mixtures, serial dilutions were performed with each sample and Millipore water.

Three QHECE solutions with concentrations of 0.200, 0.100, and 0.0500% w/v were prepared by dissolving 40.0, 20.0, or 10.0 mg QHECE, respectively, in Millipore water (20.0 mL) in a 20 mL vial. Lower concentration QHECE solutions were prepared via serial dilutions using the 0.0500% w/v QHECE solution and Millipore water.

To make gels, a volume (4.0 mL) with a known concentration of S-WP mixture was placed in a new 20 mL vial. The vial was then handheld on the vortex at a speed setting of 1.0. A volume

(4.0 mL) with a known concentration of QHECE solution was added to the S-WP vial, while vortex mixing at a speed of 1.0, over the course of a recorded time. The vial was vortexed for an additional mixing time at a speed setting of 1.0. See Figure A1.14 for images of hydrogels, QHECE addition/mixing times, and final S-WP/QHECE concentrations. From here, a localized gel was determined to be made if: (1) There was one cohesive hydrogel with minimal amounts of small polyionic complexes that were not connected to the gel. (2) The vial could be rotated 90° from a vertical to horizontal position without the localized gel breaking into smaller complexes.

Additionally, rheology performed on hydrogels suggested that gels made with this procedure are elastic, crosslinked networks. Rheological measurements can be found in the "rheological characterization of hydrogels" section. Hydrogels for rheology were made such that the final S-WP and QHECE concentrations were both 0.200% w/v.

To understand the charge balance, between S-WPs and QHECE, required to make hydrogels, a molar charge ratio[6] (f^-) was calculated according to Equation A1.1. f^- was calculated for each S-WP sample according to the example in Figure A1.15. f^- values of 0.00, 0.30, 0.45, 0.51, and 0.59 were calculated for gels made using S-WP0.0, S-WP0.53, S-WP1.0, S-WP1.3, and S-WP18, respectively.

Figure A1.14. Determining the minimum amount of material needed to make S-WP-based hydrogels.

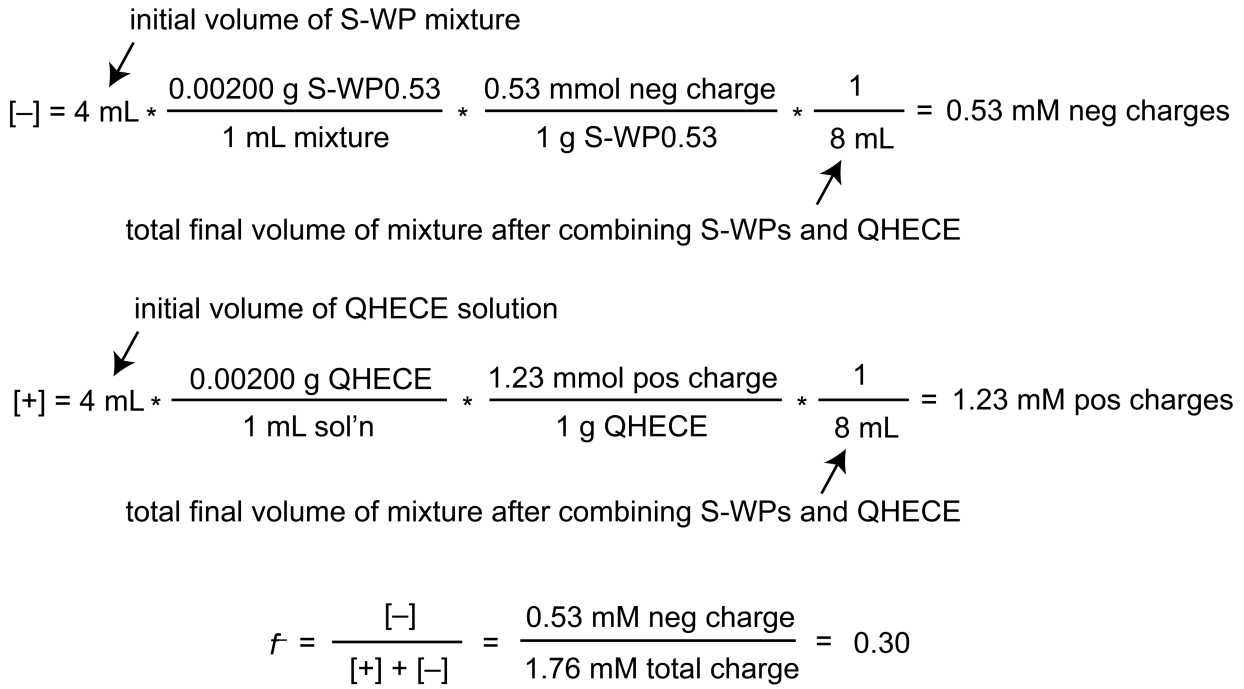

Figure A1.15. Calculating f^- for S-WP0.53-based hydrogels.

VIII. Evaluating Hydrogel Swelling

A. General procedure for making gels during swelling studies

A S-CNF or S-WP mixture (4.0 mL), with known concentration, was placed in a new 20 mL vial. The vial was then handheld on the vortex mixer at a predetermined speed. A QHECE solution (4.0 mL), with known concentration, was carefully added to the S-CNF or S-WP mixture over the course of a recorded time while vortex mixing at the predetermined speed. The vial was vortexed for an additional "mixing" time using the predetermined speed, removed from the vortex, and a gel was observed. To remove the gel from the vial, excess water was first removed via pipette. After that, the gel was scooped out with a spatula, placed in a pre-weighed vial, and dried at 110 °C. The leftover dry mass was measured, and the swell ratio was calculated according to the following equation:

$$\text{swell ratio} = \frac{\text{mass wet gel-mass dry gel}}{\text{mass dry gel}}$$

Equation A1.2. Calculating swell ratio.

Three gels were made for each set of S-CNF or S-WP and QHECE conditions, and the average swell ratio was determined by averaging these samples.

B. Procedure for measuring S-CNF-based hydrogel swelling as a function of charge density

S-CNF fibers (25.0 mg) were placed in a 20 mL vial and soaked in Millipore water (12.5 mL) for 5 min. The mixture was then homogenized at 10k rpm for 1 min. This procedure was repeated to give three 0.200% w/v S-CNF mixtures of S-CNF0.77, S-CNF1.1, S-CNF1.5, and S-CNF1.9. A 0.200% w/v QHECE solution was prepared by dissolving QHECE (40.0 mg) in Millipore water (20.0 mL) in a 20 mL vial. This procedure was repeated to generate 3 0.200% w/v QHECE solutions.

To make gels, an aliquot of 0.200% w/v QHECE solution was added to a 0.200% w/v S-CNF mixture according to the general procedure. Vortex mixing speeds are given in Table A1.4.

To understand the polyelectrolyte complex stoichiometry between S-CNFs and QHECE in gels, the cellulose (S-CNF+QHECE) mass incorporated into the gels was examined with respect to the total mass added. The percentage (%) of cellulose in each gel was calculated by dividing the mass of the dry gel by the total mass of cellulose added:

$$\%\ \text{cellulose in gel} = \frac{\text{mass dry gel}}{\text{total cellulose mass added}}$$

Equation A1.3. Calculating % cellulose in gels.

The total cellulose mass added in each of these experiments was 16 mg. An average % cellulose in gel was then calculated as a function of S-CNF charge density (Table A1.5). Consistently, we observed that ~60% of the added cellulose was incorporated into the gels.

Table A1.4. Swelling of hydrogels prepared with various S-CNFs.

S-CNF sample	QHECE addition/ mixing time (s)	vortex setting	swell ratio	avg swell ratio
S-CNF0.77	20/20	1	77.0	
S-CNF0.77	20/20	1	76.8	75 ± 3
S-CNF0.77	20/20	1	71.2	
S-CNF1.1	18/20	1	82.8	
S-CNF1.1	20/20	1	71.3	80 ± 8
S-CNF1.1	20/20	1	86.5	
S-CNF1.5	20/20	1	101.6	
S-CNF1.5	18/20	1	92.9	92 ± 10
S-CNF1.5	20/20	1	82.6	
S-CNF1.9	20/15	1.5	101.5	
S-CNF1.9	20/15	1.5	101.2	105 ± 7
S-CNF1.9	24/15	1.5	112.9	

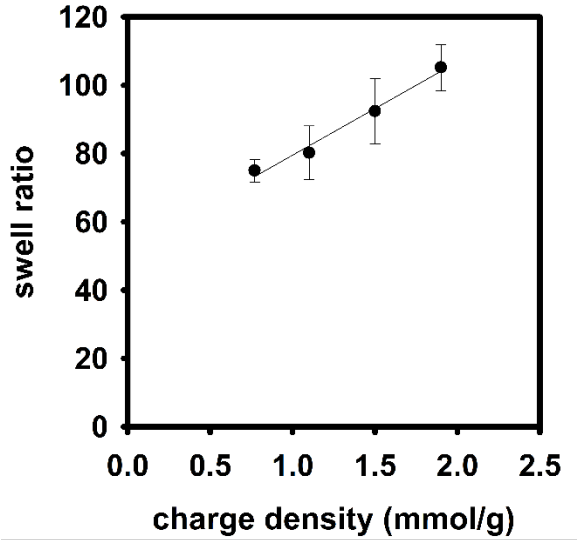

Figure A1.16. Hydrogel swell ratio as a function of S-CNF charge density. The line is present only to guide the eye.

Table A1.5. Percentage of cellulose mass incorporated into gels using various S-CNFs.

S-CNF sample	mass dry gel (mg)	% cellulose in gel	avg % cellulose in gel
S-CNF0.77	8.5	53	
S-CNF0.77	8.9	56	54 ± 1
S-CNF0.77	8.5	53	
S-CNF1.1	9.4	59	
S-CNF1.1	9.6	60	57 ± 5
S-CNF1.1	8.2	51	
S-CNF1.5	9.4	59	
S-CNF1.5	8.8	55	58 ± 3
S-CNF1.5	9.7	61	
S-CNF1.9	10.7	67	
S-CNF1.9	10.5	66	64 ± 3
S-CNF1.9	9.7	61	

C. Procedure for measuring S-WP-based hydrogel swelling as a function of charge density

S-WP fibers (50.0 mg) were placed in a 20 mL vial and soaked in Millipore water (12.5 mL) for 5 min. The mixture was then homogenized at 10k rpm for 1 min. This procedure was repeated to give three 0.400% w/v S-WP mixtures of S-WP0.53, S-WP1.0, S-WP1.3, and S-WP1.8. For S-WP1.8 only, the mixtures were made instead using 37.5 mg to make three 0.300% w/v mixtures. A 0.400% w/v QHECE solution was prepared by dissolving QHECE (80.0 mg) in Millipore water (20.0 mL) in a 20 mL vial. A 0.300% w/v QHECE solution was prepared by dissolving QHECE (60.0 mg) in Millipore water (20.0 mL) in a 20 mL vial.

To make S-WP0.53, S-WP1.0, and S-WP1.3 gels, an aliquot of 0.400% w/v QHECE solution was added to a S-WP0.53, S-WP1.0, or S-WP1.3 mixture according to the general procedure. To make S-WP1.8 gels, an aliquot of 0.300% w/v QHECE solution was added to a S-WP1.8 mixture according to the general procedure (Table A1.6). A vortex mixing speed of 1.0 was utilized at all times in these experiments.

To understand the polyelectrolyte complex stoichiometry between S-WPs and QHECE in gels, the cellulose (S-WP+QHECE) mass incorporated into the gels was examined with respect to the

total mass added. The percentage (%) of cellulose in each gel was calculated by dividing the mass of the dry gel by the total mass of cellulose added (Equation A1.3).

The total cellulose mass added was 32 mg when using S-WP0.53, S-WP1.0, and S-WP1.3, and 24 mg when using S-WP1.8. An average % cellulose in gel was then calculated as a function of S-WP charge density (Table A1.7). Consistently, we observed that ~50% of the added cellulose was incorporated into the gels.

Table A1.6. Swelling of hydrogels prepared with various S-WPs.

S-WP sample	QHECE addition/mixing time (s)	swell ratio	avg swell ratio
S-WP0.53	20/15	24.2	
S-WP0.53	20/20	26.9	25 ± 2
S-WP0.53	18/20	24.0	
S-WP1.0	20/20	39.9	
S-WP1.0	20/20	37.3	38 ± 2
S-WP1.0	20/20	36.4	
S-WP1.3	17/20	35.1	
S-WP1.3	20/15	36.9	35 ± 2
S-WP1.3	16/22	32.9	
S-WP1.8	18/20	54.2	
S-WP1.8	20/15	54.5	53 ± 2
S-WP1.8	20/20	51.7	

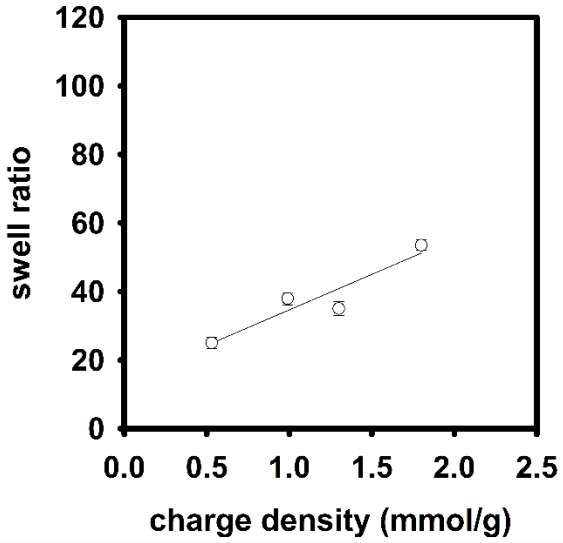

Figure A1.17. Hydrogel swell ratio as a function of S-WP charge density. The line is present only to guide the eye.

Table A1.7. Percentage of cellulose mass incorporated into gels using various S-WPs.

S-CNF sample	mass dry gel (mg)	% cellulose in gel	avg % cellulose in gel
S-WP0.53	13.4	42	
S-WP0.53	13.1	41	43 ± 2
S-WP0.53	14.3	45	
S-WP1.0	16.8	53	
S-WP1.0	16.6	52	53 ± 1
S-WP1.0	17.3	54	
S-WP1.3	15.7	49	
S-WP1.3	14.6	46	46 ± 3
S-WP1.3	14.0	44	
S-WP1.8	13.1	55	
S-WP1.8	13.0	54	54 ± 1
S-WP1.8	12.8	53	

D. Procedure for measuring S-CNF-based hydrogel swelling as a function of mass ratio

S-CNF1.8 fibers (25.0 mg) were soaked in a 20 mL vial with Millipore water (12.5 mL) for 5 min. The mixture was homogenized at 10k rpm for 1 min. This method made a 0.200% w/v S-CNF1.8 mixture, and the procedure was repeated to generate 6 samples.

Five QHECE solutions with concentrations of 0.600, 0.400, 0.300, 0.200, and 0.150% w/v were made by dissolving 120.0, 80.0, 60.0, 40.0, and 30.0 mg of QHECE, respectively, in Millipore water (20.0 mL) in a 20 mL vial.

To make gels, an aliquot of one of the QHECE solutions, with known concentration, was added to a S-CNF1.8 mixture according to the general procedure (Table A1.8). A vortex mixing speed of 1.5 was used at all times in these experiments.

To understand the polyelectrolyte complex stoichiometry between S-CNFs and QHECE in gels, the cellulose (S-CNF+QHECE) mass incorporated into the gels was examined with respect to the total mass added. The percentage (%) of cellulose in each gel was calculated by dividing the mass of the dry gel by the total mass of cellulose added (Equation A1.3).

An average % cellulose in gel was then calculated as a function of S-CNF:QHECE mass ratio (mg S-CNF/mg QHECE) (Table A1.9).

Table A1.8. Swelling of S-CNF-based hydrogels with various mass ratios.

mass ratio (mg S-CNF/mg QHECE)	initial QHECE concentration (% w/v)	QHECE addition/ mixing time (s)	swell ratio	avg swell ratio
1.33	0.150	15/10	109.3	113 ± 4
		15/15	113.6	
		17/17	117.1	
1.00	0.200	13/5	103.8	103 ± 6
		18/13	96.7	
		20/10	107.6	
0.67	0.300	16/10	89.9	87 ± 3
		16/8	83.6	
		15/7	86.6	
0.50	0.400	15/5	81.3	77 ± 7
		17/5	68.9	
		15/8	81.9	
0.33	0.600	16/10	73.0	66 ± 6
		17/5	60.8	
		18/10	65.1	

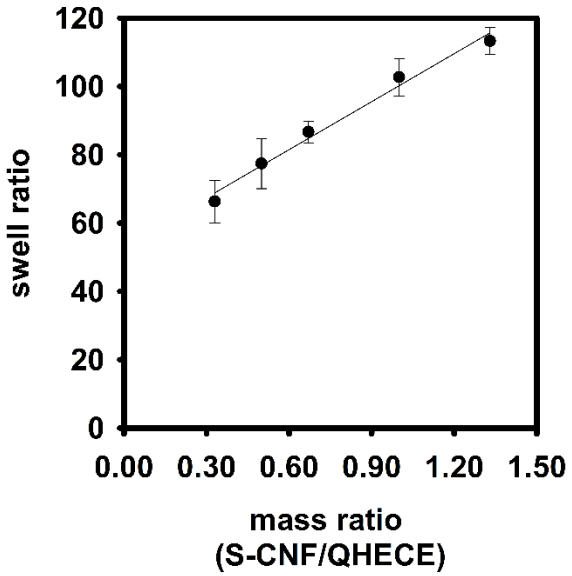

Figure A1.18. Hydrogel swell ratio as a function of mass ratio between S-CNFs and QHECE. The line is present only to guide the eye.

Table A1.9. Percentage of cellulose mass incorporated into gels at various S-CNF:QHECE mass ratios.

mass ratio (mg S-CNF/mg QHECE)	mass dry gel (mg)	total cellulose added (mg)	% cellulose in gel	avg % cellulose in gel
1.33	10.3	14.0	74	71 ± 3
	9.6	14.0	69	
	10.0	14.0	71	
1.00	10.2	16.0	64	64 ± 1
	10.3	16.0	64	
	10.4	16.0	65	
0.67	10.5	20.0	53	55 ± 2
	11.0	20.0	55	
	11.2	20.0	56	
0.50	11.5	24.0	48	46 ± 1
	10.8	24.0	45	
	11.1	24.0	46	
0.33	11.9	32.0	37	38 ± 1
	12.1	32.0	38	
	12.8	32.0	40	

E. Procedure for measuring S-WP-based hydrogel swelling as a function of mass ratio

S-WP1.8 fibers (37.5 mg) were soaked in a 20 mL vial with Millipore water (12.5 mL) for 5 min. The mixture was homogenized at 10k rpm for 1 min. This method made a 0.300% w/v S-WP1.8 mixture, and the procedure was repeated to generate 6 samples.

Five QHECE solutions with concentrations of 0.900, 0.600, 0.450, 0.300, and 0.225% w/v were made by dissolving 180.0, 120.0, 90.0, 60.0, and 45.0 mg of QHECE, respectively, in Millipore water (20.0 mL) in a 20 mL vial.

To make gels, an aliquot of one of the QHECE solutions, with known concentration, was added to a S-WP1.8 mixture according to the general procedure (Table A1.10). A vortex mixing speed of 1.0 was used at all times in these experiments.

To understand the polyelectrolyte complex stoichiometry between S-WPs and QHECE in gels, the cellulose (S-WP+QHECE) mass incorporated into the gels was examined with respect to the

total mass added. The percentage (%) of cellulose in each gel was calculated by dividing the mass of the dry gel by the total mass of cellulose added (Equation A1.3).

An average % cellulose in gel was then calculated as a function of S-WP:QHECE mass ratio (mg S-WP/mg QHECE) (Table A1.11).

Table A1.10. Swelling of S-WP-based hydrogels with various mass ratios.

mass ratio (mg S-WP/mg QHECE)	initial QHECE concentration (% w/v)	QHECE addition/ mixing time (s)	swell ratio	avg swell ratio
1.33	0.225	20/20	61.9	62 ± 1
		20/20	62.4	
		20/20	60.4	
1.00	0.300	18/20	54.2	53 ± 2
		20/15	54.5	
		20/20	51.7	
0.67	0.450	20/20	60.2	58 ± 3
		20/20	57.9	
		17/20	54.5	
0.50	0.600	23/20	51.6	53 ± 2
		20/20	55.0	
		20/20	50.9	
0.33	0.900	20/25	49.1	52 ± 3
		20/25	55.2	
		20/20	52.3	

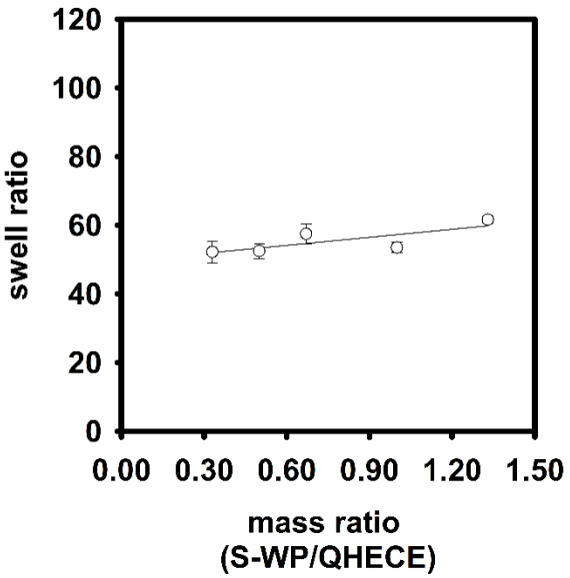

Figure A1.19. Hydrogel swell ratio as a function of mass ratio between S-WPs and QHECE. The line is present only to guide the eye.

Table A1.11. Percentage of cellulose mass incorporated into gels at various S-WP:QHECE mass ratios.

mass ratio (mg S-WP/mg QHECE)	mass dry gel (mg)	total cellulose added (mg)	% cellulose in gel	avg % cellulose in gel
1.33	11.6	21.0	55	54 ± 6
	10.2	21.0	49	
	12.5	21.0	60	
1.00	13.1	24.0	55	54 ± 1
	13.0	24.0	54	
	12.8	24.0	53	
0.67	11.2	30.0	37	40 ± 2
	12.0	30.0	40	
	12.5	30.0	42	
0.50	12.5	36.0	35	36 ± 2
	13.9	36.0	39	
	12.8	36.0	36	
0.33	13.1	48.0	27	26 ± 3
	11.1	48.0	23	
	13.7	48.0	29	

IX. Rheological Characterization of Hydrogels

A. Procedure for characterizing S-CNF- and S-WP-based gels

An AR2000ex rheometer (TA Instruments) equipped with a stainless steel 20 mm crosshatch parallel plate was used to perform rheological measurements. S-CNF-based hydrogels were made using the same procedure as in the "Procedure for measuring S-CNF-based hydrogel swelling as a function of charge density" subsection (Appendix 1 section VIII). S-CNF-based hydrogels were made using final S-CNF and QHECE concentrations of 0.100% w/v (~16 mg of total dry material). S-WP-based hydrogels were made using the same procedure as in the "Procedure for measuring S-WP-based hydrogel swelling as a function of charge density" subsection (Appendix 1 section VIII). S-WP-based hydrogels made with S-WP1.8 were made using final S-WP and QHECE concentrations of 0.150% w/v (~24 mg of total dry material). S-WP-based hydrogels made with S-WP0.53, S-WP1.0, and S-WP1.3 were made using final S-WP and QHECE concentrations of 0.200% w/v (~32 mg of total dry material) because more hydrogel sample was needed to fill the gap. Within 5 min of a gel being made, it was loaded on the rheometer using a spatula. The gap was then fixed at either 500 or 1000 μm, and a solvent trap filled with water was utilized to limit solvent evaporation. All measurements were performed at 25 °C. Each sample was pre-sheared using a stress of 0.064 Pa for 30 s and then equilibrated for 5 min before performing either a frequency or oscillating stress sweep experiment. Frequency sweep experiments were performed from 0.1–100 rad/s using a stress of 1 Pa. Oscillating stress sweep experiments were performed from 0.1–1000 Pa using a frequency of 1 rad/s.

Rheology of S-CNF0.77- and S-WP0.53-based gels were performed using a gap of 500 μm, because of their small volume, while all other gels were tested with a gap of 1000 μm.

To ensure that gap height does not affect rheological properties, frequency sweeps were performed on S-CNF1.5-based gels at 500 and 1000 μm. We observed no significant difference in G′ or G″ when the gap size was changed (Figure A1.23).

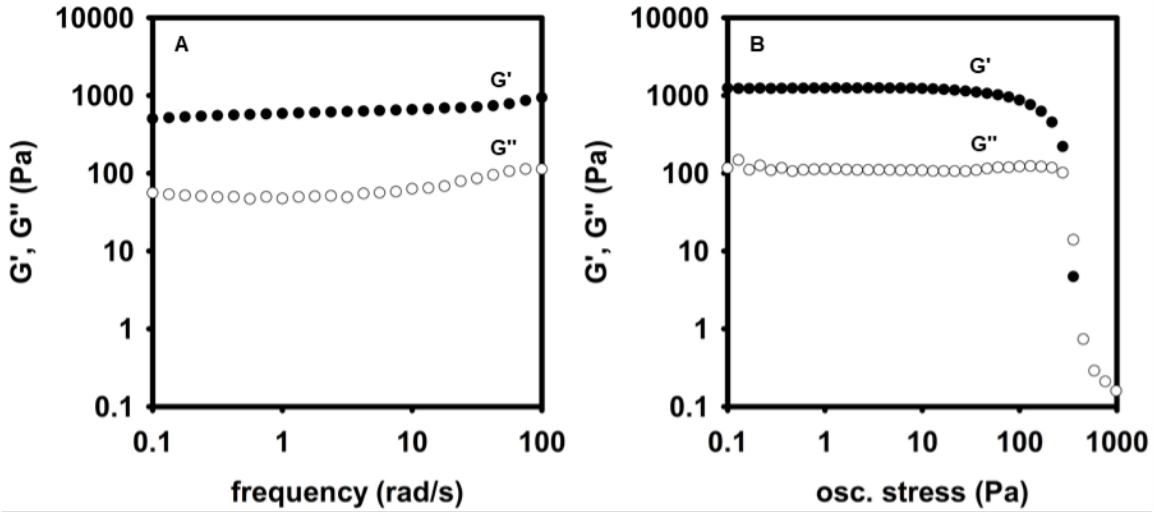

Figure A1.20. (A) Frequency and (B) oscillating stress sweep of S-CNF0.77 gels.

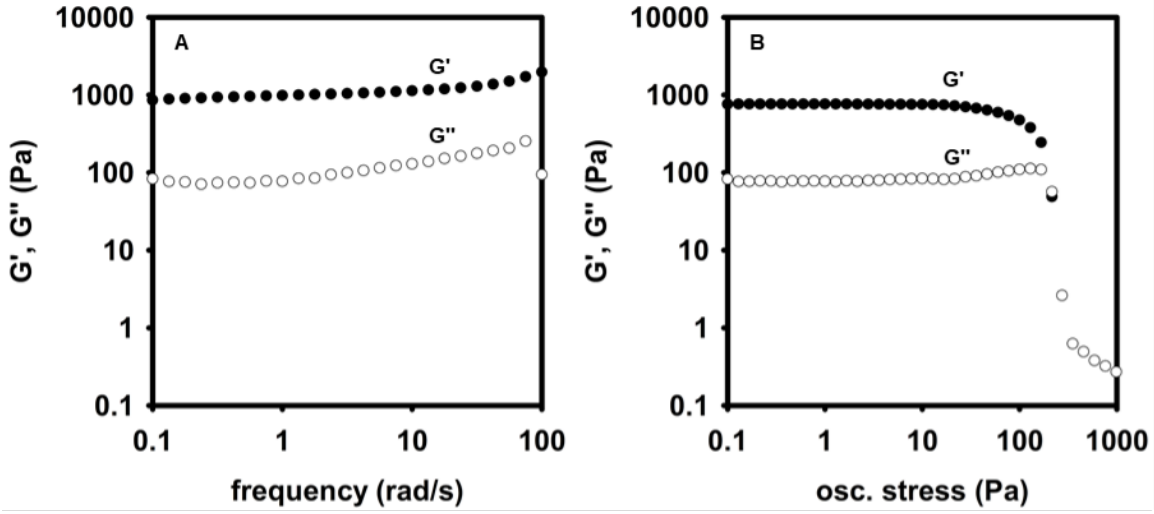

Figure A1.21. (A) Frequency and (B) oscillating stress sweep of S-CNF1.1 gels.

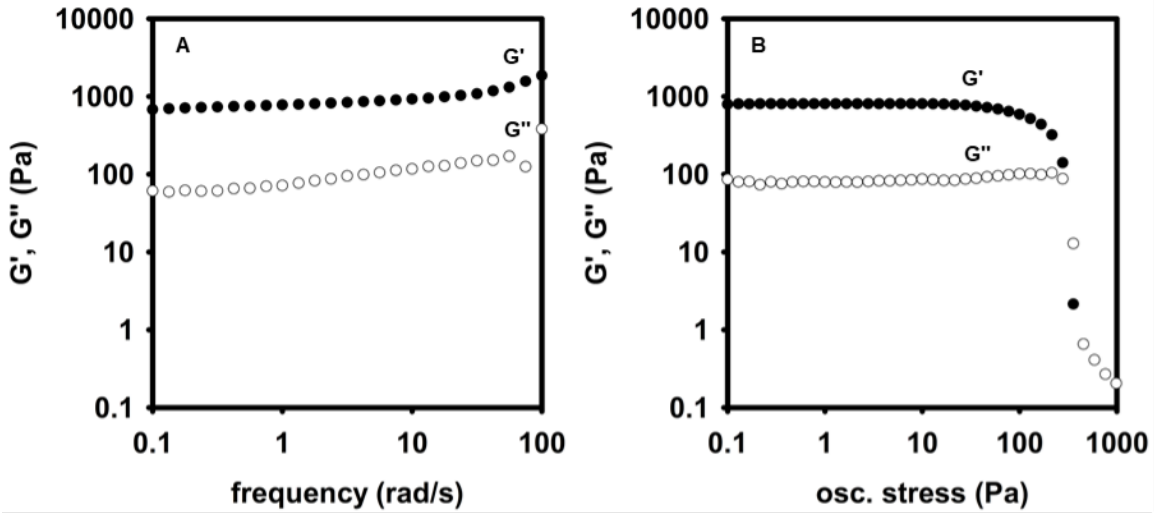

Figure A1.22. (A) Frequency and (B) oscillating stress sweep of S-CNF1.5 gels.

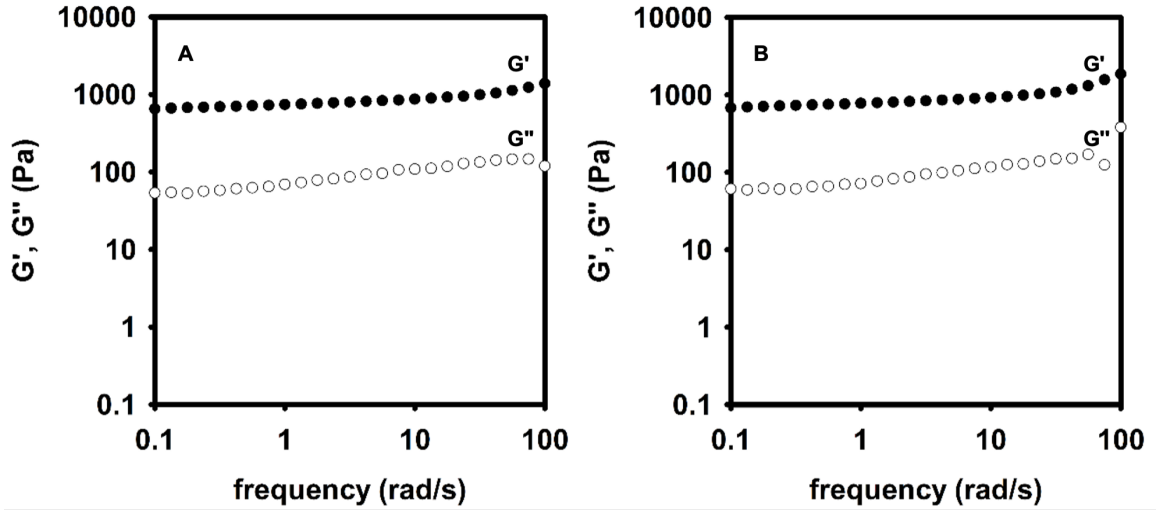

Figure A1.23. Frequency sweeps of S-CNF1.5 gels using gap heights of (A) 500 and (B) 1000 μm.

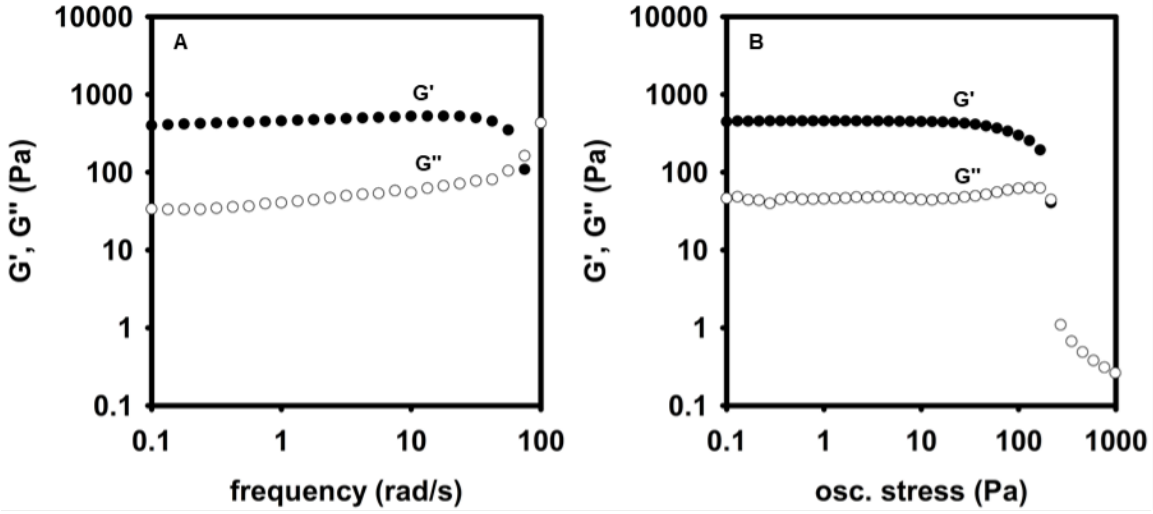

Figure A1.24. (A) Frequency and (B) oscillating stress sweep of S-CNF1.9 gels.

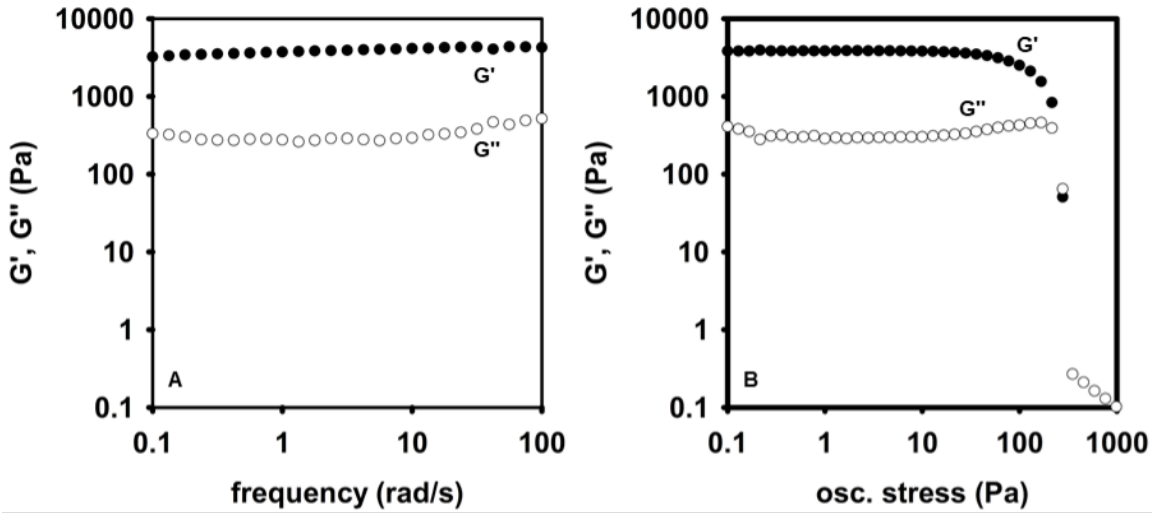

Figure A1.25. (A) Frequency and (B) oscillating stress sweep of S-WP0.53 gels.

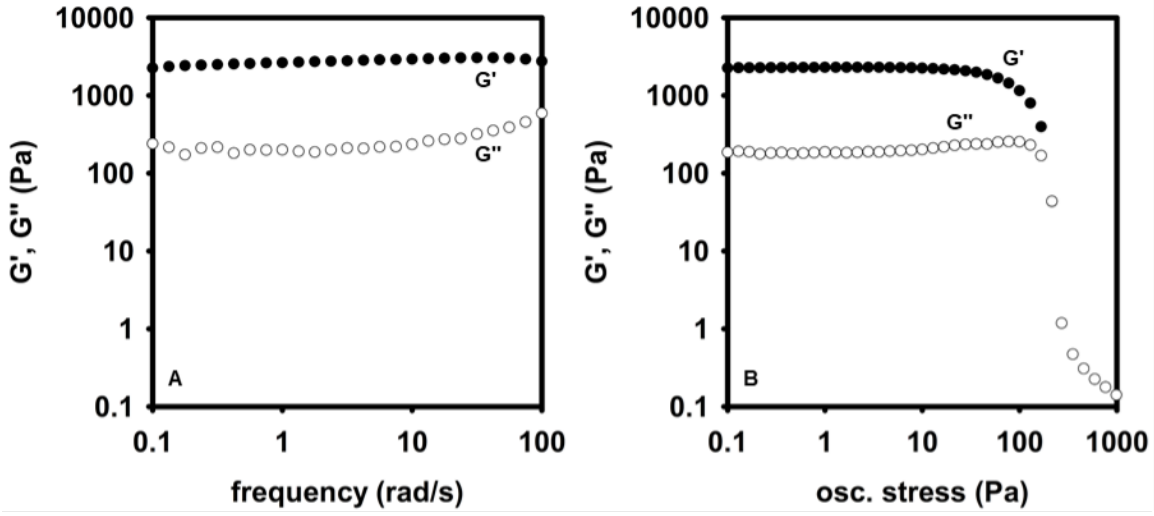

Figure A1.26. (A) Frequency and (B) oscillating stress sweep of S-WP1.0 gels.

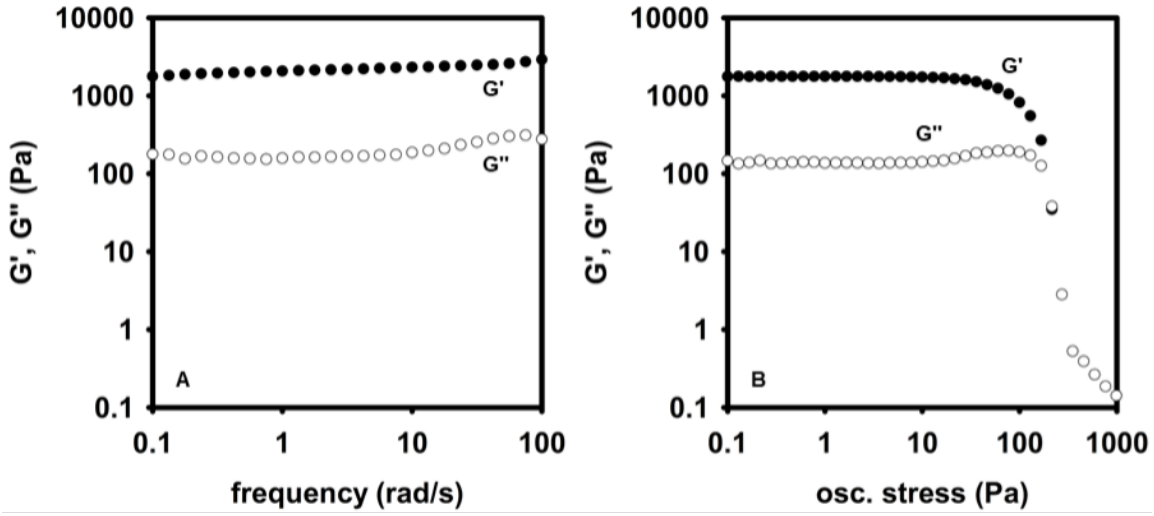

Figure A1.27. (A) Frequency and (B) oscillating stress sweep of S-WP1.3 gels.

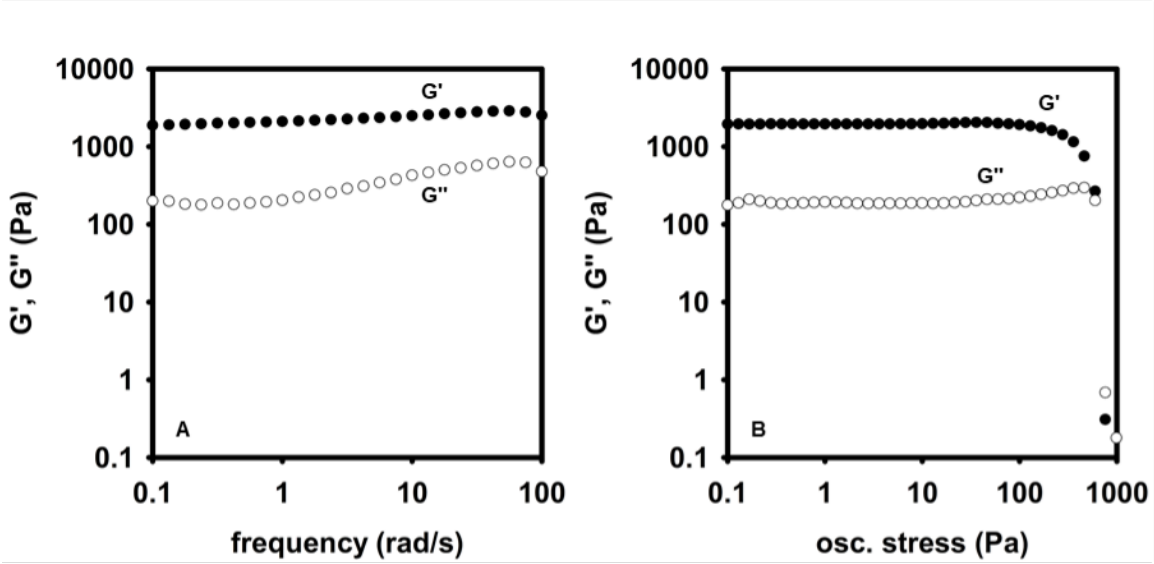

Figure A1.28. (A) Frequency and (B) oscillating stress sweep of S-WP1.8 gels.

B. Procedure for characterizing MB-loaded gels and flocs

An AR2000ex rheometer (TA Instruments) equipped with a stainless steel 20 mm crosshatch parallel plate was used to perform rheological measurements. The hydrogels/flocs were made using the procedures given in Section XF and Section XL. A pair of hydrogels were also prepared without adding MB. S-CNF-based hydrogels and flocs were made using final S-CNF and QHECE concentrations of 0.0800% w/v and 0.0600% w/v, respectively (~14 mg of total dry material).

Within 10 min of being made, gels/flocs were removed from their polypropylene tubes. First, excess water was removed via pipette (for gels) or by decanting the supernatant (for flocs). Gels/flocs were then loaded on the rheometer using a spatula. The gap was fixed at 1000 μm, and a solvent trap filled with water was utilized to limit solvent evaporation. All measurements were performed at 25 °C. Each sample was pre-sheared using a stress of 0.064 Pa for 30 s and then equilibrated for 5 min before performing a frequency sweep experiment from 0.1–100 rad/s using a stress of 1 Pa.

The rheological properties of MB-loaded gels/flocs were compared by averaging the frequency sweep spectra from either 2 or 3 gel/floc samples. For gels made with initial MB concentrations of either 0 μM or 313 μM, 2 samples were averaged. For flocs made with initial MB concentrations of 814 μM, 1628 μM, or 3130 μM, 3 samples were averaged.

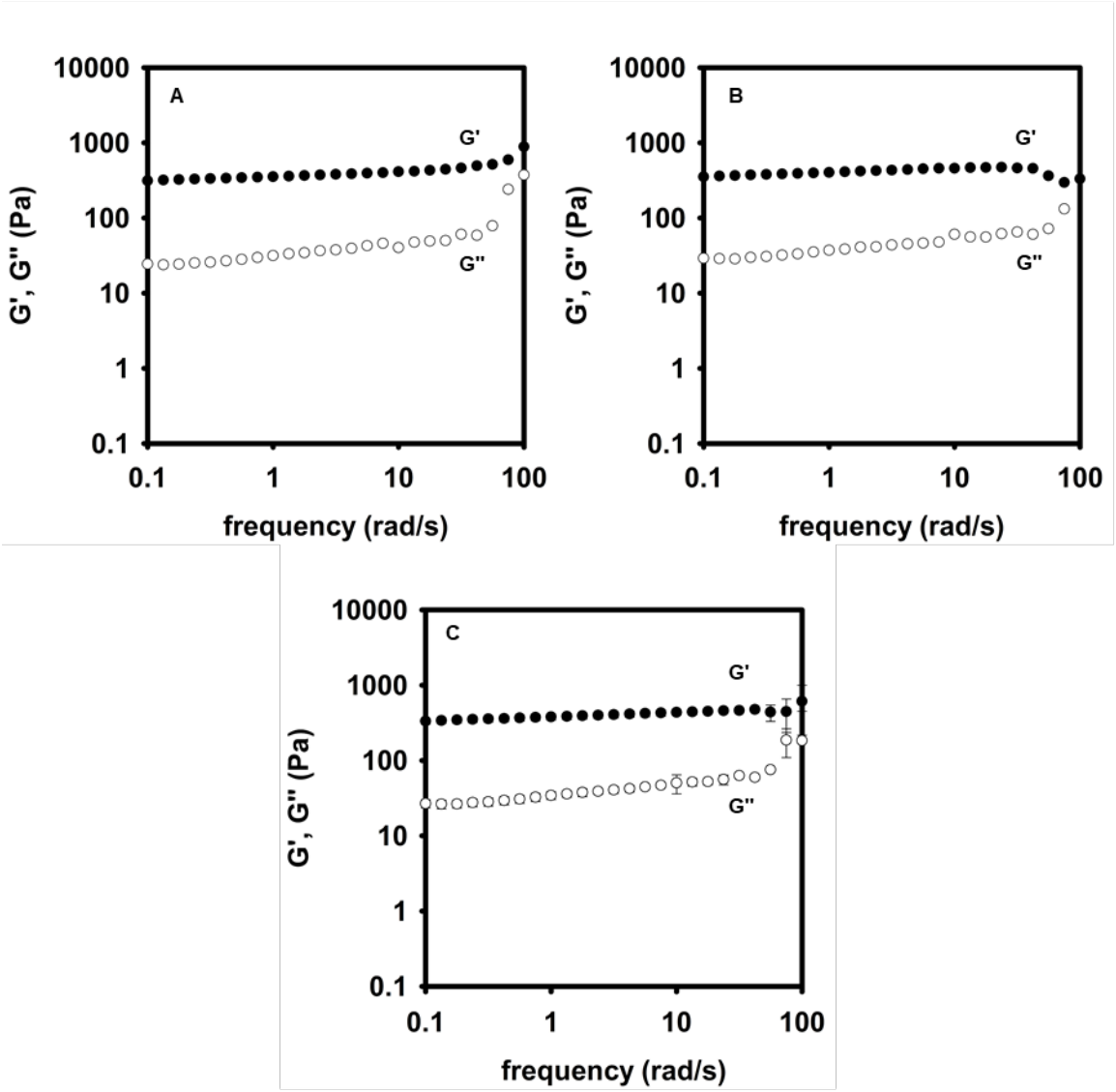

Figure A1.29. Frequency sweeps for SCNF1.8 gels made with a 0 μM initial MB concentration: (A) sample 1 and (B) sample 2. (C) Average frequency sweep from samples 1 and 2.

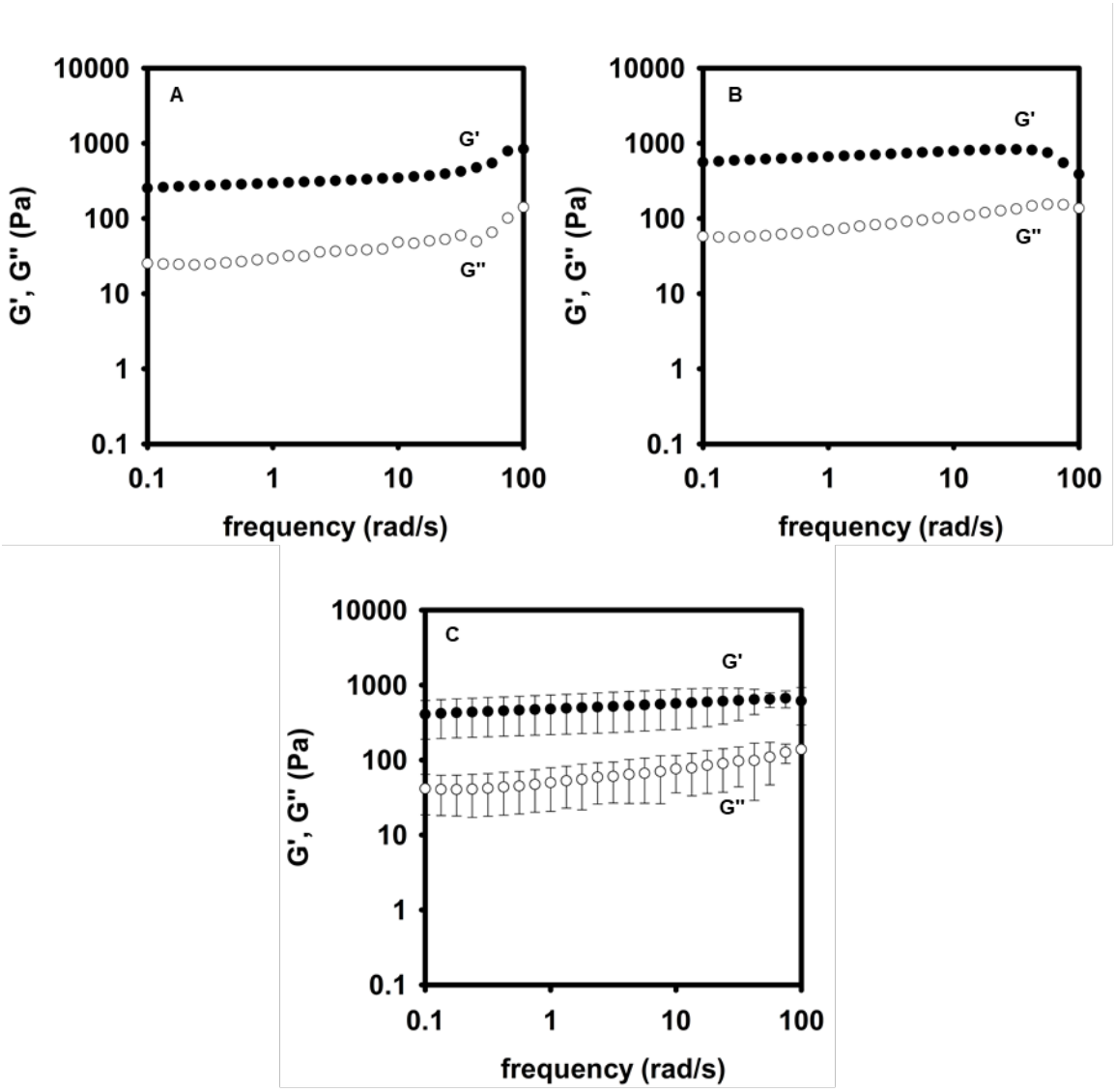

Figure A1.30. Frequency sweeps for SCNF1.8 gels made with a 313 μM initial MB concentration: (A) sample 1 and (B) sample 2. (C) Average frequency sweep from samples 1 and 2.

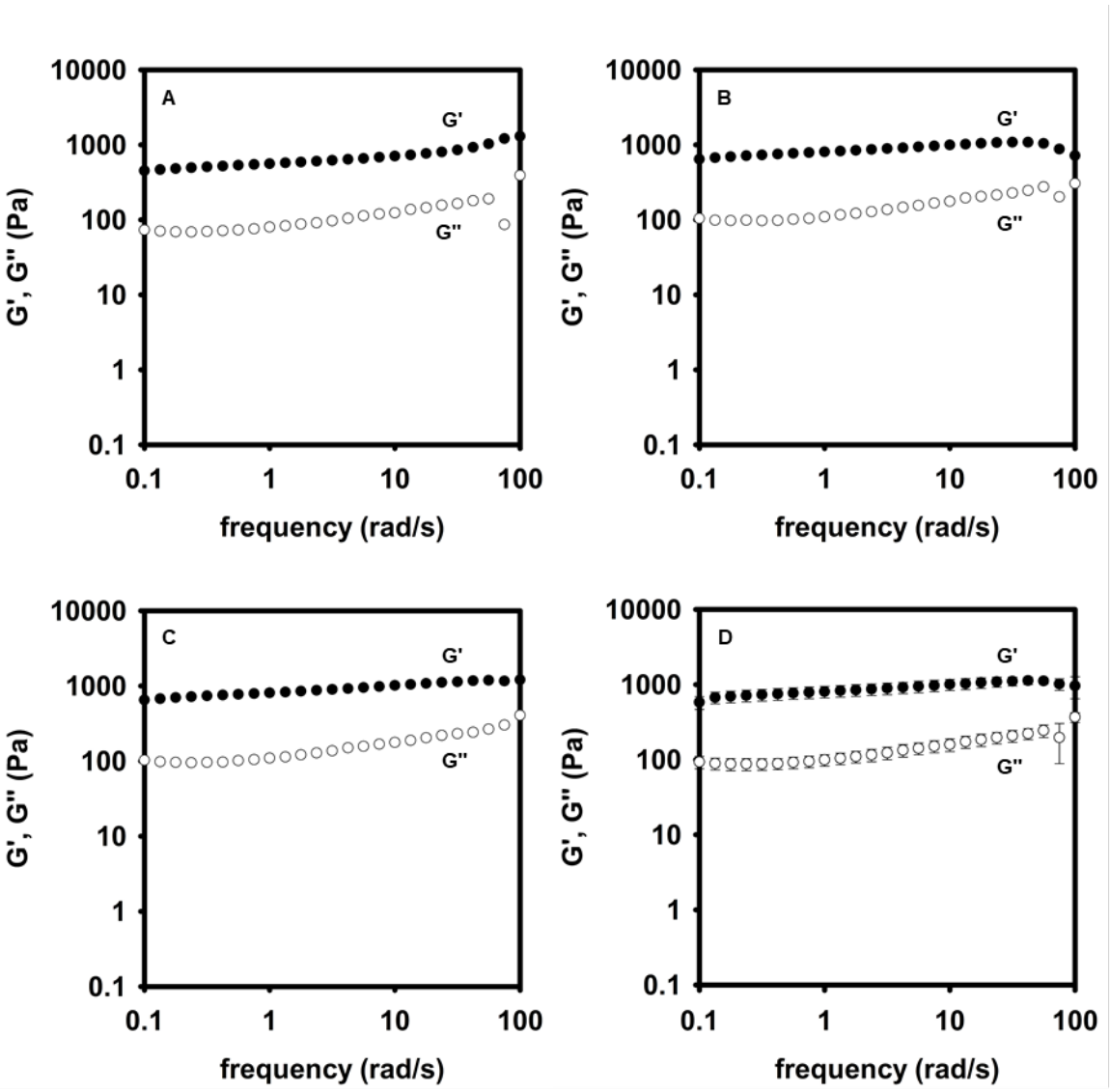

Figure A1.31. Frequency sweeps for SCNF1.8 flocs made with an 814 μM initial MB concentration: (A) sample 1, (B) sample 2, and (C) sample 3. (D) Average frequency sweep from samples 1, 2, and 3.

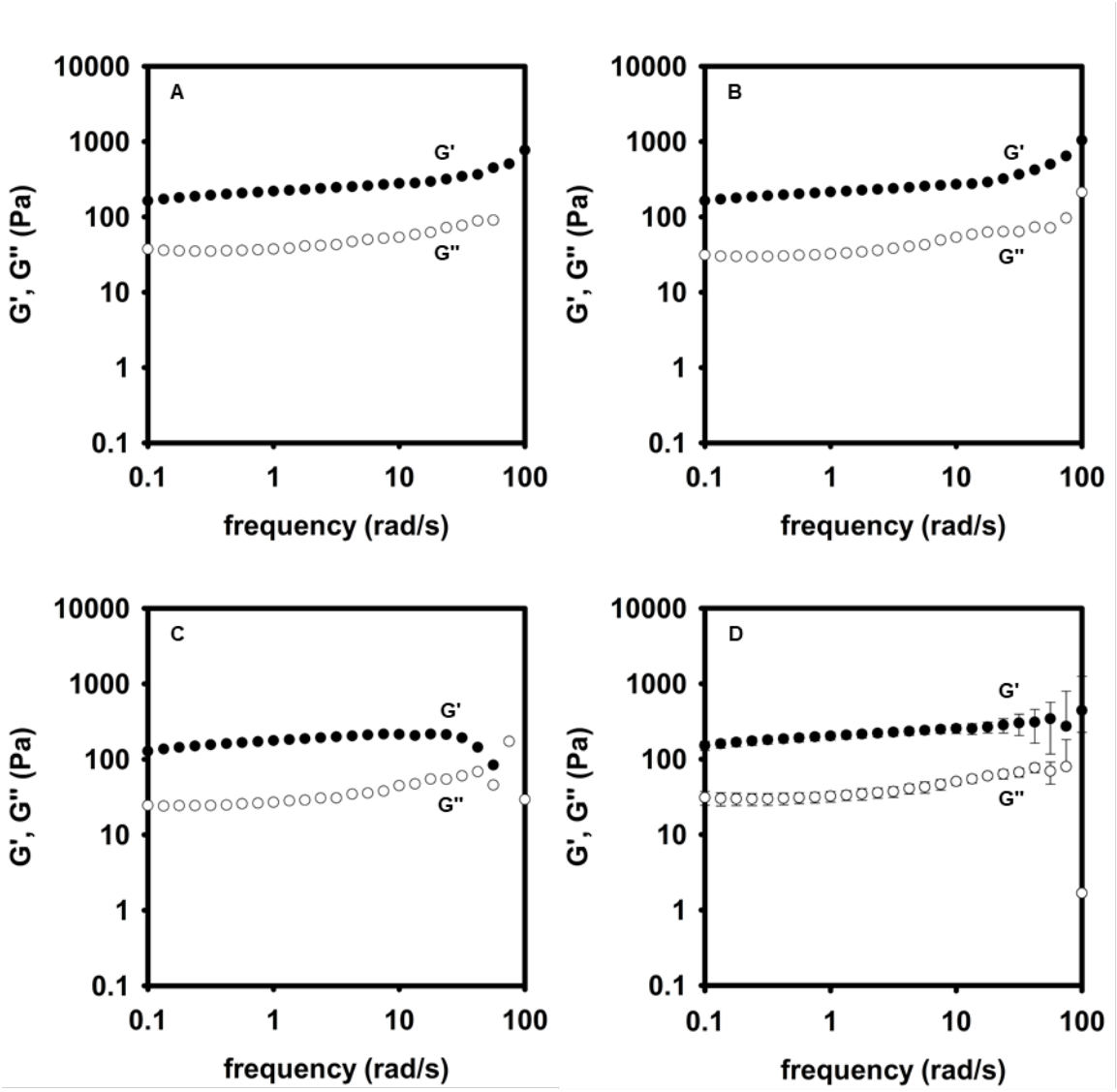

Figure A1.32. Frequency sweeps for SCNF1.8 flocs made with a 1628 μM initial MB concentration: (A) sample 1, (B) sample 2, and (C) sample 3. (D) Average frequency sweep from samples 1, 2, and 3.

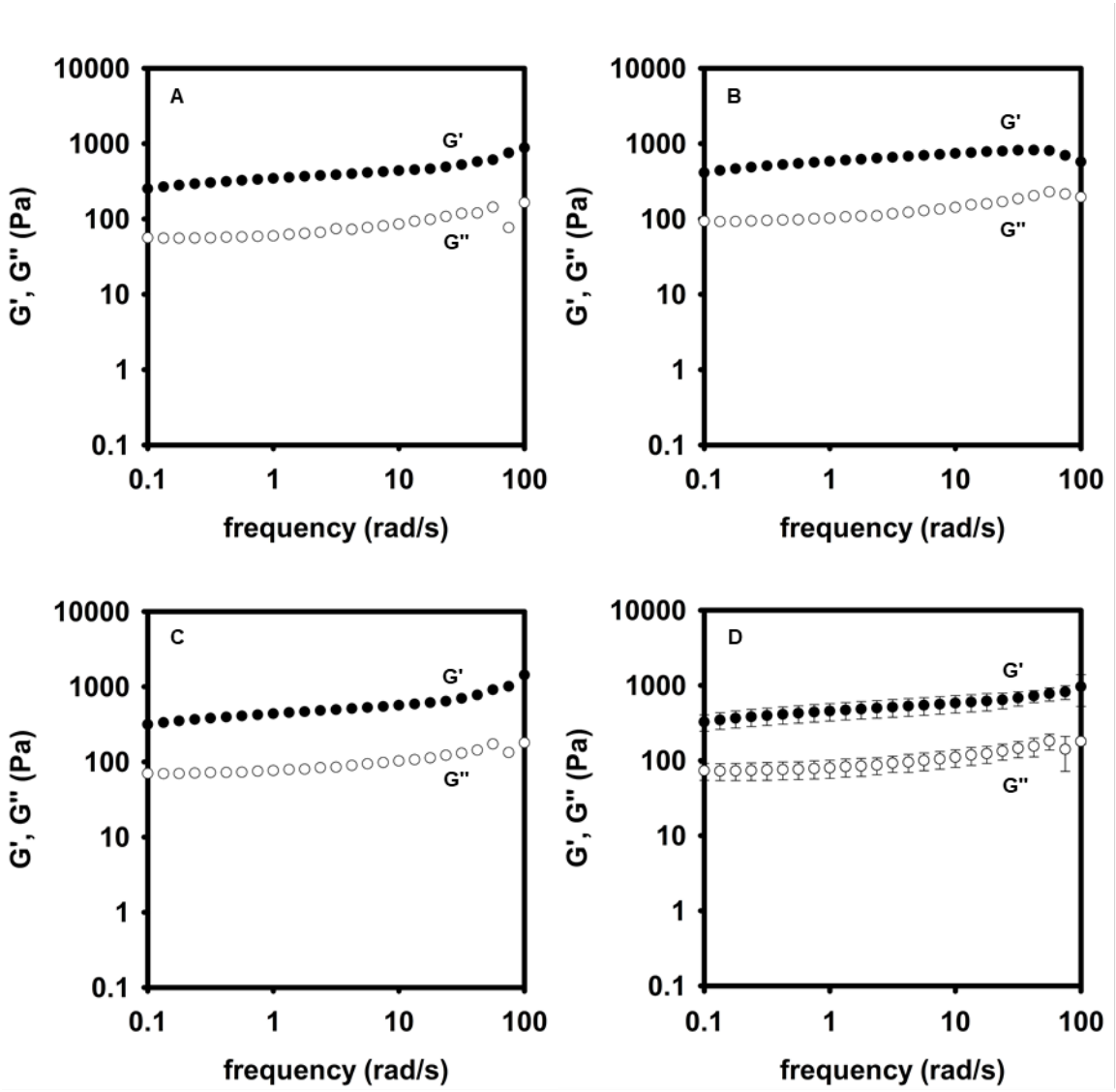

Figure A1.33. Frequency sweeps for SCNF1.8 flocs made with a 3130 μM initial MB concentration: (A) sample 1, (B) sample 2, and (C) sample 3. (D) Average frequency sweep from samples 1, 2, and 3.

X. Dye Adsorption Experiments

Note: 50 mL polypropylene centrifuge tubes were used when working with MB because we observed significant MB adsorption on glass vials during preliminary experiments.

A. General preparation of S-CNF mixtures

See Chapter 2 experimental section for details.

B. General preparation of QHECE solutions

See Chapter 2 experimental section for details.

C. General preparation of MB solutions

63 mM MB solutions were made by dissolving MB (100.0 mg, 312.6 μmol) in Millipore water (5.0 mL) in a 50 mL centrifuge tube. 31 mM MB solutions were made by dissolving MB (60.0 mg, 188 μmol) in Millipore water (6.0 mL) in a 50 mL centrifuge tube. MB solutions with lower concentrations were made by performing serial dilutions with either the 63 mM or 31 mM MB solutions and Millipore water.

D. General procedure for calculating MB adsorption in gels and flocs

To make gels or flocs, a volume of MB solution, with known concentration, was added to a 50 mL centrifuge tube followed by Millipore water to give a total volume of 2.0 mL. Then, an aliquot (4.0 mL) of S-CNF1.8 mixture and an aliquot (4.0 mL) of QHECE solution were added simultaneously, over a recorded time, directly to the bottom of the centrifuge tube with vortex mixing at a speed setting of 1.5. The centrifuge tube was then vortex mixed using a speed setting of 1.5 for an additional recorded "mixing" time. The centrifuge tube was then removed from the vortex mixer, and it was determined if a gel was formed. A gel was considered formed if: (1) There was one cohesive hydrogel with minimal amounts of small polyionic complexes that were not

connected to the gel. (2) The vial could be rotated 90° from a vertical to horizontal position without the localized gel breaking into smaller complexes.

If a gel formed, an aliquot of leftover solution was removed from the centrifuge tube, placed in a cuvette, and its UV-vis absorbance from 400–750 nm was measured. The UV-vis measurement was performed within 1 min of the gel being formed.

If a gel did not form, the mixtures were centrifuged for 2 min at ~1,500 × g, and then an aliquot of the supernatant was removed and placed in a cuvette. The absorbance spectrum of the solution was then collected from 400–750 nm within 4 min of the gel being formed.

A baseline correction was performed on all MB absorbance spectra to account for non-zero baselines. More specifically, the absorbance values for wavelengths 740–750 nm were averaged (because 740–750 nm was a region where the spectrum's absorbance was closest to 0), and this average absorbance was then subtracted from the entire spectrum. The corrected absorbance at 661 nm was then recorded for each MB solution. The concentration (C) of MB that was not adsorbed by a gel or floc was determined using the MB calibration curve (Figure A1.34).

The MB adsorption % was then determined using the following equation:

$$\text{MB adsorption \%} = \frac{C_0\text{-}C}{C_0} \text{ x } 100$$

Equation A1.4. Calculating MB adsorption %.

where C_0 is the initial dye concentration in the centrifuge tube. The initial dye concentration (in μM) was determined by calculating the mols of MB that were originally added to the centrifuge tube and using a total volume of 10 mL.

All MB adsorption experiments were performed in triplicate, unless noted, and average MB adsorption % values from the 3 trials are reported for each set of experimental conditions.

E. Generating a calibration curve for MB dissolved in Millipore water

MB (10.0 mg, 31.3 μmol, λ_{max} = 661 nm) was dissolved in Millipore water (10.0 mL) in a 50 mL centrifuge tube to make a 3.13 mM MB solution. Then, using Millipore water, serial dilutions were performed to make 0.313, 0.625, 1.56, 2.50, 3.13, 6.25, 15.6, 25.0, and 31.3 μM solutions in 50 mL centrifuge tubes. The UV-vis spectrum from 400–750 nm of each MB solution was acquired and corrected according to the baseline correction procedure in "general procedure for calculating MB adsorption in gels and flocs." This procedure was repeated to generate a second set of MB solutions and absorbance values. The absorbances of each MB concentration were averaged, and a plot of average absorbance versus MB concentration was generated (Figure A1.34 and Table A1.12).

Table A1.12. Absorbance (661 nm) of MB solutions with various concentrations.

MB concentration (μM)	trial 1 absorbance	trial 2 absorbance	avg absorbance
0.313	0.02	0.02	0.02 ± 0.00
0.625	0.04	0.04	0.04 ± 0.00
1.56	0.10	0.09	0.09 ± 0.01
2.50	0.15	0.15	0.15 ± 0.01
3.13	0.22	0.22	0.22 ± 0.00
6.25	0.43	0.40	0.41 ± 0.02
15.6	1.05	1.03	1.04 ± 0.01
25.0	1.59	1.56	1.58 ± 0.02
31.3	1.90	1.90	1.90 ± 0.00

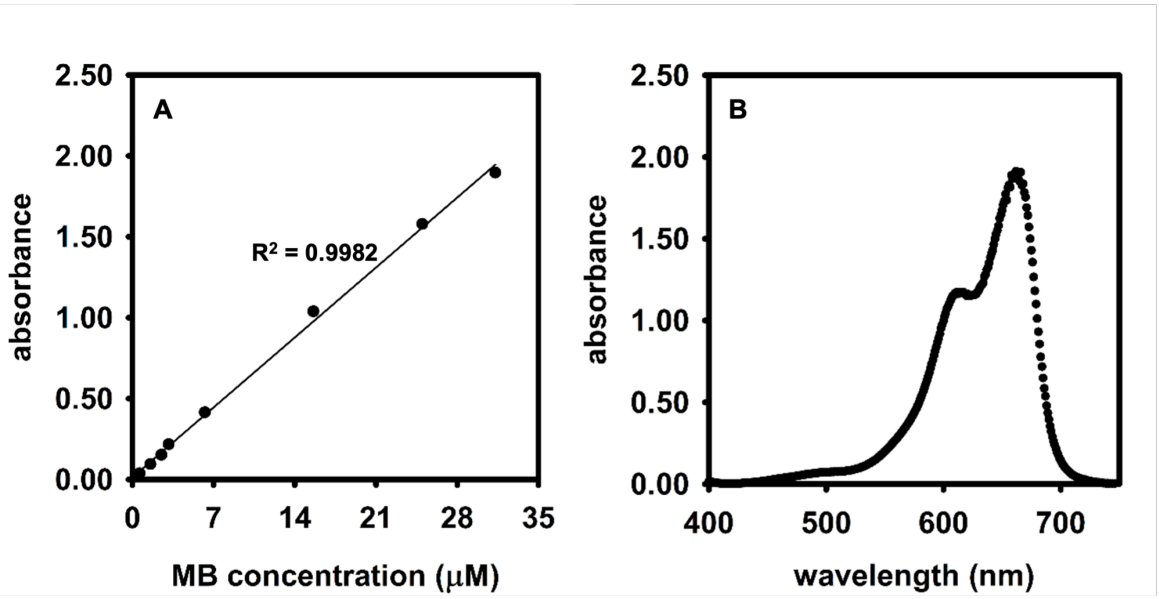

Figure A1.34. (A) Plot of absorbance (661 nm) versus concentration for MB in Millipore water. (B) Sample UV-vis spectrum of MB using the 31.3 μM solution.

F. Procedure for quantifying MB adsorption in S-CNF-based hydrogels for dye concentration versus MB adsorption % plot

0.200% w/v S-CNF1.8 mixtures, 0.150% w/v QHECE solutions, and a 31 mM MB solution were prepared according to the general procedures. Gel formation and MB adsorption calculations were performed according to the general procedure using the mixtures/solutions described in this section (Table A1.13). Only gels were formed in these experiments (no flocs). When larger initial MB concentrations were used (i.e., 406 μM), small pieces of the gel broke from the main gel during gelation, and these pieces were avoided when removing aliquots.

The following figure (Figure A1.35) is an example of a MB UV-vis spectrum following dye adsorption in a S-CNF-based gel (trial 4, Table A1.13). The spectrum is overlaid with a 31.3 μM MB spectrum that was used to make the calibration curve.

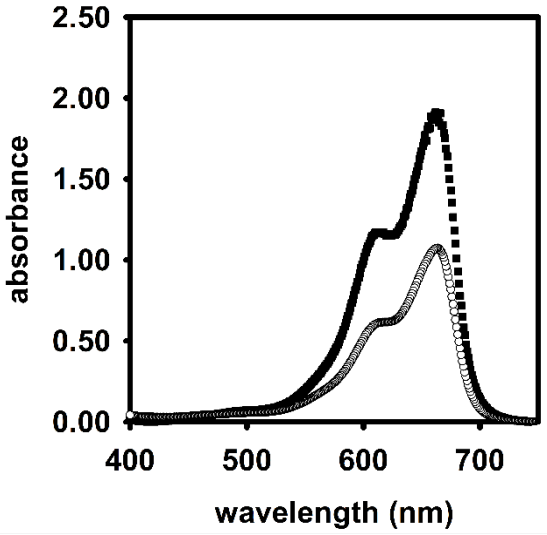

Figure A1.35. UV-vis spectra of a 31.3 μM MB solution used in the MB calibration curve (■), and a MB solution after hydrogel dye adsorption using an initial MB concentration of 94 μM (○).

Table A1.13. MB adsorption % by S-CNF-based hydrogels as a function of initial MB concentration.

trial	S-CNF and QHECE addition/mixing time (s)	volume of 31 mM MB (μL)	initial MB concentration (μM)	MB adsorption (%)	avg MB adsorption (%)
1	22/4	10.0	31	91	
2	20/6	10.0	31	93	92 ± 1
3	20/5	10.0	31	93	
4	20/8	30.0	94	82	
5	20/6	30.0	94	86	84 ± 2
6	20/8	30.0	94	86	
7	20/3	100.0	313	90	
8	20/3	100.0	313	87	88 ± 1
9	20/5	100.0	313	89	
10	20/1	130.0	406	96	
11	20/1	130.0	406	89	91 ± 4
12	20/2	130.0	406	89	

G. Procedure for quantifying MB adsorption in S-WP-based hydrogels for dye concentration vs MB adsorption % plot

S-WP1.8 fibers (50.0 mg) were soaked in Millipore water (12.5 mL) for 5 min. The mixture was then homogenized at 10k rpm for 1 min to make a 0.400% w/v S-WP1.8 mixture. This procedure was repeated to make 5 identical mixtures. QHECE (60.0 mg) was dissolved in Millipore water (20.0 mL) to make a 0.300% w/v QHECE solution. A 31 mM MB solution was prepared according to the general procedure. A 3.1 mM MB solution was also made by diluting the 31 mM MB solution (1.0 mL) with Millipore water (9.0 mL).

To make gels, a volume of either 31 or 3.1 mM MB stock solution was added to a 50 mL centrifuge tube followed by Millipore water to give a total volume of 2 mL. Then, gels were made, and MB adsorption calculations were performed according to the procedure using the 0.400% w/v S-WP1.8 mixtures and 0.300% w/v QHECE solutions described in this section (Table A1.14). Only gels were formed in these experiments (no flocs). When larger initial MB concentrations were used (i.e., 94 μM), small pieces of the gel broke from the main gel during gelation, and these pieces were avoided when removing aliquots.

The following figure (Figure A1.36) is an example of a MB UV-vis spectrum following dye adsorption in a S-WP-based gel (trial 7, Table A1.14). The spectrum is overlaid with a 31.3 μM MB spectrum that was used to make the calibration curve.

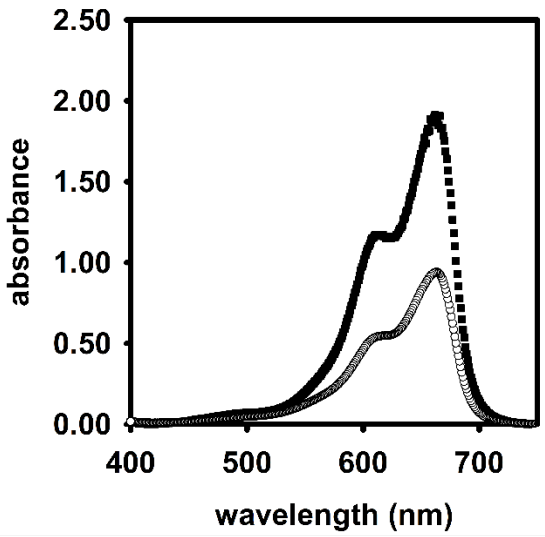

Figure A1.36. UV-vis spectra of a 31.3 μM MB solution used in the MB calibration curve (■), and a MB solution after hydrogel dye adsorption using an initial MB concentration of 31 μM (○).

Table A1.14. MB adsorption % by S-WP-based hydrogels as a function of initial MB concentration.

trial	S-WP and QHECE addition/ mixing time (s)	volume of MB stock sol'n (μL)	MB stock sol'n (mM)	initial MB concentration (μM)	MB adsorption (%)	avg MB adsorption (%)
1	20/3	10.0	3.1	3.1	55	
2	20/3	10.0	3.1	3.1	55	56 ± 1
3	20/2	10.0	3.1	3.1	57	
4	20/3	50.0	3.1	16	60	
5	20/3	50.0	3.1	16	58	59 ± 1
6	22/3	50.0	3.1	16	58	
7	20/10	10.0	31	31	52	
8	20/8	10.0	31	31	58	58 ± 6
9	20/7	10.0	31	31	64	
10	20/2	30.0	31	94	68	
11	20/3	30.0	31	94	63	66 ± 2
12	20/3	30.0	31	94	65	

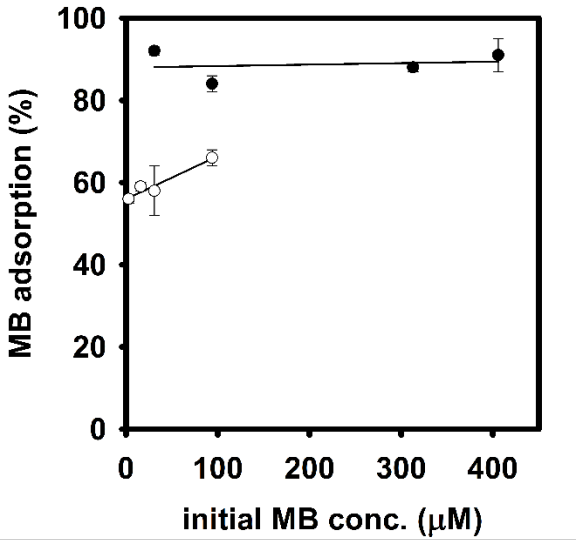

Figure A1.37. Dye adsorption % as a function of the initial dye concentration for gels made with S-CNF1.8 (●) and S-WP1.8 (○), respectively. The lines are present only as guides for the eye.

H. Procedure for measuring MB adsorption % as a function of S-CNF concentration

S-CNF1.8 fibers (37.5 mg) were soaked in Millipore water (12.5 mL) for 5 min. The mixture was then homogenized at 10k rpm for 1 min to make a 0.300% w/v S-CNF1.8 mixture. This procedure was repeated to make 3 identical mixtures. Using these mixtures, serial dilutions were performed to make 0.0500, 0.100, and 0.200% w/v S-CNF1.8 mixtures. Four QHECE solutions with concentrations of 0.0500, 0.100, 0.200, and 0.300% w/v were prepared by dissolving known amounts of QHECE in Millipore water (20.0 mL) in a 20 mL vial. A 63 mM MB solution was prepared according to the general procedure.

The procedure for making gels and adsorbing MB in this experiment is *slightly different* than the general procedure. To make gels, 4.0 mL of a known concentration S-CNF mixture was placed in a 50 mL polypropylene centrifuge tube. An aliquot of 63 mM MB solution (40.0 μL, 2.5 μmol) was directly added to the S-CNF mixture. The mixture was then vortex mixed using a

predetermined speed setting for 15 s, followed by addition of QHECE solution (4.0 mL), with a specific concentration, over a recorded time while vortex mixing at the predetermined speed (Table A1.15). The centrifuge tube was then vortex mixed for an additional recorded "mixing" time (Table A1.15) using the predetermined speed. The general procedure was then used to determine if gels were made and to calculate MB adsorption amounts. The initial dye concentration was determined to be 311 μM in these experiments by calculating the mols of MB that were originally added to the centrifuge tube and using a total volume of 8.04 mL.

The following figure (Figure A1.38) is an example of a MB UV-vis spectrum following dye adsorption in a S-CNF-based gel (trial 4, Table A1.15). The spectrum is overlaid with a 31.3 μM MB spectrum that was used to make the calibration curve.

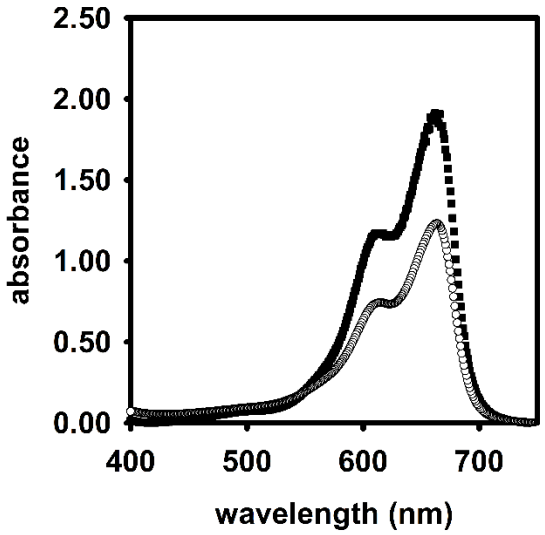

Figure A1.38. UV-vis spectra of a 31.3 μM MB solution used in the MB calibration curve (■), and a MB solution after hydrogel dye adsorption using an initial MB concentration of 311 μM (○).

Table A1.15. MB adsorption % by S-CNF-based hydrogels as a function of S-CNF concentration.

trial	final S-CNF conc. (% w/v)	final QHECE conc. (% w/v)	QHECE addition/ mixing time (s)	vortex speed setting	MB adsorption (%)	avg MB adsorption (%)
1	0.15	0.15	15/5	2	96.3	
2	0.15	0.15	18/4	2	93.1	94 ± 2
3	0.15	0.15	16/4	2	92.5	
4	0.10	0.10	18/5	1.5	93.7	
5	0.10	0.10	16/4	1.5	94.8	94.4 ± 0.6
6	0.10	0.10	17/4	1.5	94.6	
7	0.050	0.050	15/3	1.5	94.4	
8	0.050	0.050	15/1	1.5	94.5	94.6 ± 0.2
9	0.050	0.050	15/1	1.5	94.7	
10	0.025	0.025	15/1	1.5	87.5	
11	0.025	0.025	18/1	1.5	87.3	87.7 ± 0.5
12	0.025	0.025	15/1	1.5	88.2	

Using trials 7–9, the average adsorption capacity of S-CNF-based hydrogels was calculated to be 94.5 ± 0.2 mg MB/g hydrogel. The average adsorption capacity was determined by first using the MB calibration curve to find the mass of MB leftover in solution. This amount was subtracted from the initial mass of MB in solution to give a mass of MB adsorbed. The adsorption capacity for each trial was then calculated using the equation:

$$\text{adsorption capacity} = \frac{\text{MB adsorbed (mg)}}{0.0080\ \text{g}}$$

Equation A1.5. Calculating MB adsorption capacity in gels.

where the denominator is the total mass of hydrogel material (i.e., S-CNFs + QHECE). The adsorption capacities for the 3 trials were then averaged and reported above.

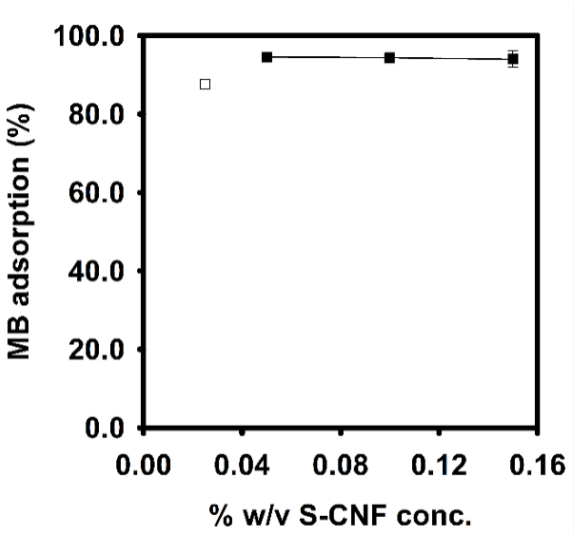

Figure A1.39. Dye adsorption % as a function of the final S-CNF1.8 concentration for samples where gels were (■) and were not (□) observed, respectively. The line is present only to guide the eye.

I. Determining the maximum ratios of dye/negative sites where gelation occurs

Three ratios were calculated to describe when the initial concentration of MB inhibits gelation for the hydrogels. The maximum ratio of dye/negative sites where hydrogels are formed (max ratio) is defined as the ratio between the maximum initial MB moles in solution to the moles of negative sites (i.e., sulfate groups) in the hydrogel:

$$\text{max ratio of dye/negative sites} = \frac{\text{maximum initial MB moles}}{\text{moles of negative sites}}$$

Equation A1.6. Calculating the max ratio of MB/negative sites.

The ratios were determined using the data from Table A1.13, Table A1.14, and Table A1.15. Note: these ratios were not calculated based on the moles of MB adsorbed.

For S-CNF-based hydrogels where MB adsorption % is monitored as a function of initial MB concentration, the max ratio was calculated using the hydrogels that were made in the presence of 4.06 μmol of MB (Table A1.13, trials 10–12). In each of these hydrogels, 8.0 mg S-CNF1.8 was

utilized, which corresponds to 14.4 μmol of negative sites. Accordingly, the max ratio is computed to be 0.28. For S-WP-based hydrogels, the max ratio was calculated using hydrogels made in the presence of 0.94 μmol of MB (Table A1.14, trials 10–12). In these hydrogels, 16 mg S-WP1.8 was used, which corresponds to 28.8 μmol of negative sites. The max ratio is then calculated to be 0.033.

For S-CNF-based hydrogels where MB adsorption % is monitored as a function of S-CNF concentration, the max ratio was calculated using the hydrogels made with 0.05% w/v S-CNFs (Table A1.15, trials 7–9). In these hydrogels, 4 mg S-CNF1.8, or 7.2 μmol of negative sites, was used along with 2.5 μmol of MB, giving a max ratio of 0.35.

J. Monitoring MB adsorption in S-CNF-based hydrogels over time

To study the MB adsorption process, we followed the decrease of MB in solution over time in the presence of hydrogels. It was found that the MB concentration decreases more over time when in the presence of S-CNF-based gels compared to a control MB solution. We attribute this decrease in MB concentration to intraparticle MB diffusion within the hydrogels.[3,4]

S-CNF1.8 mixtures, 0.200% w/v QHECE solutions, and a 63 mM MB solution were prepared according to the general procedure.

To make gels and monitor MB adsorption over time, 4.0 mL of 0.200% w/v S-CNF mixture was placed in a 50 mL polypropylene centrifuge tube. MB solution (40.0 μL, 63 mM, 2.5 μmol) was directly added to the S-CNF mixture. The mixture was then vortex mixed using a speed setting of 1.5 for 15 s, followed by addition of 0.200% w/v QHECE solution (4.0 mL) over a recorded time (QHECE addition) while vortex mixing with a speed setting of 1.5 (Table A1.16). The centrifuge tube was then vortex mixed for an additional recorded “mixing” time (Table A1.16)

using a speed setting of 1.5. The centrifuge tube was removed from the vortex mixer, and a gel was observed. An aliquot of solution was removed from the centrifuge tube, placed in a cuvette, and the absorbance spectrum of the solution from 400–750 nm was obtained. Then, the aliquot was returned to the centrifuge tube with the gel, and the centrifuge tube was wrapped in aluminum foil and placed in a closed, dark drawer to prevent light from degrading the MB. Then, at recorded time intervals, the centrifuge tube was removed from the drawer, an aliquot of solution was placed in a cuvette, the absorbance spectrum of the solution from 400–750 nm was obtained, the aliquot was returned to the centrifuge tube, and the centrifuge tube was placed back in a closed drawer. This procedure was performed for 3 hydrogel samples (Table A1.17 and Figure A1.41) to monitor the decrease of MB in solution with time.

Table A1.16. Gelation conditions for monitoring MB adsorption over time.

gel sample	QHECE addition/ mixing time (s)
1	20/5
2	18/5
3	19/4

A control MB solution was also monitored to determine the decrease of MB in solution over time. MB solution (40.0 μL, 63 mM, 2.5 μmol) was added to a centrifuge tube with Millipore water (8.0 mL) to make a 310 μM MB solution. Then, the 310 μM MB solution (500 μL) was combined with Millipore water (9.5 mL) in a centrifuge tube to make a 16 μM MB solution, which is called "the control" sample. The control sample was wrapped in aluminum foil and placed in a closed, dark drawer. Then, at recorded time intervals, the centrifuge tube was removed from the drawer, an aliquot of solution was placed in a cuvette, the absorbance spectrum of the solution from 400–

750 nm was obtained, the aliquot was returned to the centrifuge tube, and the centrifuge tube was placed back in a closed drawer.

The absorbance spectra at each time interval for the gel and control samples were obtained and baseline corrected according to the general procedure with *one exception*: for gel sample 2, the 20 min spectrum was corrected instead using the average absorbance for wavelengths 400–410 nm because this was the region where the spectrum's absorbance was closest to 0.

The following figure (Figure A1.40) contains examples of MB UV-vis spectra following dye adsorption in a S-CNF-based gel (using the spectra from gel sample 1 at 3 and 3000 min). The spectra are overlaid with a 31.3 μM MB spectrum that was used to make the calibration curve.

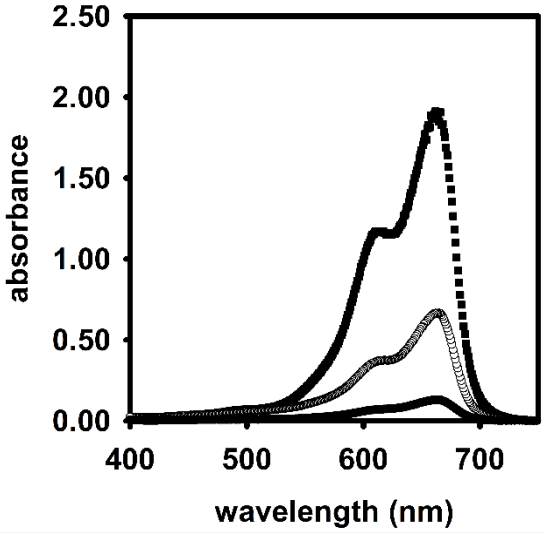

Figure A1.40. UV-vis spectra of a 31.3 μM MB solution used in the MB calibration curve (■), a MB solution after hydrogel dye adsorption for 3 min (○), and a MB solution after hydrogel dye adsorption for 3000 min (●).

Table A1.17. Decrease in MB concentration (conc.) over time in control and hydrogel-containing solutions.

time (min)	MB conc. in gel sample 1 (μM)	time (min)	MB conc. in gel sample 2 (μM)	time (min)	MB conc. in gel sample 3 (μM)	time (min)	MB conc. in control solution (μM)
3	11	2	9.1	2	9.8	2	17
17	7.9	20	8.9	15	8.9	15	16
34	6.6	33	6.3	31	7.3	30	16
60	5.6	60	5.2	60	5.4	60	16
120	4.1	120	4.0	120	4.1	120	16
241	3.1	240	3.2	240	3.2	240	15
480	2.6	480	2.5	480	2.7	420	15
1380	2.1	1380	2.3	1380	2.3	1380	15
3000	1.9	3000	1.8	3000	2.3	3000	15

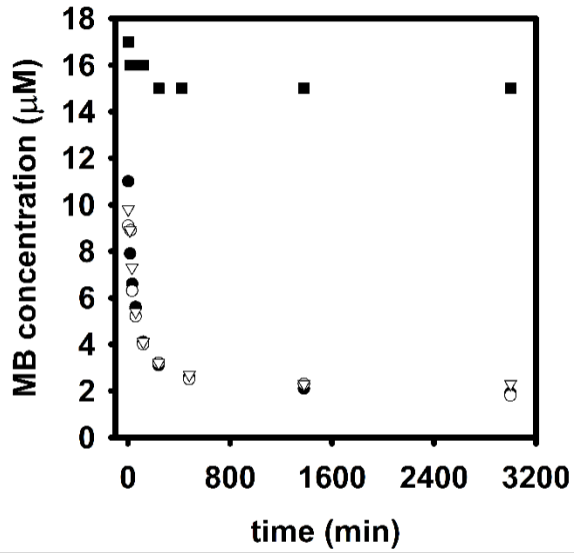

Figure A1.41. MB concentration over time in a control solution (■) and solutions containing gel sample 1 (●), gel sample 2 (▽), and gel sample 3 (○).

K. Procedure for quantifying MB adsorption in S-CNF-based flocs for dye concentration versus MB adsorption % plot

S-CNF1.8 mixtures, 0.150% w/v QHECE solutions, and a 31 mM MB solution were prepared according to the general procedure.

Flocs were formed according to the general procedure using the mixtures/solutions described in this section (Table A1.18). Gels were not formed, and only flocs were observed. Additionally, dilutions were performed to quantify the MB leftover in solution: after centrifuging, an aliquot (1 mL) of the supernatant was removed and diluted with Millipore water in a fresh polypropylene tube. An aliquot of the diluted MB sample was placed in a cuvette, and the absorbance spectrum of the solution from 400–750 nm was obtained and corrected according to the procedure in "general procedure for calculating MB adsorption in gels and flocs." The concentration (C_D) of MB in the diluted sample was determined using the MB calibration curve in "generating a calibration curve for MB dissolved in Millipore water." The concentration (C) of MB that was not adsorbed by the floc was determined by multiplying C_D by the dilution factor (D) used to prepare the diluted MB sample (Table A1.18). MB adsorption calculations were then performed according to the procedure.

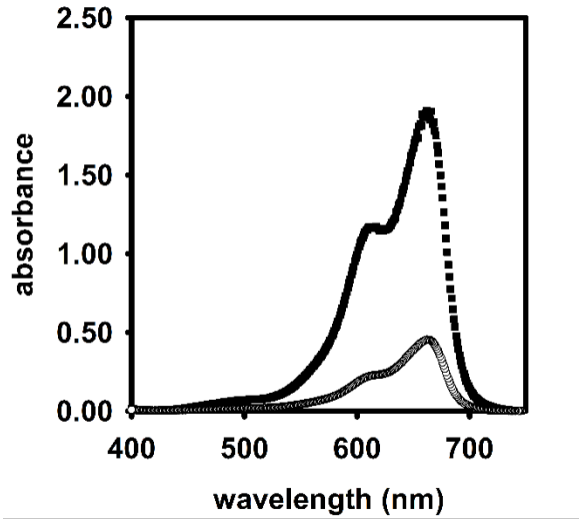

Figure A1.42. UV-vis spectra of a 31.3 μM MB solution used in the MB calibration curve (■), and a MB solution after floc dye adsorption using an initial MB concentration of 814 μM (○).

Table A1.18. MB adsorption % by S-CNF-based flocs as a function of initial MB concentration.

trial	S-CNF and QHECE addition/mixing time (s)	volume of 31 mM MB (μL)	initial MB concentration (μM)	dilution factor	MB adsorption (%)	avg MB adsorption (%)
1	21/4	260	814	10	93	
2	18/5	260	814	10	93	92 ± 1
3	21/5	260	814	10	91	
4	20/5	520	1628	15	71	
5	21/5	520	1628	15	69	70 ± 1
6	20/5	520	1628	15	69	
7	18/5	1000	3130	500	42	
8	20/5	1000	3130	500	52	48 ± 5
9	18/5	1000	3130	500	50	

L. Calculating MB adsorption capacity for S-CNF-based hydrogels and flocs

Average adsorption capacities of S-CNF-based gels and flocs were calculated as a function of initial MB concentration. Adsorption capacities were determined using the trials given in Table A1.13 and Table A1.18. The average adsorption capacity for each initial MB concentration was determined by first using the MB calibration curve to find the mass of MB leftover in solution after each adsorption trial. This amount was subtracted from the initial mass of MB in solution to give a mass of MB adsorbed. The adsorption capacity for each trial was then calculated using the equation:

$$\text{adsorption capacity} = \frac{\text{MB adsorbed (mg)}}{0.0140\ \text{g}}$$

Equation A1.7. Calculating adsorption capacity for flocs.

where the denominator is the total mass of the cellulose material (i.e., S-CNFs + QHECE). The adsorption capacities for the 3 trials were then averaged and reported below.

Table A1.19. S-CNF-based hydrogel (white) and floc (gray) adsorption capacity as a function of initial MB concentration.

initial MB concentration (μM)	adsorption capacity (mg dye adsorbed/g cellulose)
31	6.6 ± 0.1
94	18.1 ± 0.5
313	63 ± 1
406	85 ± 4
814	172 ± 2
1628	259 ± 5
3130	343 ± 36

M. Procedure for quantifying MB adsorption in S-CNF0.77-based flocs

A 0.200% w/v S-CNF0.77 mixture, 0.150% w/v QHECE solution, and 31 mM MB solution were prepared according to the general procedure.

Experiments were started by combining an aliquot of 31 mM MB solution (1.0 mL) with Millipore water (1.0 mL) in a 50 mL centrifuge tube to give a total volume of 2.0 mL. Flocs were then formed according to the general procedure using the mixtures/solutions described in this section (Table A1.20). Gels were not formed, and only flocs were observed. Additionally, dilutions were performed to quantify the MB leftover in solution: after centrifuging, an aliquot (1 mL) of the supernatant was removed and diluted 500x with Millipore water in new polypropylene tubes. An aliquot of the diluted MB sample was placed in a cuvette, and the absorbance spectrum of the solution from 400–750 nm was obtained and corrected according to the general procedure. The concentration (C_D) of MB in the diluted sample was determined using the MB calibration curve. The concentration (C) of MB that was not adsorbed by the floc was determined by multiplying C_D by the dilution factor (500) used to prepare the diluted MB sample. MB adsorption calculations were then performed according to the procedure. The initial dye concentration, C_0, in the centrifuge tube before adding S-CNFs and QHECE was 3130 μM.

Table A1.20. MB adsorption % by S-CNF0.77-based flocs.

trial	S-CNF and QHECE addition/mixing time (s)	MB adsorption (%)	avg MB adsorption (%)
1	20/12	17	
2	20/13	25	22 ± 4
3	22/10	23	

The average adsorption capacity of S-CNF0.77-based flocs was also calculated, and the adsorption capacity were determined using the trials given in Table A1.20. The average adsorption

capacity was determined by first using the MB calibration curve to find the mass of MB leftover in solution after each adsorption trial. This amount was subtracted from the initial mass of MB in solution to give a mass of MB adsorbed. The adsorption capacity for each trial was then calculated using Equation A1.7. The adsorption capacities for the 3 trials were then averaged to give 160 ± 30 mg MB adsorbed/g cellulose.

N. Influence of solution pH on dye adsorption

0.200% w/v S-CNF1.8 mixtures, 0.150% w/v QHECE solutions, and a 31 mM MB solution were prepared according to the general procedure.

Three solutions with different pHs were then prepared so that the final solution pH, when mixed with the S-CNF and QHECE mixtures, would be ~2.5, ~7, and ~11.5. The solution with a pH of ~7 was prepared with NaCl to ensure that this experiment probed the effects of pH and not ion concentration.

1) pH~7 solution: NaCl (23.1 mg, 0.395 mmol) was dissolved with Millipore water in a 25.0 mL volumetric flask to make a 15.8 mM NaCl solution. The pH of the solution was measured with a calibrated pH meter, but an accurate pH could not be measured due to large fluctuations in the observed pH, presumably because there were not enough H_3O^+ or OH^- ions present to obtain a stable reading. Thus, the NaCl solution was assumed to have a pH of 7 according to Millipore's website.[5]

2) pH~2.5 solution: concentrated HCl (2.6 mL, 12.1 M) was diluted with Millipore water in a 200 mL volumetric flask to make a 0.157 M HCl solution. Then, the 0.157 M solution (2.0 mL) was transferred to a 20 mL vial and diluted with Millipore water (18.0 mL) to give a 15.7 mM HCl

solution. The pH of the solution was measured with a calibrated pH meter and the solution pH was found to be 1.87, which corresponds to a true concentration of 13.5 mM HCl.

3) pH~11.5 solution: NaOH (15.8 mg, 0.395 mmol) was dissolved with Millipore water in a 25.0 mL volumetric flask to make a 15.8 mM NaOH solution. The pH of the solution was measured with a calibrated pH meter and the solution pH was found to be 12.22, which corresponds to a true concentration of 16.6 mM NaOH.

To make gels, one of the solutions with a known pH (1.97 mL) was placed in the bottom of a polypropylene centrifuge tube with 31 mM MB solution (30.0 μL) to give a total volume of 2.0 mL. Next, gels were formed, and MB adsorption was calculated according to the general procedure using the S-CNF and QHECE mixtures/solutions described in this section (Table A1.21). Only gels were formed in these experiments, and no flocs were observed. The initial dye concentration was determined to be 94 μM by calculating the mols of MB that were originally added to the centrifuge tube and using a total volume of 10 mL.

The following figure (Figure A1.43) shows examples of MB UV-vis spectra following dye adsorption in solutions with pH 11.51 and 2.58 (trials 1 and 7, Table A1.21). The spectra are overlaid with a 31.3 μM MB spectrum that was used to make the calibration curve.

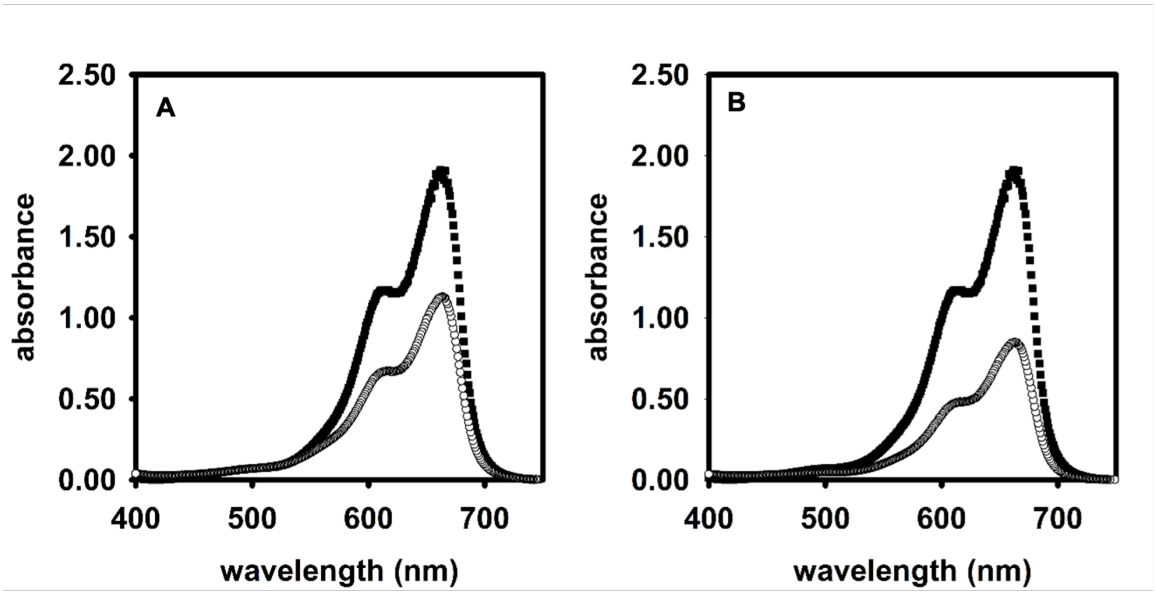

Figure A1.43. (A) UV-vis spectra of a 31.3 μM MB solution used in the MB calibration curve (■), and a MB solution after hydrogel dye adsorption in a pH 11.51 solution (○). (B) UV-vis spectra of a 31.3 μM MB solution used in the MB calibration curve (■), and a MB solution after hydrogel dye adsorption in a pH 2.58 solution (○).

Table A1.21. MB adsorption % by S-CNF-based hydrogels in solutions with various pH values.

trial	final solution pH	S-CNF and QHECE addition/ mixing time (s)	MB adsorption (%)	avg MB adsorption (%)
1	11.51	17/4	81	
2	11.51	20/4	84	80 ± 4
3	11.51	16/5	76	
4	7.00	17/5	78	
5	7.00	15/5	82	79 ± 2
6	7.00	20/5	78	
7	2.58	20/8	86	
8	2.58	20/5	87	84 ± 3
9	2.58	18/5	81	

O. Influence of salt concentration on dye adsorption

0.200% w/v S-CNF1.8 mixtures, 0.150% w/v QHECE solutions, and a 31 mM MB solution were prepared according to the general procedure.

Three solutions with different [NaCl] were then prepared so that the final [NaCl], when mixed with the S-CNF and QHECE mixtures, would be 31.1, 98.5, and 311 mM:

1) NaCl (230.8 mg, 3.949 mmol) was dissolved with Millipore water in a 25.0 mL volumetric flask to make a 158 mM NaCl solution.

2) NaCl (730.5 mg, 12.50 mmol) was dissolved with Millipore water in a 25.0 mL volumetric flask to make a 500 mM NaCl solution.

3) NaCl (2.308 g, 39.49 mmol) was dissolved with Millipore water in a 25.0 mL volumetric flask to make a 1.58 M NaCl solution.

To make gels, one of the NaCl solutions (1.97 mL) was placed in the bottom of a polypropylene centrifuge tube with 31 mM MB solution (30.0 μL) to give a total volume of 2.0 mL. Next, gels were formed, and MB adsorption was calculated according to the general procedure using the S-CNF and QHECE mixtures/solutions described in this section (Table A1.22). Gels were formed for all trials except when a final [NaCl] of 311 mM was utilized; thus, no MB adsorption % is reported for the 311 mM NaCl trials. The initial dye concentration was determined to be 94 μM by calculating the mols of MB that were originally added to the centrifuge tube and using a total volume of 10 mL.

The following figure (Figure A1.44) is an example of a MB UV-vis spectrum following dye adsorption in a 98.5 mM NaCl solution (trial 12, Table A1.22). The spectrum is overlaid with a 31.3 μM MB spectrum that was used to make the calibration curve.

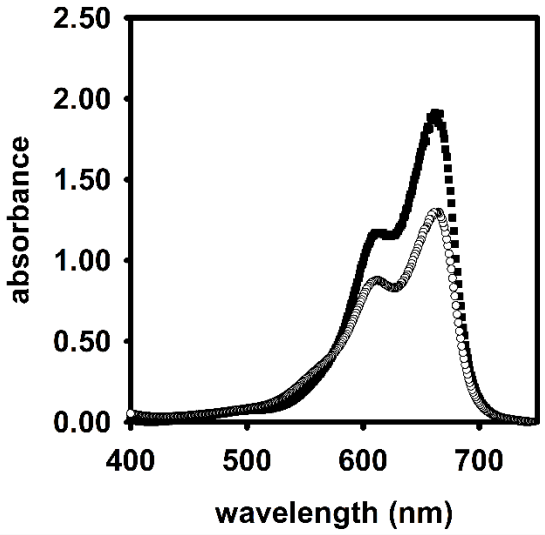

Figure A1.44. UV-vis spectra of a 31.3 μM MB solution used in the MB calibration curve (■), and a MB solution after hydrogel dye adsorption in a 98.5 mM NaCl solution (○).

Table A1.22. MB adsorption % with S-CNF-based hydrogels in various NaCl solutions.

trial	final [NaCl] (mM)	S-CNF and QHECE addition/ mixing time (s)	MB adsorption (%)	avg MB adsorption (%)
1	0	20/8	82	
2	0	20/6	86	84 ± 2
3	0	20/8	86	
4	3.11	17/5	78	
5	3.11	15/5	82	79 ± 2
6	3.11	20/5	78	
7	31.1	18/4	80	
8	31.1	20/4	78	80 ± 2
9	31.1	19/4	81	
10	98.5	20/3	78	
11	98.5	20/3	77	78 ± 0.5
12	98.5	18/3	78	
13	311	20/2	N/A[a]	
14	311	20/3	N/A[a]	N/A[a]
15	311	20/2	N/A[a]	

[a]MB adsorption % is not available because gels were not made in these samples.

P. Generating a calibration curve for MB dissolved in acidic ethanol

Note: "acidic ethanol" is used as shorthand to denote a 1:1 (v:v) ethanol:0.10 M aq. HCl solution. This calibration curve was generated because we wanted to measure MB desorption from hydrogels using acidic ethanol. In preliminary trials, it was noticed that the intensity of MB spectra in acidic ethanol was different than in Millipore water, so a new curve was generated to quantify MB as it desorbs.

First, 12.1 M aq. HCl (8.3 mL) was placed in a 1 L bottle with Millipore water (992.0 mL) to make a 0.10 M aq. HCl solution. MB (10.0 mg, 31.3 μmol, λ_{max} = 661 nm) was dissolved in acidic ethanol (10.0 mL) in a 50 mL centrifuge tube to make a 3.13 mM MB solution. Then, using acidic ethanol, serial dilutions were performed to make 0.313, 0.625, 1.56, 2.50, 3.13, 6.25, 15.6, 25.0, and 31.3 μM MB solutions in 50 mL centrifuge tubes. The UV-vis spectrum from 400–750 nm of each MB solution was acquired, and the spectra were adjusted to account for the non-zero baseline. More specifically, the absorbance values for wavelengths 740–750 nm were averaged (because 740–750 nm was a region where the spectrum's absorbance was closest to 0, and the protonated MB peak (~745 nm)[6] was not observed), and this average absorbance was then subtracted from the entire spectrum. The corrected absorbance at 661 nm was then recorded for each MB solution. This procedure was repeated to generate a second set of MB solutions and absorbance values. The absorbances of each MB concentration were averaged, and a plot of average absorbance versus MB concentration was generated (Figure A1.45 and Table A1.23).

Table A1.23. Absorbance (661 nm) of MB in acidic ethanol solutions with various concentrations.

MB concentration (μM)	trial 1 absorbance	trial 2 absorbance	avg absorbance
0.313	0.03	0.02	0.03 ± 0.00
0.625	0.05	0.04	0.04 ± 0.00
1.56	0.11	0.10	0.10 ± 0.00
2.50	0.17	0.17	0.17 ± 0.00
3.13	0.22	0.22	0.22 ± 0.00
6.25	0.47	0.39	0.43 ± 0.06
15.6	1.22	1.24	1.23 ± 0.02
25.0	2.07	2.10	2.08 ± 0.02
31.3	2.51	2.63	2.57 ± 0.08

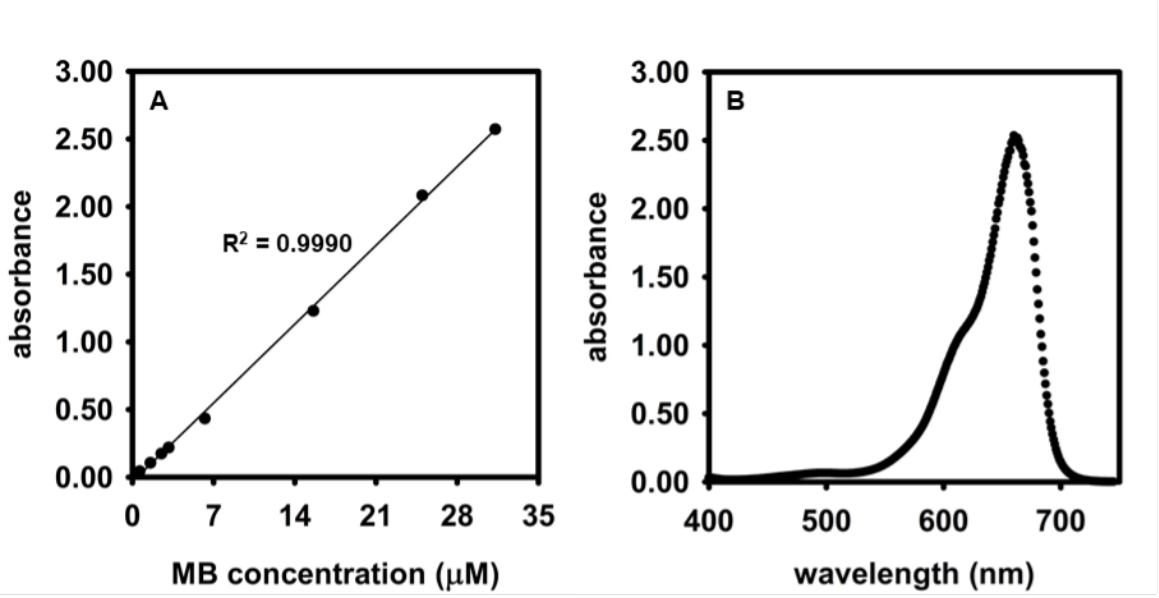

Figure A1.45. (A) Plot of absorbance (661 nm) versus concentration for MB in acidic ethanol. (B) Sample UV-vis spectrum of MB in acidic ethanol using the 31.3 μM solution.

Q. Monitoring MB desorption from S-CNF-based hydrogels over time

The reusability of S-CNF-based hydrogels was evaluated by monitoring the desorption of MB from gels in acidic ethanol. Acidic ethanol was chosen as the solvent because acid can disrupt the electrostatic interactions between S-CNFs and MB and enable MB desorption. The procedure for this experiment was carried out similar to Tam and coworkers.[7]

Note: “acidic ethanol” is used as shorthand to denote a 1:1 (v:v) ethanol:0.10 M aq. HCl solution, and the 0.10 M aq HCl solution employed here was also used to prepare the calibration curve for MB in acidic ethanol. 0.200% w/v S-CNF1.8 mixtures, 0.150% w/v QHECE solutions, and a 31 mM MB solution were prepared according to the general procedure.

Before monitoring MB desorption, an acidic ethanol solution (50.0 mL) was prepared in a 50 mL polypropylene centrifuge tube (“tube 1”). The tube was wrapped in aluminum foil to prevent light from hitting the solution, and the tube was set aside for later use.

Millipore water (1.92 mL) was combined with an aliquot of 31 mM MB solution (80.0 μL) in a 50 mL polypropylene centrifuge tube (“tube 2”), and the solution was vortex mixed using a speed setting of 1.5 for 15 s. Then, S-CNF1.8-based gels were produced according to the general procedure using the S-CNF and QHECE mixtures/solutions described in this section (Table A1.24). After a gel was formed, the gel was removed from tube 2 using a spatula and placed in tube 1. Tube 1 was capped and placed in a closed, dark drawer. Then, an aliquot of leftover solution from tube 2 was placed in a cuvette, and an absorbance spectrum from 400–750 nm was obtained and corrected according to the general procedure. Using the corrected absorbance value at 661 nm and the calibration curve, the mass of MB adsorbed in the gel was determined.

Then, at recorded time intervals, tube 1 was removed from the closed drawer and inverted to mix the contents of the tube. An aliquot of solution was then placed in a cuvette, and the absorbance spectrum of the solution was obtained and corrected according to the procedure. The aliquot was returned to tube 1, and the tube was placed back in a closed drawer. For the aliquots removed from tube 1, the concentration of MB in solution at each time point was determined using the MB calibration curve in “generating a calibration curve for MB dissolved in acidic ethanol” and the corrected absorbance of the solutions at 661 nm.

The initial dye concentration in tube 2 was determined to be 250 μM by calculating the mols of MB that were originally added to the centrifuge tube and using a total volume of 10 mL. The mass of adsorbed MB (MAMB) was determined by subtracting the mass of MB leftover in solution from the initial MB mass in solution (800 μg).

The mass of desorbed MB (MDMB) in solution was calculated assuming a total volume of 50.0 mL. The MB desorption % was calculated at each time point using the following equation:

$$\text{MB desorption \%} = \frac{\text{MDMB}}{\text{MAMB}} \text{ x } 100$$

Equation A1.8. Calculating MB desorption %.

This procedure was performed for 3 hydrogel samples (Table A1.25 and Figure 2.5) to monitor the desorption of MB with time. The MB desorption % at 24 h (1440 min) was found to be 55 ± 2 % by averaging the MB desorption % at 24 h for the 3 hydrogel samples.

Table A1.24. S-CNF1.8-based hydrogels for MB desorption.

gel sample	S-CNF and QHECE addition/ mixing time (s)	MB adsorption (%)
1	20/8	89
2	20/5	89
3	19/5	91

The following figure (Figure A1.46) contains examples of MB UV-vis spectra following dye desorption from a S-CNF-based gel (gel sample 1 at 1440 min). The spectrum is overlaid with a 31.3 μM MB spectrum that was used to make the MB calibration curve in acidic ethanol.

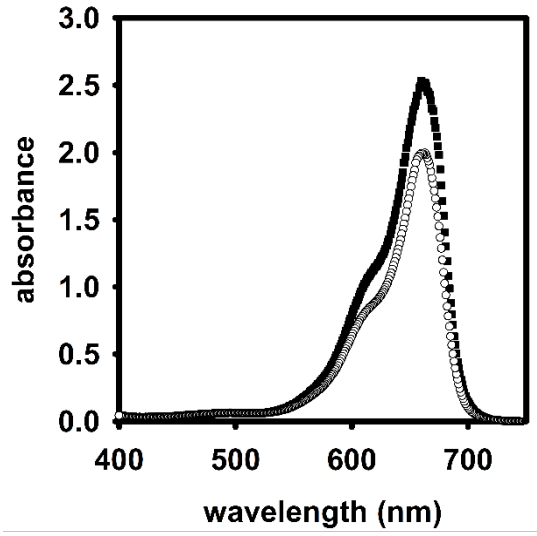

Figure A1.46. UV-vis spectra of a 31.3 μM MB in acidic ethanol (■), and a MB solution 1440 min after desorption from a hydrogel (○).

Table A1.25. MB desorption % over time from S-CNF1.8-based hydrogels.

time (min)	MB desorption (%) from gel sample 1	time (min)	MB desorption (%) from gel sample 2	time (min)	MB desorption (%) from gel sample 3
6	1.1	6	1.1	5	1.1
67	9.5	60	6.6	61	10
120	22	120	21	120	23
240	30	240	28	240	33
1140	49	1140	46	1140	53
1440	55	1440	53	1440	57
1680	59	1680	56	1680	61
2880	67	2880	65	2880	68

R. Determining the pH of acidic ethanol solutions

Note: "acidic ethanol" is used as shorthand to denote a 1:1 (v:v) ethanol:0.10 M aq. HCl solution. First, 12.1 M aq. HCl (8.3 mL) was placed in a 1 L bottle with Millipore water (992.0 mL) to make a 0.10 M aq. HCl solution. Then, an acidic ethanol solution (50.0 mL) was prepared by combining 0.1 M aq. HCl solution (25.0 mL) and ethanol (25.0 mL) in a 50 mL polypropylene centrifuge tube. A pH meter was inserted into the acidic ethanol solution and equilibrated for 10 min. The pH of the acidic ethanol was found to be 1.55.

‘

S. Comparing MB adsorption on S-CNF fibers and in S-CNF-based gels

Control experiments were performed in this section and section "MB adsorption in premade S-CNF gels" (below) to assess the efficiency of S-CNF-based gels made in the presence of MB. Here, S-CNF fibers were added to MB solutions without QHECE, and MB adsorption was quantified.

For these experiments, a S-CNF1.9 sample was synthesized and characterized according to the procedure with *one exception*. After quenching the reaction mixture with methanol, the mixture was vacuum filtered using a polyamide filter and buchner funnel. The remaining fibers were rinsed on the filter with Millipore water (~10 mL) and then 0.1 M NaOH (~15 mL) to ensure that any leftover acid was quenched and to introduce Na counterions to sulfate groups on the fibers. The pH of the filtrate was found to be ~12. The fibers were then rinsed on the filter with Millipore water (~140 mL) until the pH of the filtrate was ~6/7 and the conductivity was ~400 μS/cm. The fibers were then placed in smaller glass vials, frozen in liquid N_2, and dried under vacuum on a Schlenk line to remove excess water.

0.200% w/v S-CNF1.9 mixtures, 0.200% w/v QHECE solutions were prepared according to the general procedure. A 31 mM MB solution were prepared by dissolving MB (70.0 mg, 0.219 mmol) in Millipore water (7.0 mL) in a 50 mL polypropylene tube. A 0.10 M HCl solution was prepared.

First, gel formation experiments and MB adsorption calculations were performed according to the general procedure, using the mixtures/solutions described in this section, to serve as a direct comparison for the control experiments. The results from these experiments are trials 1–3 in Table A1.26. Only gels were formed in these experiments (no flocs).

Next, S-CNFs *only* were used to adsorb MB. These experiments were carried out according to the general procedure except that Millipore water (4 mL) was added with the S-CNFs to the MB solution instead of QHECE. After the water/S-CNFs/MB were combined, the centrifuge tube was removed from the vortex mixer, and no gel was formed. The tube was centrifuged at ~3200 × g for 2 min, and an aliquot of clear, violet-colored supernatant (1 mL) was removed from the tube and diluted with 0.1 M HCl (9 mL) in a fresh polypropylene tube.[8] This caused the color of the diluted supernatant sample to change from violet to blue. An aliquot of the diluted solution was then placed in a cuvette, and its UV-vis absorbance from 400–750 nm was measured. MB adsorption calculations were performed according to the general procedure except that the sample's spectrum was corrected instead using the average absorbance for wavelengths 415-425 nm because this was the region where the spectrum's absorbance was closest to 0. No significant peak at ~745 nm, corresponding to protonated MB,[6] was observed. The S-CNF *only* experiments were performed in triplicate (trials 4–6 in Table A1.26), and an average MB adsorption % values from the 3 trials is reported.

Table A1.26. Comparing MB adsorption in S-CNF fibers and S-CNF-based gels.

trial	S-CNF and QHECE/water addition/ mixing time (s)	MB adsorption (%)	avg MB adsorption (%)
1	20/17	91	
2	20/15	94	92 ± 1
3	20/17	92	
4	17/13	85	
5	17/12	86	85.4 ± 0.3
6	18/12	85	

T. MB adsorption in premade S-CNF gels

A second control experiment was performed by monitoring MB adsorption over time when premade S-CNF-based gels were added to MB solutions. The results from these control experiments show that S-CNF based gels made in MB solutions adsorb more MB in 2 min than when premade gels are added to MB solutions. Additionally, it was observed that when gels are premade and added to MB solutions, the gels completely break down into flocs after 120 min, likely because MB is preferentially interacting with anionic sites on the S-CNFs and disrupting electrostatic crosslinking with QHECE. This behavior suggests that MB adsorption occurs primarily through charge driven complexation as opposed to osmotically driven adsorption within the gel matrix.

The S-CNF1.9 fibers made in section "Comparing MB adsorption on S-CNF fibers and in S-CNF-based gels", above, were used for these experiments. 0.200% w/v S-CNF1.9 mixtures, 0.200% w/v QHECE solutions were prepared according to the general procedure. A 31 mM MB solution were prepared by dissolving MB (70.0 mg, 0.219 mmol) in Millipore water (7.0 mL) in a 50 mL polypropylene tube.

Millipore water (9.9 mL) and 31 mM MB solution (100.0 μL, 3.1 μmol) were combined in a 50 mL polypropylene centrifuge tube. The tube was wrapped in aluminum foil and designated as "tube 1".

Next, Millipore water (2.0 mL) was added to a different 50 mL polypropylene centrifuge tube ("tube 2"). Then, aliquots of 0.200% w/v S-CNF1.9 mixture and 0.200% w/v QHECE solution were combined in tube 2 according to the general procedure except that no MB was present (see Table A1.27 for details). A gel was produced, removed from tube 2 using a spatula, and placed in tube 1. Tube 1 was then placed in a closed, dark drawer. At specific time points, tube 1 was removed from the drawer, and an aliquot of solution (0.5 mL) was removed and diluted with Millipore water (4.5 mL) in a fresh 50 mL polypropylene centrifuge tube. Tube 1 was then placed back in the closed, dark drawer. The diluted sample was placed in a cuvette, and its UV-vis absorbance from 400–750 nm was measured. Aliquots from tube 1 were measured like this for the first 30 min of the gel soaking in tube 1. For a 60-min time point, tube 1 was removed from the drawer, an *undiluted* aliquot of solution was placed in a cuvette, the absorbance spectrum of the solution from 400–750 nm was obtained, the aliquot was returned to the centrifuge tube, and the centrifuge tube was placed back in a closed, dark drawer. The MB adsorption % at each time point was calculated according to the general procedure. The initial dye concentration was determined to be 310 μM by calculating the mols of MB that were originally added to the centrifuge tube and using a total volume of 10 mL. This procedure was repeated for 3 samples, and the MB adsorption % values were averaged for each time point (Table A1.28). Qualitatively, in all 3 samples, the gels began to break down into flocs after soaking in MB for ~30 min. After 120 min of soaking, the gels were completely dissociated into flocs.

Table A1.27. Mixing conditions for making the S-CNF1.9-based hydrogels that were added to 310 μM MB solutions.

gel sample	S-CNF and QHECE addition/ mixing time (s)
1	18/14
2	20/15
3	18/13

Table A1.28. MB adsorption % over time when S-CNF1.9-based hydrogels are added to 310 μM MB solutions.

time (min)	MB adsorption (%) in gel sample 1	time (min)	MB adsorption (%) in gel sample 2	time (min)	MB adsorption (%) in gel sample 3	time (min)	avg MB adsorption (%)
2	12	2	32	2	13	2	20 ± 10
15	46	15	68	15	60	15	40 ±10
30	73	30	89	30	86	30	83 ± 8
60	91	60	97	60	97	60	95 ± 4

XI. References

(1) Hasani, M.; Cranston, E.; Westman, G.; Gray, D. Cationic surface functionalization of cellulose nanocrystals. *Soft Matter*. **2008**, *4*, 2238–2244.

(2) Lemmers, M.; Spruijt, E.; Beun, L.; Fokkink, R.; Leermakers, F.; Portale, G.; Cohen Stuart, M.; van der Gucht, J. The influence of charge ratio on transient networks of polyelectrolyte complex micelles *Soft Matter*, **2012**, *8*, 104–117.

(3) Jiang, F.; Dinh, D.; Hsieh, D. Y-L. Adsorption and desorption of cationic malachite green dye on cellulose nanofibril aerogels. *Carbohydr. Polym*. **2017**, *173*, 286–294.

(4) Deng, H.; Lu, J.; Li, G.; Zhang, G.; Wang, X. Adsorption of methylene blue on adsorbent materials produced from cotton stalk. *Chem. Eng. J*. **2011**, *172*, 326–334.

(5) Millipore Sigma. Water for pH measurement. https://www.emdmillipore.com/US/en/water-purification/learning-centers/applications/inorganic-analysis/ph-measurement/water-impact/MK6b.qB.3g4AAAFUNWISsxU6,nav?ReferrerURL=https%3A%2F%2Fwww.google.com%2F (accessed November 11, 2019).

(6) Ghosh, A. Study of the self-association of methylene blue from protonation equilibriums. *J. Am. Chem. Soc.* **1970**, *92*, 6415–6418.

(7) Mohammed, N.; Grishkewich, N.; Berry R.;, Tam, K. Cellulose nanocrystal–alginate hydrogel beads as novel adsorbents for organic dyes in aqueous solutions. *Cellulose* **2015**, *22*, 3725–3738.

(8) According to literature, MB appears violet in alkaline solutions (see Adamcikova, L.; Pavlikova, K.; Sevcik, P. The decay of methylene blue in alkaline solution. *React. Kinet. Catal. Lett.*, **2000**, *69*, 91–94). Thus, 0.10 M HCl was used to dilute the supernatant and cause the supernatant sample to become blue again so MB could be quantified in solution using the calibration curve in "generating a calibration curve for MB dissolved in Millipore water."

Appendix 2 Supporting Information for Chapter 3

I. Materials 168

II. General Experimental 169

III. Synthesis and Characterization of Quaternized Wood Pulps (QWPs) 170

A. Synthesis of QWPs 170

B. Conductometric titrations for QWPs 170

C. Elemental analysis (EA) 171

D. Raman spectroscopy of QWPs 172

IV. PFAS adsorption experiments 175

A. General preparation of QWP mixtures 175

B. General preparation of 20.0 mg/L PFOS and PFOA solutions 175

C. Preparation of PFOS and PFOA standards for HPLC-MS 175

D. General procedure for adsorption experiments 176

E. General procedure for analyzing PFOS/PFOA solutions in-house 176

F. Eurofins procedure for analyzing PFAS concentrations 180

G. General procedure for calculating PFAS adsorption % and capacity 181

H. Procedure for determining effect of QWP CD on PFOS adsorption over time 182

I. Procedure for determining effect of QWP CD on PFOA adsorption over time 184

J. Procedure for determining effect of QWP1.5 concentration on PFOS adsorption 187

K. PFOS/PFOA adsorption over time with QWP1.5 188

L. Calculating pseudo-second order adsorption parameters 191

M. Adsorption isotherms for PFOS/PFOA adsorption with QWP1.5 193

N. Calculating distribution coefficients 199
O. Fitting isotherm data with Langmuir and Freundlich models 199
P. Adsorbing multiple PFASs over time with QWP1.5 203
Q. Calculating Specific UV Absorbance ($SUVA_{254}$) of humic acid (HA) 209
R. Adsorbing PFOS and PFOA in solutions with different pHs 211
S. Adsorbing PFOS and PFOA in the presence of NaCl 217
V. References 221

I. Materials

Bleached hardwood pulp was generously donated by Cellulose Lab. Hydrochloric acid (ACS reagent, 37%), acetone, sodium hydroxide (NaOH), 2-propanol (IPA), glycidyl trimethyl ammonium chloride (GMAC), sodium nitrate, humic acid (HA), perfluorooctanoic acid (PFOA, CAS# 335-67-1), heptadecafluorooctane sulfonic acid potassium salt (PFOS, CAS# 2795-39-3), potassium nonafluoro-1-butanesulfonate (PFBS, CAS# 29420-49-3), and heptafluorobutyric acid (PFBA, CAS# 375-22-4) were purchased from Aldrich and used without further purification. Undecafluoro-2-methyl-3-oxahexanoic acid (GenX, CAS# 13252-12-6) was purchased from Synquest Laboratories and used without further purification. Sodium 1H,1H,2H,2H-perfluorooctane sulfonate (6:2 FTS, CAS# 27619-94-9, 50 μg/mL in methanol) was purchased from Wellington Laboratories and used without further purification. Perfluorooctane sulfonamide (PFOSA, Acros, CAS# 754-91-6), sodium chloride (NaCl), silver nitrate ($NaNO_3$), methanol (certified ACS), methanol (purge and trap suitable for volatile organic residue analysis), 20 mL vials, plain glass microscope slides, Thermo Scientific 11 mm glass crimp top vials (2 mL), Thermo Scientific national target Kim-Snap 2 mL caps, 3 mL air-tite all-plastic Henke-Ject syringes, and disposable polypropylene 50 mL centrifuge tubes were purchased from Fisher and

used without further purification. Parafilm was purchased from Pechiney Plastic Packaging. Medline disposable polypropylene 15 mL centrifuge tubes (MLAB15012) were generously donated by Eurofins Eaton Analytical (Eurofins). Cellulose acetate (CA) syringe filters (0.2 μm, catalog #729226) were purchased from Machery-Nagel. VWR grade 413 qualitative filter paper (5.5 cm) was purchased from VWR.

Deionized (DI) water purified by a Millipore Synergy water purification system was used as a water source and is referred to as "Millipore water" where appropriate. DI water purified by a Millipore Milli-Q Academic system was obtained from Eurofins Eaton Analytical and used as another water source during experiments where samples would be sent to Eurofins for analysis. This water is referred to as "Eurofins water". The pH of both water sources was assumed to be 7.00 according to Millipore's website.[1] The conductivity of both water sources was measured with a calibrated conductivity meter and found to be ~1 μS/cm.

II. General Experimental

A Thermo Scientific Orion Star A215 pH/conductivity meter was used for the conductometric titrations. Before use each day, the pH and conductivity meters were calibrated. The pH meter was calibrated using Orion 4.01 (fisher catalog # 910104), 7.00 (fisher catalog # 910107), and 10.01 (fisher catalog # 910110) pH buffers. The conductivity meter was calibrated using Orion 1413 μS/cm (fisher catalog # 011007) conductivity standards.

An IKA T25 digital Ultra-Turrax homogenizer equipped with a S25N-10G-ST dispersing tool was utilized for homogenizing wood pulp (WP) mixtures.

A Thermo Scientific Sorvall ST8 centrifuge was used along with disposable polypropylene 50 mL centrifuge tubes during QWP synthesis and PFAS adsorption experiments.

A Fisher Scientific standard microplate vortex mixer (catalog number 02-216-100) was used during adsorption experiments.

Elemental analysis was performed by Midwest Microlab.

Eurofins Eaton Analytical (South Bend, IN) analyzed solutions containing PFAS when the initial [PFAS] was less than or equal to 2.5 mg/L.

Quaternized Wood Pulp (QWP) samples are identified by material type followed by the charge density (e.g., QWP0.65 is a QWP sample with a charge density of 0.65 mmol NR_3^+/g).

III. Synthesis and Characterization of Quaternized Wood Pulps (QWPs)

A. Synthesis of QWPs

See Chapter 3 experimental section.

Table A2.1. QWP experimental conditions.

sample	volume of GMAC added (mL)	[GMAC] in reaction mixture (M)	number of centrifuge cycles for purification
QWP0.0	0.00	0.00	2
QWP0.65	3.00	0.422	3
QWP0.97	5.50	0.739	4
QWP0.99	5.50	0.739	4
QWP1.5	12.48	1.49	7

B. Conductometric titrations for QWPs

See Chapter 3 experimental section.

Table A2.2. QWP conductometric titration results.

sample	first charge density (mmol/g)[a]	second charge density (mmol/g)[a]	average charge density (mmol/g)
QWP0.0	0.00	0.00	0.00 ± 0.00
QWP0.65	0.640	0.663	0.65 ± 0.02
QWP0.97	0.976	0.968	0.97 ± 0.01
QWP0.99	0.983	0.991	0.99 ± 0.01
QWP1.5	1.50	1.52	1.51 ± 0.01

[a]The data in this column contain one extra significant figure to show how the average charge density was calculated for each sample.

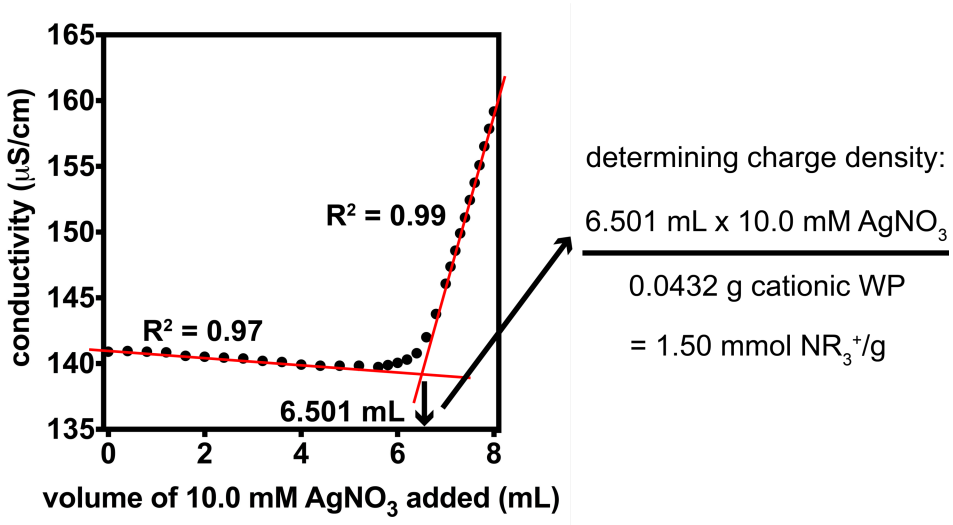

Figure A2.1. Calculating the charge density of a QWP1.5 sample. Points were included in the linear regression lines based on linearity and inclusion of extra points near the equivalence point did not significantly affect charge density calculations.

C. Elemental analysis (EA)

EA was performed on 5 QWP samples to determine the nitrogen content (wt% N) in each sample. The results from EA were then compared to nitrogen contents found using conductometric titrations, assuming that all N are from the -NR_3^+ groups. Table A2.3 shows that nitrogen contents from EA are in good agreement with the nitrogen contents from conductometric titrations.

Table A2.3. Comparing QWP nitrogen contents (wt% N) as determined with conductometric titrations and elemental analysis.

sample	wt% N by titration	wt% N by EA
QWP0.0	0.00	0.00
QWP0.65	0.91	0.87
QWP0.97	1.37	1.19
QWP0.99	1.39	1.33
QWP1.5	2.10	2.00

D. Raman spectroscopy of QWPs

See Chapter 3 experimental section for details.

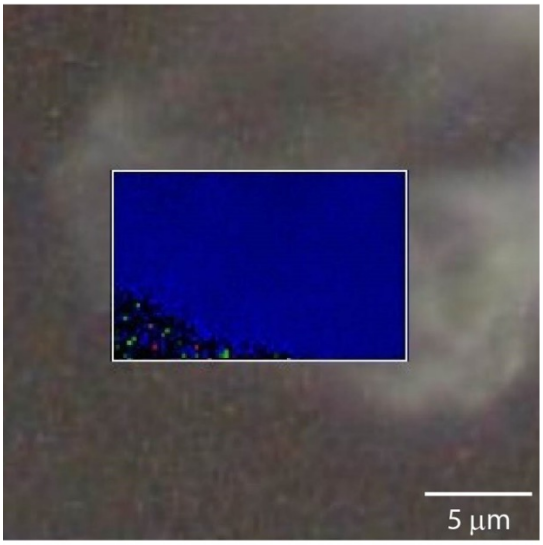

Figure A2.2. An image of a QWP1.5 fiber cross section overlayed with a Raman intensity ratio map using the intensity ratio between the peak at 724–810 cm^{-1} to the peak at 924–1183 cm^{-1}. The peak at 724–810 cm^{-1} corresponds to the symmetric $(CH_3)_3$-N^+ stretching from the quaternary amine group,[2] and the peaks at 924–1183 cm^{-1} are C-C and C-O stretching in cellulose.[3] The uniform color on the Raman intensity ratio map indicates that uniform amine functionalization occurred across the fiber cross section. The intensity ratio map was created using the Renishaw WiRE 5.3 software package.

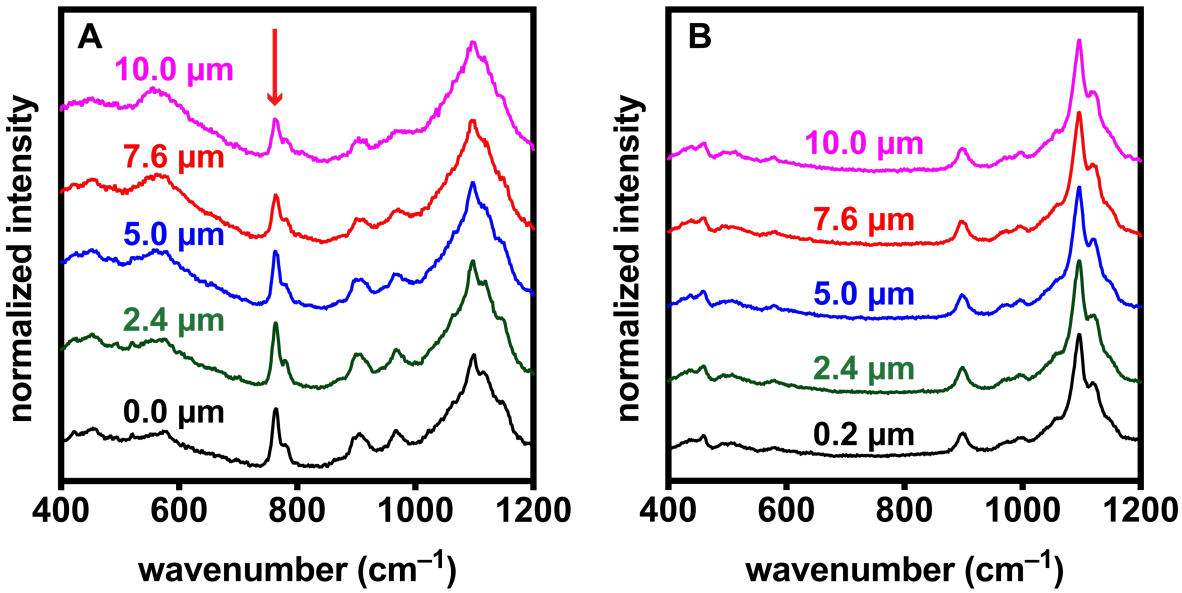

Figure A2.3. Raman spectra of (A) QWP1.5 and (B) QWP0.0 fibers at various depths in the fibers. The arrow in (A) indicates the symmetric $(CH_3)_3$-N^+ stretching at 764 cm^{-1} from the quaternary amine group.[2]

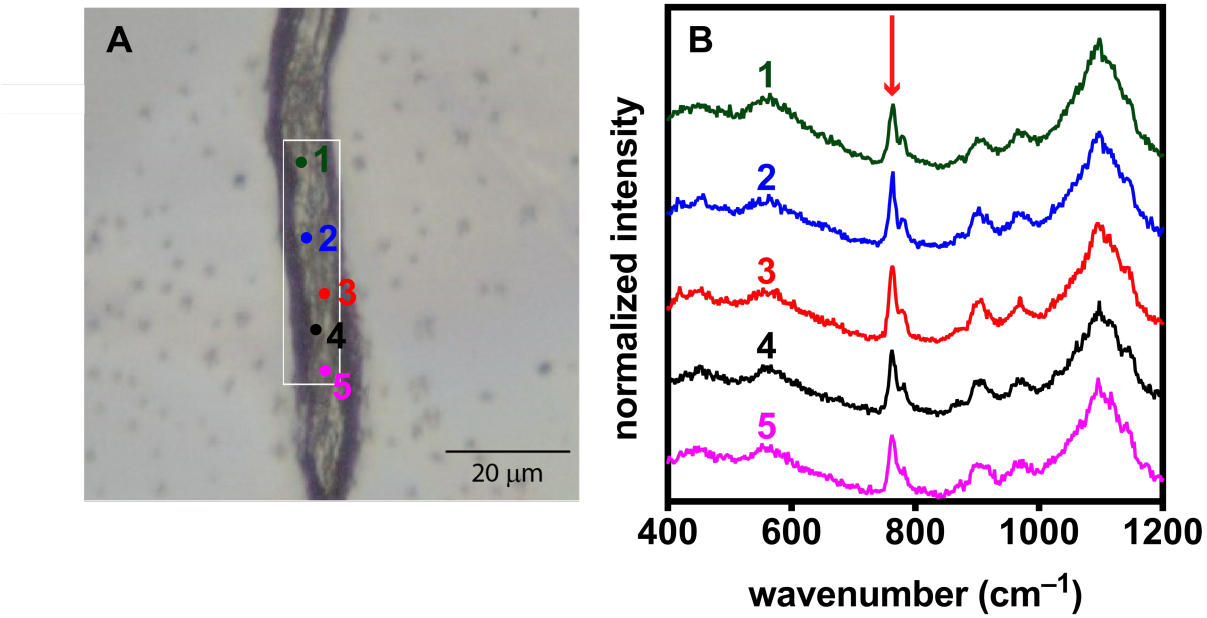

Figure A2.4. (A) QWP1.5 fiber image along with (B) Raman spectra acquired at various positions on the fiber's surface. The colors of the dots in the fiber image correspond with the Raman spectra of similar color. The arrow in (B) indicates the symmetric $(CH_3)_3$-N^+ stretching at 764 cm^{-1} from the quaternary amine group.[2]

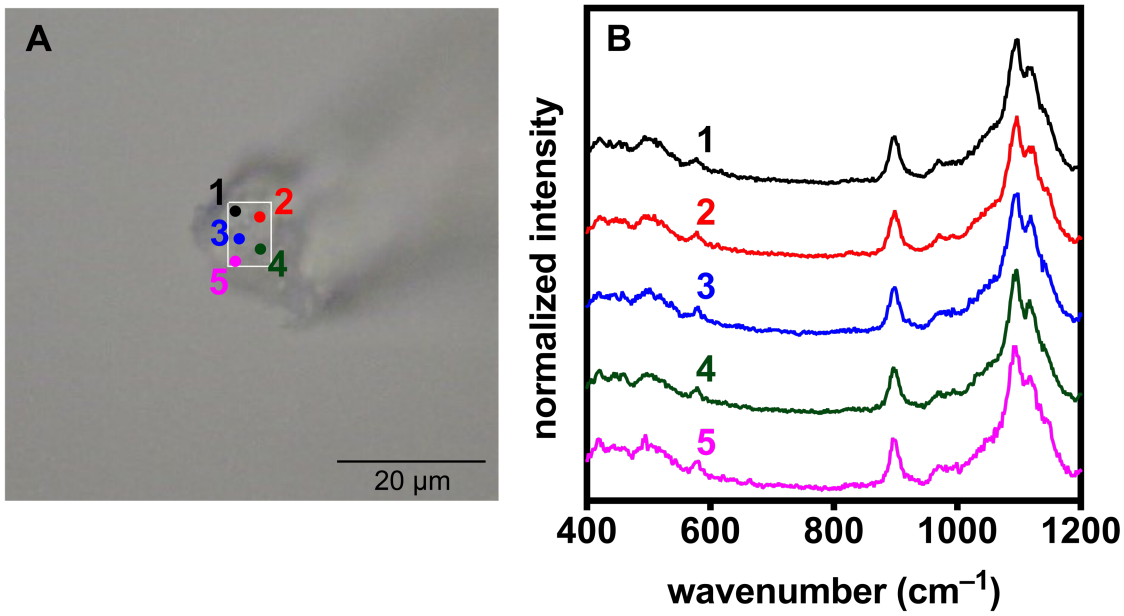

Figure A2.5. (A) Cross section microscope image of a QWP0.0 fiber. (B) Raman spectra acquired at various positions on the fiber's cross section. The Raman spectra were normalized to the peak at 1096 cm^{-1}.

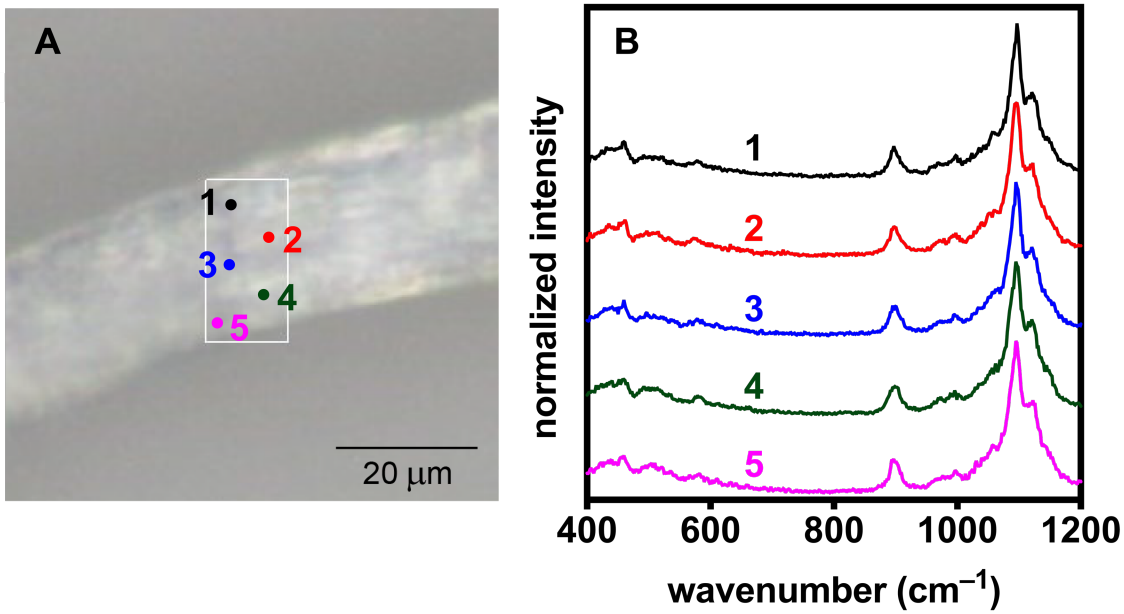

Figure A2.6. (A) QWP0.0 fiber image along with (B) Raman spectra acquired at various positions on the fiber's surface. The colors of the dots in the fiber image correspond with the Raman spectra of similar color.

IV. PFAS adsorption experiments

Note: When performing experiments that would be analyzed in-house, Millipore water was used to prepare the PFAS solutions, the QWP mixtures, and the mixtures probing PFAS adsorption. When performing experiments with samples that were sent to Eurofins Eaton Analytical for analysis, Eurofins water was used instead of Millipore water for all of the above.

A. General preparation of QWP mixtures

QWP mixtures with concentrations of 0.100 and 0.125 mg/mL were used for adsorption experiments. To make a 0.125 mg/mL mixture, QWPs (12.5 mg) were first soaked with water (10.0 mL) for 5 min in a 20 mL vial. The mixture was homogenized at 18k rpm for 1 min to generate a 1.25 mg/mL QWP mixture. The 0.125 mg/mL mixture was then made by combining the 1.25 mg/mL QWP mixture (2.0 mL) and water (18.0 mL) in a new 20 mL vial. A similar procedure was followed to make the 0.100 mg/mL QWP mixtures except that 12.5 mL water was used in the first step instead of 10.0 mL.

B. General preparation of 20.0 mg/L PFOS and PFOA solutions

PFOS or PFOA (10.0 mg) was added to a 500 mL glass container with water (500.0 mL). The container was sonicated (~2–3 min) to get all the PFOS or PFOA to dissolve.

C. Preparation of PFOS and PFOA standards for HPLC-MS

Every time a new 20.0 mg/L PFOS or PFOA solution was prepared, 6 new PFOS or PFOA standard solutions were also prepared for use as in-house HPLC-MS standards. PFOS standards with concentrations of 5.0, 1.0, 0.50, 0.10, 0.050, and 0.010 mg/L were made in 50 mL

polypropylene tubes via serial dilution using the 20.0 mg/L PFOS solution and water. PFOA standards with concentrations of 5.0, 1.0, 0.50, 0.10, 0.050, and 0.010 mg/L were made in 50 mL polypropylene tubes via serial dilution using the 20.0 mg/L PFOA solution and water. After preparing each solution, an aliquot (~1.5 mL) was removed via syringe, filtered through a cellulose acetate (CA) syringe filter, placed in a 2 mL vial, and the vial was capped. The standard solutions were stored in a fridge when not in use to minimize evaporation. Every time after using a standard, the cap was replaced with a new cap, so that the standards could be repeatedly used and provide consistency between experiments. Each standard was used for ~2 weeks.

D. General procedure for adsorption experiments

See Chapter 3 experimental section for details.

E. General procedure for analyzing PFOS/PFOA solutions in-house

Note: Water (Optima LC/MS grade, Fisher), acetonitrile (Optima LC/MS grade, Fisher), and formic acid (Optima LC/MS grade, Fisher) were used as the solvents when performing HPLC-MS. The software used to operate the HPLC was Agilent MassHunter Workstation LC/MS Data Acquisition for 6500 Series TOF, and the software used to analyze sample chromatograms was Agilent MassHunter Qualitative Analysis 10.0.

When large initial [PFAS] (>2.5 mg/L) were used during adsorption experiments, PFOS and PFOA samples were analyzed in-house with an Agilent Technologies 1200 Series high performance liquid chromatography instrument coupled to an Agilent Technologies 6520 Accurate Mass Q-TOF LC/MS spectrometer. The mobile phase contained (A) water and (B) acetonitrile:water = 95:5, and each contained 0.1% formic acid. Samples were injected at 20 μL

volumes and loaded onto a ZORBAX Eclipse Plus C-18 column (Agilent, Rapid Resolution HD, 2.1 x 50 mm, particle size 1.8 μm) which was kept at 25 °C. Solvent was passed through the column with a loading pump operated at 400 μL/min. The total sample run time was 4 min, and the solvent composition was changed over this run time. From 0–1 min, the mobile phase was linearly changed from 1:1 A:B to 3:7 A:B. From 1–2 min, the mobile phase was linearly changed from 3:7 A:B to 1:9 A:B. From 2–4 min, the mobile phase was held constant at 1:9 A:B. The Q-TOF LC/MS was operated with electrospray ionization in negative polarity mode, and reference masses of 112.98 and 1033.99 were used to calibrate the system.

To begin analysis each day, 6 PFOS or PFOA standards (0.010–5.0 mg/L) were run to generate a calibration curve. Then, all the samples from an adsorption experiment were run. After each standard or sample run, an extracted ion chromatogram (EIC) was obtained from the total ion chromatogram (TIC) using a mass of either 498.93 (PFOS) or 412.96 (PFOA). The EIC was then smoothed and the area under the analyte peak was acquired. PFOS eluted over ~1 min between the retention times of ~1.8 and 2.8 min. PFOA eluted over ~1 min between the retention times of ~1.2–2.2 min. For the standards, the area under the EIC curve was correlated with the standard's concentration to make a calibration curve. For the samples, the area under the EIC curve was used to calculate the analyte concentration in solution via the calibration curve. Figure A2.7 and Figure A2.8 show representative examples of chromatograms collected for PFOS and PFOA standards, respectively. Figure A2.9 and Figure A2.10 show representative examples of chromatograms collected for PFOS and PFOA samples after an adsorption experiment, respectively. Figure A2.11 displays representative examples of calibration curves that were generated with the 6 PFOS or PFOA standards.

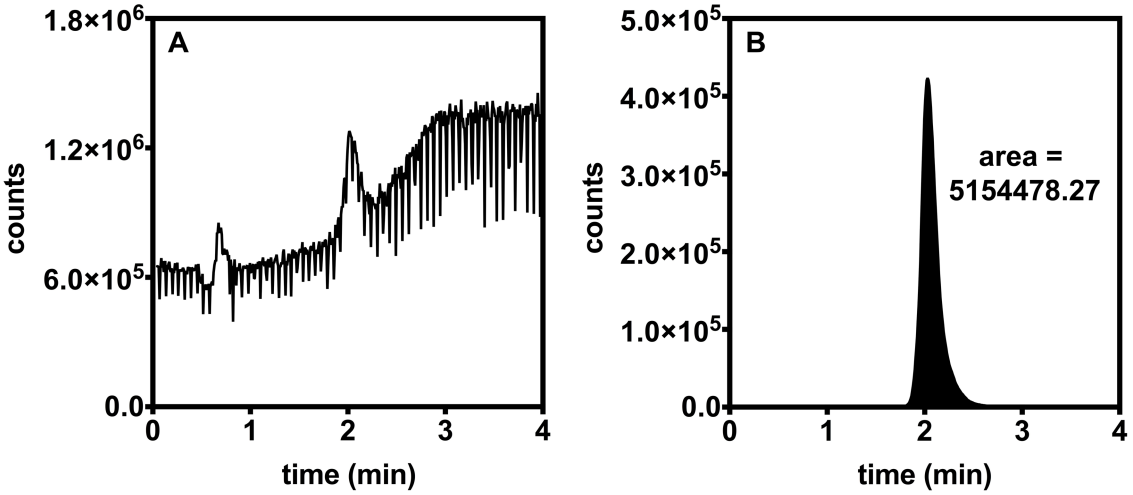

Figure A2.7. (A) TIC and (B) smoothed EIC for a 1.0 mg/L PFOS standard.

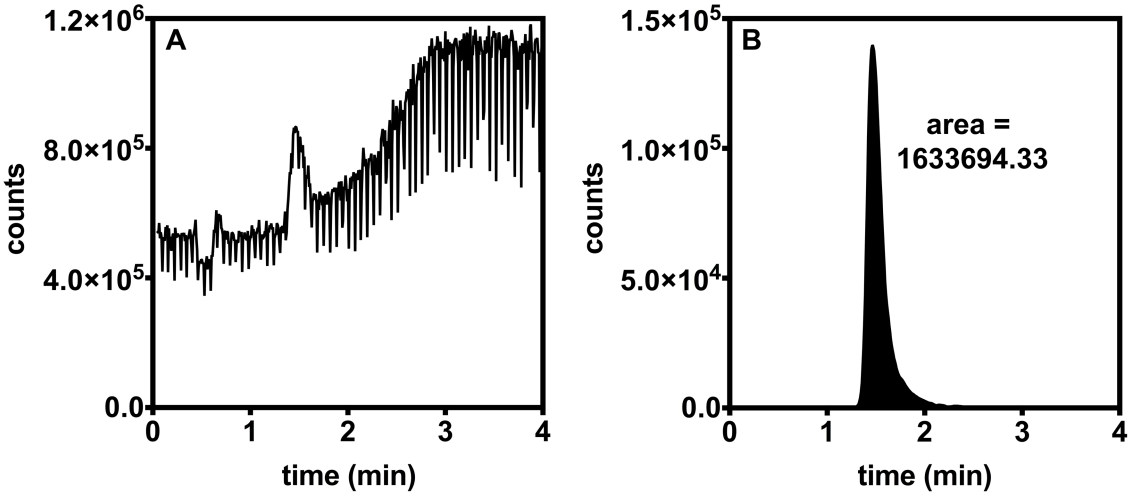

Figure A2.8. (A) TIC and (B) smoothed EIC for a 1.0 mg/L PFOA standard.

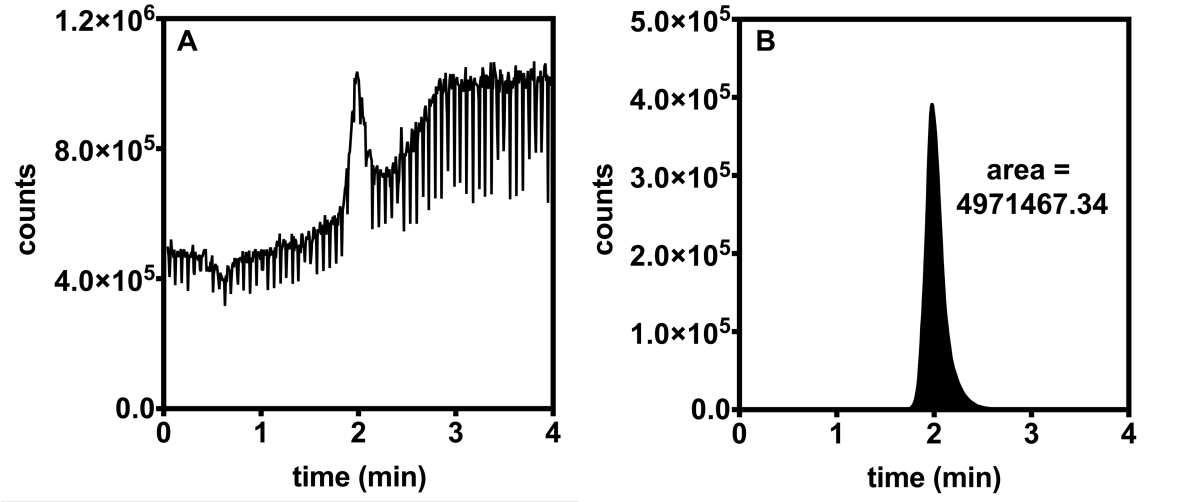

Figure A2.9. (A) TIC and (B) smoothed EIC for a PFOS sample 0.167 min after mixing with QWP1.5.

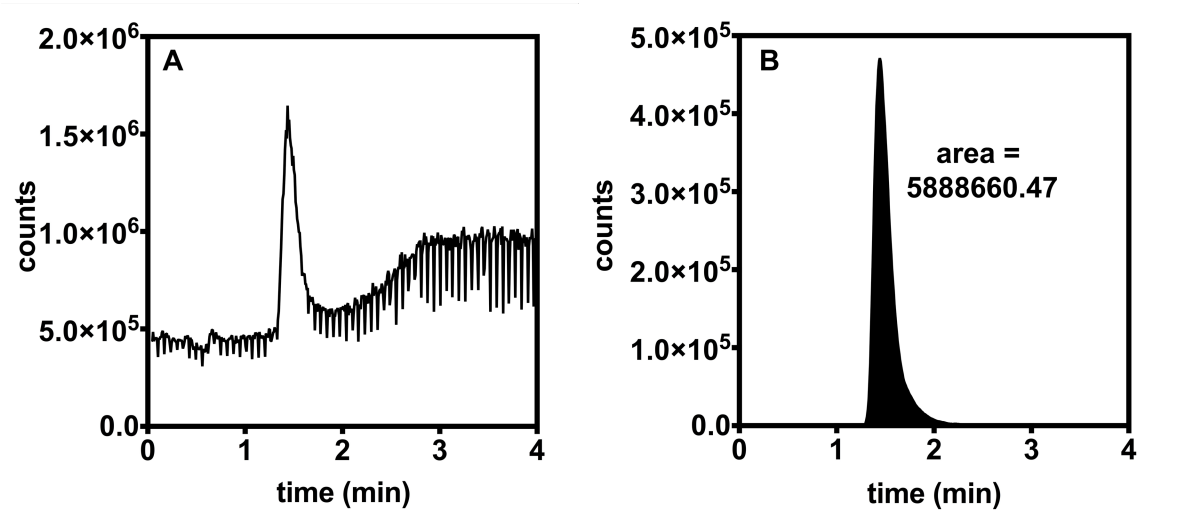

Figure A2.10. (A) TIC and (B) smoothed EIC for a PFOA sample 0.167 min after mixing with QWP1.5.

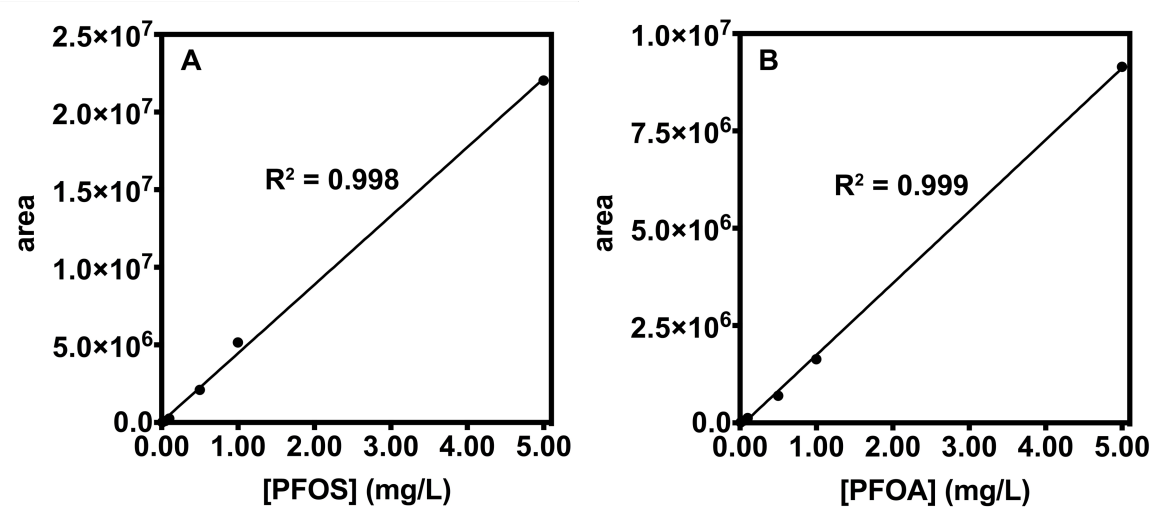

Figure A2.11. Examples of calibration curves generated for measuring (A) [PFOS] and (B) [PFOA].

F. Eurofins procedure for analyzing PFAS concentrations

Samples prepared using initial PFAS concentrations less than or equal to 2.5 mg/L were sent to Eurofins for analysis of the residual PFAS concentration in solution (unless otherwise noted).

Purge-and-trap grade methanol was purchased from Fisher Scientific. All PFAS (analytes and isotopically labeled analogues) were purchased from Wellington Laboratories.

Water analysis was carried out by using a Water's Acquity UPLC-H Class and Xevo TQ-S system. Separation was carried out using a Phenomenex's Gemini C18 (2 mm x 50 mm, 3 µm particle size) column. The mobile phase was a gradient mobile phase of 20 mM ammonium acid and methanol at a flowrate of 0.6 mL/min. The column oven temperature was 40 ºC. The injection volume was 3 µL. Isotope dilution analysis was performed for quantifying all analytes against their own isotopically labeled analogues. The correlation coefficients (r) of the linear regression curves were 0.998 or better for all analytes. The calibration standards and samples were prepared with a 1:1 ratio of water to methanol in 15 mL conical polypropylene tubes purchased from Fisher Scientific, referring to ASTM D7979-17. This procedure follows the standard test method for

determining per- and polyfluoroalkyl substances in water, sludge, influent, effluent and wastewater by liquid chromatography tandem mass spectrometry (LC/MS/MS), according to ASTM International, ASTM D7979-17.

After testing, Eurofins reported PFAS concentrations in the range of 0.02–125 µg/L, with 0.02 µg/L being the limit of quantification. More information about Eurofins can be found at https://www.eurofinsus.com/environment-testing/laboratories/eurofins-eaton-analytical/ (accessed March 25, 2021).

G. General procedure for calculating PFAS adsorption % and capacity

Using the general procedure for analyzing PFOS/PFOA solutions in-house or the data that Eurofins provided, residual concentrations of PFAS (C, µg/L) were calculated for each adsorption and control sample. In the control samples (if there was more than 1), the residual concentrations were averaged, and the average was used as the initial PFAS concentration (C_0, µg/L). The PFAS adsorption (%) for each sample was determined using the following equation:

$$\text{PFAS adsorption (\%)} = \frac{C_0\text{-}C}{C_0} \text{ x } 100$$

Equation A2.1. Calculating PFAS adsorption %.

The adsorption capacity (q, mg/g) for each sample was determined using the following equation:

$$q = \frac{C_0\text{-}C}{C_A}$$

Equation A2.2. Calculating PFAS adsorption capacity.

where C_A (mg/L) is the adsorbent concentration.

All adsorption experiments were performed in triplicate, and average adsorption % and capacity values from the 3 trials are reported with their standard deviations for each set of experimental conditions.

H. Procedure for determining effect of QWP CD on PFOS adsorption over time

General experimental

Mixtures of QWPs (0.125 mg/mL) with various charge densities were made according to the general procedure. A 20.0 mg/L PFOS solution was made according to the general procedure. All the samples in this experiment were analyzed in-house.

Adsorption experiments

To perform adsorption experiments, 2.5 mL of 20.0 mg/L PFOS was placed in a 50 mL polypropylene tube. Next, 4 mL of a 0.125 mg/mL QWP mixture and 3.5 mL of Millipore water were syringed over 10 s into the bottom of the centrifuge tube while vortex mixing at a speed of 1.5. The tube was then vortex mixed for an additional 10 s using a speed of 1.5. Aliquots (1000 μL) of mixture were then removed at various time intervals and placed in a 4 mL vial. The aliquot was placed in a 3 mL plastic syringe, filtered through a CA syringe filter, and placed in a 2 mL glass vial, and the vial was capped. After each aliquot was removed, the centrifuge tube was wrapped in parafilm and left undisturbed at rt. This procedure was repeated 3 times for each of the QWPs with varying charge densities. Aliquots for QWP0.65 and QWP0.99 were removed at 0.167, 60, 480, and 1440 min after mixing the QWPs with PFOS. Aliquots for QWP0.0 and QWP1.5 were removed at 0.167, 80, 480, and 1440 min. The targeted initial PFOS concentration in these experiments was 5.0 mg/L, the adsorbent dosage was 50.0 mg/L, and total volume was 10.0 mL.

In addition, 3 control experiments were performed following the above procedure except that only Millipore water (no QWPs) was added to give a total volume of 10.0 mL. Aliquots were removed from these controls at 0.167 and 1440 min after mixing. These samples were analyzed to

determine the initial PFOS concentration in solution and to demonstrate that minimal PFOS was lost after 24 h to other mechanisms besides adsorption on QWPs.

PFAS solution analysis

The samples were analyzed using the general procedure for analyzing PFOS/PFOA solutions in-house and the general procedure for calculating PFAS adsorption % and capacity (Table A2.4). Based on the control samples at 0.167 min, the initial PFOS concentration was calculated as 4.2 ± 0.1 mg/L. The PFOS adsorption capacity data in Figure A2.12 were fit using the pseudo second order model to generate lines to guide the eye.[4]

Table A2.4. PFOS adsorption (%) and capacity (mg/g) as a function of QWP charge density (mmol NR_3^+/g).

	PFOS adsorption 0.167 min after mixing		**PFOS adsorption 60 or 80 min after mixing**		**PFOS adsorption 480 min after mixing**		**PFOS adsorption 1440 min after mixing**	
QWP	ads %	capacity	ads %	capacity	ads %	capacity	ads %	capacity
no QWP	0 ± 3	0 ± 2	–		–		9 ± 2	7 ± 1
QWP0.0	–3 ± 1	–2 ± 1	9 ± 7	8 ± 5	12 ± 3	10 ± 2	6 ± 1	5 ± 1
QWP0.65	4 ± 5	3 ± 4	14 ± 8	12 ± 6	63 ± 7	52 ± 6	76 ± 10	63 ± 8
QWP0.99	16 ± 4	13 ± 3	52 ± 4	43 ± 3	95 ± 1	79 ± 1	99.11 ± 0.05	82.26 ± 0.04
QWP1.5	99.3 ± 0.1	82.42 ± 0.09	99.47 ± 0.03	82.57 ± 0.02	99.5 ± 0.1	82.56 ± 0.04	99.51 ± 0.01	82.60 ± 0.01

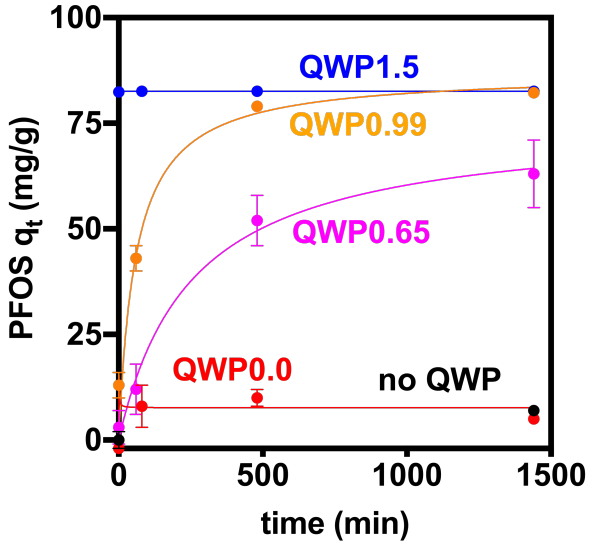

Figure A2.12. Plot of PFOS adsorption capacity (mg/g) over time (min) for QWP1.5 (blue), QWP0.99 (orange), QWP0.65 (magenta), QWP0.0 (red), and no QWPs (black). [QWP] = 50.0 mg/L. The data were fit using the pseudo second order model.

I. Procedure for determining effect of QWP CD on PFOA adsorption over time

General experimental

Mixtures of QWPs (0.125 mg/mL) with various charge densities were made according to the general procedure. A 20.0 mg/L PFOA solution was made according to the general procedure. All the samples in this experiment were analyzed in-house.

Adsorption experiments

To perform adsorption experiments, 2.5 mL of 20.0 mg/L PFOA was placed in a 50 mL polypropylene tube. Next, 4 mL of a 0.125 mg/mL QWP mixture and 3.5 mL of Millipore water were syringed over 10 s into the bottom of the centrifuge tube while vortex mixing at a speed of 1.5. The tube was then vortex mixed for an additional 10 s using a speed of 1.5. Aliquots (1000 µL) of mixture were then removed at various time intervals and placed in an 8 mL vial. The aliquot

was placed in a 3 mL plastic syringe, filtered through a CA syringe filter, and placed in a 2 mL glass vial, and the vial was capped. After each aliquot was removed, the centrifuge tube was wrapped in parafilm and left undisturbed at rt. This procedure was repeated 3 times for each of the QWPs with varying charge densities. Aliquots were removed at 0.167, 80, 480, and 1440 min after mixing the QWPs with PFOA. The targeted initial PFOA concentration in these experiments was 5.0 mg/L, the adsorbent dosage was 50.0 mg/L, and total volume was 10.0 mL.

In addition, 3 control experiments were performed following the above procedure except that only Millipore water (no QWPs) was added to give a total volume of 10.0 mL. Aliquots were removed from these controls at 0.167, 80, 480, and 1440 min after mixing. These samples were analyzed to calculate the initial PFOA concentration in solution and to demonstrate that minimal PFOA was lost after 24 h to other mechanisms besides adsorption on QWPs.

PFAS solution analysis

The samples were analyzed using the general procedure for analyzing PFOS/PFOA solutions in-house and the general procedure for calculating PFAS adsorption % and capacity (Table A2.5). Based on the control samples at 10 s, the initial PFOA concentration was calculated as 3.9 ± 0.1 mg/L. The PFOA adsorption capacity data in Figure A2.13 were fit using the pseudo second order model to generate lines to guide the eye.[4] The only exception was the QWP1.5 adsorption data, which was fit with the pseudo first order model because the graphing program (Prism 8) was unable to generate a line according to the pseudo second order model.

Table A2.5. PFOA adsorption (%) and capacity (mg/g) as a function of QWP charge density (mmol NR_3^+/g).

	PFOA adsorption 0.167 min after mixing		PFOA adsorption 80 min after mixing		PFOA adsorption 480 min after mixing		PFOA adsorption 1440 min after mixing	
QWP	ads %	capacity	ads %	capacity	ads %	capacity	ads %	capacity
no QWP	0 ± 2	0 ± 1	10 ± 1	8 ± 1	8 ± 2	6 ± 1	4 ± 2	3 ± 1
QWP0.0	5 ± 1	4 ± 1	10 ± 1	8 ± 1	8 ± 2	7 ± 1	6.2 ± 0.3	4.9 ± 0.3
QWP0.65	12 ± 1	9 ± 1	30 ± 2	23 ± 2	48 ± 10	37 ± 8	50 ± 10	39 ± 8
QWP0.99	23 ± 1	18 ± 1	53 ± 2	42 ± 1	90 ± 1	70 ± 1	96.3 ± 0.4	75.3 ± 0.3
QWP1.5	67.7 ± 0.4	52.9 ± 0.3	83 ± 2	65 ± 2	94 ± 1	73 ± 1	98 ± 1	77.1 ± 0.4

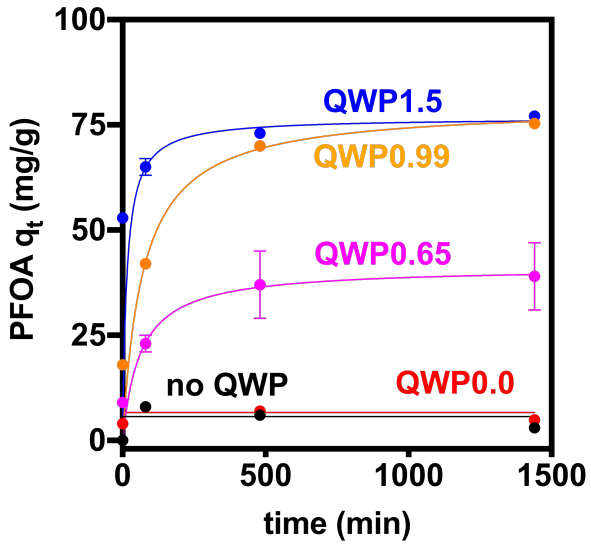

Figure A2.13. Plot of PFOA adsorption capacity (mg/g) over time (min) with QWP1.5 (blue), QWP0.99 (orange), QWP0.65 (magenta), QWP0.0 (red), and no QWPs (black). [QWP] = 50.0 mg/L. The data were fit using either the pseudo first or second order models to generate lines to guide the eye.

J. Procedure for determining effect of QWP1.5 concentration on PFOS adsorption

General experimental

A mixture of QWP1.5 (0.125 mg/mL) was made according to the general procedure. In addition, a 0.0125 mg/mL QWP1.5 mixture was made by combining 2.0 mL of 0.125 mg/mL QWP1.5 and 18.0 mL of Millipore water in a new 20 mL vial. A 20.0 mg/L PFOS solution was made according to the general procedure. All the samples in this experiment were analyzed in-house.

Adsorption experiments

To perform adsorption experiments, 2.5 mL of 20.0 mg/L PFOS was placed in a 50 mL polypropylene tube. Then, the general procedure for adsorption experiments was followed for each sample (see Table A2.6 for specific details). An aliquot (~1.5 mL) of mixture was removed from the centrifuge tube with a 3 mL plastic syringe 10 s after mixing the QWPs with PFOS, and it was passed through a CA syringe filter and placed in a 2 mL vial. This procedure was repeated 3 times for each concentration of QWP1.5 used. The targeted initial PFOS concentration was 5.0 mg/L, and the total volume was 10.0 mL.

Note: For this experiment, only 1 control sample was made following the above procedure, and only Millipore water (no QWPs) was added in this sample to give a total volume of 10.0 mL. This control sample was analyzed to determine the initial PFOS concentration in solution in the absence of adsorbent.

PFAS solution analysis

All samples were analyzed using the general procedure for analyzing PFOS/PFOA solutions in-house and the general procedure for calculating PFAS adsorption % and capacity (Table A2.6 and Figure 3.3). Based on the control sample, the initial PFOS concentration was calculated as 4.81 mg/L. Note: The PFOS adsorption % and capacity for the 50.0 mg/L data point was taken from the section "Procedure for determining effect of QWP CD on PFOS adsorption over time" at the 0.167 min time point (Table A2.4).

Table A2.6. PFOS adsorption (%) and capacity (mg/g) as a function of QWP1.5 concentration (mg/L).

QWP1.5 concentration (mg/L)	QWP mixture used to prepare samples (mg/mL)	volume of QWP mixture used to prepare samples (mL)	PFOS adsorption %	PFOS adsorption capacity
1.25	0.0125	1	-1.8 ± 0.3	-71 ± 10
6.25	0.0125	5	25 ± 2	190 ± 10
12.5	0.125	1	68 ± 1	263 ± 3
50.0	0.125	4	99.3 ± 0.1	82.42 ± 0.09

K. PFOS/PFOA adsorption over time with QWP1.5

General experimental

Mixtures of QWP1.5 (0.100 mg/mL) were made according to the general procedure. PFOS and PFOA solutions (20.0 mg/L) were made according to the general procedure. All the samples in this experiment were analyzed in-house.

Adsorption experiments

To perform adsorption experiments, 2.5 mL of either 20.0 mg/L PFOS or PFOA was placed in a 50 mL polypropylene tube. Next, 1 mL of 0.100 mg/mL QWP1.5 mixture and 6.5 mL of

Millipore water were syringed over 10 s into the bottom of the centrifuge tube while vortex mixing at a speed of 1.5. The tube was then vortex mixed for an additional 10 s using a speed of 1.5. Aliquots (1000 μL) of mixture were removed at various time intervals and placed in a 4 mL vial. The aliquot was then placed in a 3 mL plastic syringe, filtered through a CA syringe filter, and placed in a 2 mL glass vial, and the vial was capped. After each aliquot was removed, the centrifuge tube was wrapped in parafilm and left undisturbed at rt. This procedure was repeated 3 times with PFOS and PFOA as the analytes. Aliquots were removed at 0.167, 60, 480, and 1440 min after mixing the QWPs with either PFOS or PFOA. The targeted initial PFOS/PFOA concentrations were 5.0 mg/L, the adsorbent dosage was 10.0 mg/L, and total volume was 10.0 mL.

In addition, 2 control experiments were performed following the above procedure for both PFOS and PFOA. The only difference is that only Millipore water (no QWPs) was added to the tubes to give a total volume of 10.0 mL. Aliquots were removed from these controls at 0.167, 60, 480, and 1440 min after mixing. These samples were analyzed to determine the initial PFOS/PFOA concentrations in solution and to demonstrate that minimal PFOS/PFOA was lost after 24 h to other mechanisms besides adsorption on QWPs.

PFAS solution analysis

All samples were analyzed using the general procedure for analyzing PFOS/PFOA solutions in-house and the general procedure for calculating PFAS adsorption % and capacity (Table A2.7 and Table A2.8). Based on the PFOS control samples, the initial PFOS concentration was calculated as 3.5 ± 0.1 mg/L, and based on the PFOA control samples, the initial PFOA concentration was calculated as 3.9 ± 0.1 mg/L. Figure A2.14 shows the measured PFOS and PFOA adsorption over time. Because the control samples showed some loss of PFOS/PFOA over

time, we also calculated adjusted adsorption capacities, and the adjusted capacities are reported in the manuscript. The adjusted capacities were calculated by subtracting the average PFOS or PFOA control adsorption capacity from the average measured PFOS or PFOA adsorption capacity at each time point (Table A2.7 and Table A2.8). The PFOS adsorption data in Figure 3.2 and Figure A2.14 was fit using the pseudo first order model to generate a line to guide the eye. The PFOA adsorption data in Figure 3.2 and Figure A2.14 was fit using the pseudo second order model to generate a line to guide the eye. The pseudo second order model was not used for PFOS because the graphing program (Prism 8) was unable to generate a line according to the pseudo second order model.[4]

Table A2.7. Measured and adjusted PFOS adsorption over time using QWP1.5.

time (min)	measured PFOS adsorption (%)	measured PFOS adsorption capacity (mg/g)	PFOS control adsorption (%)	PFOS control adsorption capacity (mg/g)	adjusted PFOS adsorption capacity (mg/g)
0.167	67 ± 1	238 ± 5	0 ± 2	0 ± 7	238 ± 5
60	76 ± 4	270 ± 20	4 ± 1	13 ± 4	260 ± 20
480	89 ± 3	320 ± 10	3.0 ± 0.2	12 ± 1	300 ± 10
1440	96 ± 3	340 ± 10	5.0 ± 0.6	19 ± 2	320 ± 10

Table A2.8. Measured and adjusted PFOA adsorption over time using QWP1.5.

time (min)	measured PFOA adsorption (%)	measured PFOA adsorption capacity (mg/g)	PFOA control adsorption (%)	PFOA control adsorption capacity (mg/g)	adjusted PFOA adsorption capacity (mg/g)
0.167	20 ± 3	80 ± 10	0 ± 2	0 ± 7	80 ± 10
60	42 ± 1	164 ± 3	4 ± 1	16 ± 3	148 ± 3
480	70 ± 2	273 ± 3	2 ± 1	8 ± 4	265 ± 3
1440	83 ± 2	324 ± 9	2 ± 1	8 ± 2	316 ± 9

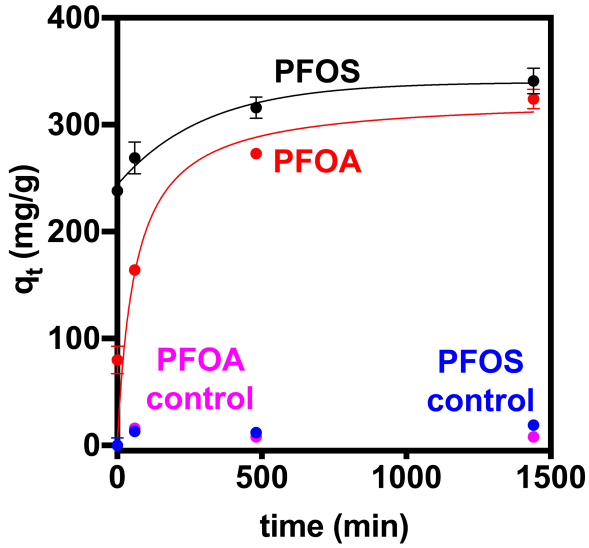

Figure A2.14. Plot of measured PFOS (black) and PFOA (red) adsorption capacities over time. PFOS (blue) and PFOA (magenta) control adsorption capacities over time are also given. Some error bars are not visible due to their small size.

L. Calculating pseudo-second order adsorption parameters

The pseudo-second-order adsorption model was then used to fit the adjusted PFOS and PFOA data in Table A2.7 and Table A2.8 to calculate rate constants and equilibrium adsorption capacities for PFOS and PFOA adsorption.[4] The linear pseudo-second-order adsorption model is given by:

$$\frac{t}{q_t} = \frac{t}{q_e} + \frac{1}{k_2 q_e^2}$$

Equation A2.3. Calculating pseudo-second order adsorption kinetics.

where q_t (mg/g) is the adsorption capacity at a given time, t (min) is time, q_e (mg/g) is the adsorption capacity at equilibrium, and k_2 is the pseudo-second-order rate constant (g/(mg·min)). Plotting (t/q_t) vs t (Figure A2.15) for both the PFOS and PFOA data results in linear regression lines where the slope equals $1/q_e$ and values of k_2 are calculated from the y-intercept and q_e. The rate constants and equilibrium adsorption capacities for PFOS and PFOA adsorption are given in

Table A2.9. k_2 was converted to units of g/(mg·h) for easy comparison with values in literature, which are typically reported with units of g/(mg·h).

Table A2.9. Pseudo-second-order adsorption parameters for PFOS and PFOA adsorption on QWP1.5. [QWP1.5] = 10 mg/L, $[PFOS]_0$ = 3.5 ± 0.1 mg/L, $[PFOA]_0$ = 3.9 ± 0.1 mg/L.

analyte	k_2 (g/(mg*h))	q_e (mg/g)
PFOS	0.014	323
PFOA	0.0035	323

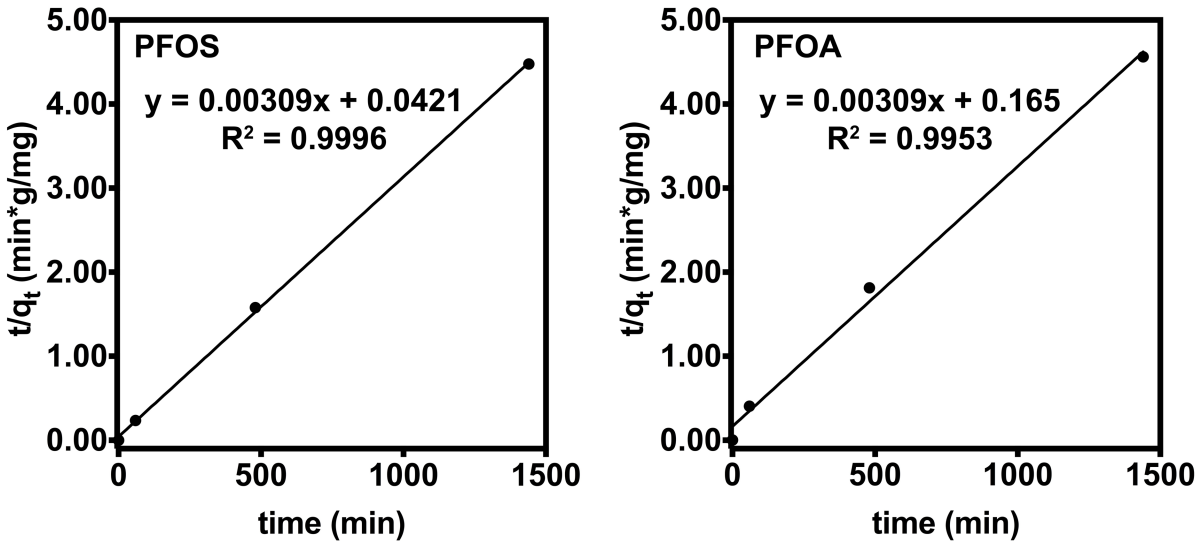

Figure A2.15. Plot of t/q_t (min·g/mg) at various time (min) points for PFOS and PFOA adsorption over time.

M. Adsorption isotherms for PFOS/PFOA adsorption with QWP1.5

General experimental

Mixtures of QWP1.5 (0.100 mg/mL) were made according to the general procedure. PFOS and PFOA solutions (20.0 mg/L) were made according to the general procedure. All the samples in this experiment were analyzed by Eurofins. The 50 mL polypropylene tubes used in this experiment were rinsed with methanol (purge and trap grade, ~1.5 mL) and air-dried prior to use to ensure no PFOS/PFOA was in the tube.

Adsorption experiments

Note: Each trial in this experiment probed either PFOS or PFOA adsorption. Every sample sent to Eurofins for analysis contained 1 aliquot of solution from a PFOS trial and 1 aliquot of solution from a PFOA trial. Furthermore, because Eurofins could only analyze samples with PFOS/PFOA concentrations between 0.02 – 125 μg/L, adsorption trials were diluted with additional Eurofins water and methanol (purge and trap grade) such that the samples contain 1:1 methanol:water solutions.

To perform adsorption trials, a volume of either 20.0 mg/L PFOS or PFOA solution was added to a 50 mL polypropylene "initial tube" (Table A2.10). Then, 1.0 mL of 0.100 mg/mL QWP1.5 mixture and Eurofins water (a volume to make the adsorption mixture 10.0 mL) were syringed over 10 s into the bottom of the centrifuge tube while vortex mixing at a speed of 1.5. The tube was then vortex mixed for an additional 10 s using a speed of 1.5. Following this mixing time, one of two procedures was followed:

1) In control trials where only water (no QWP1.5) was added to give a total volume of 10.0 mL, an aliquot (~1 mL) of solution was removed immediately from the initial tube with a 3

mL syringe, filtered through a CA syringe filter, and placed in a 4 mL vial. A portion of this filtered solution (either 50 or 100 μL) was then placed in a 15 mL centrifuge tube (called "final sample"). The remaining solution in the initial tube was then capped and parafilm was used to seal the tube. This procedure was performed to determine the initial PFOS/PFOA concentrations in solution in the absence of adsorbent. To dilute these "final samples" for analysis, a volume of Eurofins water (dependent on the combined aliquot volumes from 1 PFOS trial and 1 PFOA trial added to the 15 mL tube) was added to the 15 mL "final sample" followed by methanol (5.00 mL), and the tube was sealed with parafilm. In Table A2.10, these control samples are final samples 1–5. Note: Only 1 control trial was prepared for each targeted initial PFOS/PFOA concentration in this experiment.

2) In trials containing QWP1.5, the "initial tube" was simply capped and wrapped in parafilm to seal the tube.

Trials were left undisturbed at rt for 24 h. Following this contact time, an aliquot (~1.5 mL) of mixture was removed from the initial tube with a 3 mL plastic syringe, filtered through a CA syringe filter, and placed in a 4 mL vial. A portion of this filtered solution was placed in a 15 mL "final sample" (Table A2.10). Again, note that 1 PFOS aliquot and 1 PFOA aliquot were combined into 1 "final sample".

Once aliquots from a PFOS and PFOA trial were in a given 15 mL "final sample", Eurofins water (dependent on the combined aliquot volumes from 1 PFOS and 1 PFOA trial) was added to the tube with methanol (a volume equal to the total volume of water added to the tube), and the 15 mL tube was sealed with parafilm. In Table A2.10, final samples 6, 10, 14, 18, and 22 are the 24 h aliquots for the control final samples 1–5, respectively. These samples were prepared to

demonstrate that minimal PFOS/PFOA was lost after 24 h to other mechanisms besides adsorption on QWPs.

Adsorption trials were performed in triplicate for each targeted initial PFOS/PFOA concentration. The targeted initial PFOS/PFOA concentrations were 1000, 2500, 5000, 7500, and 10,000 ug/L. The [QWP1.5] was 10.0 mg/L.

PFAS solution analysis

All samples were analyzed using the Eurofins general procedure for analyzing PFAS concentrations. Using the data from Eurofins, the PFOS and PFOA equilibrium adsorption capacities, q_e (mg/g), and the equilibrium PFOS and PFOA solution concentrations (C_e, μg/L) were calculated according to the following method. First, because the "final samples" sent to Eurofins contained diluted PFOS/PFOA concentrations, the reported concentrations of PFOS/PFOA in each sample were multiplied by the dilution factor provided in Table A2.10 to obtain undiluted PFOS/PFOA concentrations for each sample. For samples 1–5, this undiluted PFOS/PFOA concentration was used as the true initial PFOS/PFOA concentration (C_0). For samples 6–25, this undiluted PFOS/PFOA concentration was the sample's C_e. Then, the q_e for each sample was found with:

$$q_e = \frac{C_0 - C_e}{C_A}$$

Equation A2.4. Calculating equilibrium adsorption capacity.

where C_A is the adsorbent concentration (10.0 mg/L). Averages and standard deviations of 3 samples are reported in Table A2.11 and Table A2.12 for the PFOS/PFOA equilibrium adsorption capacities and corresponding equilibrium solution concentrations.

Table A2.10. Parameters for preparing adsorption isotherm samples.

final sample	volumes (mL) of 20.0 mg/L PFOS or PFOA added to "initial tube"	aliquot volumes (µL) of filtered solutions added to "final sample"[a]	Eurofins water (mL) added to "final sample"	methanol (mL) added to "final sample"	dilution factor	targeted initial PFOS/PFOA concentrations (µg/L)
1	0.5000	100.0	4.800	5.00	100	1000
2	1.250	100.0	4.800	5.00	100	2500
3	2.500	100.0	4.800	5.00	100	5000
4	3.750	50.0	4.900	5.00	200	7500
5	5.000	50.0	4.900	5.00	200	10000
6	0.500	100.0	4.800	5.00	100	1000
7	0.500	500.0	0	1.00	4	1000
8	0.500	500.0	0	1.00	4	1000
9	0.500	500.0	0	1.00	4	1000
10	1.250	100.0	4.800	5.00	100	2500
11	1.250	1000	3.000	5.00	10	2500
12	1.250	1000	3.000	5.00	10	2500
13	1.250	1000	3.000	5.00	10	2500
14	2.500	100.0	4.800	5.00	100	5000
15	2.500	500.0	4.000	5.00	20	5000
16	2.500	500.0	4.000	5.00	20	5000
17	2.500	500.0	4.000	5.00	20	5000
18	3.750	50.0	4.900	5.00	200	7500
19	3.750	250.0	4.500	5.00	40	7500
20	3.750	250.0	4.500	5.00	40	7500
21	3.750	250.0	4.500	5.00	40	7500
22	5.000	50.0	4.900	5.00	200	10000
23	5.000	100.0	4.800	5.00	100	10000
24	5.000	100.0	4.800	5.00	100	10000
25	5.000	100.0	4.800	5.00	100	10000

[a]Note: Two aliquots were added to each final sample: one from a PFOS trial and one from a PFOA trial.

Table A2.11. PFOS adsorption isotherm data.

final sample	C_e (µg/L)	average C_e (µg/L)	q_e (mg/g)	average q_e (mg/g)
1*	745	–	–	–
2*	2011	–	–	–
3*	4272	–	–	–
4*	5683	–	–	–
5*	7940	–	–	–
6*	736	–	0.878	–
7	6.53		73.8	
8	8.82	9 ± 3	73.6	73.5 ± 0.3
9	13.0		73.2	
10*	2081	–	-7.00	–
11	25.9		199	
12	40.4	35 ± 8	197	198 ± 1
13	39.1		197	
14*	4150	–	12.2	–
15	53.3		422	
16	49.9	48 ± 6	422	422 ± 1
17	40.8		423	
18*	6031	–	-34.8	–
19	140		554	
20	119	140 ± 20	556	554 ± 2
21	158		553	
22*	7963	–	-2.28	–
23	1007		693	
24	921	900 ± 100	702	700 ± 10
25	761		718	

*Indicates the sample was a control.

Table A2.12. PFOA adsorption isotherm data.

final sample	C_e (µg/L)	average C_e (µg/L)	q_e (mg/g)	average q_e (mg/g)
1*	920	–	–	–
2*	2234	–	–	–
3*	4545	–	–	–
4*	6296	–	–	–
5*	8336	–	–	–
6*	881	–	3.90	–
7	144		77.6	
8	119	120 ± 20	80.1	80 ± 2
9	111		80.8	
10*	2181	–	5.27	–
11	149		208	
12	257	220 ± 60	198	202 ± 6
13	239		199	
14*	4436	–	10.9	–
15	387		416	
16	396	393 ± 6	415	415 ± 1
17	396		415	
18*	6426	–	-13.0	–
19	1091		520	
20	1215	1180 ± 80	508	511 ± 8
21	1237		506	
22*	8380	–	-4.40	–
23	2994		534	
24	3198	3200 ± 200	514	520 ± 20
25	3303		503	

*Indicates the sample was a control.

N. Calculating distribution coefficients

Distribution coefficients (K_D, L/g) that describe PFOS and PFOA affinity to adsorb on QWP1.5 were approximated by evaluating the linear regions of the PFOS and PFOA adsorption isotherms. More specifically, q_e was plotted against C_e for the 3 smallest C_es on the PFOS and PFOA adsorption isotherms. The data was fit using a linear trendline, and the slope of the line was taken as the K_D for PFOS and PFOA adsorption (Figure A2.16). More info on K_D can be found in the provided references.[5,6,7]

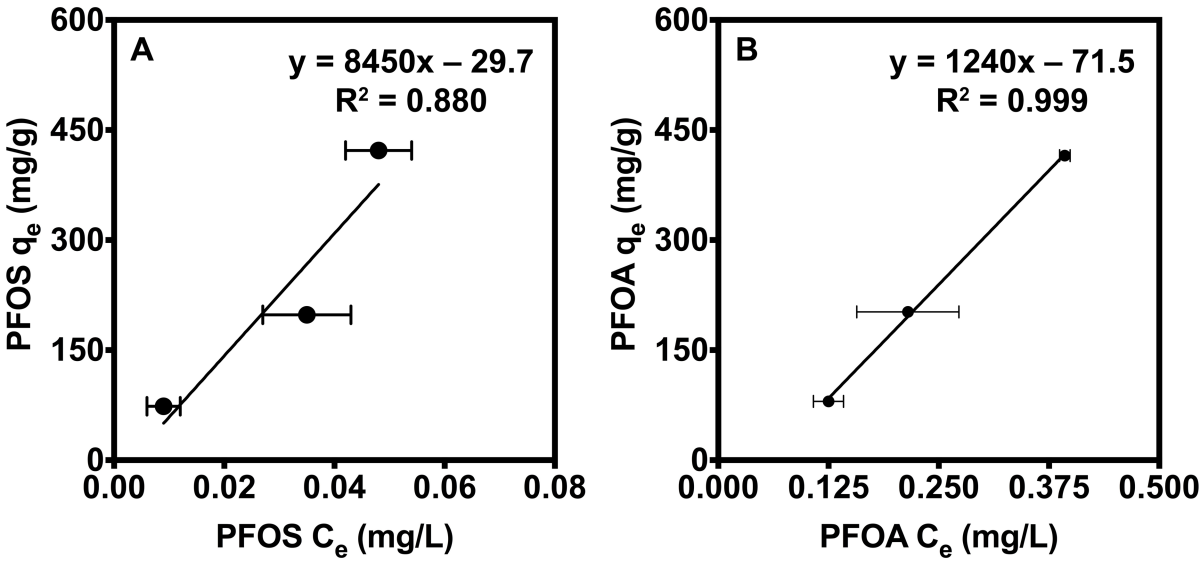

Figure A2.16. Plot of adsorption capacity (mg/g) as a function of (A) PFOS and (B) PFOA equilibrium concentration (mg/L).

O. Fitting isotherm data with Langmuir and Freundlich models

Langmuir and Freundlich models were used to understand PFOS and PFOA adsorption on QWP1.5. The Langmuir model is given by:

$$q_e = \frac{q_{max} b C_e}{1 + b C_e}$$

Equation A2.5. Langmuir model equation.

where q_e (mg/g) is the adsorption capacity, b is the Langmuir constant, q_{max} (mg/g) is the maximum capacity of PFAS adsorbate, and C_e (mg/L) is the concentration of PFAS left in solution after reaching equilibrium. The Freundlich model is given by:

$$q_e = K_F C_e^{1/n}$$

Equation A2.6. Freundlich model equation.

where q_e and C_e are defined the same as in the Langmuir model, K_F ((mg/g)(L/mg)$^{1/n}$) is the Freundlich constant which is related to adsorption capacity, and n is a constant indicating the intensity of adsorption.

To calculate q_{max} and b for PFOS and PFOA adsorption, C_e/q_e was plotted versus C_e according to the following linear Langmuir equation:

$$\frac{C_e}{q_e} = \frac{1}{bq_{max}} + \frac{C_e}{q_{max}}$$

Equation A2.7. Calculating Langmuir parameters.

q_{max} was calculated from the slope (which is $1/q_{max}$) of the line, and b was calculated from q_{max} and the intercept of the linear regression line (Figure A2.17 and Table A2.13).

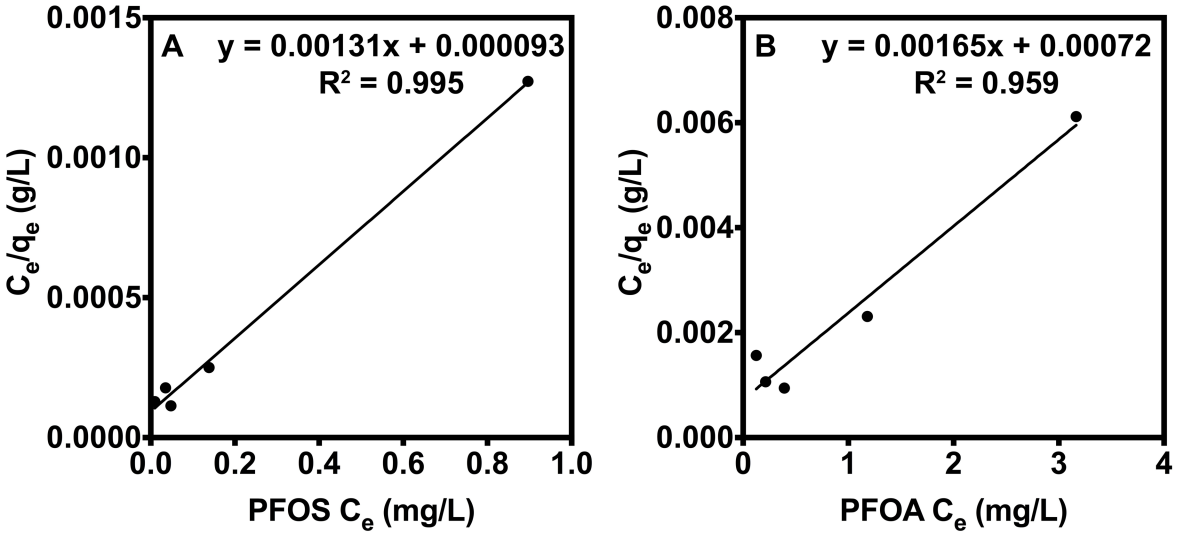

Figure A2.17. Plot of C_e/q_e (g/L) as a function of (A) PFOS and (B) PFOA equilibrium concentration (mg/L).

Table A2.13. Langmuir isotherm parameters for PFOS and PFOA adsorption on QWP1.5.

	q_{max} (mg/g)	b	R^2
PFOS	763	14.1	0.99
PFOA	605	2.29	0.96

To calculate K_F and n for PFOS and PFOA adsorption, log q_e was plotted versus log C_e according to the following linear Freundlich equation:

$$\log q_e = \log K_F + \frac{1}{n} \log C_e$$

Equation A2.8. Calculating Freundlich parameters.

K_F was calculated from the intercept of the linear regression line and n was calculated from the slope (which is 1/n) (Figure A2.18 and Table A2.14).

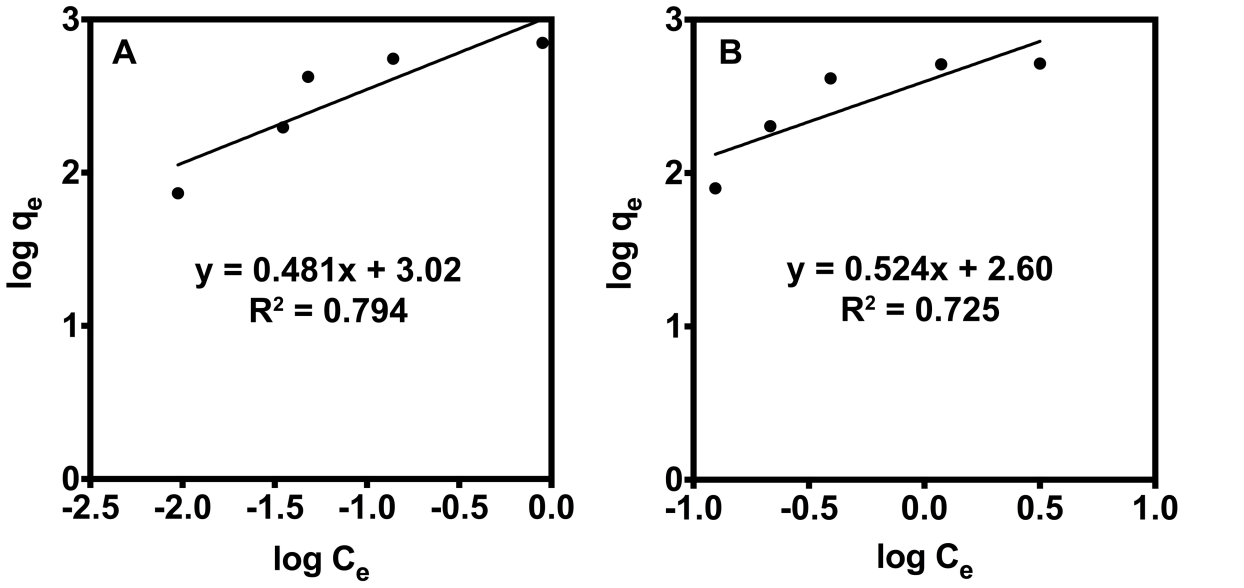

Figure A2.18. Plot of log q_e against log C_e for (A) PFOS and (B) PFOA adsorption.

Table A2.14. Freundlich isotherm parameters for PFOS and PFOA adsorption on QWP1.5.

	K_F ((mg/g)(L/mg)$^{1/n}$)	1/n	R^2
PFOS	1060	0.48	0.79
PFOA	395	0.52	0.72

P. Adsorbing multiple PFASs over time with QWP1.5

General experimental

Mixtures of QWP1.5 (0.100 mg/mL) were made according to the general procedure. All the samples in this experiment were analyzed by Eurofins. The 50 mL polypropylene tubes used in this experiment were rinsed with methanol (purge and trap grade, ~1.5 mL) and air-dried prior to use to ensure no PFAS was in the tube.

PFAS and humic acid (HA) stock solutions

The 20.0 mg/L PFOS and PFOA solutions from the adsorption isotherm experiment were used in this experiment. The other PFASs tested in this experiment were PFBS, PFOSA, PFBA, GenX, and 6:2 FTS.

PFBS and PFOSA solutions (20.0 mg/L) were made according to the same procedure used to make 20.0 mg/L PFOS and PFOA solutions. The only difference is that for PFOSA, isopropanol (IPA) was used as solvent instead of water because PFOSA is more soluble in IPA at this high concentration.

For liquid PFASs (i.e., PFBA and GenX), the PFASs were diluted with a solvent to reach 20.0 mg/L. To make the 20.0 mg/L PFBA solution, 60.8 µL of PFBA was first combined with 9.939 mL of Eurofins water in a 50 mL polypropylene tube to make a 1.00 x 10^4 mg/L PFBA solution. A 20.0 mg/L PFBA solution was made by diluting 80.0 µL of the 1.00 x 10^4 mg/L PFBA solution with 39.920 mL of Eurofins water in a new 50 mL polypropylene tube. To make the 20.0 mg/L GenX solution, 54.1 µL of GenX was first combined with 9.946 mL of methanol (purge and trap grade) in a 50 mL polypropylene tube to make a 1.00 x 10^4 mg/L GenX solution. A 20.0 mg/L

GenX solution was made by diluting 80.0 µL of the 1.00 x 10^4 mg/L GenX solution with 39.920 mL of Eurofins water in a 50 mL polypropylene tube.

After the 20.0 mg/L PFOS, PFOA, PFBS, PFOSA, PFBA, and GenX solutions were made, a "cocktail" solution containing all 7 PFASs was prepared so that the final concentration of each PFAS was 250 µg/L. The cocktail solution was made by first combining 500.0 µL of 20.0 mg/L PFOSA, PFBS, PFBA, and GenX into a 50 mL polypropylene tube. Then, 625 µL of 20.0 mg/L PFOS and 556 µL of 20.0 mg/L PFOA were added to the tube. Next, 200 µL of 50 µg/mL 6:2 FTS was added to the tube. Lastly, 36.619 mL of Eurofins water was added to the tube to give 40.0 mL of a solution that was 250 µg/L in each of the 7 PFASs. Note: 625 µL of 20.0 mg/L PFOS and 556 µL of 20.0 mg/L PFOA were used (instead of 500 µL) because it was found in the adsorption isotherm experiment that the initial PFOS and PFOA solutions were about 80% and 90%, respectively, of the targeted concentrations (Table A2.11 and Table A2.12). Thus, in this experiment, to make sure PFOS and PFOA concentrations were close to 250 µg/L, the volume of 20.0 mg/L PFOS and PFOA added to the cocktail was increased by 25% and 11%, respectively.

A 2000 mg/L HA mixture was made by combining HA (40.0 mg) and Eurofins water (20.0 mL) in a 50 mL polypropylene tube. The mixture was vortex mixed at full speed for ~1 min and sonicated for 5 min.

Adsorption experiments

Note: Eurofins requested that samples contain 1:1 methanol:water solutions, so every sample sent to Eurofins contained an aliquot of solution (1 mL) from an adsorption trial and methanol (purge and trap grade, 1 mL). Thus, the adsorption trials had a dilution factor of 2.

To perform adsorption trials, the 250 µg/L cocktail solution (100.0 µL) was added to a 50 mL polypropylene "initial tube" with a volume (0 or 100.0 µL) of 2000 mg/L HA mixture. Eurofins water (800.0 or 900.0 µL, dependent on if HA was added) was also added to the tube to give a total initial volume of 1.00 mL. Next, 1.0 mL of 0.100 mg/mL QWP1.5 mixture and 8.0 mL of Eurofins water were syringed over 10 s into the bottom of the centrifuge tube while vortex mixing at a speed of 1.5. The tube was then vortex mixed for an additional 10 s using a speed of 1.5. An aliquot of mixture (~1.5 mL) was removed from the tube with a 3 mL plastic syringe 10 s after mixing, filtered through a CA syringe filter, and placed in a 4 mL vial. A portion of the filtered solution (1000 µL) was then placed in a 15 mL "final sample" polypropylene centrifuge tube. Methanol (1000 µL) was added to the "final sample", and the 15 mL tube was sealed with parafilm.

Control trials with and without HA were performed in duplicate following the above procedure except that only Eurofins water (no QWP1.5) was added during the mixing step to give a total sample volume of 10.0 mL. These controls were analyzed to determine the initial PFAS concentrations in solution in the absence of adsorbent.

Adsorption and control trials were also performed according to the above procedure to determine PFAS adsorption after 60 min. The only difference is that after mixing QWP1.5 (or just water in controls) with PFASs, the initial tube was left undisturbed at rt for 60 min before an aliquot was removed.

The targeted initial PFAS concentrations in the adsorption and control trials were 2.50 µg/L, and the adsorbent dosage was 10.0 mg/L. Final samples 1–5 were performed without HA, and final samples 6–10 were performed with a HA concentration of 20.0 mg/L. Aliquots in final samples 1–10 were acquired immediately after mixing. Final samples 11–15 were performed without HA,

and final samples 16–20 were performed with a HA concentration of 20.0 mg/L. Aliquots in final samples 11–20 were acquired 60 min after mixing.

PFAS solution analysis

All samples were analyzed using the Eurofins general procedure for analyzing PFAS concentrations. PFAS adsorption % and capacities were calculated according to the general procedure using data from Eurofins (Table A2.15, Table A2.16, and Table A2.17). Note: Because the samples were diluted by a factor of 2, the concentrations that Eurofins reported were multiplied by 2 to find the actual PFAS concentrations in the adsorption and control trials. In addition, the PFAS concentrations in the control samples with and without HA were used as the initial PFAS concentrations for calculating adsorption % and capacity. Conclusions about PFOSA removal were not made because PFOSA was the only PFAS significantly removed by cellulose acetate syringe filters used to prepare the samples.

Table A2.15. Leftover PFAS concentrations when adsorbing multiple PFASs with QWP1.5. Trials 1–5 and 11–15 were performed without HA, and trials 6–10 and 16–20 were performed with a HA concentration of 20.0 mg/L.

final sample	[PFBA] (µg/L)	[PFBS] (µg/L)	[GenX] (µg/L)	[6:2 FTS] (µg/L)	[PFOA] (µg/L)	[PFOS] (µg/L)	[PFOSA] (µg/L)
1	3.30	2.61	2.40	2.02	2.89	2.36	0.0993
2	3.54	2.83	3.22	2.05	2.95	2.48	0.0912
3	3.16	1.96	2.70	0.211	0.616	0.040*	0.0400*
4	2.76	1.85	1.91	0.137	0.467	0.040*	0.0400*
5	3.03	1.96	1.99	0.158	0.560	0.040*	0.0400*
6	3.03	2.52	2.64	1.95	2.71	2.13	0.0641
7	3.22	2.71	3.58	2.05	2.84	2.42	0.0685
8	3.06	2.47	2.42	1.89	2.61	1.80	0.1036
9	2.94	2.34	2.24	1.73	2.45	1.72	0.0701
10	3.06	2.39	2.44	1.91	2.64	1.96	0.0867
11	2.78	2.33	2.55	2.173	2.57	2.17	0.0641
12	2.68	2.30	2.61	2.120	2.46	2.05	0.0893
13	2.01	1.34	1.71	0.0933	0.324	0.040*	0.040*
14	2.27	1.45	1.75	0.0678	0.327	0.040*	0.040*
15	2.23	1.47	1.87	0.0841	0.330	0.040*	0.040*
16	2.88	2.47	2.73	2.43	2.75	2.50	0.145
17	2.75	2.39	2.56	2.23	2.56	2.35	0.128
18	2.84	2.22	2.41	2.18	2.47	1.79	0.191
19	2.59	2.09	2.34	2.03	2.35	1.63	0.181
20	2.65	2.22	2.52	2.12	2.47	1.73	0.227

*Indicates that the measured PFAS concentration was below the limit of quantification (0.02 µg/L). Therefore, the limit of quantification was assumed to be the PFAS concentration and then multiplied by the dilution factor (2).

Table A2.16. QWP1.5 adsorption % and capacity for 7 PFASs after 30 s of contact time between QWP1.5 and PFASs.

PFAS	adsorption (%) without HA	adsorption capacity (mg/g) without HA	adsorption (%) with HA	adsorption capacity (mg/g) with HA
PFBA	13 ± 6	0.04 ± 0.02	3 ± 2	0.010 ± 0.007
PFBS	29 ± 2	0.08 ± 0.01	8 ± 3	0.021 ± 0.007
GenX	20 ± 20	0.06 ± 0.04	24 ± 3	0.07 ± 0.01
6:2 FTS	92 ± 2	0.187 ±0.004	8 ± 5	0.02 ± 0.01
PFOA	81 ± 3	0.237 ± 0.008	8 ± 4	0.02 ± 0.01
PFOS	98 ± 0*	0.238*	20 ± 5	0.05 ± 0.01
PFOSA	58 ± 0*	0.006*	-30 ± 30	–

*Indicates that the measured PFAS concentration was below the limit of quantification (0.02 µg/L). Therefore, the limit of quantification was assumed to be the PFAS concentration. Accurate standard deviations could not be calculated for these entries because of this estimation.

Table A2.17. QWP1.5 adsorption % and capacity for 7 PFASs after 60 min of contact time between QWP1.5 and PFASs.

PFAS	adsorption (%) without HA	adsorption capacity (mg/g) without HA	adsorption (%) with HA	adsorption capacity (mg/g) with HA
PFBA	21 ± 5	0.06 ± 0.01	4 ± 5	0.01 ± 0.01
PFBS	39 ± 3	0.09 ± 0.01	10 ± 3	0.03 ± 0.01
GenX	31 ± 3	0.08 ± 0.01	8 ± 3	0.02 ± 0.01
6:2 FTS	96 ± 1	0.206 ± 0.001	9 ± 3	0.02 ± 0.01
PFOA	87.0 ± 0.1	0.2190 ± 0.0003	8 ± 3	0.02 ± 0.01
PFOS	98 ± 0*	0.21*	29 ± 3	0.07 ± 0.01
PFOSA	48 ± 0*	0.037*	-50 ± 20	–

*Indicates that the measured PFAS concentration was below the limit of quantification (0.02 µg/L). Therefore, the limit of quantification was assumed to be the PFAS concentration. Accurate standard deviations could not be calculated for these entries because of this estimation.

Q. Calculating Specific UV Absorbance ($SUVA_{254}$) of humic acid (HA)

A $SUVA_{254}$ was calculated to characterize the HA's hydrophobic/hydrophilic nature.[8] We determined that the $SUVA_{254}$ was 4.1, which suggests that the HA was mainly composed of hydrophobic and aromatic materials. Note: The $SUVA_{254}$ was calculated for HA assuming the total organic carbon (TOC) was equal to the non-purgeable organic carbon (NPOC), and the purgeable organic carbon (POC) was negligible.

A 20.0 mg/L HA solution was prepared by first combining HA (10.0 mg) with Millipore water (450.0 mL) in a 500 mL glass container. NaOH (0.1 M, 25.0 mL) was then added to the container to ensure all the HA was dissolved, and the container was bath sonicated for 3 min to obtain a clear brown solution. The pH was found to be ~11 using pH paper. Aqueous HCl (0.1 M, 25.0 mL) was then added to the container to make the pH of the solution neutral, and the jar was hand mixed for ~30 s. The solution pH was found to be ~7 using pH paper.

UV-vis spectra were collected using a Thermo Scientific Evolution 220 UV-Visible Spectrophotometer and quartz cuvettes (Starna Cells, 1.0 cm pathlength). Millipore water (~2 mL) was placed in a quartz cuvette, and an absorbance spectrum from 200–750 nm was collected and used as a background spectrum. Then, the 20.0 mg/L HA solution (~2 mL) was placed in a quartz cuvette, and an absorbance spectrum from 200–750 nm was obtained. The HA's absorbance spectrum was baseline-corrected to account for the non-zero baseline. More specifically, the absorbance values for wavelengths 740–750 nm were averaged (because 740–750 nm was a region where the spectrum's absorbance was closest to 0), and this average absorbance was then subtracted from the entire spectrum. The corrected absorbance at 254 nm (Abs_{254}, au/cm) was then recorded as 0.70 for the HA solution (Figure A2.19).

The NPOC content (mg/L) of the 20.0 mg/L HA solution was found using a Shimadzu ON-LINE TOC-V_{CSH}, operated with TOC grade air. Standards and samples were analyzed using 3×80 µL injections, 1 wash, sparge times of 4.5 min, 4.0% acid add., max. integration times of 4.8 min, and 1 auto dilution. The NPOC of the 20.0 mg/L HA solution was determined to be 17 mg/L.

The $SUVA_{254}$ (L/(mg·m)) of the 20.0 mg/L HA solution was calculated according to the following equation,[9] assuming the NPOC was equal to the TOC:

$$SUVA_{254} = \frac{Abs_{254}}{NPOC} \times 100$$

Equation A2.9. Calculating SUVA of HA.

where 100 is the conversion factor between cm and m.

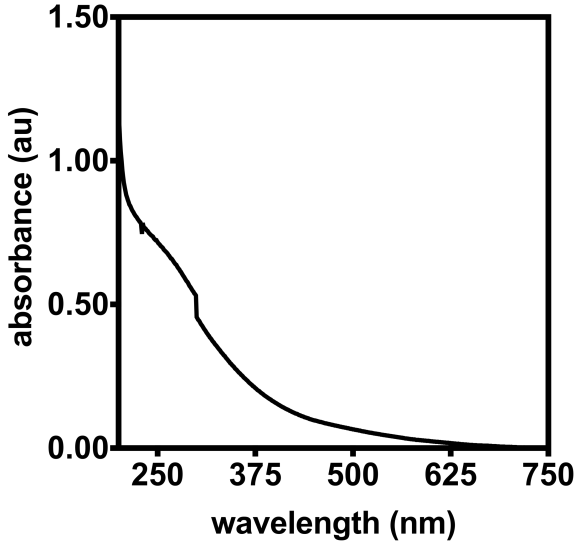

Figure A2.19. UV-vis spectrum of a 20.0 mg/L humic acid solution.

R. Adsorbing PFOS and PFOA in solutions with different pHs

General experimental

Mixtures of QWP1.5 (0.100 mg/mL) were made according to the general procedure. All the samples in this experiment were analyzed by Eurofins. The 50 mL polypropylene tubes used in this experiment were rinsed with methanol (purge and trap grade, ~1.5 mL) and air-dried prior to use to ensure no PFOS/PFOA was in the tube.

PFOS and PFOA stock solutions

The 20.0 mg/L PFOS and PFOA solutions from the adsorption isotherm experiment were used in this experiment. A 250 µg/L PFOS solution was made by diluting 625 µL of a 20.0 mg/L PFOS solution with 39.375 mL of Eurofins water in a 50 mL polypropylene tube. A 250 µg/L PFOA solution was made by diluting 556 µL of a 20.0 mg/L PFOA with 39.444 mL of Eurofins water in a 50 mL polypropylene tube. Note: 625 µL of 20.0 mg/L PFOS and 556 µL of 20.0 mg/L PFOA were used (instead of 500 µL) because it was found in the adsorption isotherm experiment that the initial PFOS and PFOA solutions were about 80% and 90%, respectively, of the targeted concentrations (Table A2.11 and Table A2.12). Thus, in this experiment, to make sure PFOS and PFOA concentrations were close to 250 ug/L, the volume of 20.0 mg/L PFOS and PFOA added to the cocktail was increased by 25% and 11%, respectively.

pH stock solutions

Three solutions with different pHs (~4, ~7, and ~10) were prepared so that when mixed with QWP1.5 and PFOS or PFOA, the final solution pH would be ~5, ~7, and ~9. The solution with a

pH of ~7 was prepared with NaCl to ensure that this experiment probed the effects of pH and not ion concentration.

1) pH ~4 solution: Concentrated HCl (2.65 mL, 12.1 M) was diluted with Eurofins water in a 200 mL volumetric flask to make a 0.100 M HCl solution. Then, 20.0 µL of the 0.100 M HCl solution was transferred to a 20 mL vial and diluted with 19.980 mL of Eurofins water to give a 0.100 mM HCl solution. The pH of the 0.100 mM solution was measured with a calibrated pH meter to be ~5. Thus, a small volume (~30.0 µL) of 0.100 M HCl was added to the 0.100 mM solution. The pH of the solution was measured again and found to be 4.06. The conductivity of the solution was measured with a calibrated conductivity meter and found to be 214 µS/cm.
2) pH ~10 solution: NaOH (40.0 mg, 1 mmol) was dissolved in 20.0 mL of Eurofins water in a 20 mL vial to make a 50.0 mM NaOH solution. Then, 40.0 µL of the 50.0 mM solution was transferred to a new 20 mL vial and diluted with 19.960 mL of Eurofins water to make a 0.100 mM NaOH solution. The pH of the 0.100 mM NaOH solution was measured with a calibrated pH meter to be ~9.75. Thus, a small volume (~20.0 µL) of 50.0 mM NaOH solution was added to the 0.100 mM solution. The pH of the 0.100 mM NaOH solution was measured again and found to have a pH of 10.00. The conductivity of the solution was measured with a calibrated conductivity meter and found to be 156 µS/cm.
3) pH ~7 solution: NaCl (20.0 mg, 0.342 mmol) was dissolved in 20.0 mL of Eurofins water in a 20 mL vial to make a 17.1 mM NaCl solution. Then, 116.9 µL of the 17.1 mM NaCl solution was transferred to a new 20 mL vial and diluted with 19.883 mL of Eurofins water to make a 0.100 mM NaCl solution. The pH of the solution was measured with a calibrated pH meter to be ~8.5, but the pH value was not stable. Thus, a small volume (~10.0 µL) of 0.100 M HCl

was added to the 0.100 mM NaCl solution. The pH of the 0.100 mM NaCl solution was measured again and found to be 6.60. The conductivity of the solution was measured with a calibrated conductivity meter and found to be 186 μS/cm.

4) The pH of Eurofins water without NaCl, HCl, or NaOH was also measured with a calibrated pH meter, and the pH of the water was found to fluctuate between ~6 and ~8 over 10 min. Thus, the pH of this water cannot be accurately measured, likely because the concentration of dissolved ions is small. The pH of the solution was assumed to be 7.00 according to Millipore's website.[1] The conductivity of the water was measured with a calibrated conductivity meter and found to be ~1 μS/cm, emphasizing the small concentration of ions present.

Adsorption experiments

Note: Each trial in this experiment probed either PFOS or PFOA adsorption in the presence of solutions with different pHs. Every sample sent to Eurofins for analysis contained 1 aliquot of solution from a PFOS trial and 1 aliquot of solution from a PFOA trial. Additionally, Eurofins requested that samples contain 1:1 methanol:water solutions, so every sample sent to Eurofins contained analyte solution (1 mL total) and methanol (purge and trap grade, 1 mL). Thus, the adsorption trials had a dilution factor of 4, stemming from the combination of 2 aliquots into a sample and the addition of methanol.

To perform adsorption trials, 100.0 μL of either 250 μg/L PFOS or PFOA solution was added to a 50 mL polypropylene tube (called "initial tube") followed by 900.0 μL of Eurofins water and 1000 μL of one of the solutions with a known pH. Then, 1.0 mL of 0.100 mg/mL QWP1.5 mixture and Eurofins water (a volume to make the adsorption mixture 10.0 mL) were syringed over 10 s into the bottom of the centrifuge tube while vortex mixing at a speed of 1.5. The tube was then

vortex mixed for an additional 10 s using a speed of 1.5. An aliquot (~1.5 mL) of mixture was removed from the initial tube using a 3 mL plastic syringe 10 s after mixing, and the aliquot was passed through a CA syringe filter and placed in a 4 mL vial. A 500.0 µL portion of this filtered solution was placed in a 15 mL "final sample" polypropylene centrifuge tube. Again, note that 1 PFOS trial aliquot and 1 PFOA trial aliquot were combined into 1 "final sample". After the "final sample" contained 1 PFOS aliquot and 1 PFOA aliquot, 1000 µL of methanol was added to the tube, and the 15 mL tube was sealed with parafilm.

Adsorption trials were performed in triplicate for each final solution pH. Final solution pHs were calculated by first dividing the $[H^+]$ or $[OH^-]$ in the pH 4.06 and 10.00 solutions by 10 to get $[H^+]_{final}$ and $[OH^-]_{final}$. The $[H^+]$ or $[OH^-]$ concentrations were divided by 10 because that is how much the pH 4.06 and 10.00 solutions were diluted by in the adsorption trial. Then, for the solutions containing $[H^+]$, the final solution pH was calculated according to:

$$pH = -\log[H^+]_{final}$$

Equation A2.10. pH equation.

For the solution containing $[OH^-]$, the final solution pH was calculated according to:

$$pH = 14 + \log[OH^-]_{final}$$

Equation A2.11. Calculating pH for basic water solution.

The final pH for trials using the pH 6.60 solution was assumed to be 7.00 according to Millipore's website.[1]

Control trials at each final solution pH were performed in duplicate following the above procedure except that only Eurofins water (no QWP1.5) was added during the mixing step to give a total sample volume of 10.0 mL. These controls were analyzed to determine the initial PFAS concentrations in solution in the absence of adsorbent. Samples 1 and 2 are the controls for the

final solution pH of 5.06, samples 6 and 7 are the controls for the final solution pH of 7.00, and samples 11 and 12 are the controls for the final solution pH of 9.00.

The targeted initial PFAS concentrations in the adsorption and control trials were 2.50 μg/L, and the adsorbent dosage was 10.0 mg/L. Samples 1–5 were performed with final solution pHs of 5.06, trials 6–10 were performed with final solution pHs of 7.00, and trials 11–15 were performed with final solution pHs of 9.00.

PFAS solution analysis

All samples were analyzed using the Eurofins general procedure for analyzing PFAS concentrations. PFOS and PFOA adsorption % and capacities were calculated according to the general procedure using data from Eurofins (Table A2.18). Because the samples were diluted by a factor of 4, the concentrations that Eurofins reported were multiplied by 4 to find the actual PFOS and PFOA concentrations in the adsorption and control trials. In addition, the PFOS and PFOA concentrations in the control samples at each final solution pH were used as the initial PFOS and PFOA concentrations for calculating adsorption % and capacity.

Table A2.18. PFOS and PFOA adsorption in solutions with various pHs.

final sample	solution pH	[PFOS] (µg/L)	PFOS adsorption (%)	PFOS adsorption capacity (mg/g)	[PFOA] (µg/L)	PFOA adsorption (%)	PFOA adsorption capacity (mg/g)
1		1.97	–	–	2.61	–	–
2		1.89			2.53		
3	5.06	0.08*			0.699		
4		0.08*	96 ± 0*	0.19	0.831	73 ± 6	0.19 ± 0.02
5		0.08*			0.526		
6		2.30	–	–	2.55	–	–
7		2.29			2.58		
8	7.00	0.08*			0.947		
9		0.08*	97 ± 0*	0.22	0.818	60 ± 10	0.15 ± 0.03
10		0.08*			1.40		
11		2.41	–	–	2.81	–	–
12		2.27			2.73		
13	9.00	0.08*			1.71		
14		0.08*	97 ± 0*	0.23	0.930	60 ± 20	0.16 ± 0.05
15		0.08*			0.812		

*Indicates that the measured PFAS concentration was below the limit of quantification (0.02 µg/L). Therefore, the limit of quantification was assumed to be the PFAS concentration and multiplied by the dilution factor (4). Accurate standard deviations could not be calculated for these entries because of this estimation.

S. Adsorbing PFOS and PFOA in the presence of NaCl

General experimental

Mixtures of QWP1.5 (0.100 mg/mL) were made according to the general procedure. All the samples in this experiment were analyzed by Eurofins. The 50 mL polypropylene tubes used in this experiment were rinsed with methanol (purge and trap grade, ~1.5 mL) and air-dried prior to use to ensure no PFOS/PFOA was in the tube.

PFOS, PFOA, and NaCl stock solutions

The 20.0 mg/L PFOS and PFOA solutions from the adsorption isotherm experiment were used in this experiment. The 250 μg/L PFOS and PFOA solutions were prepared using the same method as in "Adsorbing PFOS and PFOA in solutions with different pHs." A 1000 mg/L NaCl solution was made by dissolving NaCl (20.0 mg, 0.342 mmol) in Eurofins water (20.0 mL) in a 20 mL vial.

Adsorption experiments

Note: Each trial in this experiment probed either PFOS or PFOA adsorption in the presence of solutions with different [NaCl]. Every sample sent to Eurofins for analysis contained 1 aliquot of solution from a PFOS trial and 1 aliquot of solution from a PFOA trial. Additionally, Eurofins requested that samples contain 1:1 methanol:water solutions, so every sample sent to Eurofins contained analyte solution (1 mL) and methanol (purge and trap grade, 1 mL). Thus, the adsorption trials had a dilution factor of 4, stemming from the combination of 2 aliquots into a sample and the addition of methanol.

To perform adsorption trials, 100.0 μL of either 250 μg/L PFOS or PFOA solution was added to a 50 mL polypropylene tube (called "initial tube") followed by 900.0 μL of Eurofins water and

a volume of 1000 mg/L NaCl solution (0, 500.0, or 1000 µL). Then, 1.0 mL of 0.100 mg/mL QWP1.5 mixture and Eurofins water (a volume to make the adsorption mixture 10.0 mL) were syringed over 10 s into the bottom of the centrifuge tube while vortex mixing at a speed of 1.5. The tube was then vortex mixed for an additional 10 s using a speed of 1.5. An aliquot (~1.5 mL) of mixture was removed from the initial tube using a 3 mL plastic syringe 10 s after mixing, and the aliquot was passed through a CA syringe filter and placed in a 4 mL vial. A 500.0 µL portion of this filtered solution was placed in a 15 mL "final sample" polypropylene centrifuge tube. Again, note that 1 PFOS trial aliquot and 1 PFOA trial aliquot were combined into 1 "final sample". After the "final sample" contained 1 PFOS aliquot and 1 PFOA aliquot, 1000 µL of methanol was added to the tube, and the 15 mL tube was sealed with parafilm.

Adsorption trials were performed in triplicate for each final [NaCl]. In samples 1–5, 0 µL of 1000 mg/L was added giving a final [NaCl] of 0 mg/L. In samples 6–10, 500.0 µL of 1000 mg/L was added giving a final [NaCl] of 50.0 mg/L. In samples 11–15, 1000 µL of 1000 mg/L was added giving a final [NaCl] of 100 mg/L. In addition, to add a 4th data point to the PFOS/PFOA adsorption vs [NaCl] plot, the trials from the pH 7 data point in the section "adsorbing PFOS and PFOA in solutions with different pHs" (Table A2.18) were utilized and given as samples 16–20 in Table A2.19.

Control trials for each [NaCl] were performed in duplicate following the above procedure except that only Eurofins water (no QWP1.5) was added during the mixing step to give a total sample volume of 10.0 mL. These controls were analyzed to determine the initial PFAS concentrations in solution in the absence of adsorbent. Samples 1 and 2 are the controls for the [NaCl] = 0 mg/L, samples 6 and 7 are the controls for the [NaCl] = 50.0 mg/L, and samples 11 and 12 are the controls for the [NaCl] = 100 mg/L.

The targeted initial PFOS and PFOA concentrations in the adsorption and control trials were 2.50 µg/L, and the adsorbent dosage was 10.0 mg/L.

Calculating [NaCl] for samples 16–20 in Table A2.19

The conductivities of the PFOS/PFOA adsorption trials used to make samples 16–20 in Table A2.19 were 18.6 µS/cm. This value was utilized because the conductivity of the solution used to make the PFOS/PFOA adsorption trials was 186 µS/cm before being diluted by a factor of 10 (section "adsorbing PFOS and PFOA in solutions with different pHs"). Then, using 18.6 µS/cm as the conductivity for samples 16–20, the [NaCl] was calculated according to the following equation[10] that relates conductivity and ion concentration:

$$TDS = kC$$

Equation A2.12. Calculating salt concentration from conductivity.

where TDS (mg/L) is the total dissolved solids in solution, C is conductivity (µS/cm), and k is a constant relating conductivity and TDS. In this case, a k value of 0.5 was used because the adsorption and control trials' conductivity was estimated to be 18.6 µS/cm, and this is close to the conductivity for distilled water.[10] Thus, the TDS was calculated to be 9.30 mg/L, and this concentration was assumed to be the final [NaCl].

PFAS solution analysis

All samples were analyzed using the Eurofins general procedure for analyzing PFAS concentrations. PFOS and PFOA adsorption % and capacities were calculated according to the general procedure using data from Eurofins (Table A2.19). Note: Because the samples were diluted by a factor of 4, the concentrations that Eurofins reported were multiplied by 4 to find the actual PFOS and PFOA concentrations in the adsorption and control trials. In addition, the PFOS and

PFOA concentrations in the control samples at each [NaCl] were used as the initial PFOS and PFOA concentrations for calculating adsorption % and capacity.

Table A2.19. PFOS and PFOA adsorption in solutions with various [NaCl].

final sample	[NaCl] (mg/L)	[PFOS] (µg/L)	PFOS adsorption (%)	PFOS adsorption capacity (mg/g)	[PFOA] (µg/L)	PFOA adsorption (%)	PFOA adsorption capacity (mg/g)
1		2.49	–	–	2.67	–	–
2		2.26			2.64		
3	0.00	0.08*			1.21		
4		0.08*	97 ± 0*	0.23	0.342	80 ± 20	0.2 ± 0.1
5		0.08*			0.304		
6		1.86	–	–	2.79	–	–
7		1.65			2.34		
8	50.0	0.08*			1.53		
9		0.08*	95 ± 0*	0.17	1.97	40 ± 10	0.09 ± 0.03
10		0.08*			1.36		
11		1.87	–	–	2.66	–	–
12		1.72			2.54		
13	100	0.100			1.93		
14		0.08*	95 ± 1	0.171 ± 0.001	1.80	31 ± 5	0.08 ± 0.01
15		0.08*			1.66		
16		2.30	–	–	2.55	–	–
17		2.29			2.58		
18	9.30	0.08*			0.947		
19		0.08*	97 ± 0*	0.22	0.818	60 ± 10	0.15 ± 0.03
20		0.08*			1.40		

*Indicates that the measured PFAS concentration was below the limit of quantification (0.02 µg/L). Therefore, the limit of quantification was assumed to be the PFAS concentration and multiplied by the dilution factor (4). Accurate standard deviations could not be calculated for these entries because of this estimation.

V. References

(1) Millipore Sigma. Water for pH measurement. https://www.emdmillipore.com/US/en/water-purification/learning-centers/applications/inorganic-analysis/ph-measurement/water-impact/MK6b.qB.3g4AAAFUNWISsxU6,nav?ReferrerURL=https%3A%2F%2Fwww.google.com%2F (accessed March 10, 2021).

(2) Pigorsch, E. Spectroscopic characterisation of cationic quaternary ammonium starches. *Starch* **2009**, *61*, 129–138.

(3) Wiley, J.; Atalla, R. Band assignments in the raman spectra of celluloses. *Carbohydr. Res.* **1987**, *160*, 113–129.

(4) Ho, Y.; McKay, G. Sorption of dye from aqueous solution by peat. *Chem. Eng. J.* **1998**, *70*, 115–124.

(5) Kamlet, M.; Doherty, R.; Abraham, M.; Taft, R. Linear solvation energy relationships. 33. An analysis of the factors that influence adsorption of organic compounds on activated carbon. *Carbon* **1985**, *23*, 549–554.

(6) Luehrs, D.; Hickey, J.; Nilsen, P.; Godbole, K.; Rogers, T. Linear solvation energy relationship of the limiting partition coefficient of organic solutes between water and activated carbon. *Environ. Sci. Technol*. **1996**, *30*, 143–152.

(7) Ling, Y.; Klemes, M.; Steinschneider, S.; Dichtel, W.; Helbling, D. QSARs to predict adsorption affinity of organic micropollutants for activated carbon and ß-cyclodextrin polymer adsorbents. *Water Res*. **2019**, *154*, 217–226.

(8) Sillanpaa, M; Matilainen, A.; Lahtinen, T. Characterization of NOM. In *Natural organic matter in water*, 1st edition; IWA Publishing, **2015**; pp 17–53.

(9) Potter, B.B.; Wimsatt, J.C. *Method 415.3 determination of total organic carbon and specific UV absorbance at 254 nm in source water and drinking water*; EPA/600/R-05/055; U.S. Environmental Protection Agency. Cincinnati, OH, **2005**.

(10) Walton, N.R.G. Electrical conductivity and total dissolved solids-what is their precise relationship? *Desalination* **1989**, *72*, 275–292.

Appendix 3 Supporting Information for Chapter 4

I. General Experimental 223

II. Synthesis and characterization of sulfated wood pulps (SWPs), quaternized wood pulps (QWPs), and primary amine wood pulps (PWPs) 224

A. Synthesis and purification of SWPs 224

B. Synthesis and purification of QWPs 224

C. Synthesis of PWPs 225

D. SWP Conductometric Titration Data 225

E. QWP Conductometric Titrations 227

F. PWP Conductometric Titrations 228

G. Elemental Analysis (EA) of SWPs and QWPs 229

H. EA of PWPs 229

III. Swelling of hydrogels made with SWPs and QWPs 230

A. General preparation of QWP and SWP mixtures 230

B. Procedure for making gels and calculating swell ratios 230

IV. Methyl orange (MO) adsorption experiments 232

A. Generating a calibration curve for MO in Millipore water 232

B. Adsorbing MO as a function of SWP and QWP charge density 233

C. MO adsorption experiments with either unfunctionalized WP, SWP, or QWP fibers 235

D. Adsorbing MO as a function of QWP0.77 concentration 238

E. Adsorbing MO as a function of SWP:QWP mass ratio 240

I. General Experimental

A Thermo Scientific Orion Star A215 pH/conductivity meter was used for the conductometric titrations. Before use each day, the pH and conductivity meters were calibrated. The pH meter was calibrated using Orion 4.01 (catalog number 910104), 7.00 (catalog number 910107), and 10.01 (catalog number 910110) pH buffers. The conductivity meter was calibrated using Orion 1413 μS/cm (catalog number 011007) conductivity standards.

An IKA T25 digital Ultra-Turrax homogenizer equipped with a S25N-10G-ST dispersing tool was utilized for homogenizing cellulose nanofiber (CNF) and wood pulp (WP) mixtures.

All UV-vis spectra were collected using a Thermo Scientific Evolution 220 UV-visible Spectrophotometer.

During syntheses, two centrifuges were used: a Thermo Scientific Sorvall ST8 centrifuge along with disposable polypropylene 50 mL centrifuge tubes, and a Sorvall RC5C Plus centrifuge equipped with a Thermo Scientific SLA-1500 rotor with 250 mL Thermo Scientific Nalgene PPCO centrifuge bottles (catalog number 3141-0250).

In dye adsorption studies, when gels did not form, a Thermo Scientific Sorvall ST8 centrifuge was used along with disposable polypropylene 50 mL centrifuge tubes.

A Fisher Scientific standard microplate vortex mixer (catalog number 02-216-100) was used for making S-CNF- and S-WP-based hydrogels.

Elemental analysis was performed by Midwest Microlab.

A VWR ultrasonic cleaner (model 97043-992) was used to dissolve MO in water.

II. Synthesis and characterization of sulfated wood pulps (SWPs), quaternized wood pulps (QWPs), and primary amine wood pulps (PWPs)

A. Synthesis and purification of SWPs

See Chapter 4 experimental section for details.

Table A3.1. SWP experimental conditions.

SWP sample	initial WP mass (mg)	volume of DMF added (mL)	1st homoge-nization (rpm)	2nd homoge-nization (rpm)	CSA added (mL)	CSA conc. (mM)
SWP0.0	300	50	4 min@11k	4 min@11k	0	0
SWP0.53	400	50	1 min@15k 3 min@11k	1 min@15k 3 min@11k	1.1	43
SWP0.83	1000	125	3 min@23k	3 min@23k	5.0	77
SWP1.1	1000	125	3 min@23k	3 min@23k	8.5	130
SWP1.7	1000	50	1 min@15k 3 min@11k	1 min@15k 3 min@11k	3.2	120

B. Synthesis and purification of QWPs

See Chapter 4 experimental section for details.

Table A3.2. QWP experimental conditions.

QWP sample	QWP0.77	QWP1.2	QWP1.3	QWP1.6
initial WP mass (mg)	1000	1000	1000	300
water used during homogenization (mL)	50	50	50	15
IPA (mL)	50	50	50	15
NaOH (mg, mmol)	333.4, 8.335	333.4, 8.335	333.4, 8.335	150.0, 3.750
GMAC (mL)	3.355	6.218	9.390	3.730
[GMAC] in rxn mixture (M)	0.469	0.824	1.18	1.48
total purification cycles	4	4	6	7

C. Synthesis of PWPs

See Chapter 4 experimental section for details.

Table A3.3. PWP synthesis conditions.

sample	TEA (mL)	[TEA] in rxn 1 (mM)	TsCl (g)	[TsCl] in rxn 1 (mM)	EDA (mL)	[EDA] in rxn 2 (mM)
PWP1	0.877	137	0.600	68.6	0.600	221
PWP2	0.877	137	1.20	137	0.600	221
PWP3	0.877	137	0.600	68.6	1.20	436
PWP4	1.754	269	0.600	67.3	0.600	221
PWP5	1.754	269	1.20	135	0.600	221
PWP6	1.754	269	1.20	135	0.600	221
PWP7	1.754	269	1.20	135	0.600	221

D. SWP Conductometric Titration Data

Table A3.4. SWP conductometric titration results.

sample	first charge density (mmol/g)[a]	second charge density (mmol/g)[a]	average charge density (mmol/g)
SWP0.0	0.0439	0.0471	0.046 ± 0.002
SWP0.53	0.529	0.530	0.53 ± 0.00
SWP0.83	0.849	0.803	0.83 ± 0.03
SWP1.1	1.04	1.10	1.1 ± 0.0
SWP1.7	1.66	1.66	1.7 ± 0.0

[a]The data in this column contain one extra significant figure to show how the average charge density was calculated for each sample.

1) determining mass of SWP mixture in titration beaker:

mass beaker + water + weigh paper + protonated SWPs = 83.1266 g

– (mass beaker + weigh paper) = 62.4482 g

mass protonated SWP mixture = 20.6784 g

2) determining concentration of SWPs in titration beaker:

mass aliquot 1 = 2.3946 g → dry mass of aliquot 1 = 4.4 mg → SWP conc. = 1.837 mg/g

mass aliquot 2 = 2.5891 g → dry mass of aliquot 2 = 4.9 mg → SWP conc. = 1.893 mg/g

→ average SWP conc. = 1.865 mg/g

3) determining mass of SWPs titrated:

mass protonated SWP mixture after aliquot removal = 15.6947 g

mass protonated SWP = 29.3 mg

4) conductometric titration plot:

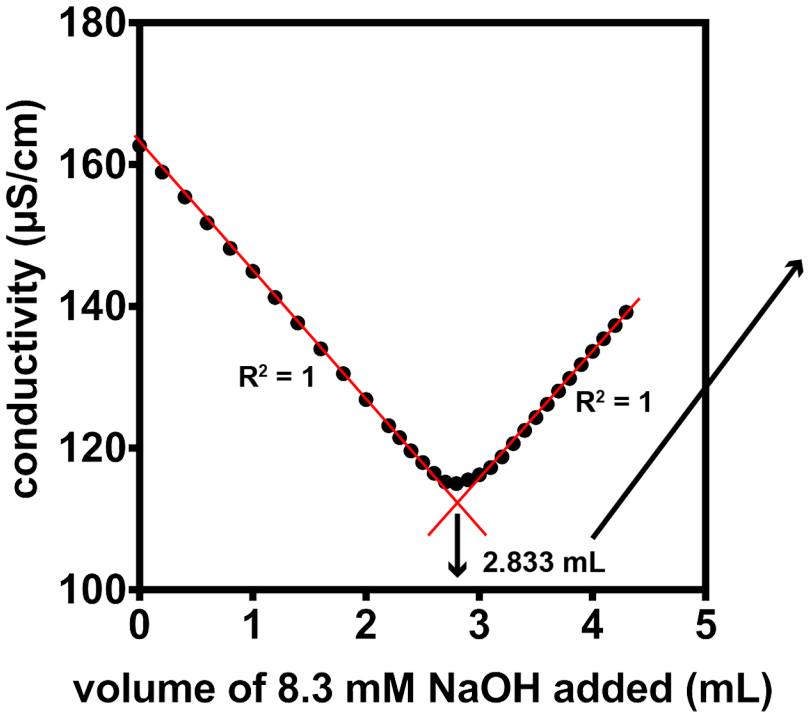

5) determining charge density:

$$\frac{2.833 \text{ mL} \times 0.0083 \text{ M NaOH}}{0.029 \text{ g SCNF}} = 0.80 \text{ mmol } SO_3^- \text{ g}^{-1}$$

Figure A3.1. Plot of conductivity (µS/cm) versus volume of 8.3 mM NaOH added (mL) during a titration to calculate the charge density of a SWP0.83 sample.

E. QWP Conductometric Titrations

Table A3.5. QWP conductometric titration results.

sample	first charge density (mmol/g)[a]	second charge density (mmol/g)[a]	average charge density (mmol/g)
QWP0.77	0.776	0.761	0.77 ± 0.01
QWP1.2	1.19	1.19	1.2 ± 0.0
QWP1.3	1.34	1.36	1.3 ± 0.0
QWP1.6[b]	1.60	–	1.60

[a]The data in this column contain one extra significant figure to show how the average charge density was calculated for each sample.
[b]Only one titration was performed on QWP1.6.

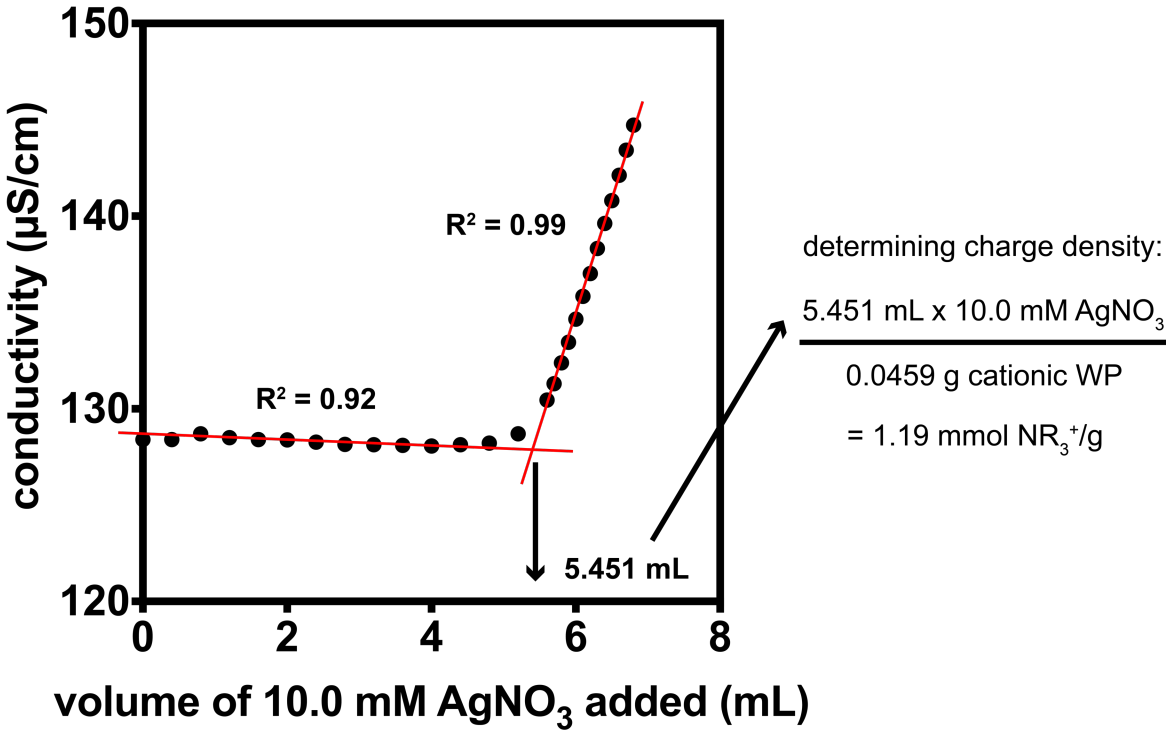

Figure A3.2. Plot of conductivity (µS/cm) versus volume of 10.0 mM $AgNO_3$ added (mL) during a titration to calculate the charge density of a QWP1.2 sample. Points were included in the linear regression lines based on linearity and inclusion of extra points near the equivalence point did not significantly affect charge density calculations.

F. PWP Conductometric Titrations

Table A3.6. PWP conductometric titration results.

sample	charge density (mmol/g)
PWP1	0.15
PWP2[a]	0.18 ± 0.01
PWP3	0.15
PWP4	0.17
PWP5	0.20
PWP6	0.14
PWP7	0.17

[a]This sample was titrated 2 times.

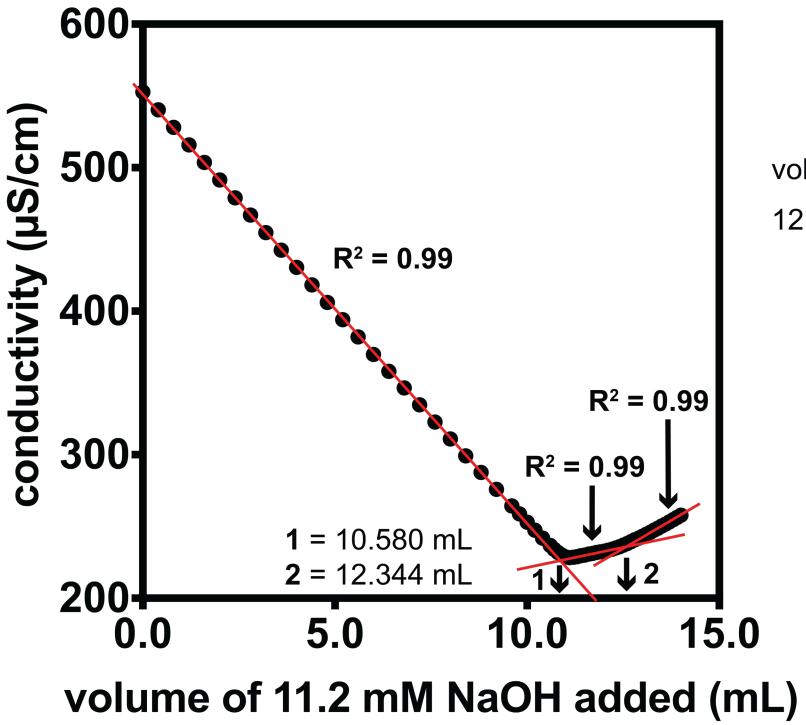

volume difference between **1** and **2**:

12.344 mL – 10.580 mL = 1.764 mL

determining charge density:

$$\frac{1.764\ \text{mL} \times 11.2\ \text{mM NaOH}}{0.100\ \text{g PWP}}$$

$$= 0.20\ \text{mmol } -NH_3^+/\text{g}$$

Figure A3.3. Plot of conductivity (µS/cm) versus volume of 11.2 mM NaOH added (mL) during a titration to calculate the charge density of the PWP5 sample. Points were included in the linear regression lines based on linearity and inclusion of extra points near the equivalence point did not significantly affect charge density calculations.

G. Elemental Analysis (EA) of SWPs and QWPs

Although EA was not performed on the SWPs and QWPs described in this appendix, it was performed on the SWPs and QWPs in Appendices 1 and 2, where we found that the charge densities calculated with conductometric titrations are accurate.

H. EA of PWPs

EA was performed on the PWP samples to determine the nitrogen content (wt% N) in each sample. The wt% N found via EA were then divided by 2 to compare with the wt% N determined by conductometric titrations, which only account for the primary amine N in the ethylene diamine groups linked to PWPs. Table A3.7 shows that conductometric titrations underestimate the PWPs' nitrogen contents, but the reason for the underestimation is not currently known.

Table A3.7. Comparing PWP nitrogen contents (wt% N) as determined with conductometric titrations and elemental analysis.

sample	wt% N by titration	wt% N found by EA	adjusted wt% N from EA
PWP1	0.22	0.60	0.30
PWP2	0.25	0.61	0.31
PWP3	0.21	0.67	0.34
PWP4	0.24	0.70	0.35
PWP5	0.28	0.69	0.35
PWP6	0.20	0.65	0.33
PWP7	0.23	0.70	0.35

III. Swelling of hydrogels made with SWPs and QWPs

A. General preparation of QWP and SWP mixtures

QWP and SWP mixtures with concentrations of 2.00 mg/mL were made by first soaking QWPs or SWPs (25.0 mg) with Millipore water (12.5 mL) for 5 min in a 20 mL vial. Then, the mixture was homogenized at 18k rpm for 1 min.

B. Procedure for making gels and calculating swell ratios

A volume (4.0 mL) of 2.00 mg/mL SWP mixture and a volume (4.0 mL) of 2.00 mg/mL QWP mixture were simultaneously added via syringe to either a 20 mL vial or 50 mL polypropylene centrifuge tube over a recorded time (14–20 s) while vortex mixing at a speed of 1.5 (Table A3.8). The vial or centrifuge tube was vortexed for an additional "mixing" time using a speed of 1.5 (Table A3.8), and then the vial or centrifuge tube was removed from the vortex mixer with a gel being observed. The gel was removed from the vial or centrifuge tube using a spatula, placed in a pre-weighed vial to measure the mass of the gel, and dried at 110 ºC. The leftover dry mass was measured, and the swell ratio was calculated according to the following equation:

$$\text{swell ratio} = \frac{\text{mass wet gel - mass dry gel}}{\text{mass dry gel}}$$

Equation A3.1. Calculating WP-based hydrogel swell ratios.

Samples 1–6 in Table A3.8 examined swelling of hydrogels made with SWP0.53 and 3 different QWPs. Two gels were made for each combination of SWP0.53 and QWP, and the average swell ratio was determined by averaging these samples. Samples 7–15 in Table A3.8 probed swelling of hydrogels made with SWP1.7 and 3 different QWPs. Three gels were made for each combination of SWP1.7 and QWP, and the average swell ratio was determined by averaging these samples. Note: Samples 13–15 were the only samples made using a centrifuge tube instead of vial.

Table A3.8. Swell ratio of hydrogels prepared with various SWPs and QWPs.

Gel sample	SWP charge density (mmol SO_3^- /g)	QWP charge density (mmol -NR_3^+/g)	SWP and QWP combination/additional mixing time (s)	swell ratio	average swell ratio
1	0.53	0.77	20/5	51.9	51.8 ± 0.1
2		0.77	18/2	51.8	
3		1.2	15/2	68.8	65 ± 6
4		1.2	15/2	60.9	
5		1.6	18/2	79.2	80 ± 1
6		1.6	16/2	81.3	
7	1.7	0.77	14/2	76.7	73 ± 4
8		0.77	15/2	73.7	
9		0.77	16/1	68.7	
10		1.2	18/2	90.7	90 ± 1
11		1.2	17/2	90.3	
12		1.2	20/1	88.5	
13		1.6	16/2	101.9	94 ± 7
14		1.6	15/2	87.5	
15		1.6	17/2	91.5	

IV. Methyl orange (MO) adsorption experiments

A. Generating a calibration curve for MO in Millipore water

MO (10.0 mg, 30.6 μmol, λ_{max} = 464 nm) was dissolved in Millipore water (10.0 mL) in a 50 mL centrifuge tube to make a 3.06 mM MO solution. Then, using Millipore water, serial dilutions were performed to make 0.306, 0.611, 1.53, 2.44, 3.06, 6.11, 15.3, 24.4, 30.6, 61.1, and 91.7 μM solutions in 50 mL centrifuge tubes. The UV-vis spectrum from 400–750 nm of each MO solution was acquired and corrected according to the baseline correction procedure in "General procedure for adsorbing MO with SWP/QWP gels."

Table A3.9. Baseline-corrected absorbance (464 nm) of MO solutions with various concentrations.

MO concentration (μM)	absorbance
0.306	0.007
0.611	0.012
1.53	0.036
2.44	0.054
3.06	0.063
6.11	0.121
15.3	0.330
24.4	0.556
30.6	0.685
61.1	1.503
91.7	2.373

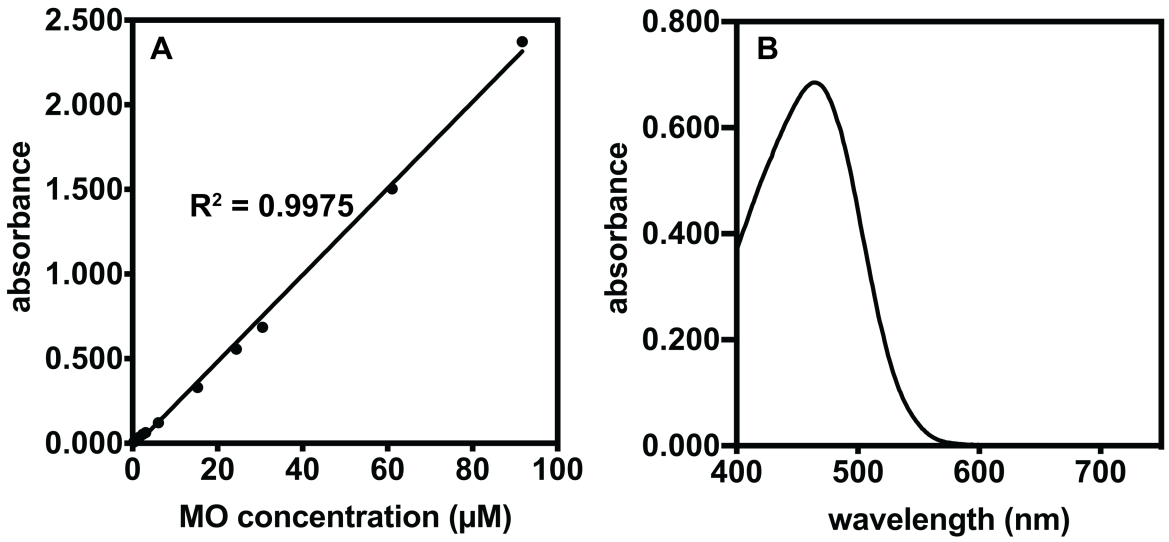

Figure A3.4. (A) Plot of absorbance (464 nm) versus MO concentration in Millipore water. (B) Sample UV-vis spectrum of MO using the 30.6 μM solution.

B. Adsorbing MO as a function of SWP and QWP charge density

SWP0.83 and SWP1.7 mixtures (1.50 mg/mL) were made according to the general procedure using 18.8 mg of SWP and 12.5 mL of Millipore water. QWP0.77 and QWP1.6 mixtures (2.00 mg/mL) were made according to the general procedure using 25.0 mg of QWP and 12.5 mL of Millipore water. The general procedure for adsorbing MO with SWP/QWP gels was followed to calculate MO adsorption % as a function of SWP and QWP charge density (Table A3.10).

The following figure (Figure A3.5) is an example of a MO UV-vis spectrum following dye adsorption with hydrogels. The spectrum is overlaid with a 30.6 μM MO spectrum that was used to make the calibration curve.

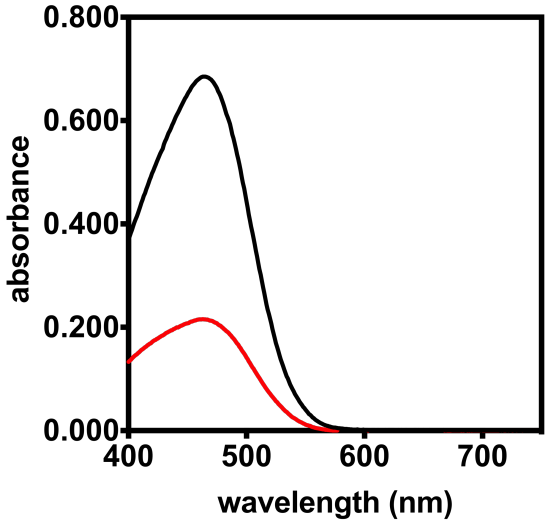

Figure A3.5. UV-vis spectra of a 30.6 µM solution used in the MO calibration curve (black), and a MO solution after dye adsorption using a hydrogel made with SWP0.83 and QWP1.6 (red).

Table A3.10. MO adsorption as a function of SWP and QWP charge density.

trial	SWP charge density (mmol SO_3^-/g)	QWP charge density (mmol - NR_3^+/g)	SWP and QWP combination/additional mixing time (s)	MO adsorption (%)	avg MO adsorption (%)
1	0.83	1.6	15/2	58	61 ± 2
2			17/2	63	
3			18/2	62	
4		0.77	20/2	64	64 ± 3
5			20/2	66	
6			18/2	61	
7	1.7	1.6	20/2	58	54 ± 3
8			18/2	52	
9			21/3	52	
10		0.77	17/3	53	54 ± 3
11			18/2	57	
12			18/2	51	

C. MO adsorption experiments with either unfunctionalized WP, SWP, or QWP fibers

Experiments were performed to determine if MO adsorption occurred on unfunctionalized WP, SWP, or QWP fibers without making hydrogels. SWP0.0 and SWP1.1 mixtures (2.00 mg/mL) were made according to the general procedure using 25.0 mg of SWP and 12.5 mL of Millipore water. QWP0.77 and QWP1.6 mixtures (2.00 mg/mL) were made according to the general procedure using 25.0 mg of QWP and 12.5 mL of Millipore water. The general procedure for adsorbing MO with SWP/QWP gels was followed with 3 modifications to calculate MO adsorption % in samples containing fibers (Table A3.11):

(1) Instead of combining a SWP and a QWP mixture into a centrifuge tube containing MO, 4.0 mL of either a SWP or a QWP mixture was combined simultaneously with 4.0 mL of Millipore water via syringe to the centrifuge tube over a recorded time while vortex mixing at a speed setting of 1.5.

(2) After mixing SWPs or QWPs with water and MO, the mixture was centrifuged for 2 min at 3260 × g because a gel did not form. Then, an aliquot (~2 mL) of the supernatant was removed and placed in a cuvette without dilution. The absorbance spectrum of the solution was measured from 400–750 nm within 4 min of mixing the components together.

(3) After centrifuging trial 1 in Table A3.11, the supernatant was diluted by a factor of 10 using Millipore water before the UV-vis spectrum was acquired. Thus, to find the true leftover MO concentration for this trial, the MO concentration calculated from calibration curve was multiplied by 10.

Finally, 2 control trials were performed by only adding 8.0 mL of Millipore water (no SWP or QWP) to the MO solution, and these controls were averaged and analyzed to determine if any MO adsorption is lost to other processes besides adsorption. Because these control samples showed

some loss of MO, we calculated adjusted MO adsorption %, which are reported in Chapter 4, and the final column of Table A3.11. The adjusted % were calculated by subtracting the average control MO adsorption % from the average measured MO adsorption % for each sample (Table A3.11).

The following figure (Figure A3.6) is an example of a MO UV-vis spectrum following dye adsorption with SWP1.1 and QWP0.77 fibers. The spectra are overlaid with a 30.6 μM MO spectrum that was used to make the calibration curve.

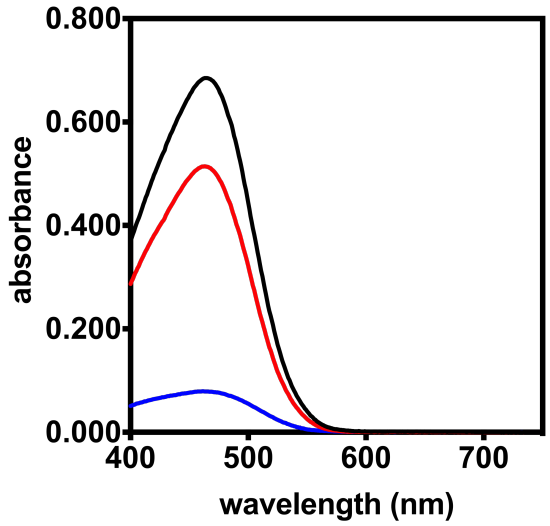

Figure A3.6. UV-vis spectra of a 30.6 μM solution used in the MO calibration curve (black), and MO solutions after adsorption using SWP1.1 (red) and QWP0.77 (blue) fibers.

Table A3.11. MO adsorption with only SWP and QWP fibers.

trial	SWP, QWP, or water added	SWP or QWP or water combination/additional mixing time (s)	MO adsorption (%)	avg measured MO adsorption (%)	avg adjusted MO adsorption (%)
1	SWP0.0	19/11	9	8 ± 2	0 ± 2
2		18/10	6		
3		17/10	7		
4	SWP1.1	20/10	7	7.3 ± 0.3	-1 ± 0.3
5		15/10	7		
6		18/10	8		
7	QWP1.6	16/10	81	81 ± 1	73 ± 1
8		18/10	80		
9		20/10	80		
10	QWP0.77	20/10	89	90 ± 1	82 ± 1
11		19/9	90		
12		20/8	91		
13	water	20/10	8	8.3 ± 0.5	–
14		20/10	9		

D. Adsorbing MO as a function of QWP0.77 concentration

A SWP0.83 mixture (6.00 mg/mL) was made according to the general procedure using 78.0 mg of SWP0.83 and 13.0 mL of Millipore water. A QWP0.77 mixture (8.00 mg/mL) was made according to the general procedure using 104.0 mg of QWP and 13.0 mL of Millipore water. Using the 6.00 mg/mL SWP0.83 mixture, serial dilutions were performed with Millipore water to make SWP mixtures with concentrations of 4.50, 3.00, 1.50, 0.75, and 0.38 mg/mL. Using the 8.00 mg/mL QWP0.77 mixture, serial dilutions were performed to make QWP mixtures concentrations of 6.00, 4.00, 2.00, 1.00, and 0.50 mg/mL. The general procedure for adsorbing MO with SWP/QWP gels was followed to calculate MO adsorption % as a function of QWP0.77 concentration (Table A3.12). The mass ratio of SWP0.83:QWP0.77 was held constant at 0.75, and only one adsorption trial was performed for each SWP0.83/QWP0.77 concentration. The MO adsorption capacity (q, mg/g) for each trial was determined using the following equation:

$$q = \frac{(C_0 - C) \times 327.33}{C_A \times 1000}$$

Equation A3.2. Calculating MO adsorption capacity in WP-based hydrogels.

where C_A (mg/mL) is the total concentration of WP in the mixture, 327.33 is the MO molar mass (μg/μmol), and 1000 is the conversion ratio between mL and L.

The following figure (Figure A3.7) is an example of a MO UV-vis spectrum following dye adsorption with 1.6 mg/mL QWP0.77. The spectrum is overlaid with a 30.6 μM MO spectrum that was used to make the calibration curve.

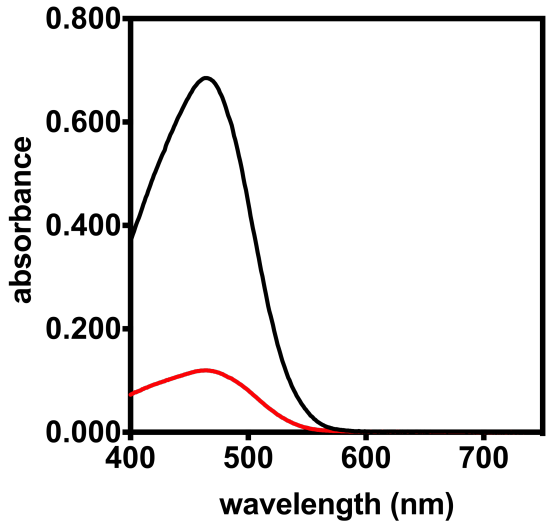

Figure A3.7. UV-vis spectra of a 30.6 µM solution used in the MO calibration curve (black), and a MO solution after adsorption using a hydrogel made with 1.2 mg/mL SWP0.83 and 1.6 mg/mL QWP0.77 (red).

Table A3.12. MO adsorption (%) and capacity (mg/g) as a function of SWP and QWP concentration.

trial	final SWP conc. (mg/mL)	final QWP conc. (mg/mL)	SWP and QWP combi-nation/additional mixing time (s)	MO adsorption (%)	MO q (mg/g)
1	2.4	3.2	20/15	78	1.0
2	1.8	2.4	20/15	86	1.5
3	1.2	1.6	18/12	75	2.0
4	0.6	0.8	18/8	64	3.4
5	0.3	0.4	18/6	42	4.5
6	0.15	0.2	18/5	29	6.1

E. Adsorbing MO as a function of SWP:QWP mass ratio

A SWP0.83 mixture (4.00 mg/mL) was made according to the general procedure using 52.0 mg of SWP0.83 and 13.0 mL of Millipore water. A QWP0.77 mixture (4.00 mg/mL) was made according to the general procedure using 52.0 mg of QWP and 13.0 mL of Millipore water. Using the 4.00 mg/mL SWP0.83, serial dilutions were performed with Millipore water to make SWP mixtures concentrations of 1.00 and 0.25 mg/mL. The general procedure for adsorbing MO with SWP/QWP gels was followed to calculate MO adsorption % as a function of SWP0.83:QWP0.77 mass ratio (Table A3.13). The final QWP concentration was 1.6 mg/mL.

The following figure (Figure A3.8) is an example of a MO UV-vis spectrum following dye adsorption with a SWP0.83:QWP0.77 mass ratio of 0.25. The spectrum is overlaid with a 30.6 μM MO spectrum that was used to make the calibration curve.

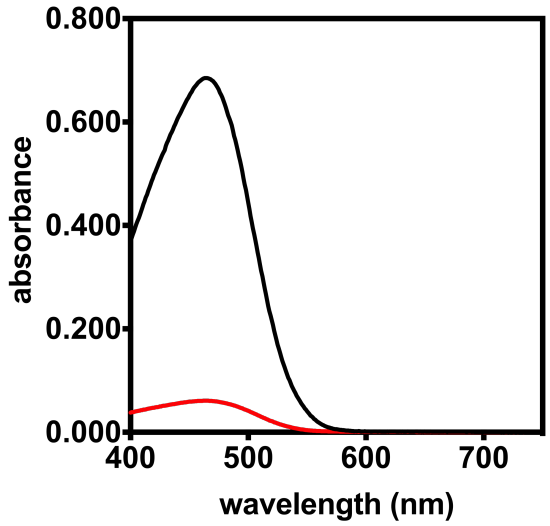

Figure A3.8. UV-vis spectra of a 30.6 μM solution used in the MO calibration curve (black), and a MO solution after adsorption in a hydrogel with a SWP0.83:QWP0.77 mass ratio of 0.25 (red).

Table A3.13. MO adsorption as a function of SWP0.83:QWP0.77 mass ratio.

trial	final SWP conc. (mg/mL)	mass ratio (SWP:QWP)	MO adsorption (%)
1	1.6	1.0	70
2	0.40	0.25	85
3	0.10	0.063	81